frontiers | Research Topics

Petal development: From cell biology to EvoDevo

Edited by
Tengbo Huang, Elena M. Kramer and Deshu Lin

Published in
Frontiers in Plant Science

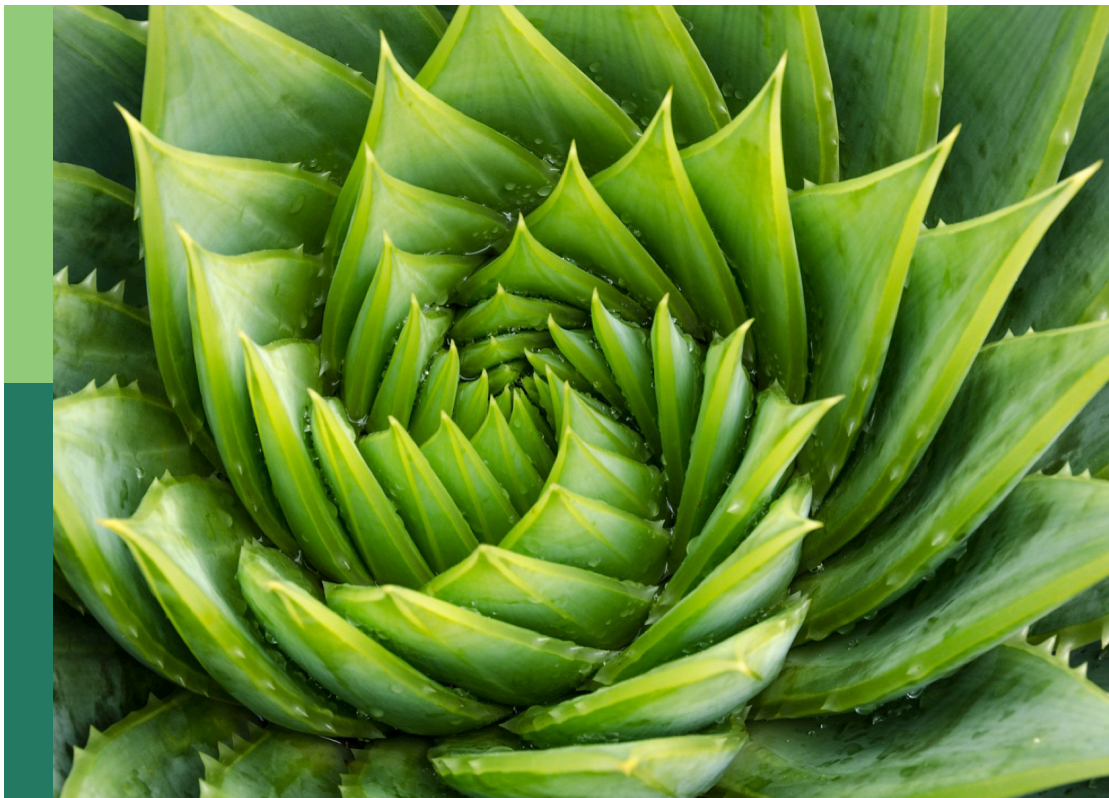

ISSN 1664-8714
ISBN 978-2-83251-528-0
DOI 10.3389/978-2-83251-528-0

About Frontiers

Frontiers is more than just an open access publisher of scholarly articles: it is a pioneering approach to the world of academia, radically improving the way scholarly research is managed. The grand vision of Frontiers is a world where all people have an equal opportunity to seek, share and generate knowledge. Frontiers provides immediate and permanent online open access to all its publications, but this alone is not enough to realize our grand goals.

Frontiers journal series

The Frontiers journal series is a multi-tier and interdisciplinary set of open-access, online journals, promising a paradigm shift from the current review, selection and dissemination processes in academic publishing. All Frontiers journals are driven by researchers for researchers; therefore, they constitute a service to the scholarly community. At the same time, the *Frontiers journal series* operates on a revolutionary invention, the tiered publishing system, initially addressing specific communities of scholars, and gradually climbing up to broader public understanding, thus serving the interests of the lay society, too.

Dedication to quality

Each Frontiers article is a landmark of the highest quality, thanks to genuinely collaborative interactions between authors and review editors, who include some of the world's best academicians. Research must be certified by peers before entering a stream of knowledge that may eventually reach the public - and shape society; therefore, Frontiers only applies the most rigorous and unbiased reviews. Frontiers revolutionizes research publishing by freely delivering the most outstanding research, evaluated with no bias from both the academic and social point of view. By applying the most advanced information technologies, Frontiers is catapulting scholarly publishing into a new generation.

What are Frontiers Research Topics?

Frontiers Research Topics are very popular trademarks of the *Frontiers journals series*: they are collections of at least ten articles, all centered on a particular subject. With their unique mix of varied contributions from Original Research to Review Articles, Frontiers Research Topics unify the most influential researchers, the latest key findings and historical advances in a hot research area.

Find out more on how to host your own Frontiers Research Topic or contribute to one as an author by contacting the Frontiers editorial office: frontiersin.org/about/contact

Petal development: From cell biology to EvoDevo

Topic editors

Tengbo Huang — Shenzhen University, China
Elena M. Kramer — Harvard University, United States
Deshu Lin — Fujian Agriculture and Forestry University, China

Citation

Huang, T., Kramer, E. M., Lin, D., eds. (2023). *Petal development: From cell biology to EvoDevo*. Lausanne: Frontiers Media SA. doi: 10.3389/978-2-83251-528-0

Table of contents

frontiers | Frontiers in Plant Science

EDITORIAL
published: 15 June 2022
doi: 10.3389/fpls.2022.951442

Editorial: Petal Development: From Cell Biology to EvoDevo

Tengbo Huang[1]*, *Elena M. Kramer*[2]* and *Deshu Lin*[3]*

[1] Guangdong Provincial Key Laboratory for Plant Epigenetics, College of Life Sciences and Oceanography, Shenzhen University, Shenzhen, China, [2] Department of Organismic and Evolutionary Biology, Harvard University, Cambridge, MA, United States, [3] Key Laboratory of Ministry of Education for Genetics, Breeding and Multiple Utilization of Crops, Fujian Agriculture and Forestry University, Fuzhou, China

Keywords: petal organogenesis, cell proliferation and expansion, cell type specification, plant-pollinator interaction, plant evolution

Editorial on the Research Topic

Petal Development: From Cell Biology to EvoDevo

The petal is an excellent model system for studying plant organogenesis because it is simple in structure and dispensable for plant viability (Irish, 2008). The petal is also a useful system for investigating plant-animal interactions, as it is the major plant part that attracts pollinators in many outcrossing species (Fenster et al., 2004; Stuurman et al., 2004). The nine articles in this Research Topic focus on several important aspects of research associated with petal development and function. We organize this collection of studies into several groups based on common themes as described below.

OPEN ACCESS

Edited and reviewed by:
Jill Christine Preston, University of Vermont, United States

***Correspondence:**
Tengbo Huang
tengbohuang@szu.edu.cn
Elena M. Kramer
ekramer@oeb.harvard.edu
Deshu Lin
deshu.lin@fafu.edu.cn

Specialty section:
This article was submitted to Plant Development and EvoDevo, a section of the journal Frontiers in Plant Science

Received: *24 May 2022*
Accepted: *31 May 2022*
Published: *15 June 2022*

Citation:
Huang T, Kramer EM and Lin D (2022) Editorial: Petal Development: From Cell Biology to EvoDevo. Front. Plant Sci. 13:951442. doi: 10.3389/fpls.2022.951442

SPECIFICATION OF PETAL IDENTITY

In the model plant *Arabidopsis thaliana* (Arabidopsis, Brassicaceae), petal primordia arise in the second whorl of the four concentric floral whorls. Specification of petal identity depends on the combinatorial regulation of MADS box transcription factors encoded by the *APETALA1* (*AP1*), *APETALA3* (*AP3*), *PISTILLATA* (*PI*), and *SEPALLATA* (*SEP*) genes (Wellmer et al., 2014). In this Research Topic, Deveaux et al. investigate an ortholog of *AP3*, *NdAP3-3,* in *Nigella damascena* (Ranunculaceae). They analyze the putative target genes of *NdAP3-3* and compare them with those of the *AP3* homologs in Arabidopsis and *Aquilegia coerulea* (Ranunculaceae). They identify a number of common genes in each comparison, which shows the functional conservation of *AP3* genes during plant evolution.

PETAL GROWTH MEDIATED BY THE CELL PROLIFERATION TO EXPANSION TRANSITION

The growth of petal primordia in the second whorl occurs through two waves:early stage cell division and late stage post-mitotic expansion (Huang and Irish, 2016). Coordination of cell division and expansion in petal development is critical for the regulation of cell number and size that determine the morphology of the mature petal. In this Research Topic, several articles focus on studies related to this theme. For example, Galipot et al. investigate the growth of nectariferous petals in *N. damascena* and identify the allometric nature of petal shape and size dynamics. They also find that the patterning of petal shape is primarily determined by the activities of cell proliferation, while the change of petal size is mainly driven by the dynamics of cell expansion. These data uncover an important cellular mechanism that sculpts the elaborate *N. damascena*

petal. Furthermore, in a study of another ornamental species, *Gerbera hybrida* (Asteraceae), Lin et al. characterize two 14-3-3 protein-coding genes that mediate brassinosteroid-induced ray petal elongation. They find that these two 14-3-3 genes play a key role in controling petal growth by promoting petal cell elongation.

The timing of transition from cell proliferation to expansion is a key control point that determines mature organ morphology. Two transcription factors, RABBIT EARS (RBE) and TCP5, play vital roles in the regulation of cell proliferation-to-expansion transition in the Arabidopsis petal (Huang and Irish, 2015). In this Research Topic, Huang et al. propose a model that RBE may repress *TCP5* by recruiting epigenetic modifiers to induce chromatin-mediated silencing at the *TCP5* locus, which adds a new layer of epigenetic regulation to the RBE/TCP5-mediated transcriptional control of cell proliferation-to-expansion transition in petal morphogenesis.

REGULATION OF PETAL CELL MATURATION

Following the transition from cell division to expansion, another critical factor that controls petal growth is the degree of expansion and final cell shape. Zhang and Zhang show that genome size of *Paphiopedilum* (Orchidaceae) species is negatively correlated with labellum epidermal cell size, and positively correlated with the size of leaf epidermal cells, which suggests that genome size may be a strong predictor of cell size. Moreover, Cavallini-Speisser et al. write a review to summarize the major cell types in the petal and their functions. They also conclude the actions of the key regulators of petal development in the specification of different cell types in the petal. This collection of information provides us with a good resource for further studying the genetic control of petal organogenesis at the cellular level.

RELATIONSHIP BETWEEN PETAL DEVELOPMENT AND POLLINATION

Variation in petal development that results in the diversity of petal morphologies has important implications in attracting specific pollinators for different plant species (Fenster et al., 2004; Stuurman et al., 2004). One such relationship between petal development and pollination is investigated by Hsu and Kuo, who analyze the nectar guide patterns in Ligeriinae (Gesneriaceae) by examining the petal contours and vasculatures. They identify four modes of nectar guide patterns and show that two of the four modes, distal and proximal, have the strongest associations with pollination types. These results are helpful for further understanding the diversity of nectar guide patterns and its relationship with plant-pollinator interaction in Ligeriinae.

SUMMARY

The diverse and interconnected subjects presented in this Research Topic provide comprehensive information about ongoing studies of petal development and functions. These studies also raise some interesting questions worthy of future investigation. For example, what role do epigenetic mechanisms play in the transcriptional regulation of petal growth? How is variation in growth patterns during petal development, which has been shown in this topic to be critical for determining petal morphology, regulated by temporal- and spatial-specific factors? It is worth noting that we include two articles that are not directly related with petal development in this topic: one uses tissue-specific analyses to investigate the interaction between tomato and a parasitic plant *Cuscuta campestris* (Jhu et al.); while the other assesses the miRNA profiles in Mepiquat chloride-mediated inhibition of internode elongation in cotton (Wang et al.). The strategies and results of these two studies, such as the tissue-specific approaches and the roles of the epigenetic regulator miRNAs, may shed light on the above questions. By addressing these critical questions, we hope to have a more in-depth dissection of the complex network that controls petal growth, which may serve as the basis for a better understanding of plant organ development in the future.

AUTHOR CONTRIBUTIONS

TH, EK, and DL were contributed to the writing of this editorial. All authors approved it for publication.

FUNDING

Our work on petal organogenesis has been supported by grants from the Guangdong Basic and Applied Basic Research Foundation (2021A1515011035) and Guangdong Special Support Program for Young Talents in Innovation Research of Science and Technology (2019TQ05N940) to TH, and NSF IOS-1456217 to EK.

ACKNOWLEDGMENTS

The guest editors would like to acknowledge all contributors to this Research Topic.

REFERENCES

Fenster, C. B., Armbruster, W. S., Wilson, P., Dudash, M. R., and Thomson, J. D. (2004). Pollination syndromes and floral specialization. *Annu. Rev. Ecol. Evol. Syst.* 35, 375–403. doi: 10.1146/annurev.ecolsys.34.011802.132347

Huang, T., and Irish, V. F. (2015). Temporal control of plant organ growth by TCP transcription factors. *Curr. Biol.* 25, 1765–1770. doi: 10.1016/j.cub.2015.05.024

Huang, T., and Irish, V. F. (2016). Gene networks controlling petal organogenesis. *J. Exp. Bot.* 67, 61–68. doi: 10.1093/jxb/erv444

Irish, V. F. (2008). The Arabidopsis petal: a model for plant organogenesis. *Trends Plant Sci.* 13, 430–436. doi: 10.1016/j.tplants.2008.05.006

Stuurman, J., Hoballah, M. E., Broger, L., Moore, J., Basten, C., and Kuhlemeier, C. (2004). Dissection of floral pollination syndromes in Petunia. *Genetics* 168, 1585–1599. doi: 10.1534/genetics.104.031138

Wellmer, F., Graciet, E., and Riechmann, J. L. (2014). Specification of floral organs in Arabidopsis. *J. Exp. Bot.* 65, 1–9. doi: 10.1093/jxb/ert385

Conflict of Interest: The authors declare that the research was conducted in the absence of any commercial or financial relationships that could be construed as a potential conflict of interest.

Publisher's Note: All claims expressed in this article are solely those of the authors and do not necessarily represent those of their affiliated organizations, or those of the publisher, the editors and the reviewers. Any product that may be evaluated in this article, or claim that may be made by its manufacturer, is not guaranteed or endorsed by the publisher.

frontiers in Plant Science

ORIGINAL RESEARCH
published: 24 February 2021
doi: 10.3389/fpls.2021.643213

Profiling of MicroRNAs Involved in Mepiquat Chloride-Mediated Inhibition of Internode Elongation in Cotton (*Gossypium hirsutum* L.) Seedlings

Li Wang[1,2], Ying Yin[1], Xiuxiu Jing[1], Menglei Wang[1], Miao Zhao[1], Juanjuan Yu[1,2], Zongbo Qiu[1,2] and Yong-Fang Li[1,2]**

[1] College of Life Sciences, Henan Normal University, Xinxiang, China, [2] Henan International Joint Laboratory of Agricultural Microbial Ecology and Technology, Henan Normal University, Xinxiang, China

OPEN ACCESS

Edited by:
Deshu Lin,
Fujian Agriculture and Forestry University, China

Reviewed by:
Lianfeng Gu,
Fujian Agriculture and Forestry University, China
Wankui Gong,
Cotton Research Institute (CAAS), China

***Correspondence:**
Yong-Fang Li
li_yongfang@hotmail.com
Li Wang
wangli1015@htu.cn

Specialty section:
This article was submitted to Plant Development and EvoDevo, a section of the journal Frontiers in Plant Science

Received: 17 December 2020
Accepted: 01 February 2021
Published: 24 February 2021

Citation:
Wang L, Yin Y, Jing X, Wang M, Zhao M, Yu J, Qiu Z and Li Y-F (2021) Profiling of MicroRNAs Involved in Mepiquat Chloride-Mediated Inhibition of Internode Elongation in Cotton (Gossypium hirsutum L.) Seedlings. Front. Plant Sci. 12:643213. doi: 10.3389/fpls.2021.643213

Mepiquat chloride (MC) is the most important plant growth retardant that is widely used in cotton (*Gossypium hirsutum* L.) production to suppress excessive vegetative growth and improve plant architecture. MicroRNAs (miRNAs) are important gene expression regulators that control plant growth and development. However, miRNA-mediated post-transcriptional regulation in MC-induced growth inhibition remains unclear. In this study, the dynamic expression profiles of miRNAs responsive to MC in cotton internodes were investigated. A total of 508 known miRNAs belonging to 197 families and five novel miRNAs were identified. Among them, 104 miRNAs were differentially expressed at 48, 72, or 96 h post MC treatment compared with the control (0 h); majority of them were highly conserved miRNAs. The number of differentially expressed miRNAs increased with time after treatment. The expression of 14 known miRNAs was continuously suppressed, whereas 12 known miRNAs and one novel miRNA were continuously induced by MC. The expression patterns of the nine differentially expressed miRNAs were verified using qRT-PCR. The targets of the known and novel miRNAs were predicted. Four conserved and six novel targets were validated using the RLM-5′ RACE assay. This study revealed that miRNAs play crucial regulatory roles in the MC-induced inhibition of internode elongation. It can improve our understanding of post-transcriptional gene regulation in MC-mediated growth inhibition and could potentially facilitate the breeding of dwarf cotton.

Keywords: mepiquat chloride, internode, microRNA, cotton, target gene

INTRODUCTION

Cotton (*Gossypium hirsutum* L.) is a worldwide cultivated economic crop that provides natural fiber materials and edible oil. One of the major challenges in cotton production is the control of excessive vegetative growth during the entire developmental stage owing to its indeterminate growth habit. Serious production problems, such as auto-shading, fruit abscission, delayed maturity, and reduced

yield, often occur under excessive vegetative growth (Zhao and Oosterhuis, 2000). Therefore, the vegetative growth of cotton should be controlled. Mepiquat chloride (MC) is the most commonly used growth regulator in cotton production; it shortens internodes, decreases plant height, and reduces leaf area (Reddy et al., 1990; Rademacher, 2000; Siebert and Stewart, 2006; Curaba et al., 2013; Ren et al., 2013). The compact plant architecture and open canopy by MC application are important for maximizing cotton yield (Gwathmey and Clement, 2010; Ren et al., 2013).

Mepiquat chloride is a well-known gibberellin (GA) biosynthesis inhibitor. Early studies hypothesized that MC specifically inhibits the activity of copalyl diphosphate synthase in the early steps of GA biosynthesis (Shechter and West, 1969; Rademacher, 2000). Recently, we found that MC repressed cell division and elongation of cotton internodes by reducing not only endogenous GA but also auxin and brassinosteroid (BR) contents (Wang L. et al., 2020). Transcriptome profiling showed that MC remarkably reduced the expression of genes related to GA, auxin, BR, and ethylene metabolism and signaling but increased the expression of genes related to cytokinin and abscisic acid (Wang L. et al., 2020). Furthermore, many transcription factors (TFs), including growth regulating factor (GRF), TEOSINTE BRANCHED1/CYCLOIDEA/PCF (TCP), no apical meristem (NAC), myb domain protein (MYB), and squamosa promoter binding protein (SPLs/SBP), which play key modulating functions in plant growth, were significantly altered by MC (Wang L. et al., 2020).

MicroRNAs (miRNAs) are a class of non-coding RNAs with lengths of ∼20–24 nt. miRNAs modulate the expression of their targets post-transcriptionally through mRNA cleavage or translation inhibition in a sequence-specific manner (Addoquaye et al., 2009). Most targets of the conserved miRNAs are TFs or phytohormone-related genes (Rodriguez et al., 2016; Tang et al., 2018), therefore, miRNAs play key roles in many biological processes such as organ development, hormone signal transduction, growth phase switching, and stress response (Gao et al., 2016; Rodriguez et al., 2016; Tang et al., 2018; Yuan et al., 2019). Several miRNAs have been shown to be associated with plant height by modulating internode elongation (Schwab et al., 2005; Chuck et al., 2007; Alonso-Peral et al., 2010; Fu et al., 2012; Gao et al., 2015, 2016; Liu et al., 2017; Zhao et al., 2017; Dai et al., 2018; Jiang et al., 2018; Sun et al., 2019; Yuan et al., 2019). In rice, overexpression of miR319, miR396d, miR164b, and miR535 or suppression of miR159 shortened internodes and caused plant dwarfism (Liu et al., 2017; Zhao et al., 2017; Jiang et al., 2018; Tang et al., 2018; Sun et al., 2019). Transgenic creeping bentgrass (*Agrostis stolonifera*) overexpressing osa-miR396c exhibited shortened internodes (Yuan et al., 2019). Enhanced expression of miR156 reduced plant height in Arabidopsis, rice, maize, alfalfa, and switchgrass (Schwab et al., 2005; Chuck et al., 2007; Fu et al., 2012; Gao et al., 2016; Dai et al., 2018). TCPs regulated by miR319 have been shown to control cell proliferation in plants (Rodriguez et al., 2016). miR396 has been proven to be closely related to cell proliferation and elongation by targeting GRFs (Rodriguez et al., 2016; Tang et al., 2018), and miR396 is associated with the pathways of several hormones such as GA, auxin, and BR (Gao et al., 2015; Tang et al., 2018). miR159 positively regulates organ growth by promoting cell division via the targeting of GAMYBs (Alonso-Peral et al., 2010; Zhao et al., 2017). Suppression of miR159 in rice impaired cell cycle and hormone homeostasis (Zhao et al., 2017).

Although miRNAs associated with plant height have been identified in several crops, limited information is available on miRNAs related to cotton internode elongation. Most studies on cotton miRNAs have focused on miRNA profiling and identification of miRNAs associated with fiber initiation and elongation (Zhao et al., 2019), anther development (Zhang et al., 2018), male sterility (Nie et al., 2018), somatic embryogenesis (Yang et al., 2013), stress response (Xie et al., 2015a), and disease resistance (Shweta et al., 2018). By comparing the miRNA profiles between wild type and dwarf mutants of cotton, An et al. (2015) identified 104 differentially expressed miRNAs (DEG miRNAs) in stem apexes and revealed the roles of miRNAs in controlling cotton plant height. In our previous study, we found that many genes, including TFs, were altered by MC application (Wang L. et al., 2020); thus, we hypothesize that miRNAs may contribute to MC-induced internode elongation inhibition at post-transcriptional level. To identify the miRNAs responsive to MC treatment and reveal their potential roles in MC-mediated growth inhibition, we sequenced four small RNA (sRNA) libraries from cotton internodes at the three-leaf stage at different time points (0, 48, 72, and 96 h) post MC treatment. This study reveals the regulatory roles of miRNAs in cotton internode elongation and provides novel insights into the molecular mechanisms of MC-mediated growth inhibition, which may facilitate the breeding of dwarf cotton.

MATERIALS AND METHODS

Plant Growth and Treatments

Upland cotton (*G. hirsutum* 'CCRI49') seeds were obtained from the Institute of Cotton Research of the Chinese Academy of Agricultural Sciences (Anyang, China). Cotton seeds were immersed in water for 8 h at 37°C and then germinated in sand at 28°C in the dark for 3 days. Subsequently, uniform seedlings were transferred to plastic pots filled with aerated half-strength Hoagland solution and grown hydroponically in a growth chamber with a 14-h photoperiod at a 28/20°C day/night temperature cycle and a light intensity of 550 μmol m^{-2} s^{-1}.

Based on our previous study (Wang L. et al., 2020), 80 mg/L of MC (Hebei Guoxin ahadzi Biological Technology Co., Ltd., Hejian, Hebei, China) was applied to the cotton seedlings at the three-leaf stage by foliar spraying until the leaf was evenly wetted and started dripping (approximately 4 mL/plant). The upper halves of the second internode were harvested at 0 h (control), 48, 72, and 96 h post MC treatment (hpt), and samples at each time point were collected from 10 seedlings, immediately frozen in liquid nitrogen, and then stored at –80°C for RNA extraction, with three biological replicates for each time point. Morphological phenotypes of control and MC-treated seedlings were observed at 10 days post treatment.

sRNA Library Construction and Sequencing

Total RNA was extracted from internodes using TRIzol reagent (Invitrogen, Carlsbad, CA, United States) according to the manufacturer's instructions. The RNA quality and integrity of each sample were evaluated using 1% agarose gel electrophoresis and a Bioanalyzer (Agilent 2100). Equal amounts of total RNA from three biological replicates were mixed and sent to BGI (Shenzhen, China) for the construction of sRNA libraries. sRNAs of 18–30 nt in length were enriched using 15% denatured polyacrylamide gel electrophoresis (PAGE) and ligated to the 3′ and 5′ RNA adaptors. A reverse transcription reaction was then performed to generate cDNA, which was then used for subsequent PCR enrichment. The final PCR products were purified using PAGE (Wang et al., 2015). The constructed libraries were sequenced using the BGISEQ-500RS sequencing platform (BGI, Shenzhen, China).

Analysis of sRNA Sequencing Data

Raw sequencing reads were first processed by filtering low-quality reads and trimming the adaptor sequences, and eventually, high-quality clean reads (18–30 nt) were acquired. Any sRNAs mapping to rRNAs, tRNAs, snRNAs, protein-coding genes, or repeat sequences were filtered by alignment against the databases of Rfam, Repbase, GtRNAdb, and Silva. Subsequently, the clean reads were aligned to the *G. hirsutum* TM-1 genome (Zhang et al., 2015) using Bowtie tools with no mismatch and multiple mappings allowed. Only the mapped sRNAs were subjected to identification of cotton-known miRNAs. The mature miRNA sequences from all plant species were downloaded from miRBase 22.1[1] and combined to obtain all known plant miRNA sequences. Cotton known miRNAs in internodes were identified by BLASTN search against all known plant miRNA sequences. Only sRNAs with not more than two mismatches were identified as cotton-known miRNAs. The remaining sRNAs were used to predict novel cotton miRNAs using the miRdeep2 software (Friedländer et al., 2012).

The flanking genome sequences (150 nt upstream and 150 nt downstream) of sRNAs were used to predict the secondary hairpin structures using RNAfold software.[2] The secondary structures of the novel miRNAs were further checked manually using the MFOLD (Zuker, 2003). The criteria we used to identify novel miRNAs were based on a recent article (Axtell and Meyers, 2018).

Identification and Validation of Differentially Expressed miRNAs

For miRNA expression analysis, tags per million (TPM) were utilized to normalize the miRNA expression levels as follows: TPM = (read count/mapped reads)*1,000,000. Differential expression analysis of miRNAs between the two samples was performed using DEGseq (Wang et al., 2010a). miRNAs with $|\log_2(\text{fold change})| \geq 1.0$ between samples and p-value ≤ 0.05 were considered to be DEG miRNAs.

To validate the sRNA sequencing data, qRT-PCR was carried out. Total RNA containing sRNAs was first polyadenylated and then reverse-transcribed to cDNA using the Mir-X^{TM} miRNA First-Strand Synthesis Kit (Clontech, CA, United States). Real-time PCR was performed on a LightCycler® 96 System (Roche) with an SYBR Premix Ex Taq^{TM} kit (Takara, Japan). All reactions were performed in triplicate. The forward primers were designed based on the mature miRNA sequences, and the universal reverse primer was supplied in the Mir-X^{TM} miRNA First-Strand Synthesis Kit. The primer sequences are listed in **Supplementary Table 1**. The *U6* gene was used as an internal control for the normalization of qRT-PCR data. The expression levels of the miRNAs at 0 h were set as 1.0, and relative expression at other time points was calculated using the $2^{-\Delta\Delta CT}$ method (Livak and Schmittgen, 2001).

Prediction and Validation of the Target Genes of miRNAs

The potential target genes of cotton miRNAs were predicted using TargetFinder software (alignment score ≤4) (Kielbasa et al., 2010). To validate the predicted target genes, RNA ligase-mediated 5′- rapid amplification of cDNA ends (RLM-5′ RACE) was performed using a GeneRacer kit (Invitrogen). Total RNA from the cotton internode was directly ligated to the RNA oligo adapter. First-strand cDNA was reverse-transcribed using oligo dT primers and Superscript II reverse transcriptase (Invitrogen). Nested PCR was performed using 5′-adaptor primers and 3′ gene-specific primers (**Supplementary Table 2**). After amplification, PCR products with expected sizes were gel-purified using a QIAquick® Gel Extraction Kit (QIAGEN, Valencia, CA, United States) and cloned into the pMD19-T vector (Takara, Japan). Following transformation, positive *Escherichia coli* DH5α clones identified using colony PCR were used for isolation of plasmids, which were subjected to Sanger sequencing (Li et al., 2010).

RESULTS

Overview of the sRNA Library Sequencing Data

Application of 80 mg/L MC significantly reduced the internode length and plant height of cotton seedlings (**Figure 1**), corroborating the result of our previous study (Wang L. et al., 2020). Previously, we found that the transcriptional levels of genes related to GA biosynthesis and signaling and cell expansion were inhibited by MC after 48 h of treatment owing to the time-dependent translocation and accumulation of MC from the leaf to the internode (Wang L. et al., 2020). Therefore, the second elongating internodes were collected at four time points (0, 48, 72, and 96 h) post MC treatment for sRNA library preparation and MC-responsive miRNA identification. After discarding low-quality reads and contaminated sequences and adaptor trimming, a total of 98,906,991 clean reads representing 52,952,581 unique reads, ranging from 18 to 30 nt, were retained for subsequent

[1] http://www.mirbase.org

[2] http://rna.tbi.univie.ac.at/cgi-bin/RNAWebSuite/RNAfold.cgi

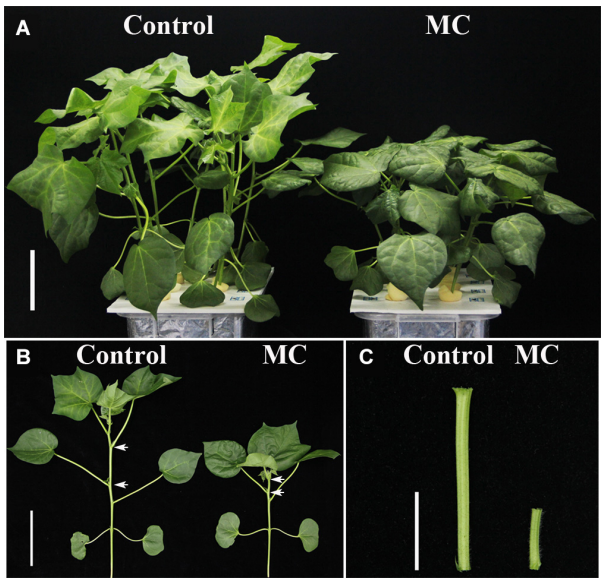

FIGURE 1 | Morphological phenotypes of MC-induced growth inhibition of cotton seedlings. **(A,B)** Control and MC-treated seedlings at 10 d post treatment. The white arrows indicate the second internode. Bar = 10 cm. **(C)** The second internode of control and MC-treated seedling at 10 d post treatment. Bar = 3 cm.

analysis (**Table 1**). The size distributions of the four sRNA libraries showed similar patterns (**Figure 2**). The 24-nt reads were the most abundant class (about 50%), followed by 21-nt reads (17%) (**Figure 2**), in agreement with previous reports on cotton and other plant species (An et al., 2015; Li et al., 2019; Zhao et al., 2020). On the average, 84.18% of the reads were successfully aligned to the AD genome of *G. hirsutum*. The reads mapping to tRNAs, rRNAs, snoRNAs, and snRNAs accounted for 0.00–2.35% of the total reads (**Table 1**). The sequencing data and mapping statistics reflect the high-quality sRNA libraries obtained in this study.

Identification of Known miRNAs in the Elongating Internode

To identify known cotton miRNAs in the sRNA libraries, we downloaded the mature miRNA sequences from all plant species deposited in miRBase 22.1 and combined them to obtain all known plant miRNA sequences. The unique reads from the four cotton sRNA libraries were subjected to a BLASTN search against all known plant miRNA sequences. The sRNAs that matched the known plant miRNA sequences with fewer than two mismatches were annotated as known cotton miRNAs. In total, 508 known miRNAs belonging to 197 families were identified in the four libraries (**Supplementary Table 3**). Among them, 21 highly conserved miRNA families were identified, and they included: miR156/157, miR159, miR160, miR162, miR164, miR165/166, miR167, miR168, miR169, miR170/171, miR172, miR319, miR390, miR393, miR394, miR395, miR396, miR397, miR398, miR399, and miR408. Currently, there are 378 mature miRNAs belonging to 217 families deposited in miRBase (22.1) for the genus *Gossypium* (*Gossypium raimondii*, *Gossypium hirsutum*, *Gossypium arboreum*, and *Gossypium herbaceum*). In this study, 309 cotton miRNAs belonging to 177 families (81.7%) were identified, indicating a good sequencing coverage of the four sRNA libraries.

The expression of known miRNAs was found to vary significantly. The highly abundant miRNAs were conserved miRNAs such as miR159, followed by miR166, miR164, miR319, miR168, miR171, miR156, miR398, and miR396. Several conserved miRNAs such as miR397, miR399, and miR172 showed relatively low expression levels. Most of the less conserved known miRNAs exhibited low expression levels; however, the abundance of miR535, miR2949, miR482, miR2947, miR3476, and miR7505 was high at different time points.

Identification of Novel miRNAs in the Elongating Internode

Excluding the identified known miRNAs, the remaining sRNA sequences were used to predict potential novel miRNAs using the miRDeep2 software. We further manually checked the hairpin structure of the predicted novel miRNAs using MFOLD software (Zuker, 2003), and only those with the typical stem-loop structure were retained. Five novel miRNAs were identified in this study and were designated as ghr-miRn1 to ghr-miRn5 (**Supplementary Table 4** and **Supplementary File 1**), and the corresponding miRNA* sequences were also detected. The lengths of these novel miRNAs and miRNAs* varied from 20 to 24 nt. Compared

TABLE 1 | Read statistics of four cotton internode small RNA libraries.

Type	Raw reads	Clean reads	Mapped reads	rRNA	snRNA	snoRNA	tRNA	Unique reads	Unique mapped reads
0 h	25,516,715	24,556,182 (100%)	20,776,551 (84.61%)	309,986 (1.21%)	13 (0.00%)	338 (0.00%)	13,392 (0.05%)	14,262,096 (100%)	11,235,293 (78.78%)
48 h	23,951,610	23,159,571 (100%)	19,102,915 (82.48%)	413,155 (1.72%)	17 (0.00%)	269 (0.00%)	12,564 (0.05%)	12,760,520 (100%)	9,691,613 (75.95%)
72 h	26,285,348	25,272,630 (100%)	21,403,498 (84.69%)	386,318 (1.47%)	18 (0.00%)	348 (0.00%)	13,802 (0.05%)	14,248,382 (100%)	11,300,636 (79.31%)
96 h	27,129,484	25,918,608 (100%)	22,014,595 (84.94%)	636,338 (2.35%)	22 (0.00%)	407 (0.00%)	15,948 (0.06%)	11,681,583 (100%)	9,138,581 (78.23%)
Total	102,883,157	98,906,991 (100%)	83,297,559	1,745,797	70	1,362	55,706	52,952,581	41,366,123

Data in parentheses are the percentages.

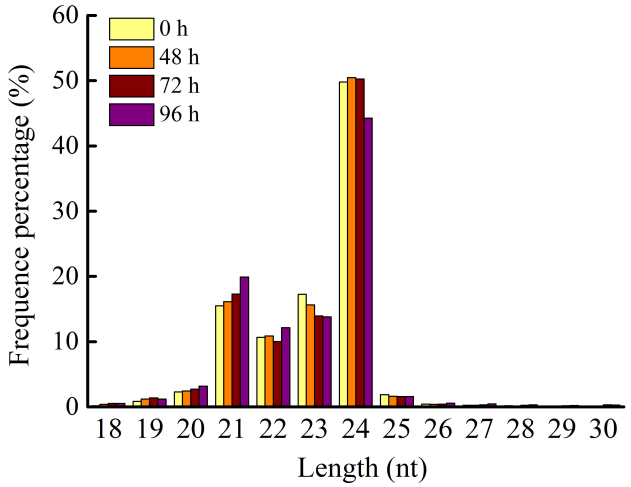

FIGURE 2 | Length distribution of sRNA in the four small RNA libraries. 0, 48, 72, and 96 h represent four time points post MC treatment.

with conserved miRNAs, the abundance of most novel miRNAs was relatively low (**Table 2**). In addition, three novel miRNA members, which belong to known miRNA families (miR390, miR3627, and miR2275), were identified in this study (**Supplementary Table 4**).

Identification of DEG miRNAs in Elongating Internode After MC Application

To identify MC-responsive miRNAs in cotton internodes, differential expression analysis of the miRNAs was performed between control (0 h) and MC treatment (48, 72, and 96 hpt). Based on the strict criteria ($|\log_2$ (fold change)$| \geq 1$, p-value ≤ 0.05, and TPM ≥ 5 in at least one sample), a total of 104 DEG miRNAs were identified (**Supplementary Table 5**). Sixty-three DEG miRNAs (61%) were highly conserved miRNAs, and 20 were cotton-specific miRNAs, which have been identified only in cotton. Compared with the control (0 h), 60 (24 upregulated and 36 downregulated), 65 (34 upregulated and 31 downregulated), and 77 (29 upregulated and 48 downregulated) DEG miRNAs were identified at 48, 72, and 96 hpt, respectively. The number of DEG miRNAs increased with time post treatment.

Generally, more downregulated miRNAs were detected than upregulated miRNAs, except at 72 hpt. All members of miR167 and miR827, and most members of miR160, miR168, miR169, miR171, miR172, and miR319 were downregulated by MC treatment (**Figure 3** and **Supplementary Table 5**). Among them, 14 miRNAs were continuously repressed by MC treatment, including miR159d, miR160 (b, e), miR166 (e, q), miR167e, miR168 (c, d), miR171m, miR319 (c, d), miR398, miR398a, and miR827b. In particular, miR168c, miR319c, and miR159d showed more than nine-fold downregulation. In contrast, 12 miRNAs were continuously induced by MC, including miR159 (h, v), miR482 (h, i, j), miR535 (b, e), miR858b, miR2948-5p, miR7122a, miR8633, and miR8634. Most of them exhibited more than a twofold upregulation. For novel DEG miRNAs, only ghr-miRn4 showed a continuous upregulation. Most DEG miRNAs were altered in response to MC at early or late post treatment time (**Figure 3** and **Supplementary Table 5**). For example, miR858a showed more than twofold downregulation at 48 and 72 hpt; miR164 members showed significant upregulation at 72 and 96 hpt, with miR164c

TABLE 2 | Expression levels of novel miRNAs identified from cotton internode in response to MC.

miRNA_id	miRNA expression (TPM)				Sequence
	0 h	48 h	72 h	96 h	
Novel miRNAs					
ghr-miRn1-5p	1.10	7.64	9.58	0.12	TTGTCCACGCGCGACACGCAC
ghr-miRn1-3p	1.55	0.99	0.63	0.96	GTGTTTCGCGCGTGGACGAC
ghr-miRn2-5p	1.26	1.64	4.43	1.16	TGTCGCAGGAGCGATGGCACTG
ghr-miRn2-3p	0.61	5.74	8.51	0.77	GTGCCATCGGCCTGCGACAAG
ghr-miRn3-5p	33.88	13.77	38.34	40.51	ACAGGTGGTGGATCAAATATGAGT
ghr-miRn3-3p	2.00	0.47	0.24	0.46	TCATATTTGTTCCACCCGCCTGTG
ghr-miRn4-5p	2.73	2.76	1.50	3.94	AGTCTCCTTCAAACGCTTCCAG
ghr-miRn4-3p	1.87	12.18	5.14	11.65	GGAAGGTTTGGAGGAGAGTGA
ghr-miRn5-5p	6.96	3.76	7.44	0.66	CAAGGCTTTGGGATACAAG
ghr-miRn5-3p	11.77	1.38	10.92	13.35	TGTATTTCAAAGCCTTGGTT
Novel conserved miRNAs					
cotton-miR3627-5p	0.29	0.78	2.53	0.42	TTGTCGCAGGAGCGATGGCACT
cotton-miR3627-3p	2.12	8.38	6.09	0.73	GTGCCTTCGGCCTGCGACAAG
cotton-miR2275-5p	0.94	0.52	1.74	0.15	TTTTTCACAAATATCACAATA
cotton-miR2275-3p	54.41	41.84	58.56	15.05	TTGTGATATTAGTGAAAAACA
cotton-miR390-5p	18.98	18.05	33.44	38.27	GAAACTCAGGATAGATAGCGC

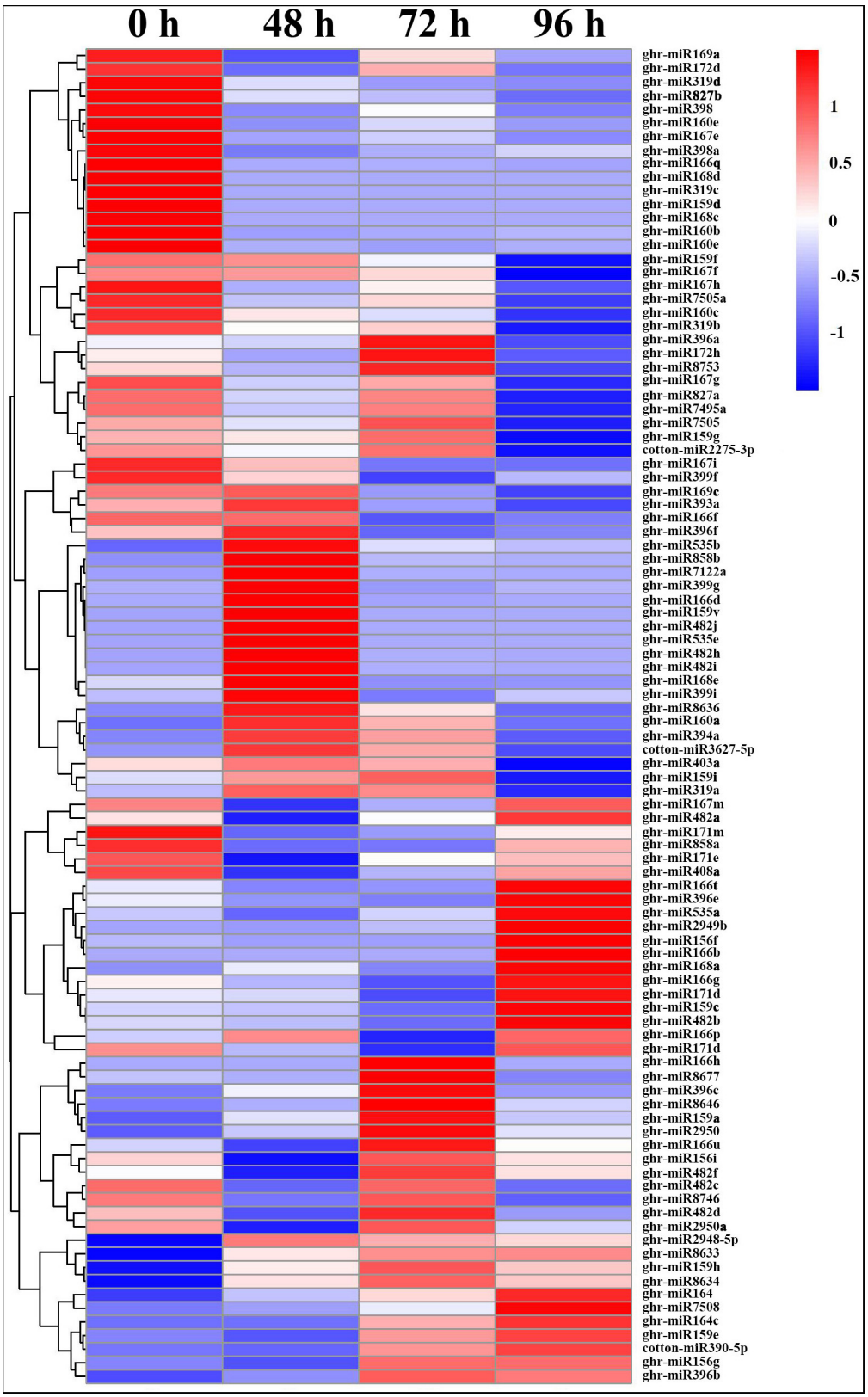

FIGURE 3 | Heat map of differentially expressed miRNAs in cotton internode between MC treatment and control. Data was presented as miRNA abundances (TPM). Blue indicates lower expression, and red indicates higher expression. 0 h: Control; 48, 72 and 96: 48, 72, and 96 h post MC treatment.

being upregulated by more than sixfold; some cotton-specific miRNAs such as miR2275, miR7495a, miR7505, miR7505a, and miR8753 were significantly downregulated only at 96 hpt. These results suggest the importance of miRNA-mediated post-transcriptional regulation in MC-induced inhibition of internode elongation.

To validate the expression patterns of DEG miRNAs obtained by sRNA-Seq, three upregulated and six downregulated miRNAs were selected for qRT-PCR. In general, the expression patterns of most DEG miRNAs obtained from qRT-PCR were in accordance with those obtained by deep sequencing (**Figure 4**), although the fold change of expression detected by qRT-PCR was not completely consistent with the sRNA-Seq results owing to the difference in sensitivity and specificity between the two techniques. The results showed that the expression profiles of miRNAs using deep sequencing were reliable for further analyses.

Target Prediction of Known and Novel miRNAs

MicroRNAs regulate many biological processes by regulating the expression of target genes. To better understand the role of miRNAs in MC-induced inhibition of internode elongation, we performed target prediction of miRNAs using the TargetFinder program (Kielbasa et al., 2010), and targets with scores less than four were considered putative cotton miRNA targets. In total, 1,638 targets for known miRNAs and 141 targets for novel miRNAs were predicted (**Supplementary Table 6**). Many targets of the conserved miRNAs were TFs, including SPL (miR156), MYB (miR159), NAC (miR164), homeobox-leucine zipper protein ATHB (miR166), nuclear transcription factor Y subunit A (miR169), TCP (miR319), and GRF (miR396). Some targets are involved in plant hormone signaling pathways. For example, auxin response factor (ARF) (miR160 and miR167),

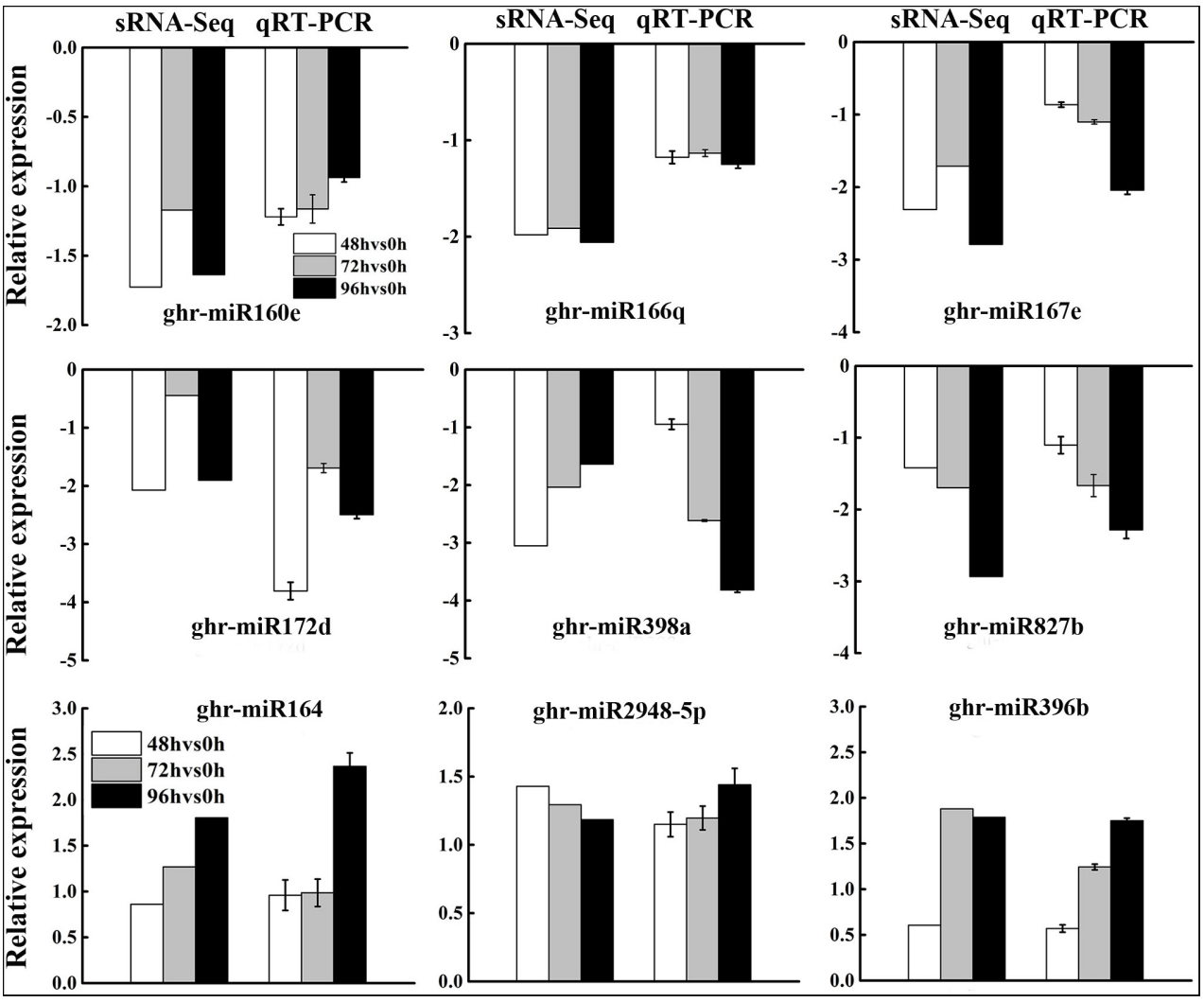

FIGURE 4 | Validation of differentially expressed miRNAs from sRNA-Seq analysis by qRT-PCR. Data from sRNA-Seq was presented as the $\log_2$ fold change values at 48, 72, and 96 h post MC treatment compared to control (0 h), while that from qRT-PCR was presented as –delt delt Ct. Each column represents mean ± SD. Error bars represent the SD of three biological and three technical replicates.

transport inhibitor response 1 (TIR1) (miR393), and auxin signaling F-box 2-like protein (miR393) are involved in the auxin signaling pathway; scarecrow-like protein (SCL) (miR171) is related to the GA signaling pathway. In addition to the previously identified conserved targets, many new targets have also been identified for known miRNAs. These novel targets include cytokinin dehydrogenase 1-like (miR159), indole-3-acetaldehyde oxidase-like (miR7505), and GA 3 oxidase 1 (miR7508), which are involved in plant hormone metabolism, indicating that these miRNAs could mediate plant hormone metabolism and signaling.

RLM-5′ RACE is a widely used technique for verifying miRNA-mediated cleavage of target genes. Thirteen predicted targets were selected to perform the RLM-5′ RACE assay, and 10 genes were confirmed as miRNA targets. Among them, four conserved targets for miR160 (Gh_D06G0360, ARF17), miR164 (Gh_D12G1761, NAC100), miR319 (Gh_D05G2713, GAMYB), and miR393 (Gh_A11G1077, TIR1) were identified (**Figure 5**). Six novel targets were validated in cotton for the first time: AGO2 (Gh_A06G1231), SPL7 (Gh_A12G0866), pentatricopeptide repeat-containing protein (PPR, Gh_D05G3392), MYB4 (Gh_A11G1005), cysteine proteinase inhibitor (CYSb, Gh_A06G1537), and putative disease resistance protein RGA1 (Gh_D03G1355), which are targeted by miR403, miR535, miR7505, miR858, miR8634, and miR8746, respectively. It is worth noting that miR8746, miR7505, and miR8634 are cotton-specific miRNAs. All 10 target genes had specific cleavage sites located in the middle of the complementary sequences between miRNAs and their target sites.

DISCUSSION

Mepiquat chloride is a widely used growth regulator for improving cotton architecture, producing compact plants by inhibiting internode elongation and reducing leaf area. Recently, we found that MC significantly altered the expression of a large number of genes related to cell cycle, cell wall structure, hormone metabolism, signal transduction, and secondary metabolism, and TFs (Wang L. et al., 2020). miRNA is a kind of important post-transcriptional regulator of gene expression. The aim of the present study was to reveal the roles of miRNAs in MC-induced growth inhibition in cotton.

In the present study, a total of 508 known miRNAs from 197 families and five novel miRNAs were identified from the elongating internode of cotton seedlings (**Supplementary Tables 3,4**). This number is much higher than that previously reported for cotton (*G. hirsutum*) stem apexes (An et al., 2015). Among the conserved miRNAs, miR159 was the most abundant in the elongating internode, followed by miR166, miR164, miR319, miR168, and miR171 (**Supplementary Table 3**). High expression of miR159, miR166, and miR171 was also found in cotton stem apexes (An et al., 2015). In addition, other miRNAs

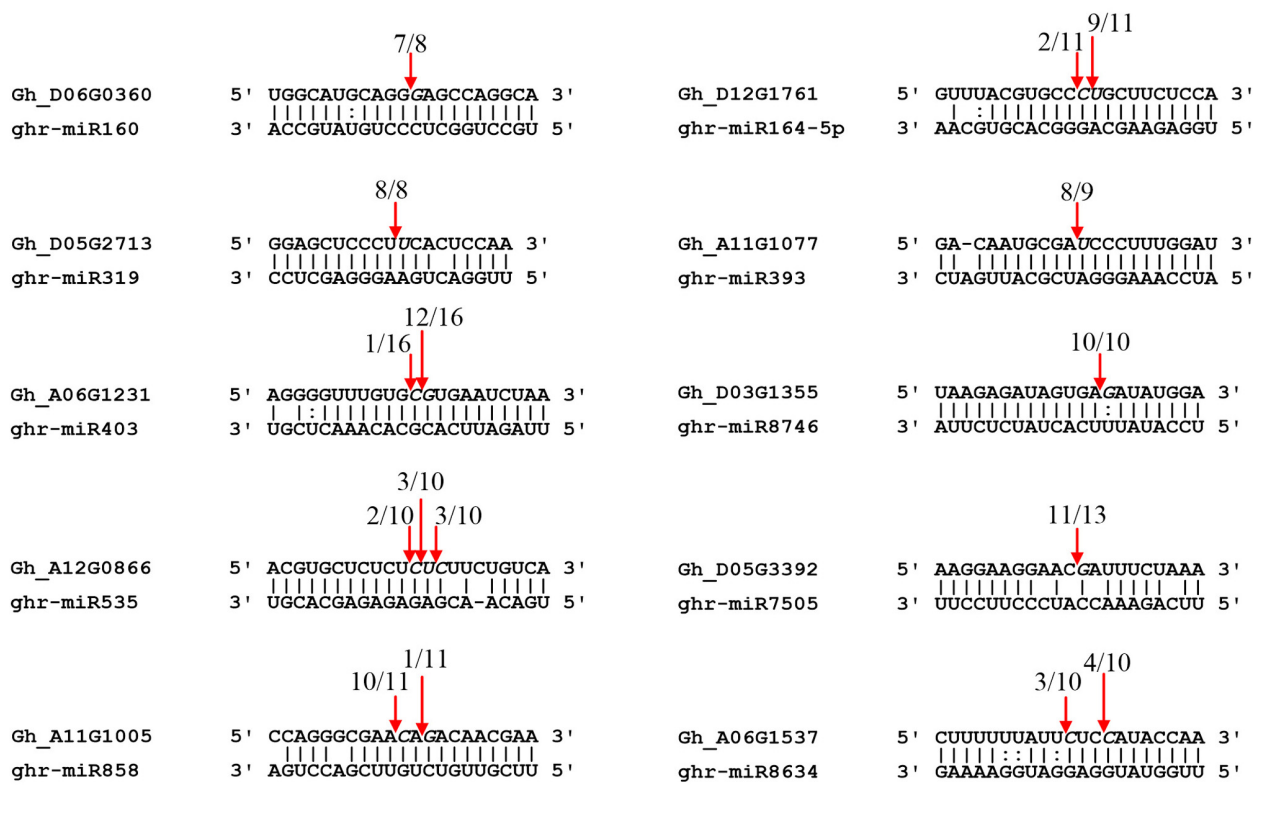

FIGURE 5 | Validation of miRNA targets by RLM-5′ RACE. Red arrows indicate the cleavage sites detected by RLM-5′ RACE.

such as miR535, miR2949, miR482, and miR2947 were also highly expressed in the elongating internode (**Supplementary Table 3**), and similar results were observed in stem apexes of cotton, except for miR2947, which was not found in the previous study (An et al., 2015). The high miRNA diversity in internodes implies that a complex mechanism is involved in cotton growth and development.

A total of 104 DEG miRNAs were found to be responsive to MC (**Figure 3** and **Supplementary Table 5**). Sixty-three DEG miRNAs (61%) were highly conserved. miRNAs regulate many biological processes through mRNA cleavage or translational repression. Identification of miRNA targets is crucial for understanding miRNA-mediated processes. In this study, 1,638 targets for known miRNAs and 141 targets for novel miRNAs were predicted based on bioinformatics analysis (**Supplementary Table 6**). Many conserved targets were TFs such as GRF, TCP, MYB, SPL, ARF, NAC domain, and SCL (**Supplementary Table 6**). Previously, we identified 497 differentially expressed TFs in response to MC (Wang L. et al., 2020); among them, 36 TFs were found to be targeted by miRNAs in this study (**Supplementary Table 6**). In addition to the known targets, many novel targets of known miRNAs and novel miRNAs were predicted (**Supplementary Table 6**). Given the false-positive rate of computationally predicted targets, experimental confirmation of these targets is necessary. Degradome sequencing provides a high-throughput strategy for the global validation of miRNA targets (Song et al., 2017). An et al. (2015) validated the interaction between miR172 and AP2; miR160 and ARF; and miR159, miR319, and miR858 and MYB based on the released cotton degradome sequencing data. In this study, we confirmed 10 miRNA target genes using RLM-5′ RACE. Among them, six genes were verified as novel targets of six miRNAs for the first time. It is worth noting that Gh_D05G3392 (PPR), Gh_A06G1537 (CYSb), and Gh_D03G1355 (RGA1) were targeted by cotton-specific miR7505b, miR8634, and miR8764, respectively (**Figure 5**). Based on the analysis of miRNA response to MC, we present a model to reveal the regulatory network between miRNAs and their targets involved in MC-induced inhibition of internode elongation (**Figure 6**).

Our previous study revealed that MC repressed both cell division and cell elongation by downregulating the expression of many genes related to cell cycle and cell wall architecture, leading to shortened internodes (Wang L. et al., 2020). Several conserved miRNAs such as miR396, miR319, and miR159 have been reported to control cell proliferation (Rodriguez et al., 2016). miR396 negatively regulates cell proliferation by targeting GRF TFs, which are usually strongly expressed in actively growing tissues (Rodriguez et al., 2016). Overexpression of miR396 in Arabidopsis and rice suppressed the expression of GRFs and cell cycle-related genes, leading to dwarfism (Rodriguez et al., 2010; Tang et al., 2018). Our result showed that the expression of three miR396 members was significantly induced by MC at 72 and 96 hpt (**Figure 3** and **Supplementary Table 5**), corroborating the result of our previous study, which revealed that 12 GRFs showed reduced expression in response to MC (Wang L. et al., 2020). High expression of miR396 was also reported in the stem apexes of cotton dwarf mutant and shoots of apple dwarf mutant (An et al., 2015; Song et al., 2017). miR396 was found to be negatively regulated by GA during cell proliferation (Lu et al., 2020). Our previous study showed that MC significantly reduced GA levels in cotton internodes (Wang L. et al., 2020). Thus, the low GA concentration caused by MC may promote the

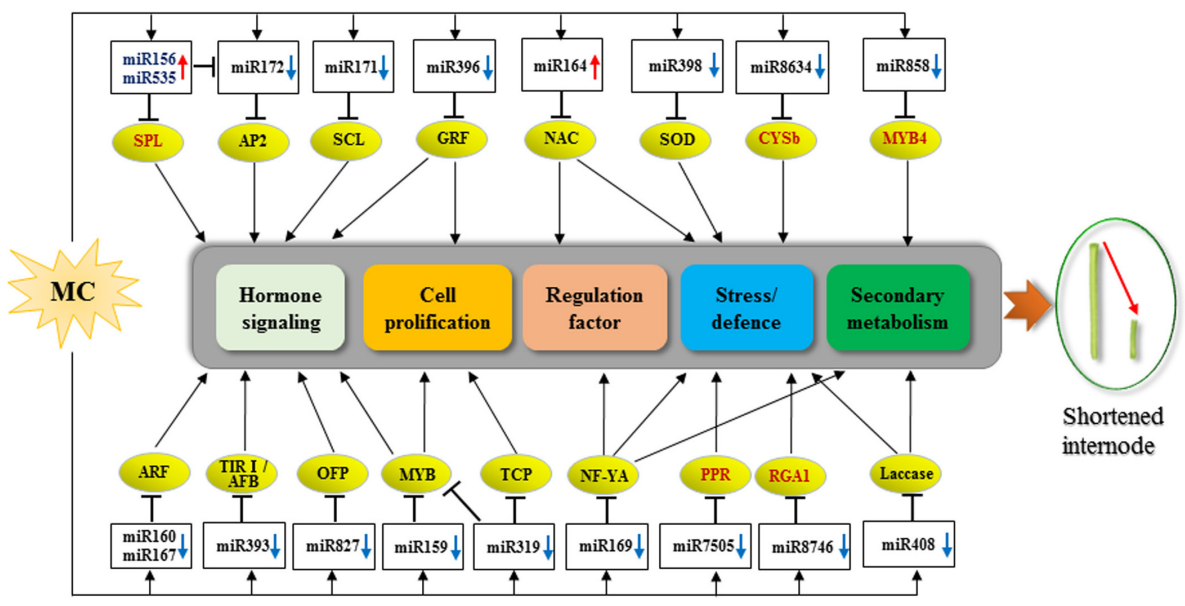

FIGURE 6 | Proposed model for the roles of miRNA-targets in MC-induced inhibition of internode elongation. Up and down arrows behind the miRNA names represent up- and down-regulation by MC, respectively. The targets in red color are novel targets validated in this study. CYSb, cysteine proteinase inhibitor; PPR, pentatricopeptide repeat-containing protein; RGA1, resistance gene analog 1.

expression of miR396, resulting in suppressed expression of GRFs and cell cycle-related genes, thus leading to inhibited internode elongation in cotton, as in rice (Lu et al., 2020).

miR319 has been demonstrated to promote cell proliferation during leaf and petal development (Nag et al., 2009; Liu et al., 2020); however, the effect of miR319 on stem elongation varies with plant species. Overexpression of sha-miR319d in tomato reduced plant height (Shi et al., 2019), whereas overexpression of osa-miR319b in switchgrass promoted stem elongation and increased plant height (Liu et al., 2020). Knockdown of miR319 using artificial miRNA target mimics (MIM) completely suppressed stem elongation in Arabidopsis (Todesco et al., 2010). In this study, all miR319 members showed significant downregulation at 96 hpt, with ghr-miR319c being downregulated by more than 10-fold (**Figure 3** and **Supplementary Table 5**). Our results suggest a positive role of miR319 in cotton internode elongation. miR159, similar in sequence to miR319, positively regulates organ size by promoting cell division (Rodriguez et al., 2016). In rice, suppressing miR159 through short tandem target mimic (STTM) resulted in short internodes and small leaves owing to the disruption of cell division, which is related to the reduced expression of genes associated with cell cycle and hormone homeostasis (Zhao et al., 2017). The Arabidopsis *mir159ab* double mutant showed a dwarf phenotype (Allen et al., 2007). The expression of four miR159 members was significantly downregulated in response to MC, and the expression of ghr-miR159d was downregulated by more than ninefold (**Figure 3** and **Supplementary Table 5**). In addition, one MYB TF DIVARICATA (DIV) (Gh_D04G0641), a target of miR159, was upregulated by MC in cotton internodes in our previous study (Wang L. et al., 2020). DIV was first reported to modulate the growth of ventral and lateral petals (Galego and Almeida, 2002). Recently, DIV has been suggested to regulate cell proliferation during stamen development in the flowers of *Plantago* (Reardon et al., 2014) and control cell expansion in the fruit pericarp of *Solanum lycopersicum* by interacting with other proteins (Machemer et al., 2011). The increased expression of DIV may contribute to the inhibition of cell division and elongation of internodes under MC treatment. These results indicate that decreased expression of miR159 members is associated with MC-induced inhibition of internode elongation, which is similar to the findings in Arabidopsis (Todesco et al., 2010) and rice (Zhao et al., 2017).

miR156 negatively regulates plant height by repressing the expression of SPLs. The dwarf phenotype has been observed in transgenic Arabidopsis, rice, maize, alfalfa, and switchgrass overexpressing miR156 (Schwab et al., 2005; Chuck et al., 2007; Fu et al., 2012; Gao et al., 2016; Dai et al., 2018). Thus, as expected, the expression of ghr-miR156f and ghr-miR156g was induced by MC in cotton internodes (**Figure 3** and **Supplementary Table 5**). miR535 shows extremely high sequence identity to miR156 sequence, and six SPLs (OsSPL4/7/11/12/16/19) were co-targeted by miR156/miR535 in rice (Liang et al., 2013; Sun et al., 2019). Overexpression of either miR535 (Sun et al., 2019) or miR156 (Xie et al., 2006) in rice shortened the internode length and thus reduced plant height by down-regulating OsSPL7. Similar to miR156, the expression of miR535 was also significantly induced by MC (**Figure 3** and **Supplementary Table 5**), suggesting their overlapping functions in inhibiting cotton internode elongation. Our previous study demonstrated that 12 SPLs, including four SPL7 TFs, which are homologous to OsSPL7, showed significant downregulation in response to MC (Wang L. et al., 2020); this correlates well with the increased levels of miR156 and miR535. Moreover, Gh_A12G0866 (GhSPL7) was confirmed to be cleaved by miR535 in cotton using the RLM-5′ RACE assay (**Figure 5**).

miR172 has been reported to act downstream of miR156 (Wu et al., 2009; Jung et al., 2011). These two miRNAs often show inverse expression patterns during plant growth and development in many plant species (Chuck et al., 2007; Wu et al., 2009; Wang et al., 2011; Bhogale et al., 2014). miR156 represses the transcription of miR172 via SPL genes in Arabidopsis, *Populus* × *canadensis*, and potato (Wu et al., 2009; Wang et al., 2011; Bhogale et al., 2014). Thus, the reduced expression of ghr-miR172d and ghr-miR172h might be ascribed to the increased expression of miR156 under MC treatment (**Figure 3** and **Supplementary Table 5**). In rice, silencing of miR172 by STTM led to severe defects in internode elongation and resulted in dwarfism (Zhang et al., 2017). Therefore, miR156 may negatively regulate internode elongation by down-regulating SPLs and miR172 in cotton under MC treatment.

miR160 mediates auxin signaling by restraining certain ARFs and further regulating plant growth (Liu et al., 2010; Zhang et al., 2017). Silencing of miR160 by STTM in Arabidopsis and rice resulted in dwarf stature (Liu et al., 2010; Zhang et al., 2017). The expression of three miR160 members was significantly downregulated by MC, and ghr-miR160b exhibited more than fourfold downregulation (**Figure 3** and **Supplementary Table 5**). GhARF18 (Gh_A13G2013), a target of miR160, was found to be significantly upregulated by MC in our previous study (Wang L. et al., 2020), which correlates well with the repression of miR160. In polyploid rapeseed, ARF18 was reported to inhibit downstream auxin genes during silique development (Liu et al., 2015). Rice transgenic plants, expressing an osa-miR160-resistant version of OsARF18, exhibited dwarf stature because of the disruption of auxin signaling (Huang et al., 2016). In addition, the transcripts of GhARF17 (Gh_D06G0360) were cleaved at the miR160 complementary site in the cotton internode (**Figure 5**). These results suggest that the miR160-ARF module plays an important role in the MC-induced inhibition of internode elongation by modifying auxin signaling.

miR164 has been shown to participate in development and stress defense in plants by targeting different NAC-domain genes, including uncharacterized CUP-SHAPED COTYLEDON (*CUC*). In rice, knocking out *OsCUC1*, a target of osa-miR164c, leads to a dwarf plant architecture (Wang J. et al., 2020). Overexpression of miR164b or downregulation of its target, OsNAC2, led to reduced plant height in rice (Jiang et al., 2018). In the present study, all miR164 members were induced by MC treatment, and ghr-miR164c was upregulated by more than sixfold at 72 and 96 hpt (**Figure 3** and **Supplementary Table 5**). Increased expression of miR164 was also found in the stem apexes of cotton dwarf mutants (An et al., 2015). In accordance with the upregulation of miR164, eight NAC TFs, including CUC2 (a target of miR164, Gh_D01G0448), CUC3, and NAC2, were

found to be downregulated by MC in cotton internodes in our previous study (Wang L. et al., 2020). In addition, GhNAC100 (Gh_D12G1761) was found to be cleaved by miR164 in cotton internodes (**Figure 5**). A recent study showed that ghr-miR164 could improve cotton plant resistance to *Verticillium dahlia* by downregulating GhNAC100 (Gh_A11G0290) (Hu et al., 2020). These results suggest that the upregulation of miR164 by MC may not only result in the inhibition of internode elongation but also improve the resistance of cotton plants to the stress caused by MC.

miR171 controls shoot development by targeting SCL6 (Wang et al., 2010b). The expression of all miR171 members was downregulated by MC (**Figure 3** and **Supplementary Table 5**), which correlates well with our previous study, which showed that two SCL6 genes (Gh_A12G0855 and Gh_D12G0935), targets of miR171, were significantly upregulated by MC (Wang L. et al., 2020). Decreased expression of miR171 was also found in the shoots of apple dwarf mutants (Song et al., 2017). Silencing of miR171 in rice caused semi-dwarf stature (Zhang et al., 2017). In contrast, overexpression of miR171 in Arabidopsis and rice or triple *scl6* mutant Arabidopsis resulted in increased plant height (Wang et al., 2010b; Fan et al., 2015). Therefore, miR171 is a positive regulator of plant height.

miR398 has been reported to function in various stress responses by repressing Cu/Zn superoxide dismutases (Sunkar et al., 2006). Little is known about the role of miR398 in plant growth and development. Recently, a positive role of miR398 in plant height has been identified based on the dwarf phenotype of STTM398 lines and increased height of miR398-overexpressing lines in rice (Zhang et al., 2017). In the present study, all miR398 members were repressed by MC (**Figure 3** and **Supplementary Table 5**), suggesting that miR398 is not only related to stress response but also might be associated with cotton internode elongation.

Besides these conserved DEG miRNAs, miR827, and miR858 were also strongly responsive to MC (**Figure 3** and **Supplementary Table 5**). Previous studies have reported the roles of miR827 in stress response and anther and fruit development (Liu et al., 2015; Nie et al., 2018; Fileccia et al., 2019). In this study, two miR827 members were significantly downregulated in response to MC (**Figure 3** and **Supplementary Table 5**), and miR827 was predicted to target the transcription repressor OVATE family protein (OFP1, Gh_D10G1150) (**Supplementary Table 6**). Overexpression of OFPs in Arabidopsis, rice, and tomato has been reported to inhibit cell elongation and reduce plant height by suppressing GA biosynthesis (Wang et al., 2007; Schmitz et al., 2015; Zhou et al., 2019). Thus, we speculate that the suppressed expression of miR827 by MC may lead to the accumulation of OFP1 and further reduce GA content, resulting in the inhibition of internode elongation. miR858 has been reported to negatively regulate flavonoid biosynthesis by targeting different MYBs in different plant species (Jia et al., 2015; Sharma et al., 2016; Li et al., 2020). In Arabidopsis, miR858a positively regulates plant growth and lignin biosynthesis (Sharma et al., 2016). Overexpression of miR858a promoted vegetative growth; however, its knockdown using MIM reduced vegetative growth and the expression of lignin biosynthetic genes (Sharma et al., 2016). In this study, the expression of ghr-miR858a was downregulated by more than twofold by MC at 48 and 72 hpt (**Figure 3** and **Supplementary Table 5**). Using the RLM-5′ RACE assay, MYB4 (Gh_A11G1005) was confirmed as a bona fide target of miR858 (**Figure 5**). Reduced expression of genes related to lignin biosynthesis was observed upon MC application in our previous study (Wang L. et al., 2020). Therefore, similar to miR858a in Arabidopsis, ghr-miR858a may be a positive regulator of internode elongation in cotton.

Several cotton-specific miRNAs, such as miR2948, miR7505, miR8633, miR8634, and miR8746, also showed altered expression in response to MC. A few of them have been reported to be related to stress response, anther development, or fiber development in cotton (Xie et al., 2015b; Peng et al., 2018; Zhang et al., 2018). Previously, we found that MC regulated the transcription levels of other hormone-related genes in a GA-dependent manner (Wang L. et al., 2020). Further studies are required to investigate whether these MC-responsive miRNAs are related to the reduced endogenous GA levels in cotton internodes.

In summary, a total of 508 known miRNAs belonging to 197 families and five novel miRNAs were identified from the elongating internode of cotton seedlings. Furthermore, 104 DEG miRNAs were identified as MC-responsive miRNAs. Most of the DEG miRNAs (61%) were highly conserved miRNAs. The expression of 14 known miRNAs was continuously suppressed, whereas 12 known miRNAs and one novel miRNA were continuously induced post MC treatment. Moreover, six novel target genes were verified using RLM-5′ RACE. This study deepens our understanding of the miRNA-mediated regulation network in cotton internode elongation and MC-mediated growth inhibition and could provide guidance for breeding new cotton varieties with better plant architecture. Future studies should focus on the detailed mechanisms of how these miRNAs are involved in the MC-mediated inhibition of internode elongation.

DATA AVAILABILITY STATEMENT

The datasets presented in this study can be found in online repositories. The names of the repository/repositories and accession number(s) can be found below: https://www.ncbi.nlm.nih.gov/, PRJNA647661.

AUTHOR CONTRIBUTIONS

Y-FL and LW conceived the idea and supervised the research. LW, YY, and XJ grew cotton seedlings and performed MC treatment, samples collection and RNA extractions. LW, YY, XJ, JY, and ZQ analyzed the sRNA library data sets. YY, XJ, MW, and MZ performed qRT-PCR analyses and miRNA target validation. LW and Y-FL wrote the manuscript. All authors read and approved the final manuscript.

FUNDING

This work was supported by the National Natural Science Foundation of China (Grant Nos. 31601241 and 3177 1703).

SUPPLEMENTARY MATERIAL

The Supplementary Material for this article can be found online at: https://www.frontiersin.org/articles/10.3389/fpls.2021.643213/full#supplementary-material

REFERENCES

Addoquaye, C., Miller, W., and Axtell, M. J. (2009). CleaveLand: a pipeline for using degradome data to find cleaved small RNA targets. *Bioinformatics* 25, 130–131. doi: 10.1093/bioinformatics/btn604

Allen, R. S., Li, J., Stahle, M. I., Dubroue, A., Gubler, F., and Millar, A. A. (2007). Genetic analysis reveals functional redundancy and the major target genes of the *Arabidopsis* miR159 family. *Proc. Natl. Acad. Sci. U.S.A.* 104, 16371–16376. doi: 10.1073/pnas.0707653104

Alonso-Peral, M. M., Li, J., Li, Y., Allen, R. S., Schnippenkoetter, W., Ohms, S., et al. (2010). The microRNA159-regulated GAMYB-like genes inhibit growth and promote programmed cell death in *Arabidopsis*. *Plant Physiol.* 154, 757–771. doi: 10.1104/pp.110.160630

An, W., Gong, W., He, S., Pan, Z., Sun, J., and Du, X. (2015). MicroRNA and mRNA expression profiling analysis revealed the regulation of plant height in *Gossypium hirsutum*. *BMC Genomics* 16:886. doi: 10.1186/s12864-015-2071-6

Axtell, M. J., and Meyers, B. C. (2018). Revisiting criteria for plant microRNA annotation in the era of big data. *Plant Cell* 30, 272–284. doi: 10.1105/tpc.17.00851

Bhogale, S., Mahajan, A. S., Natarajan, B., Rajabhoj, M., Thulasiram, H. V., and Banerjee, A. K. (2014). MicroRNA156: a potential graft-transmissible microRNA that modulates plant architecture and tuberization in *Solanum tuberosum* ssp *Andigena*. *Plant Physiol.* 164, 1011–1027. doi: 10.1104/pp.113.230714

Chuck, G., Cigan, A. M., Saeteurn, K., and Hake, S. (2007). The heterochronic maize mutant Corngrass1 results from overexpression of a tandem microRNA. *Nat. Genet.* 39, 544–549. doi: 10.1038/ng2001

Curaba, J., Talbot, M., Li, Z., and Helliwell, C. (2013). Over-expression of microRNA171 affects phase transitions and floral meristem determinancy in barley. *BMC Plant Biol.* 13:6. doi: 10.1186/1471-2229-13-6

Dai, Z., Wang, J., Yang, X., Lu, H., Miao, X., and Shi, Z. (2018). Modulation of plant architecture by the miR156f–OsSPL7–OsGH3.8 pathway in rice. *J. Exp. Bot.* 69, 5117–5130. doi: 10.1093/jxb/ery273

Fan, T., Li, X., Yang, W., Xia, K., Ouyang, J., and Zhang, M. (2015). Rice osa-miR171c mediates phase change from vegetative to reproductive development and shoot apical meristem maintenance by repressing four OsHAM transcription factors. *PLoS One* 10:e0125833. doi: 10.1371/journal.pone.0125833

Fileccia, V., Ingraffia, R., Amato, G., Giambalvo, D., and Martinelli, F. (2019). Identification of microRNAS differentially regulated by water deficit in relation to mycorrhizal treatment in wheat. *Mol. Biol. Rep.* 46, 5163–5174. doi: 10.1007/s11033-019-04974-6

Friedländer, M. R., Mackowiak, S. D., Li, N., Chen, W., and Rajewsky, N. (2012). miRDeep2 accurately identifies known and hundreds of novel microRNA genes in seven animal clades. *Nucleic Acids Res.* 40, 37–52. doi: 10.1093/nar/gkr688

Fu, C., Sunkar, R., Zhou, C., Shen, H., Zhang, J., Matts, J., et al. (2012). Overexpression of miR156 in switchgrass (*Panicum virgatum* L.) results in various morphological alterations and leads to improved biomass production. *Plant Biotechnol. J.* 10, 443–452. doi: 10.1111/j.1467-7652.2011.00677.x

Galego, L., and Almeida, J. (2002). Role of DIVARICATA in the control of dorsoventral asymmetry in *Antirrhinum* flowers. *Genes Dev.* 16, 880–891. doi: 10.1101/gad.221002

Gao, F., Wang, K., Liu, Y., Chen, Y., Chen, P., Shi, Z., et al. (2015). Blocking miR396 increases rice yield by shaping inflorescence architecture. *Nat. Plants* 2:15196. doi: 10.1038/Nplants.2015.196

Gao, R., Austin, R. S., Amyot, L., and Hannoufa, A. (2016). Comparative transcriptome investigation of global gene expression changes caused by miR156 overexpression in *Medicago sativa*. *BMC Genomics* 17:658. doi: 10.1186/s12864-016-3014-6

Gwathmey, C. O., and Clement, J. D. (2010). Alteration of cotton source-sink relations with plant population density and mepiquat chloride. *Field Crops Res.* 116, 101–107. doi: 10.1016/j.fcr.2009.11.019

Hu, G., Lei, Y., Liu, J., Hao, M., Zhang, Z., Tang, Y., et al. (2020). The ghr-miR164 and GhNAC100 modulate cotton plant resistance against *Verticillium dahlia*. *Plant Sci.* 293, 110438. doi: 10.1016/j.plantsci.2020.110438

Huang, J., Li, Z. Y., and Zhao, D. Z. (2016). Deregulation of the OsmiR160 target gene OsARF18 causes growth and developmental defects with an alteration of auxin signaling in rice. *Sci. Rep.* 6:29938. doi: 10.1038/Srep29938

Jia, X., Shen, J., Liu, H., Li, F., Ding, N., Gao, C., et al. (2015). Small tandem target mimic-mediated blockage of microRNA858 induces anthocyanin accumulation in tomato. *Planta* 242, 283–293. doi: 10.1007/s00425-015-2305-5

Jiang, D., Chen, W., Dong, J., Li, J., Yang, F., Wu, Z., et al. (2018). Overexpression of miR164b-resistant OsNAC2 improves plant architecture and grain yield in rice. *J. Exp. Bot.* 69, 1533–1543. doi: 10.1093/jxb/ery017

Jung, J. H., Seo, P. J., Kang, S. K., and Park, C. M. (2011). miR172 signals are incorporated into the miR156 signaling pathway at the SPL3/4/5 genes in *Arabidopsis* developmental transitions. *Plant Mol. Biol.* 76, 35–45. doi: 10.1007/s11103-011-9759-z

Kielbasa, S. M., Bluthgen, N., Fahling, M., and Mrowka, R. (2010). Targetfinder.org: a resource for systematic discovery of transcription factor target genes. *Nucleic Acids Res.* 38, W233–W238. doi: 10.1093/nar/gkq374

Li, Y., Cui, W., Qi, X., Lin, M., Qiao, C., Zhong, Y., et al. (2020). MicroRNA858 negatively regulates anthocyanin biosynthesis by repressing AaMYBC1 expression in kiwifruit (*Actinidia arguta*). *Plant Sci.* 296:110476. doi: 10.1016/j.plantsci.2020.110476

Li, Y., Wei, K., Wang, M., Wang, L., Cui, J., Zhang, D., et al. (2019). Identification and temporal expression analysis of conserved and novel microRNAs in the leaves of winter wheat grown in the field. *Front. Genet.* 10:779. doi: 10.3389/fgene.2019.00779

Li, Y.-F., Zheng, Y., Addo-Quaye, C., Zhang, L., Saini, A., Jagadeeswaran, G., et al. (2010). Transcriptome-wide identification of microRNA targets in rice. *Plant J.* 62, 742–759. doi: 10.1111/j.1365-313X.2010.04187.x

Liang, G., Li, Y., He, H., Wang, F., and Yu, D. (2013). Identification of miRNAs and miRNA-mediated regulatory pathways in *Carica papaya*. *Planta* 238, 739–752. doi: 10.1007/s00425-013-1929-6

Liu, J., Hua, W., Hu, Z., Yang, H., Zhang, L., Li, R., et al. (2015). Natural variation in ARF18 gene simultaneously affects seed weight and silique length in polyploid rapeseed. *Proc. Natl. Acad. Sci. U.S.A.* 112, E5123–E5132. doi: 10.1073/pnas.1502160112

Liu, W., Chen, P., Chen, L., Yang, C., Chen, S., Huang, G., et al. (2017). Suppressive effect of microRNA319 expression on rice plant height. *Theor. Appl. Genet.* 130, 1507–1518. doi: 10.1007/s00122-017-2905-5

Liu, X., Huang, J., Wang, Y., Khanna, K., Xie, Z., Owen, H. A., et al. (2010). The role of floral organs in carpels, an *Arabidopsis* loss-of-function mutation in MicroRNA160a, in organogenesis and the mechanism regulating its expression. *Plant J.* 62, 416–428. doi: 10.1111/j.1365-313X.2010.04164.x

Liu, Y., Yan, J., Wang, K., Li, D., Han, Y., and Zhang, W. (2020). Heteroexpression of Osa-miR319b improved switchgrass biomass yield and feedstock quality by repression of PvPCF5. *Biotechnol. Biofuels* 13:56. doi: 10.1186/S13068-020-01693-0

Livak, K. J., and Schmittgen, T. D. (2001). Analysis of relative gene expression data using real-time quantitative PCR and the 2(-Delta Delta C(T)) Method. *Methods* 25, 402–408. doi: 10.1006/meth.2001.1262

Lu, Y., Feng, Z., Meng, Y., Bian, L., Xie, H., Mysore, K. S., et al. (2020). SLENDER RICE1 and *Oryza sativa* INDETERMINATE DOMAIN2 regulating OsmiR396 are involved in stem elongation. *Plant Physiol.* 182, 2213–2227. doi: 10.1104/pp.19.01008

Machemer, K., Shaiman, O., Salts, Y., Shabtai, S., Sobolev, I., Belausov, E., et al. (2011). Interplay of MYB factors in differential cell expansion, and

consequences for tomato fruit development. *Plant J.* 68, 337–350. doi: 10.1111/j.1365-313X.2011.04690.x

Nag, A., King, S., and Jack, T. (2009). miR319a targeting of TCP4 is critical for petal growth and development in *Arabidopsis*. *Proc. Natl. Acad. Sci. U.S.A.* 106, 22534–22539. doi: 10.1073/pnas.0908718106

Nie, H., Wang, Y., Su, Y., and Hua, J. (2018). Exploration of miRNAs and target genes of cytoplasmic male sterility line in cotton during flower bud development. *Funct. Integr. Genomics* 18, 457–476. doi: 10.1007/s10142-018-0606-z

Peng, Z., He, S. P., Gong, W. F., Xu, F. F., Pan, Z. E., Jia, Y. H., et al. (2018). Integration of proteomic and transcriptomic profiles reveals multiple levels of genetic regulation of salt tolerance in cotton. *BMC Plant Biol.* 18:128. doi: 10.1186/s12870-018-1350-1

Rademacher, W. (2000). GROWTH RETARDANTS: effects on gibberellin biosynthesis and other metabolic pathways. *Annu. Rev. Plant Physiol. Plant Mol. Biol.* 51, 501–531. doi: 10.1146/annurev.arplant.51.1.501

Reardon, W., Gallagher, P., Nolan, K. M., Wright, H., Cardenosa-Rubio, M. C., Bragalini, C., et al. (2014). Different outcomes for the MYB floral symmetry genes DIVARICATA and RADIALIS during the evolution of derived actinomorphy in Plantago. *New Phytol.* 202, 716–725. doi: 10.1111/nph.12682

Reddy, V. R., Baker, D. N., and Hodges, H. F. (1990). Temperature and mepiquat chloride effects on cotton canopy architecture. *Agron. J.* 82, 190–195. doi: 10.2134/agronj1990.00021962008200020004x

Ren, X., Zhang, L., Du, M., Evers, J. B., Der Werf, W. V., Tian, X., et al. (2013). Managing mepiquat chloride and plant density for optimal yield and quality of cotton. *Field Crops Res.* 149, 1–10. doi: 10.1016/j.fcr.2013.04.014

Rodriguez, R. E., Mecchia, M. A., Debernardi, J. M., Schommer, C., Weigel, D., and Palatnik, J. F. (2010). Control of cell proliferation in *Arabidopsis thaliana* by microRNA miR396. *Development* 137, 103–112. doi: 10.1242/dev.043067

Rodriguez, R. E., Schommer, C., and Palatnik, J. F. (2016). Control of cell proliferation by microRNAs in plants. *Curr. Opin. Plant Biol.* 34, 68–76. doi: 10.1016/j.pbi.2016.10.003

Schmitz, A. J., Begcy, K., Sarath, G., and Walia, H. (2015). Rice ovate family protein 2 (OFP2) alters hormonal homeostasis and vasculature development. *Plant Sci.* 241, 177–188. doi: 10.1016/j.plantsci.2015.10.011

Schwab, R., Palatnik, J. F., Riester, M., Schommer, C., Schmid, M., and Weigel, D. (2005). Specific effects of microRNAs on the plant transcriptome. *Dev. Cell* 8, 517–527. doi: 10.1016/j.devcel.2005.01.018

Sharma, D., Tiwari, M., Pandey, A., Bhatia, C., Sharma, A., and Trivedi, P. K. (2016). MicroRNA858 is a potential regulator of phenylpropanoid pathway and plant development. *Plant Physiol.* 171, 944–959. doi: 10.1104/pp.15.01831

Shechter, I., and West, C. A. (1969). Biosynthesis of gibberellins. IV. Biosynthesis of cyclic diterpenes from trans-geranylgeranyl pyrophosphate. *J. Biol. Chem.* 244, 3200–3209.

Shi, X., Jiang, F., Wen, J., and Wu, Z. (2019). Overexpression of *Solanum habrochaites* microRNA319d (sha-miR319d) confers chilling and heat stress tolerance in tomato (*S. lycopersicum*). *BMC Plant Biol.* 19:214. doi: 10.1186/s12870-019-1823-x

Shweta, Y., Akhter, and Khan, J. A. (2018). Genome wide identification of cotton (*Gossypium hirsutum*)-encoded microRNA targets against cotton leaf curl Burewala virus. *Gene* 638, 60–65. doi: 10.1016/j.gene.2017.09.061

Siebert, J. D., and Stewart, A. M. (2006). Influence of plant density on cotton response to mepiquat chloride application. *Agron. J.* 98, 1634–1639. doi: 10.2134/agronj2006.0083

Song, C., Zhang, D., Zheng, L., Zhang, J., Zhang, B., Luo, W., et al. (2017). miRNA and degradome sequencing reveal miRNA and their target genes that may mediate shoot growth in spur type mutant "Yanfu 6". *Front. Plant Sci.* 8:441. doi: 10.3389/fpls.2017.00441

Sun, M., Shen, Y., Li, H., Yang, J., Cai, X., Zheng, G., et al. (2019). The multiple roles of OsmiR535 in modulating plant height, panicle branching and grain shape. *Plant Sci.* 283, 60–69. doi: 10.1016/j.plantsci.2019.02.002

Sunkar, R., Kapoor, A., and Zhu, J. K. (2006). Posttranscriptional induction of two Cu/Zn superoxide dismutase genes in *Arabidopsis* is mediated by downregulation of miR398 and important for oxidative stress tolerance. *Plant Cell* 18, 2051–2065. doi: 10.1105/tpc.106.041673

Tang, Y., Liu, H., Guo, S., Wang, B., Li, Z., Chong, K., et al. (2018). OsmiR396d affects gibberellin and brassinosteroid signaling to regulate plant architecture in rice. *Plant Physiol.* 176, 946–959. doi: 10.1104/pp.17.00964

Todesco, M., Rubiosomoza, I., Pazares, J., and Weigel, D. (2010). A collection of target mimics for comprehensive analysis of microRNA function in *Arabidopsis thaliana*. *PLoS Genet.* 6:e1001031. doi: 10.1371/journal.pgen.1001031

Wang, J., Bao, J., Zhou, B., Li, M., Li, X., and Jin, J. (2020). The osa-miR164 target OsCUC1 functions redundantly with OsCUC3 in controlling rice meristem/organ boundary specification. *New Phytol.* 229, 1566–1581. doi: 10.1111/nph.16939

Wang, J. W., Park, M. Y., Wang, L. J., Koo, Y., Chen, X. Y., Weigel, D., et al. (2011). miRNA control of vegetative phase change in trees. *PLoS Genet.* 7:e1002012. doi: 10.1371/journal.pgen.1002012

Wang, L., Feng, Z., Wang, X., Wang, X., and Zhang, X. (2010a). DEGseq: an R package for identifying differentially expressed genes from RNA-seq data. *Bioinformatics* 26, 136–138. doi: 10.1093/bioinformatics/btp612

Wang, L., Mai, Y., Zhang, Y., Luo, Q., and Yang, H. (2010b). MicroRNA171c-Targeted SCL6-II, SCL6-III, and SCL6-IV genes regulate shoot branching in *Arabidopsis*. *Mol. Plant* 3, 794–806. doi: 10.1093/mp/ssq042

Wang, L., Yin, Y., Wang, L. F., Wang, M., Zhao, M., Tian, Y., et al. (2020). Transcriptome profiling of the elongating internode of cotton (*Gossypium hirsutum* L.) seedlings in response to mepiquat chloride. *Front Plant Sci.* 10:1751. doi: 10.3389/Fpls.2019.01751

Wang, L., Zhao, J., Zhang, M., Li, W., Luo, K., Lu, Z., et al. (2015). Identification and characterization of microRNA expression in *Ginkgo biloba* L. leaves. *Tree Genet. Genomes* 11:76. doi: 10.1007/s11295-015-0897-3

Wang, S., Chang, Y., Guo, J., and Chen, J. G. (2007). *Arabidopsis* Ovate family protein 1 is a transcriptional repressor that suppresses cell elongation. *Plant J.* 50, 858–872. doi: 10.1111/j.1365-313X.2007.03096.x

Wu, G., Park, M. Y., Conway, S. R., Wang, J. W., Weigel, D., and Poethig, R. S. (2009). The sequential action of miR156 and miR172 regulates developmental timing in *Arabidopsis*. *Cell* 138, 750–759. doi: 10.1016/j.cell.2009.06.031

Xie, F., Wang, Q., Sun, R., and Zhang, B. (2015a). Deep sequencing reveals important roles of microRNAs in response to drought and salinity stress in cotton. *J. Exp. Bot.* 66, 789–804. doi: 10.1093/jxb/eru437

Xie, F., Jones, D. C., Wang, Q. L., Sun, R. R., and Zhang, B. H. (2015b). Small RNA sequencing identifies miRNA roles in ovule and fibre development. *Plant Biotechnol. J.* 13, 355–369. doi: 10.1111/pbi.12296

Xie, K., Wu, C., and Xiong, L. (2006). Genomic organization, differential expression, and interaction of SQUAMOSA promoter-binding-like transcription factors and microRNA156 in rice. *Plant Physiol.* 142, 280–293. doi: 10.1104/pp.106.084475

Yang, X., Wang, L., Yuan, D., Lindsey, K., and Zhang, X. (2013). Small RNA and degradome sequencing reveal complex miRNA regulation during cotton somatic embryogenesis. *J. Exp. Bot.* 64, 1521–1536. doi: 10.1093/jxb/ert013

Yuan, S., Zhao, J., Li, Z., Hu, Q., Yuan, N., Zhou, M., et al. (2019). MicroRNA396-mediated alteration in plant development and salinity stress response in creeping bentgrass. *Hortic. Res.* 6:48. doi: 10.1038/s41438-019-0130-x

Zhang, B., Zhang, X., Liu, G., Guo, L., Qi, T., Zhang, M., et al. (2018). A combined small RNA and transcriptome sequencing analysis reveal regulatory roles of miRNAs during anther development of Upland cotton carrying cytoplasmic male sterile *Gossypium harknessii* (D2) cytoplasm. *BMC Plant Biol.* 18:242. doi: 10.1186/s12870-018-1446-7

Zhang, H., Zhang, J., Yan, J., Gou, F., Mao, Y., Tang, G., et al. (2017). Short tandem target mimic rice lines uncover functions of miRNAs in regulating important agronomic traits. *Proc. Natl. Acad. Sci. U.S.A.* 114, 5277–5282. doi: 10.1073/pnas.1703752114

Zhang, T. Z., Hu, Y., Jiang, W. K., Fang, L., Guan, X. Y., Chen, J. D., et al. (2015). Sequencing of allotetraploid cotton (*Gossypium hirsutum* L. acc. TM-1) provides a resource for fiber improvement. *Nat. Biotechnol.* 33, 531–537. doi: 10.1038/nbt.3207

Zhao, C., Li, T., Zhao, Y., Zhang, B., and Wang, X. (2020). Integrated small RNA and mRNA expression profiles reveal miRNAs and their target genes in response to *Aspergillus flavus* growth in peanut seeds. *BMC Plant Biol.* 20:215. doi: 10.1186/s12870-020-02426-z

Zhao, D., and Oosterhuis, D. M. (2000). Pix plus and mepiquat chloride effects on physiology, growth, and yield of field-grown cotton. *J. Plant Growth Regul.* 19, 415–422. doi: 10.1007/s003440000018

Zhao, T., Xu, X., Wang, M., Li, C., Li, C., Zhao, R., et al. (2019). Identification and profiling of upland cotton microRNAs at fiber initiation stage under exogenous IAA application. *BMC Genomics* 20:421. doi: 10.1186/s12864-019-5760-8

Zhao, Y., Wen, H., Teotia, S., Du, Y., Zhang, J., Li, J., et al. (2017). Suppression of microRNA159 impacts multiple agronomic traits in rice (*Oryza sativa* L.). *BMC Plant Biol.* 17:215. doi: 10.1186/s12870-017-1171-7

Zhou, S. G., Hu, Z. L., Li, F. F., Tian, S. B., Zhu, Z. G., Li, A. Z., et al. (2019). Overexpression of SlOFP20 affects floral organ and pollen development. *Hortic Res.* 6:125. doi: 10.1038/S41438-019-0207-6

Zuker, M. (2003). Mfold web server for nucleic acid folding and hybridization prediction. *Nucleic Acids Res.* 31, 3406–3415. doi: 10.1093/nar/gkg595

Conflict of Interest: The authors declare that the research was conducted in the absence of any commercial or financial relationships that could be construed as a potential conflict of interest.

frontiers in Plant Science

ORIGINAL RESEARCH
published: 12 April 2021
doi: 10.3389/fpls.2021.650836

Nectar Guide Patterns on Developmentally Homologous Regions of the Subtribe Ligeriinae (Gesneriaceae)

*Hao-Chun Hsu and Yan-Fu Kuo**

Department of Biomechatronics Engineering, National Taiwan University, Taipei City, Taiwan

Homology is a crucial concept that should be considered while conducting a comparative analysis between organisms. In particular, in the subtribe Ligeriinae, the nectar guide pattern is associated with high diversity in petal shapes and sizes. This largely limits researchers to exclusively examining the interspecific variation in nectar guide patterns on the developmentally homologous region. Thus, to solve this problem, we proposed an approach for defining a homologous region of interest (ROI) that aligns the petal image between specimens based on petal contours and vasculatures. We identified petal contours and vasculatures from the fresh petal image and its histological image through image processing. The homologous ROI was subsequently obtained by applying geometric transformation to the contour and vasculature. The qualification and quantification of nectar guide patterns were subsequently performed based on the homologous ROI. Four patterning modes, namely vascular, random, distal, and proximal, were defined for the qualitative analysis of nectar guide patterns. In the quantitative analysis, principal component (PC) analysis was applied to homologous ROIs, and the PC score of each specimen served as the trait values of nectar guide patterns. The results of the two analyses coincided, and both showed significant associations between nectar guide patterns and pollination types. The proximal mode (corresponding to PC1) and distal mode (corresponding to PC2) together showed the strongest association with pollination types. Species exhibiting the hummingbird and bee pollination types tended to recruit the distal and proximal modes, respectively. Our study conducted a comparative analysis of nectar guide patterns on the developmentally homologous region and provided a comprehensive view of the variation in the nectar guide patterns of Ligeriinae.

Keywords: image processing, geometric transformation, Gesneriaceae, Ligeriinae, nectar guide pattern, petal vasculature, region of interest, homologous region

OPEN ACCESS

Edited by:
Dianella G. Howarth,
St. John's University, United States

Reviewed by:
Citerne Helene,
UMR 8120 Génétique Quantitative et Evolution Le Moulon, France
Miho Stephanie Kitazawa,
Osaka University, Japan

***Correspondence:**
Yan-Fu Kuo
ykuo@ntu.edu.tw

Specialty section:
This article was submitted to Plant Development and EvoDevo, a section of the journal Frontiers in Plant Science

Received: *08 January 2021*
Accepted: *22 March 2021*
Published: *12 April 2021*

Citation:
Hsu H-C and Kuo Y-F (2021) Nectar Guide Patterns on Developmentally Homologous Regions of the Subtribe Ligeriinae (Gesneriaceae). Front. Plant Sci. 12:650836. doi: 10.3389/fpls.2021.650836

INTRODUCTION

Nectar guide patterns, which are observed as contrasting pigmentation on flower petals, have attracted biologists' interest for centuries. The diversity of these patterns is considered a key morphological characteristic that facilitates the plant–pollinator interaction and angiosperm diversification (Penny, 1983; Endress, 1996; van der Kooi et al., 2019). Several studies have

examined variations in nectar guide patterns (Yoshioka et al., 2004; Lootens et al., 2007; Hsu et al., 2018; Hung et al., 2020). In addition to these nectar guide patterns, petal shape and size exhibit considerable diversity. In particular, shape differences lead to misunderstanding of the distribution of pigmented areas and overestimation of variation in nectar guide patterns. To prevent this problem, considering the developmentally homologous region of petals is essential. This study proposed an approach that considers the developmentally homologous region of petals to examine the variation in nectar guide patterns.

Petal vasculature is an ideal object for considering the developmentally homologous regions of petals. The petal, the second whorl of a flower, is considered a homologous structure across most core eudicots (Endress, 1996; Ronse De Craene, 2008). Moreover, the petal recruits many fundamental genetic bases of lateral organ development, including vascular differentiation (Walcher-Chevillet and Kramer, 2016; Basile et al., 2017). In some taxa, the vasculature is a frequently used characteristic for examining the variation in petals (Gómez and Perfectti, 2010; Wang et al., 2020). These studies have acquired spatial information not only from contours but also from the vasculature. For petals with different shapes, the vasculature, together with lobe contours, can serve as the anchor to study the distribution of pigmented areas based on the developmentally homologous region.

The inclusion of developmental homologous region in the definition of a region of interest (ROI) may facilitate the examination of nectar guide patterns in different petal shapes. In image processing analysis, defining the ROI is a frequently used approach to specify the study object in an image. Many studies have applied ROI to quantify petal color patterns among species or varieties (Yoshioka et al., 2004; Lootens et al., 2007; Hsu et al., 2018; Hung et al., 2020). Although these studies have successfully evaluated the variation in nectar guide patterns, ROIs obtained from different petal shapes may not be homologous. For example, Hung et al. (2020) defined an ROI on the basis of mechanical traits such as petal widths and lengths. In other words, the position of ROIs fluctuates between species, and even between specimens, in different petal shapes. Whibley et al. (2006) used a consistent corolla shape obtained through geometric transformation to analyze interspecific variations in flower colors. Therefore, the developmentally homologous region of the nectar guide patterns in different petal shapes can be considered. In this study, we propose a homologous ROI that aligns the contour and vasculature of different petal shapes to analyze nectar guide patterns.

The subtribe Ligeriinae is an ideal system for implementing the image-based approach to examine nectar guide patterns. The subtribe Ligeriinae was recognized as a monophyletic group in the family Gesneriaceae, and composed of the species from three genera, *Sinningia*, *Vanhouttea*, and *Paliavana*. A study reported considerable variations in corolla shapes and nectar guide patterns and the pollination types of most species in the subtribe Ligeriinae (Perret et al., 2007). The developmental anatomy of flowers is consistent throughout the subtribe. The wild varieties of all species have a zygomorphic corolla with two dorsal, two lateral, and one ventral petal (top right of **Figure 1**). The vasculature of each petal contains one middle vein and two side veins (Wang et al., 2020). In addition, the ventral petal has a showy nectar guide pattern with color gradients, dotted stripes, and spot clusters (**Figure 1**). Because the ventral petal serves as the landing and contacting platform for visiting pollinators, it has a simple and flat structure. This provides an innate advantage for capturing high-quality images of petals under optimal imaging conditions. By defining a homologous ROI in the image, we considered developmentally homologous regions in the analysis of nectar guide patterns.

In this study, we collected images of fresh ventral petals and histological images of 34 Ligeriinae species. The homologous ROI of petals was defined and obtained from the fresh petal image and the histological image through image processing. On the basis of the homologous ROI, we aimed to (1) qualify and quantify nectar guide patterns and (2) extend our understanding of the association between nectar guide patterns and pollination types in the subtribe Ligeriinae.

MATERIALS AND METHODS

Sampling and Growth Conditions

The sampled species were selected such that they covered a range of corolla morphologies (shape, size, and color) and pollination types in the subtribe Ligeriinae (**Table 1**). Plant materials used for the qualification and quantification of nectar guide patterns were sampled from the greenhouse of the Dr. Cecilia Koo Botanic Conservation Center (KBCC, Pingtung, Taiwan). The growth conditions were as follows: natural lighting with 60% net shading, humidity of 70–80%, and temperature of 22–30°C. Specimen collection was conducted from 2017 to 2019. Specimens were collected at the floral developmental stage between the anther and stigma anthesis. Specimens of the same species were collected in the same flowering season. In total, 454 specimens of 34 species were collected.

Fresh Petal Image Acquisition

After a flower was harvested, the corolla was dissected along the middle vein of the two lateral petals. From the ventral half of the corolla, the remaining lateral lobes were removed, and a necessary cut was made at the remaining lateral tube region to properly flatten the petal (**Figure 1**). An image of the adaxial surface of the petal was captured using a flatbed color scanner (Perfection V370, Epson, Nagano, Japan). The resolution ranged from 600 to 9,600 dpi. During scanning, the petal was flattened at the scanning stage and covered with a black cloth. The detailed procedure was reported by Hung et al. (2020). Subsequently, the scanned fresh petal was carefully moved to a fixative solution.

Histological Image Acquisition

The scanned fresh petal was fixed with 0.5% glycerol (v/v) in a 70% ethanol solution under a 600-mmHg vacuum until the tissue was completely infiltrated. The ethanol-fixed petal was subsequently transferred to the scanner and covered with a light emitting diode light board (A4 ultra-thin portable light box, LitEnergy, Dallas, TX, United States) under a color temperature

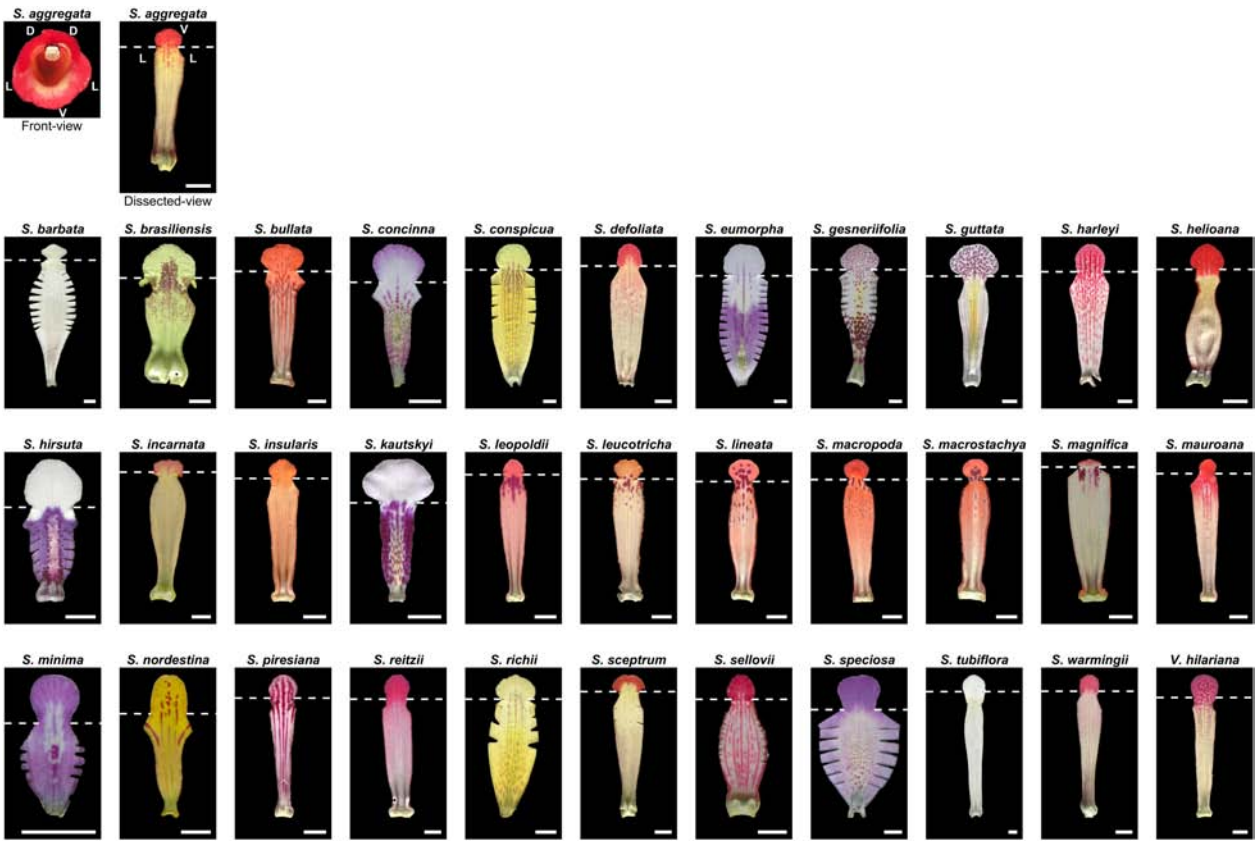

FIGURE 1 | Ventral petals of 34 Ligeriinae species. The white dashed line denotes the location of the lobe–tube connected rim. Scale bar: 0.5 cm.

of 9,000 K and a light source of 4,000 lux. The resolution was the same as that used in fresh petal image acquisition.

Extraction of the Homologous ROI

The homologous ROI was first defined as the frame combining a half-circle and a rectangle corresponding to the lobe and tube regions in the fresh petal image, respectively (**Figure 2**). The homologous ROI corresponded to the entire lobe and one-third of the tube at the distal side. Anatomical characteristics, namely the lobe contour (green line), the tracks of the middle vein (red line) and two side veins (blue line), and the tube–tube boundary between the ventral and lateral regions (black dotted line), were acquired to align the lobe contour and vasculature of specimens in different petal shapes and sizes.

Homologous ROI extraction was performed in four steps: anatomical characteristic selection, image registration, mapping, and affine transformation. The anatomical characteristic selection was performed on the histological image. Anatomical characteristics included the lobe contour, the tracks of the middle and side veins, and the tube–tube boundary. The lobe contour was automatically identified using the Gaussian-mixture-model-based segmentation algorithm (Nasios and Bors, 2006). The tracks of the middle vein and two side veins were manually identified using the cursor. The tube–tube boundary between the ventral and lateral regions was determined by examining the middle line between the track of the ventral side vein and the track of the neighboring lateral side vein. Subsequently, image registration was performed by superimposing the control points of histological images over the corresponding control points of fresh petal images (Gonzalez and Woods, 2006). The control points were landmarks found in both the images, such as the tips on the serrated lobe edge and the cutting trace of the lateral tube region. The identified anatomical characteristics were then mapped to the registered fresh petal image. Subsequently, 161 source points were arranged on the mapped characteristics (empty circles and triangles on the fresh petal image in **Figure 2**). In addition, the frame of the homologous ROI was arranged with 161 destination points. The source point and the corresponding destination point were paired. Finally, the homologous ROI was obtained through affine transformation (Gonzalez and Woods, 2006). The aforementioned procedures were performed using MATLAB (MathWorks, Natick, MA, United States).

Qualification of Nectar Guide Patterns

On the basis of the observation of homologous ROIs, four patterning modes were defined to qualify the nectar guide patterns. In addition to our previous study in which we classified the pattern of petal colors in Ligeriinae (Hung et al., 2019), we also incorporate the observation on the developmental serial to support the definition of patterning

TABLE 1 | Species list and number of specimens, pollination types, and accession numbers of the sampled individuals.

	Number of specimen	Pollination type[a]	KBCC accession number
Sinningia aggregata	26	Hummingbird	K039091, K039092, K039093, K039297
Sinningia barbata	3	Bee	K039105
Sinningia brasiliensis	17	Bat	K023999, K024028, K024030, K024040, K024074
Sinningia bullata	42	*To be determined*	K023430, K023431, K023443, K023448, K037111
Sinningia concinna	10	Bee	K039117
Sinningia conspicua	5	Bee	K039121
Sinningia defoliata	3	Hummingbird	K023265, K039125
Sinningia eumorpha	36	Bee	K039133
Sinningia gesneriifolia	9	*To be determined*	K039220, K039221
Sinningia guttata	3	Bee	K039134
Sinningia harleyi	7	Hummingbird	K039135
Sinningia helioana	6	*To be determined*	K039222
Sinningia hirsute	4	Bee	K039136
Sinningia incarnata	3	Hummingbird	K039137
Sinningia insularis	28	Hummingbird	K039142, K039145
Sinningia kautskyi	9	Bee	K039146, K039147
Sinningia leopoldii	9	Hummingbird	K039148, K039150
Sinningia leucotricha	6	Hummingbird	K039157
Sinningia lineata	43	Hummingbird	K039159, K039162, K039163
Sinningia macropoda	19	Hummingbird	K023363, K023405, K023413, K039164
Sinningia macrostachya	9	Hummingbird	K023944, K039165
Sinningia magnifica	4	Hummingbird	K039166
Sinningia mauroana	10	Hummingbird	K024149, K024154, K024169
Sinningia minima	4	*To be determined*	S82P101[b]
Sinningia nordestina	29	Hummingbird	K039168
Sinningia piresiana	9	Hummingbird	K023312, K023333
Sinningia reitzii	15	Hummingbird	K039173
Sinningia richii	5	Bee	K039176
Sinningia sceptrum	10	Hummingbird	K039178, K039182
Sinningia sellovii	21	Hummingbird	K023224, K039184, K039185
Sinningia speciosa	11	Bee	K039190
Sinningia tubiflora	4	Moth	K039191
Sinningia warmingii	14	Hummingbird	K039206, K039207
Vanhouttea hilariana	21	Hummingbird	K039218

[a] *Pollination type was referenced from the study by Perret et al. (2007).*
[b] *Plant material held by HC Hsu.*

modes (**Supplementary Figure 1**). The variegated pattern was defined as pigmentation initiating at the center of the petal, and the gradient pattern was defined as pigmentation initiating at the distal or proximal end of the petal. In this study, two patterning modes of each pattern were identified (**Figure 3**). In the variegated pattern, the pigmentation overlaying the vasculature was defined as the vascular mode (**Figure 3**, first row), and the distribution of pigmentation that does not follow the vasculature was defined as the random mode (**Figure 3**, second row). In the gradient pattern, the pigmentation initiating from the distal end was defined as the distal mode (**Figure 3**, third row), and pigmentation initiating from the proximal end was defined as the proximal mode (**Figure 3**, fourth row).

The association between the qualitative nectar guide pattern and pollination type was evaluated using the χ^2 test of independence. Cross-tabulation was performed to match the patterning modes of the variegated and gradient patterns with pollination type. The level of significance was set to 0.05.

Quantification of Nectar Guide Patterns

Nectar guide patterns were quantified by performing principal component analysis (PCA). The homologous ROI of each specimen was first converted from red–green–blue to grayscale and transformed from a two-dimensional image to a one-dimensional vector. The collection of one-dimensional vectors was then subjected to PCA. In PCA, variations in nectar guide patterns were decomposed into a series of principal components (PCs), which corresponded to an essential characteristic of nectar guide patterns. Inverse PCA was applied to PC scores to visualize variations in nectar guide patterns. In addition, stepwise multiple regression was applied to identify PCs that contributed to pollination types.

The association between quantitative nectar guide patterns and pollination types was evaluated by calculating the logarithm of the odds (LOD) score and by performing a permutation test. The LOD score in each PC is the logarithm of the ratio of the squared deviation of the PC score to the sum of the within-type

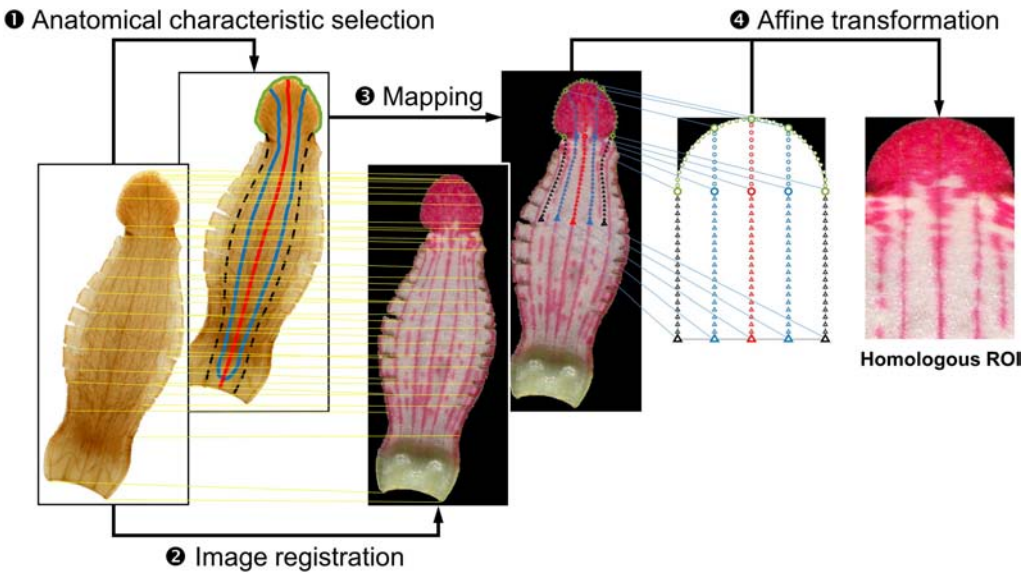

FIGURE 2 | Homologous region of interest (ROI) extraction procedure. In the histological image, the green line denotes the lobe contour, the red line denotes the track of the middle vein, the blue line denotes the track of the side vein, and the black dotted line denotes the tube–tube boundary. The yellow line connecting the histological image and fresh petal image denotes landmarks that were found in both images and used for image registration. The blue line connecting the fresh petal image and the frame of the homologous ROI denotes the source point and destination point pair.

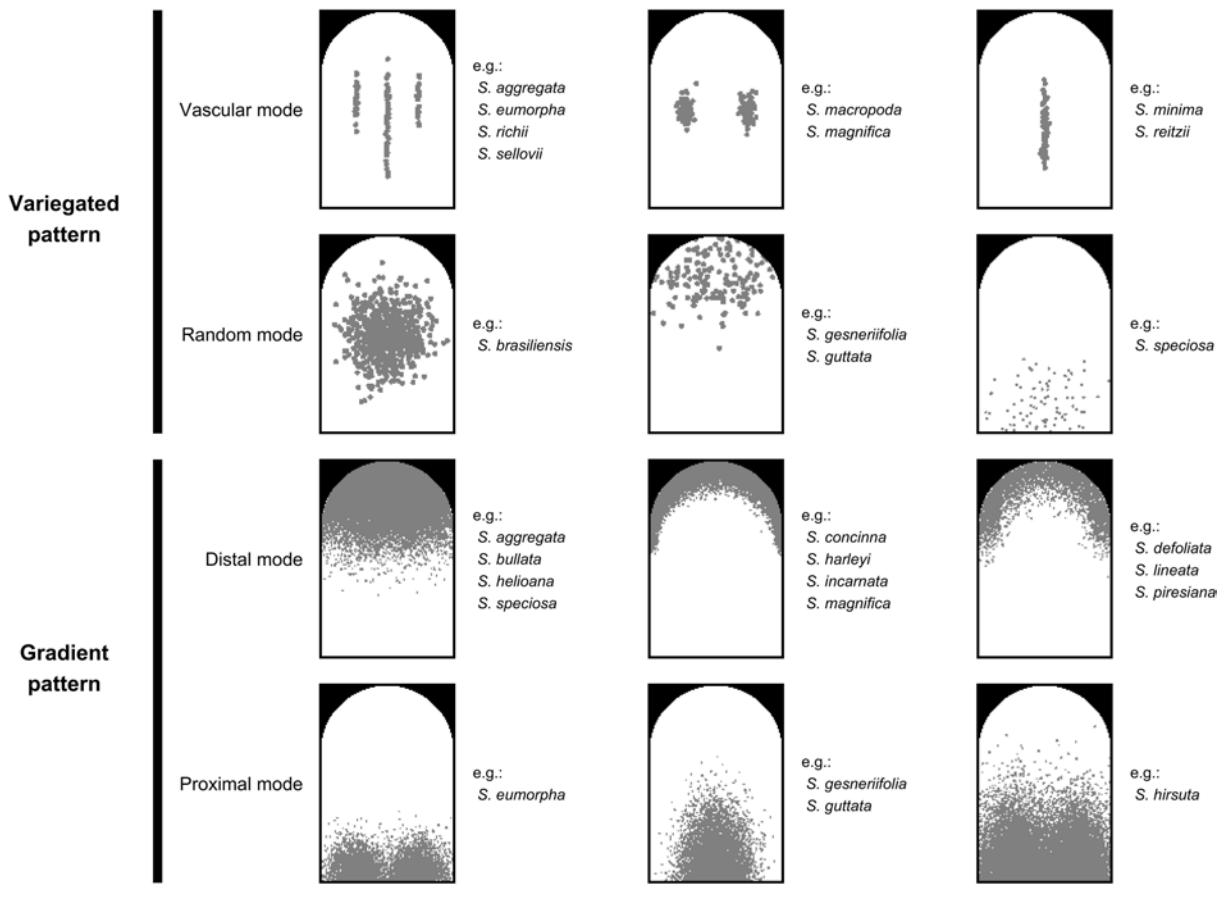

FIGURE 3 | Illustrations of four patterning modes. The gray region denotes the location of the pigmented area.

squared deviation of the PC score (Broman and Sen, 2009). The equation of LOD score is as,

$$\text{LOD score} = \frac{n}{2}\log_{10}\frac{\sum_i (y_i - \bar{y})^2}{\sum_i (y_i - \hat{y}_{pi})^2} \quad (1)$$

where the n is the sample size, the y_i is the PC score of specimen i, the $\bar{y}$ is the mean PC score of all specimens, the $\hat{y}_{pi}$ is the mean PC score of the pollination type of specimen i. The permutation test was then performed to evaluate the statistical significance of the LOD score. In the test, pairs of PC scores and their corresponding pollination types were shuffled 10,000 times. In each shuffle, the LOD score was calculated according to the shuffled pairs. The collection of LOD scores obtained from 10,000 shuffles served as the null distribution of the permutation test. The P-value for the test was subsequently calculated as the possibility that the null distribution exceeds the LOD score calculated from the original PC score–pollination type pair. A lower P-value indicated a statistically significant association between the quantified nectar guide pattern and pollination type.

RESULTS

The homologous ROI unified the lobe contour and vasculature from different species. **Figure 4** shows the homologous ROI for each species. All homologous ROIs were subsequently used for the qualification and quantification of nectar guide patterns.

Qualitative Nectar Guide Patterns and Their Association With Pollination Types

Table 2 lists the qualitative nectar guide patterns of 34 Ligeriinae species. Four patterning modes, namely the vascular and random modes of the variegated pattern and the distal and proximal modes of the gradient pattern, were determined on the basis of the location of the pigmented area in the homologous ROIs. Some species, such as *Sinningia brasiliensis* and *Sinningia conspicua*, acquired only a single patterning mode. Most of the species with complex patterns acquired two patterning modes. Moreover, the vascular and random modes were mutually exclusive in the variegated pattern, and the distal and proximal modes were mutually exclusive in the gradient pattern.

The patterning modes of the variegated and gradient patterns showed strong associations with pollination types (**Table 3**, $\chi^2 = 16.70$, $P = 1.05 \times 10^{-2}$; **Table 4**, $\chi^2 = 22.75$, $P = 8.85 \times 10^{-4}$). No pigmentation was considered a patterning mode (None in **Tables 3**, **4**). The species exhibiting the hummingbird pollination type tended to recruit the vascular mode of the variegated pattern and the distal mode of the gradient pattern.

Quantitative Nectar Guide Patterns and Their Association With the Pollination Type

Nectar guide patterns were quantified by applying PCA to all 454 homologous ROIs. The first five PCs, namely PC1–PC5,

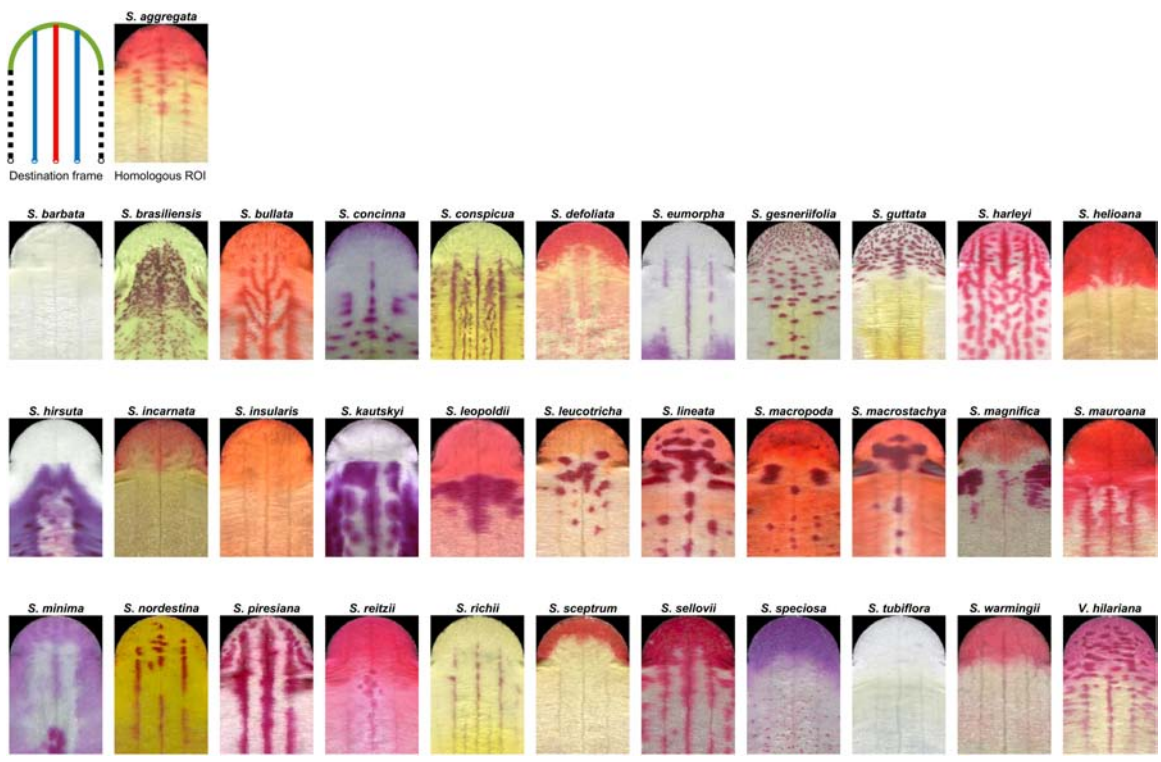

FIGURE 4 | Homologous ROIs of 34 Ligeriinae species. The legend for line colors is identical to that in **Figure 2**.

TABLE 2 | Qualitative nectar guide patterns of 34 Ligeriinae species.

	Variegated pattern (Vascular mode vs. Random mode)	Gradient pattern (Distal mode vs. Proximal mode)
Sinningia aggregata	V	D
Sinningia barbata	–	–
Sinningia brasiliensis	R	–
Sinningia bullata	V	D
Sinningia concinna	V	D
Sinningia conspicua	V	–
Sinningia defoliata	V	D
Sinningia eumorpha	V	P
Sinningia gesneriifolia	R	P
Sinningia guttata	R	P
Sinningia harleyi	V	D
Sinningia helioana	–	D
Sinningia hirsuta	R	P
Sinningia incarnata	–	D
Sinningia insularis	–	D
Sinningia kautskyi	V	P
Sinningia leopoldii	V	D
Sinningia leucotricha	V	D
Sinningia lineata	V	D
Sinningia macropoda	V	D
Sinningia macrostachya	V	–
Sinningia magnifica	V	D
Sinningia mauroana	V	D
Sinningia minima	V	D
Sinningia nordestina	V	–
Sinningia piresiana	V	D
Sinningia reitzii	V	D
Sinningia richii	V	–
Sinningia sceptrum	–	D
Sinningia sellovii	V	D
Sinningia speciosa	R	D
Sinningia tubiflora	–	–
Sinningia warmingii	–	D
Vanhouttea hilariana	V	D

TABLE 3 | χ^2 test of independence between patterning modes of the variegated pattern and pollination type in 34 Ligeriinae species.

Pollination type	Variegated pattern			χ^2	*P*-value
	Random mode	Vascular mode	None		
Bat	1	0	0	16.70	1.05×10^{-2}
Bee	3	5	1		
Hummingbird	0	15	5		
Moth	0	0	1		

accounted for 39.31, 22.49, 6.02, 3.58, and 2.15% of the total variance, respectively (**Figure 5**). In PC1–PC2 scatter plot, most of the species exhibiting bat, bee, and moth pollination types were distant from most of the species with the hummingbird pollination type. In PC3–PC4 and PC4–PC5 scatter plots, some species exhibiting the hummingbird pollination type, such as *Sinningia leopoldii* and *Sinningia piresiana*, with unique nectar guide patterns were also distant from other species exhibiting the hummingbird pollination type.

TABLE 4 | χ^2 test of independence between patterning modes of the gradient pattern and pollination type in 34 Ligeriinae species.

Pollination type	Gradient pattern			χ^2	*P*-value
	Distal mode	Proximal mode	None		
Bat	0	0	1	22.75	8.85×10^{-4}
Bee	2	4	3		
Hummingbird	18	0	2		
Moth	0	0	1		

The quantified nectar guide pattern accounting for the pollination type coincided with the patterning modes defined in the qualitative analysis. The variation in PC1, PC2, PC3, and PC5 significantly explained the variation in pollination types in the stepwise multiple regression analysis (**Table 5**, $P = 1.8187 \times 10^{-70}$). **Figure 6A** illustrates the virtual homologous ROIs of PC1, PC2, PC3, and PC5 with the PC scores (means ± standard deviations, SDs) covering negative and positive extremes. **Figure 6B** shows the deviation between the PC scores of the mean + 2 SDs and the mean – 2 SD. By determining the location of the larger gray-level deviation, we found that the variation in PC1, PC2, PC3, and PC5 corresponded to the proximal, distal, random, and vascular modes, respectively.

The quantified nectar guide pattern showed a strong association with pollination type. In the association analysis, species exhibiting bee and hummingbird pollination types were only included because only one species each demonstrated bat and moth pollination types. The LOD score and permutation test results revealed that PC1 (LOD = 19.91, $P = 1.74 \times 10^{-31}$), PC2 (LOD = 30.57, $P = 1.36 \times 10^{-36}$), and PC5 (LOD = 0.70, $P = 4.95 \times 10^{-2}$) were significantly associated with bee and hummingbird pollination types at a significance level of 0.05 (**Table 6**). The high LOD scores of PC1 and PC2 coincided with the result in the qualitative analysis that the gradient pattern had a stronger association with pollination type than that of the variegated pattern and pollination type.

DISCUSSION

In this study, we proposed defining a homologous ROI to compare nectar guide patterns on the developmentally homologous regions between species with different petal shapes and sizes. By using homologous ROIs, we qualified and quantified nectar guide patterns. In addition, we provided statistical evidence suggesting the association of nectar guide patterns with pollination types.

More Patterning Modes to Be Identified Using Homologous ROIs

In Ligeriinae, some unique patterning modes apart from the four identified patterning modes, remain to be defined and identified. The proposed homologous ROI only acquired the middle vein and two side veins to represent the petal vasculature. In *Sinningia bullata*, pigmentation following the higher-order vein was evident (**Figure 1**), forming strips that were not parallel

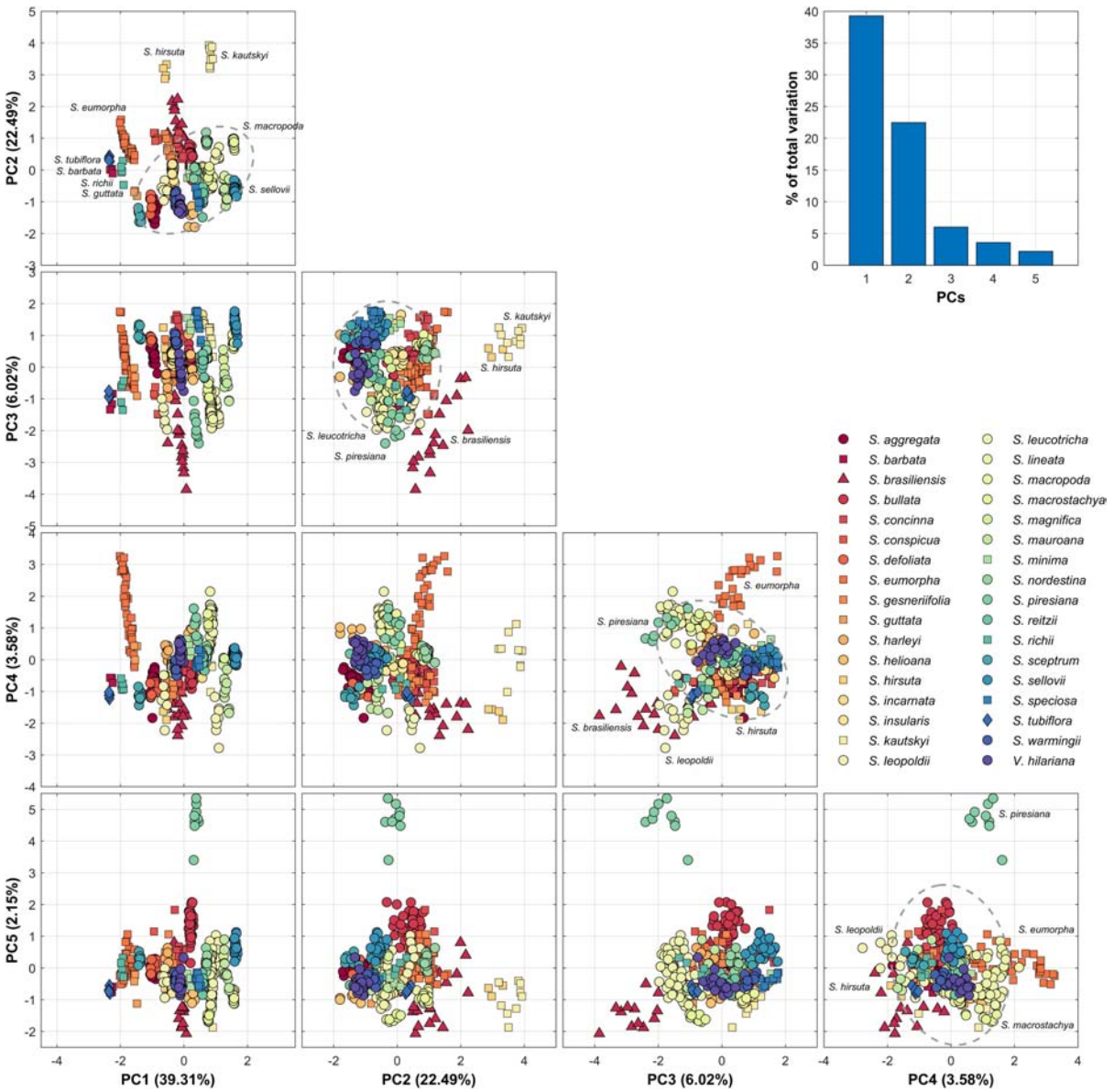

FIGURE 5 | Summary and scatter plots of PC1–5. PC scores are standardized to a mean of 0 and variance of 1. Circle, triangle, square, and diamond represent hummingbird, bat, bee, and moth pollination types, respectively. The dashed-line ellipse denotes the confidence ellipse of hummingbird pollination type.

TABLE 5 | Stepwise multiple regression analysis for PCs predicting pollination types.

	Stepwise multiple regression analysis							
	R^2 (%)	*F*-stat[a]	*P*-value	B[b]	SE[b]	*T*-stat[b]	*P*-value	Status[c]
	51.97	121.98	1.82×10^{-70}					
PC1				−0.65	0.04	−15.27	9.84×10^{-43}	In
PC2				0.66	0.04	15.49	1.03×10^{-43}	In
PC3				0.097	0.04	2.27	2.35×10^{-2}	In
PC4				0.082	0.04	1.93	5.48×10^{-2}	Out
PC5				−0.13	0.04	−3.09	2.10×10^{-3}	In

[a] *F-stat, the F-statistic of testing the final model versus the initial model (empty variable).*
[b] *B, coefficient for variables in the final model; SE, the standard error of coefficient estimates; T-stat, the T-statistic of coefficient estimation.*
[c] *Status, the decision for variables to be included in the model. The tolerance level for adding and removing variables is 0.05.*

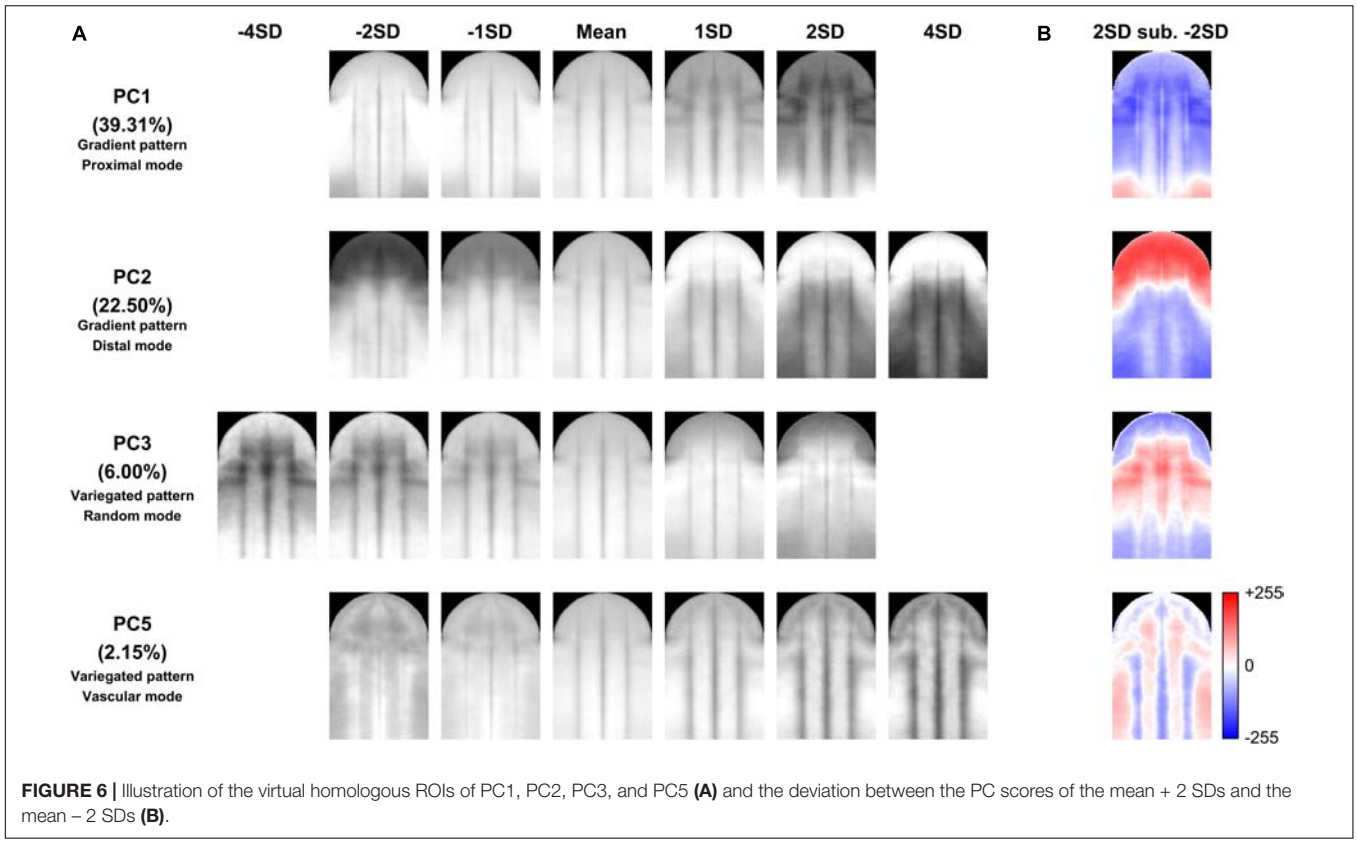

FIGURE 6 | Illustration of the virtual homologous ROIs of PC1, PC2, PC3, and PC5 **(A)** and the deviation between the PC scores of the mean + 2 SDs and the mean – 2 SDs **(B)**.

to the middle vein and two side veins in the homologous ROI (**Figure 4**). This observation implied that the vascular mode might be too coarse to describe the diversity of pigmentation patterning related to the vasculature. Regarding the higher-order vein, we also found a patterning mode contrasting with the vascular mode. In *S. conspicua*, at the region between the middle and side veins, the pigmented area evaded the vasculature of higher-order veins. In addition to the patterning modes of the variegated pattern, an undescribed patterning mode of the gradient pattern exists. In *Sinningia minima*, the process of pigmentation emerging from the neighboring lateral tube toward the side vein of the ventral tube was observed in the developmental series. Thus, an unpigmented area formed at the center of the ventral petal. The homologous ROI remains to be further refined to sufficiently and appropriately identify variations in nectar guide patterns.

TABLE 6 | Logarithm of the odds scores of PC1, PC2, PC3, and PC5 for hummingbird and bee pollination types.

	LOD score	*P*-value
PC1 (proximal mode of gradient pattern)	19.91	1.74×10^{-31}
PC2 (distal mode of gradient pattern)	30.57	1.36×10^{-36}
PC3 (random mode of variegated pattern)	0.56	9.19×10^{-2}
PC5 (vascular mode of variegated pattern)	0.70	4.95×10^{-2}

Insights Into the Pollination Type Based on the Patterning Mode of Nectar Guide Patterns

The results of our study indicate that the color distribution of petals, namely the nectar guide pattern, was strongly associated with different types of pollinators. A recent study reported the effect of petal color on pollinator preference in the neotropical Gesneriaceae (Ogutcen et al., 2021). Our study results imply that color distribution is also linked to the innate preference of pollinators and the pollination strategy in plants. Studies examining the pattern preferences of bees have shown that the color contrast between the inner and outer corolla (Lunau et al., 1996, 2006), the color patch at the center of the corolla (Free, 1970), and the pattern of dotted lines and stripes (radiating sector; Lehrer et al., 1995; Leonard and Papaj, 2011) can effectively allure bees. Our results coincide with those of these studies. A large proportion of species exhibiting the bee pollination type recruited vascular and proximal modes. Furthermore, most of the species exhibiting the hummingbird pollination type recruited vascular and distal modes. This finding also coincides with that a previous study demonstrating that long corolla tubes with color contrast is conspicuous to hummingbirds (Bergamo et al., 2019). *Sinningia tubiflora*, the only species that exhibited the moth pollination type, lacked variegated and gradient

patterns, suggesting that visual attraction is not its major strategy for attracting moths (Knudsen and Tollsten, 1993). Similarly, acoustic and scent attraction, rather than visual attraction, are major strategies for species demonstrating the bat pollination type (Gonzalez-Terrazas et al., 2016). This may explain why only *S. brasiliensis* has green petals and demonstrated a highly fluctuating random mode among specimens (**Supplementary Figure 2**). In addition, we also added more species in the analysis, which included the species with petal images captured under undesirable conditions (**Supplementary Figure 3**) and the species from the literature and image galleries on the Internet (**Supplementary Table 1**). We found that the association between patterning modes and pollination types was stronger and obvious (**Supplementary Tables 2, 3**). The present study provides insights into the association of patterning modes with pollination types from the perspective of nectar guide pattern diversity.

Application and Generalization of Homologous ROIs

The extraction of homologous ROIs integrates plant histology and image processing and provides new insights into the study of nectar guide patterns. Homologous ROIs can be applied to quantitative genetics. PC scores can serve as trait values and present trait differences between a parent and its offspring. **Supplementary Figure 4** presents the quantified nectar guide patterns of F_1 hybrids. With the use of homologous ROIs, the interspecific comparative analysis can also be expanded. **Supplementary Figure 5** shows an example in which homologous ROIs are applied to Gesneriaceae species other than Ligeriinae. PC scores can also serve as character values for phylogenetic analysis. **Supplementary Figure 6** summarizes the test of phylogenetic signals indicating the nectar guide pattern of the related species have less tendency to resemble each other in Ligeriinae.

Biologists can use homologous ROIs to gain a comprehensive understanding of nectar guide patterns with an extensive survey. In Ronse De Craene's (2008) study, the petaloid organ vasculature of Lamiales (including the family Gesneriaceae) belongs to the single bundle character state. Approximately 70% of the taxa of eudicots was determined to have this character state. The single bundle was further subdivided into fan-like and trifid branching types. Although Lamiales was identified to have the fan-like branching type, the vasculature of the single middle vein and two side veins was clearly recognized in the present study. These findings suggest that the homologous ROI has potential to be generalized to the taxa adopting a single bundle development of the petal vasculature. As aforementioned, the petal is a homologous structure across core eudicots. Thus, homologous ROIs may be applied to other Lamiales lineages, or even the core eudicot, to perform a large-scale comparative analysis of nectar guide patterns.

DATA AVAILABILITY STATEMENT

The raw data supporting the conclusions of this article will be made available by the authors, without undue reservation.

AUTHOR CONTRIBUTIONS

H-CH: conceptualization, methodology, software, validation, formal analysis, investigation, resources, data curation, writing – reviewing and editing, visualization, and project administration. Y-FK: conceptualization, resources, writing – reviewing and editing, supervision, project administration, and funding acquisition. Both authors contributed to the article and approved the submitted version.

FUNDING

This work was supported by the National Science Council (Ministry of Science and Technology) of Taiwan (grant NSC-101-2313-B-002-050-MY3).

ACKNOWLEDGMENTS

We thank Mr. Chun-Ming Chen and Dr. Cecilia Koo of the Botanic Conservation and Environmental Protection Center for maintaining plant materials. We also thank Mr. Jui-Jung Wu for providing the plant material, *Sinningia minima* and the F_1 hybrid of *Sinningia nordestina* × *brasiliensis*. This article was subsidized for English editing by the National Taiwan University under the Excellence Improvement Program for Doctoral Students (grant 108-2926-I-002-002-MY4), sponsored by Ministry of Science and Technology, Taiwan.

SUPPLEMENTARY MATERIAL

The Supplementary Material for this article can be found online at: https://www.frontiersin.org/articles/10.3389/fpls.2021.650836/full#supplementary-material

Supplementary Figure 1 | Developmental serial of *Sinningia brasiliensis* (K024074), *Sinningia eumorpha* (K039133), *Sinningia magnifica* (K039166), *Sinningia nordestina* (K039168), *Sinningia sceptrum* (K039182), and *Sinningia speciosa* (K039190). V_R: random mode of variegated pattern; V_V: vascular mode of variegated pattern; G_D: distal mode of gradient pattern; G_P: proximal mode of gradient pattern.

Supplementary Figure 2 | Homologous ROI of *Sinningia brasiliensis*.

Supplementary Figure 3 | Homologous ROI of *Sinningia aghensis*, *Sinningia allagophylla*, *Sinningia carangolensis*, *Sinningia polyantha*, and *Sinningia pusilla*. Scale bar: 0.5 cm.

Supplementary Figure 4 | Ventral petals, homologous ROIs, and quantified nectar guide patterns in the PC1 and PC2 of eight F_1 hybrids. Scale bar: 0.5 cm.

Supplementary Figure 5 | Ventral petals, homologous ROIs, and quantified nectar guide patterns in the PC1 and PC2 of eight Gesneriaceae species. Scale bar: 0.5 cm.

Supplementary Figure 6 | Phylogenetic signals of 4 PC scores. The boxplot presents the distributions of the Blomberg K values obtained from the phylogenetic trees of 1,000 replicates in the maximum likelihood analysis. Diamonds indicate the Blomberg K values calculated using the 50% majority-rule

consensus tree. The gray dots in the denote the data point of outliers. The *P*-values are provided at the right of each boxplot.

Supplementary Table 1 | Qualitative nectar guide pattern of 60 Ligeriinae species reviewed from the literature and image galleries on the Internet.

Supplementary Table 2 | χ^2 test of independence between the patterning modes of the variegated pattern and pollination type in 83 Ligeriinae species.

Supplementary Table 3 | χ^2 test of independence between the patterning modes of the gradient pattern and pollination type in 83 Ligeriinae species.

REFERENCES

Basile, A., Fambrini, M., and Pugliesi, C. (2017). The vascular plants: open system of growth. *Dev. Genes Evol.* 227, 129–157. doi: 10.1007/s00427-016-0572-1

Bergamo, P. J., Wolowski, M., Telles, F. J., De Brito, V. L. G., Varassin, I. G., and Sazima, M. (2019). Bracts and long-tube flowers of hummingbird-pollinated plants are conspicuous to hummingbirds but not to bees. *Biol. J. Linnean Soc.* 126, 533–544. doi: 10.1093/biolinnean/bly217

Broman, K. W., and Sen, S. (2009). *A Guide to QTL Mapping with R/qtl*, Vol. 46. New York: Springer.

Endress, P. K. (1996). *Diversity and evolutionary biology of tropical flowers*. New York: Cambridge University Press.

Free, J. B. (1970). Effect of flower shapes and nectar guides on the behaviour of foraging honeybees. *Behaviour* 37, 269–285.

Gómez, J. M., and Perfectti, F. (2010). Evolution of complex traits: the case of erysimum corolla shape. *Int. J. Plant Sci.* 171, 987–998. doi: 10.1086/656475

Gonzalez, R. C., and Woods, R. E. (2006). *Digital Image Processing*, 3rd Edn. Upper Saddle River, NJ: Prentice-Hall, Inc.

Gonzalez-Terrazas, T. P., Martel, C., Milet-Pinheiro, P., Ayasse, M., Kalko, E. K., and Tschapka, M. (2016). Finding flowers in the dark: nectar-feeding bats integrate olfaction and echolocation while foraging for nectar. *R. Soc. Open Sci.* 3:160199. doi: 10.1098/rsos.160199

Hsu, H. C., Hsu, K. L., Chan, C. Y., Wang, C. N., and Kuo, Y. F. (2018). Quantifying colour and spot characteristics for the ventral petals in sinningia speciosa. *Biosyst. Eng.* 167, 40–50. doi: 10.1016/j.biosystemseng.2017.12.010

Hung, T. T., Hsu, H. C., and Kuo, Y. F. (2019). *Quantifying color and textural patterns of petals and studying their association with pollinators: using genus Sinningia (GESNERIACEAE) as an example. In 2019 ASABE Annual International Meeting*. Michigan, US: American Society of Agricultural and Biological Engineers, 1.

Hung, T. T., Hsu, H. C., and Kuo, Y. F. (2020). Quantification of petal patterns and colours of genus sinningia (GESNERIACEAE). *Biosyst. Eng.* 197, 324–335. doi: 10.1016/j.biosystemseng.2020.07.008

Knudsen, J. T., and Tollsten, L. (1993). Trends in floral scent chemistry in pollination syndromes: floral scent composition in moth-pollinated taxa. *Bot. J. Linnean Soc.* 113, 263–284. doi: 10.1111/j.1095-8339.1993.tb00340.x

Lehrer, M., Horridge, G. A., Zhang, S. W., and Gadagkar, R. (1995). Shape vision in bees: innate preference for flower-like patterns. *Phil. Trans. R. Soc. Lond. B* 347, 123–137.

Leonard, A. S., and Papaj, D. R. (2011). 'X'marks the spot: the possible benefits of nectar guides to bees and plants. *Funct. Ecol.* 25, 1293–1301. doi: 10.1111/j.1365-2435.2011.01885.x

Lootens, P., Van Waes, J., and Carlier, L. (2007). Evaluation of the tepal colour of begonia x tuberhybrida Voss. for DUS testing using image analysis. *Euphytica* 155, 135–142. doi: 10.1007/s10681-006-9315-0

Lunau, K., Fieselmann, G., Heuschen, B., and van de Loo, A. (2006). Visual targeting of components of floral colour patterns in flower-naive bumblebees (bombus terrestris; apidae). *Naturwissenschaften* 93, 325–328. doi: 10.1007/s00114-006-0105-2

Lunau, K., Wacht, S., and Chittka, L. (1996). Colour choices of naive bumble bees and their implications for colour perception. *J. Comp. Physiol. A* 178, 477–489.

Nasios, N., and Bors, A. G. (2006). Variational learning for gaussian mixture models. *IEEE Trans. Syst. Man Cybernetics Part B (Cybernetics)* 36, 849–862. doi: 10.1109/TSMCB.2006.872273

Ogutcen, E., Durand, K., Wolowski, M., Clavijo, L., Graham, C., Glauser, G., et al. (2021). Chemical basis of floral color signals in gesneriaceae: the effect of alternative anthocyanin pathways. *Front. Plant Sci.* 11:604389. doi: 10.3389/fpls.2020.604389

Penny, J. H. J. (1983). Nectar guide colour contrast: a possible relationship with pollination strategy. *New Phytol.* 95, 707–721.

Perret, M., Chautems, A., Spichiger, R., Barraclough, T. G., and Savolainen, V. (2007). The geographical pattern of speciation and floral diversification in the neotropics: the tribe sinningieae (gesneriaceae) as a case study. *Evol. Int. J. Organic Evol.* 61, 1641–1660. doi: 10.1111/j.1558-5646.2007.00136.x

Ronse De Craene, L. P. (2008). Homology and evolution of petals in the core eudicots. *Syst. Bot.* 33, 301–325. doi: 10.1600/036364408784571680

van der Kooi, C. J., Dyer, A. G., Kevan, P. G., and Lunau, K. (2019). Functional significance of the optical properties of flowers for visual signalling. *Ann. Bot.* 123, 263–276. doi: 10.1093/aob/mcy119

Walcher-Chevillet, C. L., and Kramer, E. M. (2016). Breaking the mold: understanding the evolution and development of lateral organs in diverse plant models. *Curr. Opin. Genet. Dev.* 39, 79–84. doi: 10.1016/j.gde.2016.06.005

Wang, Y. H., Hsu, H. C., Chou, W. C., Liang, C. H., and Kuo, Y. F. (2020). Automatic identification of first-order veins and corolla contours in 3D floral images. *Front. Plant Sci.* 11:549699. doi: 10.3389/fpls.2020.549699

Whibley, A. C., Langlade, N. B., Andalo, C., Hanna, A. I., Bangham, A., Thébaud, C., et al. (2006). Evolutionary paths underlying flower color variation in antirrhinum. *Science* 313, 963–966. doi: 10.1126/science.1129161

Yoshioka, Y., Iwata, H., Ohsawa, R., and Ninomiya, S. (2004). Quantitative evaluation of flower colour pattern by image analysis and principal component analysis of *Primula sieboldii* E. *Morren. Euphytica* 139, 179–186. doi: 10.1007/s10681-004-3031-4

Conflict of Interest: The authors declare that the research was conducted in the absence of any commercial or financial relationships that could be construed as a potential conflict of interest.

frontiers in Plant Science

ORIGINAL RESEARCH
published: 04 June 2021
doi: 10.3389/fpls.2021.660803

Transcriptome Analysis Reveals Putative Target Genes of *APETALA3-3* During Early Floral Development in *Nigella damascena* L.

Yves Deveaux[1]†, Natalia Conde e Silva[1†], Domenica Manicacci[1], Martine Le Guilloux[1], Véronique Brunaud[2], Harry Belcram[1], Johann Joets[1], Ludivine Soubigou-Taconnat[2,3], Etienne Delannoy[2,3], Hélène Corti[1], Sandrine Balzergue[2,4], Jose Caius[2,3], Sophie Nadot[5] and Catherine Damerval[1]*

[1]Université Paris-Saclay, INRAE, CNRS, AgroParisTech, Génétique Quantitative et Evolution-Le Moulon, Gif-sur-Yvette, France, [2]Université Paris-Saclay, CNRS, INRAE, Univ Evry, Institute of Plant Sciences Paris-Saclay (IPS2), Orsay, France, [3]Université de Paris, CNRS, INRAE, Institute of Plant Sciences Paris-Saclay (IPS2), Orsay, France, [4]Univ Angers, Institut Agro, INRAE, IRHS, SFR QUASAV, Angers, France, [5]Université Paris-Saclay, CNRS, AgroParisTech, Ecologie Systématique Evolution, Orsay, France

Even though petals are homoplastic structures, their identity consistently involves genes of the APETALA3 (AP3) lineage. However, the extent to which the networks downstream of AP3 are conserved in species with petals of different evolutionary origins is unknown. In Ranunculaceae, the specificity of the AP3-III lineage offers a great opportunity to identify the petal gene regulatory network in a comparative framework. Using a transcriptomic approach, we investigated putative target genes of the AP3-III ortholog NdAP3-3 in *Nigella damascena* at early developmental stages when petal identity is determined, and we compared our data with that from selected eudicot species. We generated a *de novo* reference transcriptome to carry out a differential gene expression analysis between the wild-type and mutant *NdAP3-3* genotypes differing by the presence vs. absence of petals at early stages of floral development. Among the 1,620 genes that were significantly differentially expressed between the two genotypes, functional annotation suggested a large involvement of nuclear activities, including regulation of transcription, and enrichment in processes linked to cell proliferation. Comparing with *Arabidopsis* data, we found that highly conserved genes between the two species are enriched in homologs of direct targets of the AtAP3 protein. Integrating AP3-3 binding site data from another Ranunculaceae species, *Aquilegia coerulea*, allowed us to identify a set of 18 putative target genes that were conserved between the three species. Our results suggest that, despite the independent evolutionary origin of petals in core eudicots and Ranunculaceae, a small conserved set of genes determines petal identity and early development in these taxa.

Keywords: APETALA3, RNA-seq, AP3 target genes, petal, *Nigella damascena*, floral mutant, Ranunculaceae, *Arabidopsis*

OPEN ACCESS

Edited by:
Elena M. Kramer, Harvard University, United States

Reviewed by:
Verónica S. Di Stilio, University of Washington, United States
Chunce Guo, Pennsylvania State University (PSU), United States
Suzanne De Bruijn, John Innes Centre, United Kingdom

****Correspondence:***
Yves Deveaux
yves.deveaux@universite-paris-saclay.fr

[†]These authors have contributed equally to this work

Specialty section:
This article was submitted to Plant Development and EvoDevo, a section of the journal Frontiers in Plant Science

Received: *29 January 2021*
Accepted: *04 May 2021*
Published: *04 June 2021*

Citation:
Deveaux Y, Conde e Silva N, Manicacci D, Le Guilloux M, Brunaud V, Belcram H, Joets J, Soubigou-Taconnat L, Delannoy E, Corti H, Balzergue S, Caius J, Nadot S and Damerval C (2021) Transcriptome Analysis Reveals Putative Target Genes of APETALA3-3 During Early Floral Development in Nigella damascena L.. Front. Plant Sci. 12:660803. doi: 10.3389/fpls.2021.660803

INTRODUCTION

Petals are floral organs that play a major role in pollinator attraction. In flowers with a differentiated perianth, petals are defined as the second whorl of sterile organs surrounding the androecium; the first whorl of sterile organs is composed of sepals, which protect the fertile organs during development. A recent reconstruction of the ancestral angiosperm flower suggests that the ancestral flower has an undifferentiated perianth and floral organs inserted in whorls or along a spiral (Sauquet et al., 2017). Perianth differentiation has evolved several times independently, and consequently, the term "petal" is not indicative of organ homology across angiosperms (Irish, 2009; Ronse de Craene and Brockington, 2013).

The analysis of floral mutants in two core eudicot species, *Antirrhinum majus* and *Arabidopsis thaliana*, has been a turning point for understanding the genetic control of floral organ identity by proposing a model based on four main functions: A, B, C, and E. The A-function specifies sepals, A- and B-functions determine petals, B- and C-functions specify stamens, and C-function specifies carpels (Coen and Meyerowitz, 1991). The E-function combines with the three other functions to specify floral identity (Pelaz et al., 2001). Most genes involved in A-, B-, C-, and E-functions, encode transcription factors belonging to the MIKC-type MADS-box gene family (reviewed in Theißen and Gramzow, 2016). They are known to act in tetrameric protein complexes ("floral quartets"; Theißen et al., 2016; Yan et al., 2016). In particular, B-function relies on two proteins APETALA3/DEFICIENS (AP3) and PISTILLATA/GLOBOSA (PI) in *Arabidopsis*/*Antirrhinum*, respectively, which function as an obligate heterodimer within tetrameric complexes (Goto and Meyerowitz, 1994).

AP3 and *PI* belong to two paralogous gene lineages that result from an ancient duplication preceding the angiosperm radiation. Additional duplications took place in the *AP3* and *PI* lineages during angiosperm evolution, at different points in time (Lee and Irish, 2011). In the *AP3* lineage, an ancient duplication event occurred at the base of the core eudicots, resulting in the TM6 and euAP3 gene lineages. The euAP3 lineage is characterized by a C-terminal motif that differs from the paleoAP3 motif present in TM6 and other AP3 lineages (Kramer et al., 1998, 2006). EuAP3 genes are thought to play an important role in the formation and diversification of petals in core eudicots (Irish, 2009). Independently, two successive duplications of AP3 have occurred at the base of the order Ranunculales, the sister group to all other eudicots, giving rise to three paralogous lineages: AP3-I, AP3-II, and AP3-III (Rasmussen et al., 2009). The *PI* lineage evolution is also complex and dynamic with cases of multiple recent duplications (Zahn et al., 2005). In Ranunculales, the B-function involves generally the three AP3 paralogous and at least one PI paralogous genes. Heterodimerization of PI proteins with AP3 proteins of the different lineages has been observed in several species (Kramer et al., 2007; Wang et al., 2016; Galimba et al., 2018). While *PI* gene expression is essential for both stamen and petal identity (Kramer et al., 2007; Wang et al., 2016), the function of the different paralogous AP3 genes with regard to stamen and petal identity has diverged (Kramer et al., 2007; Sharma and Kramer, 2013; Wang et al., 2016). In particular, it has been shown that the presence of petals is strongly correlated with the expression of AP3-III orthologs (Kramer et al., 2003; Di Stilio et al., 2005; Rasmussen et al., 2009), and that the absence of petals in some species is linked to a disruption of the *AP3-3* locus (Zhang et al., 2013). In two Ranunculaceae species where functional studies can be conducted using Virus-Induced Gene Silencing (VIGS), namely, *Aquilegia coerulea* and *Nigella damascena*, it has been shown that expression of *AP3-3* genes is required for petal identity (Sharma et al., 2011; Gonçalves et al., 2013; Wang et al., 2016). These lines of evidence indicate that AP3-3 orthologs play a crucial role in determining petal identity in Ranunculaceae.

Petals, with their multiple independent origins, have been consistently associated with the expression of B-function genes (Ambrose et al., 2000; Drea et al., 2007; Mondragón-Palomino and Theissen, 2008). Therefore, they are a good case study of the conservation of gene networks downstream of B-function proteins. While *Arabidopsis AP3* gene is involved in both petal and stamen development, the petal specificity of the Ranunculaceae *AP3-3* genes offers a good opportunity to unravel a petal-specific gene regulatory network. The target genes of MADS-box proteins are beginning to be identified in model species, mainly in *Arabidopsis* (Bey et al., 2004; Kaufmann et al., 2009, 2010; Wuest et al., 2012; Ó'Maoiléidigh et al., 2013; Pajoro et al., 2014). High throughput sequencing methods now open the way for comparing possible target genes in a wider range of non-model species representing diverse organ morphologies and evolutionary origins (Thomson et al., 2017).

Expression of B-function genes is required at every stage of development to obtain full organ identity. In *N. damascena*, we observed that the presence and morphology of petals differed according to the timing of inactivation of *NdAP3-3* by VIGS (Gonçalves et al., 2013). Early inactivation results in the absence of petal formation, resulting in a phenocopy of the spontaneous mutant lacking petals known since the 16th century (Toxopéus, 1927). When inactivation takes place at later stages, a range of intermediate morphologies between petals and sepals are observed. In this paper we intended to characterize the early target genes of NdAP3-3 that determine the full petal identity. Because of the large size of the *N. damascena* genome (~10 Gb), no genomic data are available for this species yet. To circumvent this limiting factor, we assembled and annotated a floral reference transcriptome and characterized differential gene expression between wild-type and mutant genotypes at the *NdAP3-3* locus differing by the presence vs. absence of petals. The wild type vs. mutant comparison gives the unique opportunity to investigate

Abbreviations: AtAP3-BCG, 200 *Arabidopsis* genes whose expression is best correlated (100 positively and 100 negatively) with *AtAP3* expression; AtDEG, *Arabidopsis* genes whose expression differs between wild type and *ap3.3* mutant; AtBCG-DEG, *Arabidopsis* genes that are both AtDEG and AtAP3-BCG; DEG, differentially expressed genes; M_LFC, Log-fold change between the two morphs; NdH, *Nigella* genes homologous to AtDEG; NdH-BCG, *Nigella* genes homologous to AtAP3-BCG; NdH-BCG-DEG, NdH-BCG that are differentially expressed between the *Nigella* floral morphs; NdH-DEG, NdH that are differentially expressed between the *Nigella* floral morphs.

the early stages of floral development when petals are initiated or not. Therefore, differentially expressed genes are candidates for direct or indirect targets of the NdAP3-3 protein involved in petal identity and early development. Genes were annotated and compared to known or suspected targets of B-function genes in other eudicot species (Bey et al., 2004; Wuest et al., 2012; Jiang et al., 2020), and the conservation of the petal gene network is discussed.

MATERIALS AND METHODS

Plant Material and Tissue Collection

Segregating populations were obtained by selfing plants issued from two commercial seed lots obtained from horticultural companies (Royal Fleur and Truffaut) as described in Gonçalves et al. (2013). The heterozygosity level of these mother plants is unknown. For analysis of the early stages, the progeny of F2 plants (F3 offspring), which were homozygous either for the wild-type *P* allele (P morph, with petals) or the mutant *p* allele (T morph, without petals), were sown in three replicates. Each of the three replicates consisted of a mix of eight seeds from the same six *PP* or *pp* F2 mother plants. Plants were grown in pots in randomized blocks in a growth chamber under controlled conditions (18 h day at 25°C, 6 h night at 16°C). Another set of *PP* plants was grown independently to collect late developmental stages. The genotype at the *NdAP3-3* locus was checked for all plants by PCR using primers flanking the MITE element insertion site in intron 2, which is a marker for the *p* allele (Gonçalves et al., 2013).

Floral buds were collected at different stages, based on the developmental schedule previously described by Jabbour et al. (2015). Stage 1 corresponds to 1 day after floral transition marked by the beginning of stem extension; at this stage, only sepals are initiated in both genotypes. Stage 2 occurs 3 days later, and corresponded to petal initiation (*PP* plants) or internal sepal initiation (*pp* plants). Approximately 20 terminal flower meristems were dissected under a stereomicroscope allowing stage inspection for each condition (morph × stage × replicate). Flower buds were collected from 32 *PP* plants at three late stages (bud diameter 5–6 mm, 6–8 mm, and just before anthesis), and the organs were dissected and kept separately (sepals, petals, stamens, and carpels). All dissected floral tissues were immediately frozen in liquid nitrogen and stored at −80°C until RNA extraction.

RNA Extraction and RNA-Sequence Analysis

Total RNA from floral meristems and dissected organs was extracted using the RNeasy Plant Mini Kit (Qiagen) with the additional DNAse I step according to the manufacturer's instructions. Total RNA from each tissue was checked for integrity on an RNA_Nano chip, using an Agilent 2,100 bioanalyzer (Agilent Technologies, Waldbroon, Germany). Twelve libraries were constructed for the two morphs at the two earliest developmental stages in three replicates. Two additional libraries were constructed from the dissected floral organs of the P morph, the first one by pooling equal amounts of RNA from the three non-petal organs at the three late developmental stages, and the second one by pooling RNA from petals only at these three stages. The libraries were constructed with the TruSeq-stranded mRNA library Prep kit (Illumina, California, USA) with 300-bp size for libraries from early-stage material and 260-bp size for dissected material. Libraries were paired-end (PE) sequenced with a read length of 150 bp for early-stage material and 100 bp for dissected material using an Illumina HiSeq2000 at the Genoscope Laboratory (Evry, France). Lane distribution and barcoding gave approximately 20–30 million PE reads per sample. For each sample, raw data (fastq) were trimmed with Trimmomatic (Bolger et al., 2014) with a Phred Quality Score Qscore > 20, and read lengths > 30 bases. Ribosome sequences were removed with the sortMeRNA tool (Kopylova et al., 2012).

All steps of the study, from growth conditions to bioinformatic analyses, were managed in a CATdb database (Gagnot et al., 2007, http://tools.ips2.u-psud.fr/CATdb/) with ProjectID NGS2013_09_AAP-IDEEV and NGS2015_16_Ranunculaceae. This project was submitted from CATdb to the international public repository GEO (Gene Expression Omnibus, Edgar et al., 2002, http://www.ncbi.nlm.nih.gov/geo, GSE159429).

Reference Transcriptome Assembly

Assembly of the reference transcriptome was made using Trinity (version 2.4, Grabherr et al., 2011). To balance between the different genotypes, developmental stages, and organs, we combined the following six samples for a total of ~130 million oriented PE reads: four libraries were from floral buds of the P and T morphs at stages 1 and 2, and two libraries were from petal and non-petal tissues from the P morph at later stages. Trinity was run with default parameters and a kmer size of 32. Contigs that were smaller than 200 bases were removed, and 81,194 contigs were finally obtained. iAssembler (version 1.3, Zheng et al., 2011) was then used for scaffolding contigs and reducing redundancy, with 97% identity for sequence clustering. For simplicity, hereafter we use the term transcript or gene to refer to the contigs, which may include paralogs, alleles, and alternative splicing of the same gene.

Functional Annotation and Homology Search

Before annotating the transcriptome, we predicted all coding sequences. First, the TransDecoder software (v5.0.2; Perina et al., 2016; Roy et al., 2018) was used to predict all putative open reading frames (ORFs) among assembled transcript sequences (default parameters). These predicted ORFs were then searched for Pfam domain hits (v28) using the HMMER software (3.1b2, default settings; Eddy and Pearson, 2011). Final coding region predictions were achieved by running TransDecoder a second time taking into account the Pfam domain search output. Functional annotations were performed by searching for sequence similarity and protein domains. Similarity of the predicted proteins with sequences from the

UniRef90 (Suzek et al., 2015) and TAIR databases (Huala et al., 2001; Rhee et al., 2003) was determined using Blast (ncbi-blast-2.6.0+, E-value < 1.10–3; Altschul et al., 1990). InterProScan software (5.29–68.0; Zdobnov and Apweiler, 2001; Jones et al., 2014) was used to search for InterPro domain hits (default settings). We extracted Gene Ontology (GO) and GO slim terms (functions, locations, and biological roles) from Blast and InterProScan outputs with a lab script (Ashburner et al., 2000; The Gene Ontology Consortium, 2001).

BlastP tool was used to compare *N. damascena* predicted proteins to the 43,550 proteins of *A. coerulea* from Phytozome (322-v3.1). We kept only the best hit for each *Nigella* protein (E-value ≤ 0.01). Blastn was also used to search for the homology of some unannotated transcripts in the *A. coerulea* genome.

Nine transcripts with differential expression between morphs and without functional annotation were chosen randomly to check whether they could correspond to novel potentially *Nigella*-specific sequences or were misassembled transcripts. Primers were designed based on the full sequences of these nine transcripts and used to amplify from cDNA and/or gDNA (**Supplementary Table S1**).

Differential Gene Expression Analysis

Reads corresponding to the three replicates of stages 1 and stage 2 floral buds of the P and T morphs were mapped on the reference transcriptome. Every PE read in each sample was mapped against the complete list of contigs with Bowtie2 (Langmead and Salzberg, 2012, local option). Ninety six percent of the reads could be mapped, demonstrating the quality of transcriptome assembly. All PE reads with multi-hits, meaning mapped on sequence regions shared by isoforms, were removed. We kept only PE reads associated with a unique contig, ensuring specific quantification of gene expression. The method generated quantitative data for 70,491 contigs.

Low-expression genes were filtered to include only contigs (genes) that have at least 1 read count per million (CPM, counts per million) after normalization, in at least two samples. 34,614 transcripts (that include *NdAP3-3*) were thus retained for quantitative analysis. The coefficients of determination calculated on normalized counts between pairs of replicates for each stage–organ combination were high (R2 > 0.95). To assess how the overall variability is structured among the 12 datasets (2 morphs × 2 stages × 3 replicates), a principal component analysis was carried out on the normalized counts for these 34,614 informative transcripts using the FactoMineR package. Using the EdgeR package v3.8.6 (Robinson et al., 2010), we then fitted the normalized count data to a model that considered the effect of plant morph (2 levels), developmental stage (2 levels), replicate (3 levels), as well as the morph by stage and morph by replicate interactions. We performed contrasts to (i) compare the P and T morphs at stage 1, at stage 2, and at both stages on average; (ii) compare the developmental stages in the P morph, the T morph, and in both morphs on average; and (iii) test the morph by stage interaction. In each case, *p*-values for statistical significance were adjusted following the Benjamini and Hochberg's (1995) FDR method.

To quantify the level of differential expression between morphs, we calculated the log2 ratio of the mean of the normalized counts of T over P for the three replicates (hereafter M_LFC) at stage 1, stage 2, or both together. A heatmap of the log2-normalized counts of the two morphs at the two developmental stages in the three replicates was drawn with the heatmap function in R.

As a complementary approach to identify possible targets of the NdAP3-3 transcription factor, we correlated the expression of the remaining 34,613 transcripts for quantitative analysis with the expression of the *NdAP3-3* gene in the P morph. Because the effect of the developmental stage was high for *NdAP3-3* and for most transcripts, we normalized the data per stage. The Pearson's correlation coefficient was then calculated for each of the 34,613 transcripts and the corresponding FDR was calculated. Although this analysis may be of very low power (normalization and correlation based on 6 data points – three replicates for each developmental stage) and some statistical hypotheses may not be fulfilled (normality of expression data), we used it to strengthen the evidence of a functional interaction between differentially expressed genes and NdAP3-3. We chose to focus on genes with a Pearson's correlation coefficient ≥ 0.8, which corresponded to an FDR value ≤ 0.26.

Functional category enrichment/depletion among differentially expressed vs. non-differentially expressed genes were tested using Chi-squared contingency tests ($p < 0.001$).

Consistency Between RNA-Sequence Quantitative Data and Quantitative RT-PCR Results

A set of 15 genes were randomly selected for comparison of quantitative expression measured by RNAseq-normalized counts and quantitative RT-PCR. The RNA pools from the three replicates used for RNA-seq were used to synthesize cDNAs for qRT-PCR. Primer pairs were designed from the transcript sequences (**Supplementary Table S1**) and validated by qRT-PCR on a dilution series. Four genes were initially chosen as possible references, based on their stable expression within the range of expression of the 15 genes of interest. After qRT-PCR analysis, we finally selected RN20658, a pentatricopeptide repeat (PPR)-containing protein as the best reference. Relative expression was calculated using the $2^{-\Delta\Delta Ct}$ method.

Identification of Conserved Petal Genes and Homologs of Direct Target Genes of AP3 in *Nigella damascena*

First, we searched the *N. damascena* annotated transcriptome for homologs of the *A. thaliana* genes (AGI-ID) whose expression is correlated with that of MADS-box genes of the ABCE model (**Supplementary Table S4**). This was done using the Expression Angler program and the AtGenExpress Plus - Extended tissue Compendium data set (Toufighi et al., 2005), as previously described (Damerval et al., 2019).

Second, we focused on genes involved in petal formation in *Arabidopsis* and searched for their homologs in the *Nigella* transcriptome. These genes are often members of gene families and functional diversification may be species specific.

Therefore, for each gene of the *Nigella* transcriptome, we sorted the 10 best AGI-ID hits to identify homology with any member of *Arabidopsis* petal gene families. The obtained dataset was then filtered using two different AGI-ID lists to identify *Nigella* homologs of *Arabidopsis* genes that were (i) co-expressed with *AtAP3*, and/or (ii) differentially expressed between the wild type and the *ap3.3* mutant in flowers. The first AGI-ID list was composed of the 100 best positively and 100 best negatively correlated genes to *AtAP3* in *Arabidopsis* (Toufighi et al., 2005), in addition to *AtPI* and *AtAP3* (AtAP3-BCG). The second AGI-ID list contained differentially expressed genes between wild type and mutant regardless of whether they are considered in the literature to be putative direct targets of AtAP3 or not (AtDEG, Mara and Irish, 2008; Wuest et al., 2012). Whereas the first dataset aimed to identify genes associated with petal and stamen development in a broad sense, the second dataset was more specific to the AtAP3 downstream network. Both lists were then used to identify the *Nigella* genes that were homologous, respectively, to the AtAP3-BCG (NdHBCG) and the AtDEG (NdH). Finally, these genes were characterized as (i) being differentially expressed between the two *Nigella* morphs (NdHBCG-DEG and NdH-DEG, respectively) and (ii) having as best homolog, an AtAP3 direct target gene or a paralog of an AtAP3 direct target gene.

Third, to identify additional putative target genes in the set of genes differentially expressed in *Nigella*, we took advantage of the ChIP-sequence analysis of the whole genome of *A. coerulea* for the detection of AP3-3 protein (AcAP3-3) target sequences that was conducted at a late floral developmental stage (Jiang et al., 2020).

RESULTS

Reference Transcriptome Assembly and Functional Annotation

The floral reference transcriptome of *N. damascena* was assembled *de novo* from a pool of transcripts obtained from early developmental stages when organs are initiated to later stages when all organs are formed and are growing (see Material and Methods). 71,319 contigs with a mean length of 1,160 bp and an N50 length of 1843 bp were generated. These parameters were in the same range as those of another *N. damascena* transcriptome elaborated from floral buds, bracts, and leaves (95,758 unigenes, mean length 933 bp, N50 of 1711 bp, Zhang et al., 2020). As expected, compared to the data from the annotated whole genome of another Ranunculaceae species, *A. coerulea* (43,550 transcripts, mean gene length; 1755 bp, N50 length: 2133 bp, https://phytozome.jgi.doe.go), the contigs of our *Nigella* transcriptome were shorter and more numerous. Two factors may account for this difference: our material was heterozygous, and classical assembly tools tend to fall short of complete gene coverage and generate too many smaller than expected contigs.

In the absence of a fully sequenced and annotated genome of *N. damascena*, a total of 53,133 peptides were predicted from 35,409 different transcripts. InterProScan identified 19,347 transcripts encoding peptides with at least one protein domain and a GO annotation. A BLAST search of UniRef90 allowed 5,603 genes to be annotated against 5,751 proteins. Selecting the GO:0003700 (DNA-binding transcription factor activity), we found 355 genes with at least one domain corresponding to 20 types of transcription factors (**Supplementary Figure S1**). Among these, the K-box, AP2/ERF, and basic leucine zipper were the most represented (20, 19, and 15%, respectively). Homologs of all ABCE MADS-box floral genes were found, except for *AP1*.

A high percentage of coding regions could be annotated against *Arabidopsis* (29,877–84%) and *A. coerulea* (30,700–87%) proteins. The GO slim annotation of the *N. damascena* transcriptome was based on homology with *Arabidopsis* genes annotated with *Arabidopsis* GO slim terms (see Material and Methods). The two best-represented categories within biological process were "other cellular processes" (29%) and "other metabolic processes" (20%); within cellular components, the four best-represented categories were "nucleus" (17%), "other cytoplasmic components" (17%), "other intracellular components" (15%), and "chloroplast" (11%); among molecular functions, the best-represented categories were "protein binding" (12%), "hydrolase activity" (11%), and "transferase activity" (13%; **Figure 1**).

Analysis of Differential Gene Expression During Petal Initiation in the Two *Nigella damascena* Floral Morphs

Quantitative RNA-seq was conducted at two early flower developmental stages framing petal initiation, as defined in Jabbour et al. (2015). We compared gene expression in two pools of full-sib F3 genotypes homozygous for the *NdAP3-3* alleles determining the presence (*PP* genotype, P morph) or absence (*pp* genotype, T morph) of petals. Genes that are expressed differentially between the two morphs should therefore include genes from the petal initiation network downstream of *NdAP3-3*, but also a limited number of genes in close linkage disequilibrium with *NdAP3-3* that are expressed at these floral developmental stages.

Based on informative read counts, 34,614 transcripts, which include *NdAP3-3*, were included in the quantitative analysis (**Supplementary Table S2**). We tested the consistency of gene expression patterns observed with RNA-seq counts using qRT-PCR and by randomly choosing a few genes and replicates. Among a set of 14 randomly chosen transcripts and the *NdAP3-3* gene, the expression patterns were similar between the two methods for *NdAP3-3* and 11 of the 14 genes (**Supplementary Figure S2**).

To assess how variability is structured among the 12 (2 morphs x 2 stages x 3 replicates) datasets, a principal component analysis (PCA) was carried out on the expression of the 34,614 genes. The variation in expression between replicates accounted for 31% of the overall variability, while the second axis of the PCA separated developmental stages 1 and 2 (15% of the variability) and the third axis separated the two morphs (9.7%; **Figure 2**; **Supplementary Figure S3**). The relatively high part of variability between replicates may be accounted for by the residual heterozygosity in the F3 generation, even though

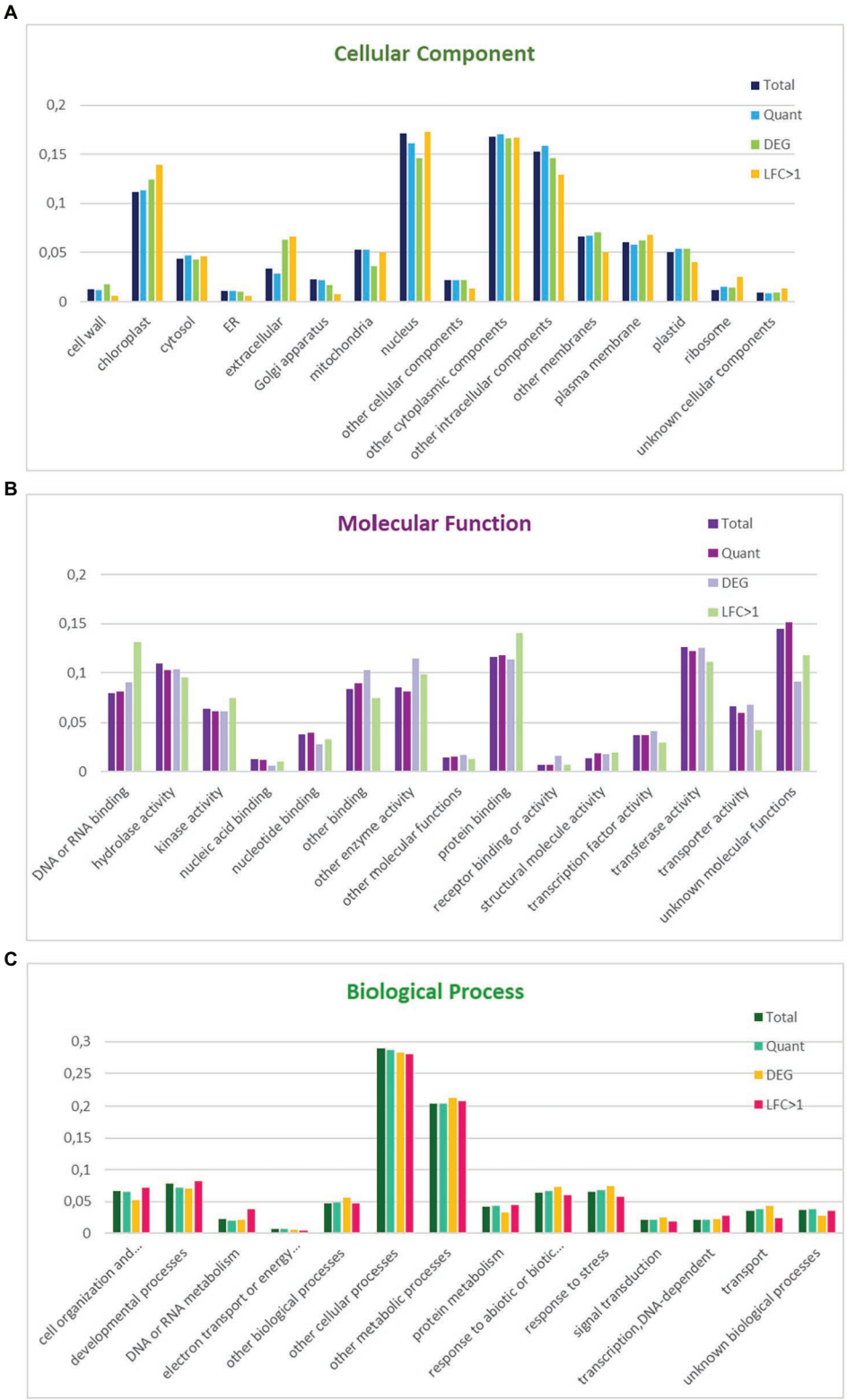

FIGURE 1 | Distribution of GO slim terms in the floral reference transcriptome, the set of informative transcripts used in the quantitative analysis, and the genes differentially expressed between floral morphs in *Nigella damascena*. Distributions are compared within GO cellular component **(A)**, molecular function **(B)**, and biological process **(C)**. Total: reference transcriptome; Quant: transcripts in quantitative analysis; DEG: genes differentially expressed between the two morphs; LFC > 1: most differentially expressed genes between the two morphs.

we tried to homogenize the background by using pools of plants. The developmental stage was the major factor for differential expression. 4,959 genes were differentially expressed (DEGs) between stages 1 and 2 (FDR < 0.05) in at least one of the two genotypes; about half of these (2,133, with twice as many genes showing an increased expression in stage 2 compared with stage 1 than vice versa) were differentially expressed in both genotypes, suggesting that they participate in a general "flower" or "sepal" developmental program but not in petal specification.

To investigate the possible direct or indirect targets of NdAP3-3, we focused on the 1,620 genes that were found to be differentially expressed between morphs at either stage or over both stages on average (FDR < 0.05, **Supplementary Table S3**; **Supplementary Figure S4**). This DEG set between morphs was highly enriched in genes also exhibiting a stage effect (652 genes, 40% vs. 14% of all genes analyzed). The number of DEGs between the two morphs was higher at stage 2 (884 genes) than at stage 1 (580 genes), which is consistent with petal initiation at stage 2 in the P morph, while at stage 2 the T morph produces additional sepal-like primordia. Interestingly, a significant morph by stage interaction was found for 74 transcripts (FDR < 0.05), most of which also exhibited a significant morph effect at one or both stages (63 out of 74). Among the B-function genes, only the three *NdAP3* paralogs were found differentially expressed between the two morphs, *NdAP3-1* (RN021161) at stage 2 but not stage 1, *NdAP3-2* (RN002991) at stage 1 but not stage 2, and *NdAP3-3* (RN035793) at both stages, as expected.

Among these 1,620 DEGs, 739 exhibited at least two-fold difference in expression level between morphs (|M_LFC| > 1) at one or both developmental stages. The most represented GO term within the 243 annotated genes in this set was "nucleus" (GO:0005634, 74 genes), including DNA binding

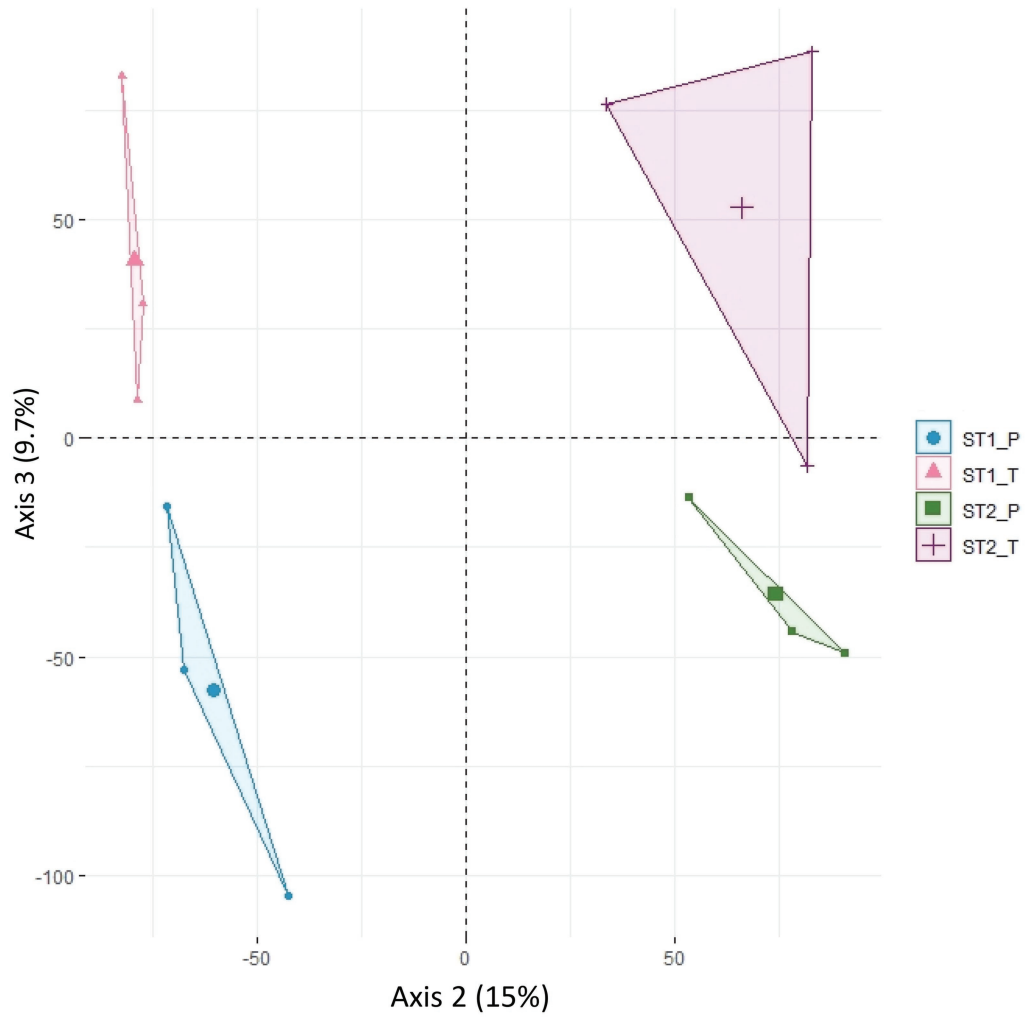

FIGURE 2 | Principal component analysis (PCA) of normalized counts for 34,614 informative transcripts. PCA was done on the four-stage x morph combinations and the three biological replicates. Axis 2 (15% of the variability) separates individuals according to developmental stage (stage 1 vs. stage 2) and axis 3 (9.7% of the variability) separates them according to morph (P morph vs. T morph). ST1_P, ST1_T: individuals at stage 1 of P and T morph, respectively; ST2_P, ST2_T: individuals at stage 2 of P and T morph, respectively.

(GO:0003677), protein binding (GO:0005515), and regulation of transcription activity (GO:0006355). Other than NdAP3-3 (RN035793), homologs of transcription factors, such as Crabs Claw (NdCRC, RN058291); Reduced Vernalization Response 1 (NdVRN1, RN059576); OBP3-responsive gene 2 (NdORG2 with two isoforms, RN057454 and RN012090), and Agamous-like 15 (NdAGL15, RN008012), as well as histones and proteins involved in the maintenance of cell division (RN047478 and RN003149) and several F-Box proteins were found (**Supplementary Table S3**). Differential expression between morphs generally showed the same trend at both stages: 400 genes were more expressed in the T morph than in the P morph (e.g., *NdCRC*), while 275 genes were more expressed in the P morph than in the T morph (e.g., *NdAP3-3*, RN047478 and RN003149) at both developmental stages (**Supplementary Table S3**; **Figure 3**). For 64 transcripts, including homologs of ORG2 genes, the difference in expression between the two morphs was reversed between the two developmental stages (e.g., P > T at stage 1 and T > P at stage 2, **Figure 3**).

To identify the petal gene network in *Nigella*, we searched for the DEGs that were most correlated with wild-type *NdAP3-3* gene expression. We calculated the correlation between the expression of the 34,613 transcripts and the expression of *NdAP3-3* in the P morph, then focused on the correlation values among the set of 739 transcripts with a |M_LFC| > 1. We found 94 transcripts with a Pearson's correlation coefficient ≥ 0.8, which corresponded to an FDR of 26%. Among these, about one-third could be annotated against the *Arabidopsis* proteome. The four most correlated transcripts (|r| > 0.99, FDR < 0.01) were unannotated and likely non-coding (**Supplementary Table S3**).

Forty-nine percent of the differentially expressed genes could not be annotated (792 out of 1,620, **Supplementary Table S3**), mostly because they did not include a coding phase longer

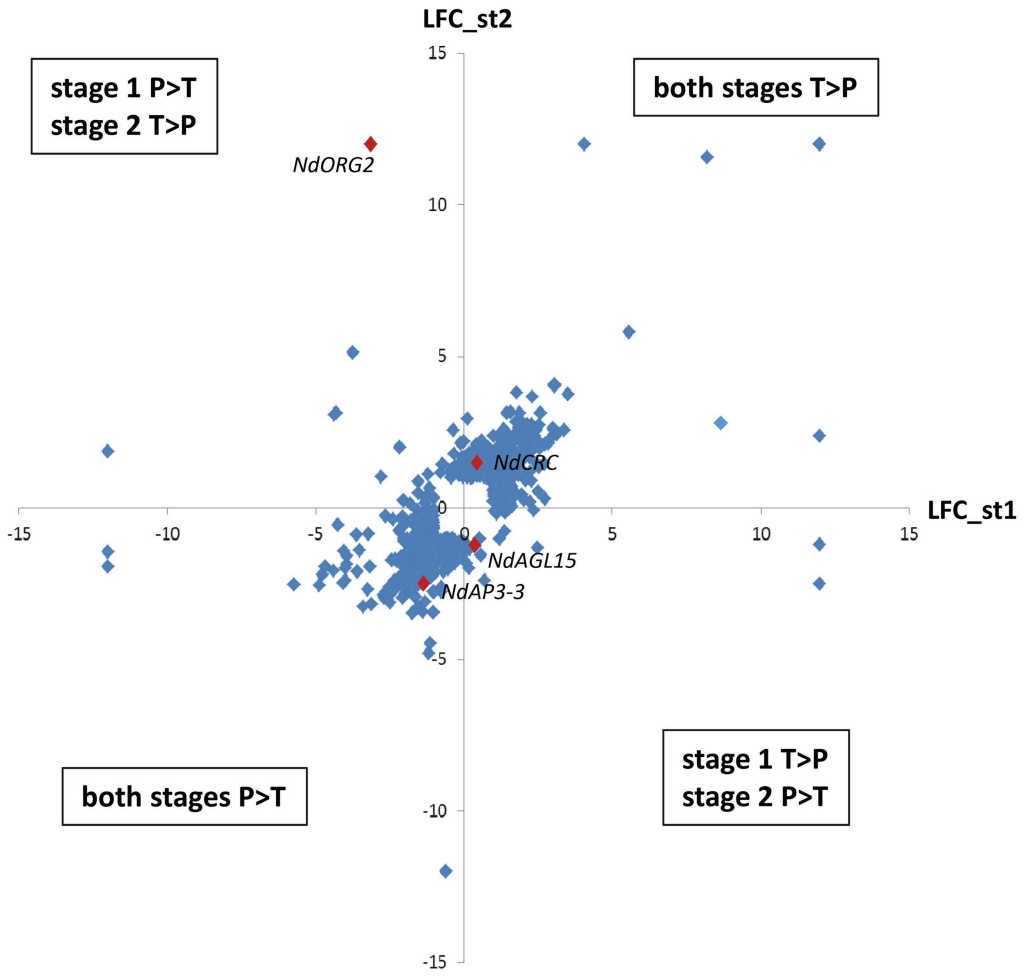

FIGURE 3 | Differential expression between morphs at the two developmental stages for the most differentially expressed genes. Differential expression is expressed by Log2fold change, and only genes with |M_LFC| > 1 at one or both developmental stages are represented. The y-axis represents differential expression between the two morphs at stage 2 and the x-axis represents differential expression at stage 1. The upper right quadrant includes genes more expressed in the T morph at both stages, while the lower left quadrant includes genes more expressed in the P morph at both stages. The two other quadrant group genes that have reversed differential expression between the two morphs at the two stages. Examples of genes illustrating these situations are represented by red diamonds. Genes not expressed at one stage have been arbitrarily attributed M_LFC = +12: (T morph) or −12: (P morph).

than 100 amino acids. This proportion appears significantly less than the proportion in the whole set of quantitatively analyzed transcripts (57%, $p < 0.00001$). The alignment of the unannotated transcripts against the genomic sequence of *A. coerulea* revealed a significant percentage of similarity for 90 transcripts. Additionally, we verified a set of nine transcripts by PCR amplification to check whether they could correspond to *N. damascena* sequences with unknown homology or misassembled transcripts. Three sequences could not be amplified and one gave a mix of two different sequences. For the remaining five sequences, the amplified fragments covered 80.8–89.6% of the total length and corresponded to the expected sequence, with a few single-nucleotide polymorphisms. Among these validated unannotated transcripts, one included a putative coding phase of at least 100 amino acids and four were likely to be non-coding.

Functional Enrichment Analyses

18,883 of the 34,614 transcripts included in the quantitative analysis, including 771 DEGs between the two morphs and 243 genes with a |M_LFC| > 1 could be annotated with GO terms. The proportion of genes represented in the different GO terms was compared between the different gene sets and with the annotation of the whole transcriptome within each of the three major GO slim categories (**Figure 1**). Compared with genes that are not differentially expressed between morphs, the morph DEG set was enriched in the extracellular, cell wall and chloroplast components, other enzyme activities, and receptor binding or receptor activity, and was depleted in mitochondrial components, cell organization, and biogenesis and protein metabolism processes. Interestingly, among the morph DEGs, those with a |M_LFC| > 1 were enriched in ribosome components, DNA or RNA binding, cell organization and biogenesis, and/or DNA or RNA or protein metabolism, and were depleted in transport and response to stress processes (**Figure 1**).

Identification of Conserved Floral Genes and Putative NdAP3-3 Target Genes Using a Comparative Approach

The shared expression patterns that result from functional constraints imposed by the developmental process and the cell microenvironment are good indicators of the conservation of floral gene regulatory networks (Davila-Velderrain et al., 2014). To determine the extent to which the gene network involved in floral organ development is conserved in eudicots, we searched for homologs of genes in *Nigella* with expression patterns that are best correlated (BCGs) with that of ABCE MADS-box genes in *A. thaliana*, as done previously in *Grevillea juniperina* (Damerval et al., 2019). Analysis of the annotated *N. damascena* transcriptome revealed a rate of conservation of BCGs that was identical to that observed in *G. juniperina* using the same approach (**Supplementary Figure S5A**). In addition, *N. damascena* and *G. juniperina* have 75% of their BCGs in common with an *r*-value ≥ 0.75 (**Supplementary Table S5**; Damerval et al., 2019). Homologs of all ABCE genes except *AP1* were found in *N. damascena*, and most of the genes that were highly correlated with them were also conserved between *Nigella* and *Arabidopsis* (**Supplementary Table S5**). Individual analyses of the 25 BCGs showed that on average, 49% of homologs of the ABCE MADS-box correlated genes were conserved. Homologs of *AP1* and *AP3* correlated genes were slightly over-represented, whereas homologs of *AG* and *SEP1/3* correlated genes were under-represented (**Supplementary Figure S5B**). Overall, good conservation of the floral genes is observed between the species.

To be considered as a direct target of a transcription factor, a gene must have a binding signal in its regulatory regions and its expression must be regulated by this protein. In *Arabidopsis*, such a study combining genome-wide site detection and wild type vs. mutant comparison was conducted to identify the target genes of the floral transcription factor AtAP3 (Wuest et al., 2012). Because no genomic data are available in *Nigella*, we opted for a comparative approach, using the *Arabidopsis* data, to identify the putative target genes of NdAP3-3. We searched for homologous genes in *Arabidopsis* and *Nigella* whose expression is altered by the inactivation of their respective AP3 petal identity genes and identify those that are homologs to AtAP3 target genes. Only 20% of the 1,075 DEGs between the *Arabidopsis ap3.3* mutant and wild type (AtDEG, **Supplementary Table S6A**) were found to be direct targets of AtAP3 (Wuest et al., 2012). Among the 4,910 *Nigella* transcripts that are homologous to AtDEG (NdH), 172 were differentially expressed between the two *Nigella* floral morphs (NdH-DEG). Twenty-eight percent of the NdH-DEG were homologous to AtAP3 direct target genes (48 out 172), either as best hits to *Arabidopsis* target genes (23 out 172, 13%) or as a paralog of the target genes (25 out 172, 15%, **Figure 4A**).

The overlapping of the AtAP3-BCG set with that of the conserved DEG set between *Arabidopsis* and *Nigella* (NdH-DEG) was also analyzed to identify the core gene set of the petal development network. When considering the 202 *AtAP3* BCGs (AtAP3-BCG, **Supplementary Table S6B**), only 9% were differentially expressed between mutant and wild type (19 AtBCG-DEG), but almost half (9 out of 19, 47%) were classified as putative direct targets of the AtAP3 protein (**Supplementary Table S6B**). Among the 1,310 *Nigella* transcripts that were homologous to the AtAP3-BCG (NdH-BCG), ~3% (37) were differentially expressed between the two *Nigella* morphs (NdH-BCG-DEG). Within this group, the proportion of homologs of AtAP3 direct target genes was 13% (5 out 37) when considering only the best hits, and 18% (7 out 37) if paralogs of target genes are included (**Figure 4A**).

When restricting the analysis to the set of *Nigella* DEG genes that were the best hits of *Arabidopsis* AtBCG-DEGs and AtDEGs, the percentage of homologs of AtAP3-target genes increased to 45% (5 out of 11, **Supplementary Table S6B**) and 49% (23 out of 47, **Supplementary Table S6A**), respectively. Thus, the highly conserved gene set between the two species seems to be enriched in direct targets of AtAP3 protein. In addition, the expression of the majority of highly conserved homologs is affected in the same way in both the *Arabidopsis ap3.3* and *Nigella NdAP3-3* null mutants, as shown by the LFC in expression level during the early stages of flower development (**Supplementary Table S7**). This further suggests

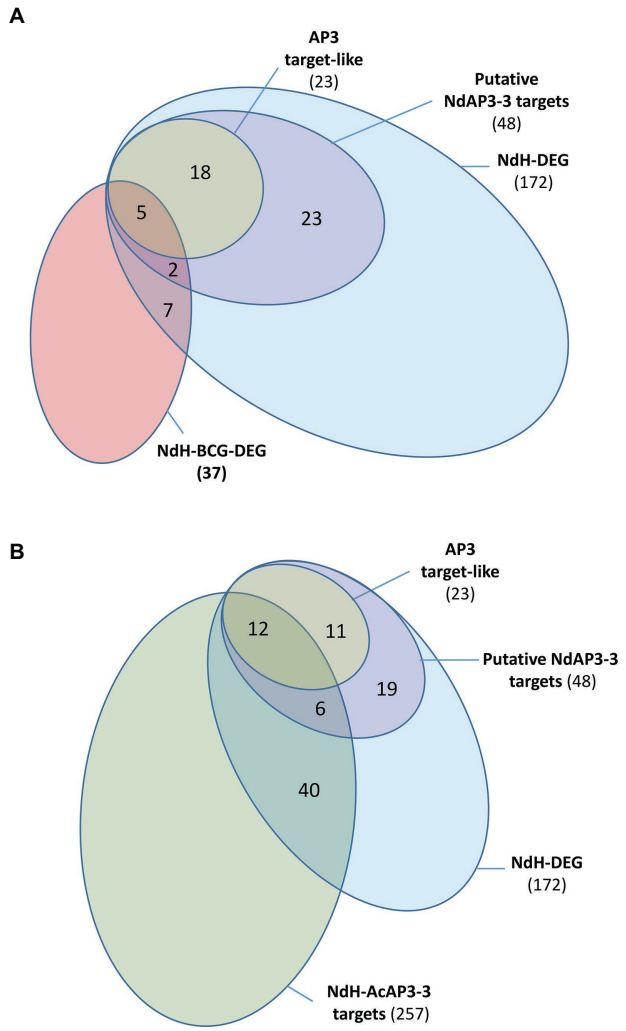

FIGURE 4 | Venn diagram representing the distribution of the *Nigella* transcripts into subcategories. **(A)** NdH-DEG and NdH-BCG-DEG are *Nigella* genes which are differentially expressed between the two morphs and homologous to *Arabidopsis* genes which are differentially expressed between the wild type and the *ap3.3* mutant and the best correlated genes to *AtAP3*, respectively. Putative AP3-3 target genes include the best homologs of the AtAP3 target genes (AP3 target-like) and paralogs of AtAP3 target genes in *Nigella* (see details in **Supplementary Table S6**). **(B)** NdH-AcAP3-3 are the *Nigella* best homologs of the *Aquilegia* AcAP3-3 target genes (see details in **Supplementary Table S8**). The other categories are the same as panel **(A)**.

that these homologs of AtAP3 target genes could be putative direct targets of the NdAP3-3 protein in *N. damascena*. Among these putative conserved target genes, we found the *AP3* paralogs themselves, other transcription factor genes, such as *CRC*, *DRNL*, *AINTEGUMENTA-like 5*, and genes involved in cell wall biogenesis, gibberellin biosynthesis, and signal transduction (**Supplementary Table S7**).

Finally, to identify additional target genes in the set of genes differentially expressed between the two floral morphs in *Nigella*, we carried out a comparative analysis with the AP3-3 (AcAP3-3) target genes detected in the full genome of *A. coerulea*, another Ranunculaceae species (Jiang et al., 2020). Among the 1,620 DEGs found in *Nigella*, 257 were homologous to AcAP3-3 target genes (NdH-AcAP3-3; **Figure 4B**). When considering the set of 172 homologs that are differentially expressed in both *Arabidopsis* and *Nigella* (NdH-DEG), 18 (12+6) putative targets were found conserved between the three species, 30 (19+11) were specific to *Arabidopsis* and *Nigella*, and 239 were specific to *Nigella* and *Aquilegia* (**Supplementary Table S8**). Interestingly, among the target genes that were conserved between the three species, one-third of the *Nigella* genes homologous to a paralog of AtAP3-target genes were found to be the best homologs of an AcAP3-3 target gene (6 out of 18, **Supplementary Table S8**). Among the 239 putative conserved target genes between *Nigella* and *Aquilegia*, 40 genes were homologous to genes that were differentially expressed between the *Arabidopsis* wild type and *ap3.3* mutant although not direct targets of the AtAP3 protein.

DISCUSSION

Petals in Ranunculaceae are believed to have evolved independently of petals in core eudicots (Irish, 2009; Carrive et al., 2020). In both Ranunculaceae and core eudicots, however, B-function genes are instrumental for their identity and development. In Ranunculaceae, of the three AP3 paralogous lineages, the AP3-III orthologs have shown to be key genes for petal identity (Sharma et al., 2011; Gonçalves et al., 2013; Wang et al., 2016). In this study, we took advantage of the spontaneous *NdAP3-3* mutation in *N. damascena* that results in a floral morph without petals to characterize early target genes of NdAP3-3, which determine petal identity and first steps of development. Then we adopted a comparative perspective to address the question of the conservation of this early gene network, using the wealth of knowledge available in *Arabidopsis* as a reference point for core eudicots, and the recently available results obtained from developing petals in *A. coerulea* (Jiang et al., 2020).

Representativeness of the *de novo* Floral Reference Transcriptome Illustrated by ABCE MADS-Box Genes

We found in our transcriptome all the MADS-box genes involved in the *N. damascena* ABCE model of floral organ identity (Wang et al., 2016). In *Arabidopsis*, *AP1* is one of the two genes involved in the A-function. In *N. damascena*, no *AP1* homolog was found, but several isoforms of the *NdAGL6* gene, which from functional analysis is suspected to be an A-function gene (Wang et al., 2016) were identified. The high proportion of homologs of the *Arabidopsis* AP1 best correlated genes in *Nigella* suggests that the A-function network is as represented as the networks of the other functions, even though it may have a different master control gene, possibly *NdAGL6*. The slight overrepresentation of homologs of AP1-BCGs, as well as of AP3-BCGs, could be due to a bias toward early developmental–stage genes and a preponderance of perianth developmental

genes at the expense of reproductive organ genes in the *Nigella* transcriptome (**Supplementary Figure S5B**). This hypothesis could also account for the comparatively slight underrepresentation of homologs of *AG* and possibly *SEP1/3*-correlated genes.

Effect of *NdAP3-3* Mutation on the Expression of Other B-Function Genes at Early Stages of Petal Development

In *Arabidopsis*, the B-function AtAP3 and AtPI proteins interact as a heterodimer to maintain their expression at a high level at late stages. However, their initial expressions are independent (Goto and Meyerowitz, 1994). In *N. damascena*, all the B-function genes are more or less expressed in petal depending on the developmental stage (Gonçalves et al., 2013; Wang et al., 2016). *NdPI1*, which encodes a protein shown to interact with NdAP3-3 in yeast two-hybrid (Wang et al., 2016), was not differentially expressed between morphs during early petal development; no differential expression was observed either for its paralog *NdPI2* (**Supplementary Table S2**). These data further support that their initial expression does not depend on AP3/PI protein–protein interaction, as shown in *Arabidopsis*. By contrast, *NdAP3-2* appeared significantly more expressed in the T morph than the P morph at stage 1, but the increase in expression between stages was higher in the P morph than in the T morph, resulting in no significant difference between morphs at stage 2. The reverse situation was observed for the *NdAP3-1* isoform with no differential expression between morphs at stage 1 but a greater increase in expression in the P morph than in the T morph resulting in a significant difference at stage 2. Thus, the differential expression profiles of *NdAP3-1* and *NdAP3-2* suggest either a regulatory control of their expression by NdAP3-3 (Wang et al., 2016; Jiang et al., 2020), or some kind of interaction between all three NdAP3 proteins that may affect their expression.

Searching for Genes Downstream of AP3 That Are Part of the Petal Identity and Development Networks

Because petals are completely suppressed in the homozygous *NdAP3-3* mutant, we assume that differentially expressed genes between the two homozygous *PP* and *pp* genotypes would include good candidates for petal identity and early development gene network in *N. damascena*. In *Arabidopsis*, AP3/PI heterodimer is bifunctional, acting either as activator or repressor of downstream target genes (Wuest et al., 2012). Interestingly, among the genes differentially expressed between the two floral morphs in *N. damascena*, we found more genes with a higher expression in the T morph than in the P morph, suggesting that NdAP3-3 and the complex it belongs to act more often as a repressor than as an activator at the early stages that we investigated.

Almost 50% of the morph DEGs could not be functionally annotated (**Supplementary Table S3**). Part of these transcripts could be non-coding sequences, or possibly misassembled sequences, a limitation of transcriptome assembly without a reference genome. Based on the results of homology searches in the genome of the closely related species *A. coerulea* and of experimental validation of a small set of unannotated sequences, we make the assumption that about 50% of these transcripts, possibly including non-coding transcripts, would be specific to *N. damascena* and could possibly be involved in species-specific processes. Annotation and GO-term assignment in the most differentially expressed gene set suggested a large involvement of nuclear activities, including regulation of transcription, and an enrichment in processes linked to cell proliferation (ribosome components, DNA or RNA binding, cell organization and biogenesis, and/or DNA or RNA or protein metabolism), which is consistent with the initiation of a novel organ. Most *Arabidopsis* homologous genes specific to or preferentially expressed in the *Nigella* petal at late developmental stages (Zhang et al., 2020) were found in our transcriptome. However, they were not differentially expressed between morphs at the early stages we investigated, supporting the hypothesis that different gene sets and networks operate during development to build the elaborate petal. Within the annotated set of DEGs between morphs, we found a homolog of *CRC*, a carpel developmental gene known to be repressed by B-function genes in early stages of floral development in *Arabidopsis* (Wuest et al., 2012). Consistent with this, we found that *NdCRC* was more expressed in the T morph than in the P morph at both stages. We found a few homologs of genes known to play a role in *Arabidopsis* petal organogenesis *sensu stricto* (Huang and Irish, 2016). A homolog of a DRNL transcription factor, one of the earliest markers of petal initiation, was found to be downregulated in the T morph, and to be a putative target of NdAP3-3 (**Supplementary Table S7**). Conversely, a homolog of KIP-RELATED PROTEIN 7, an inhibitor of petal initiation and cell proliferation, was found upregulated in the mutant. Although a homolog of *BIGPETAL* was found in the *Nigella* transcriptome, it was not differentially expressed between the two morphs. This low number of homologs in *N. damascena* may suggest a lack of functional conservation, but it may also be that the developmental stages investigated are not appropriate to observe an expression and/or an effect of NdAP3-3 on these genes. Indeed, it can be noted that a few of these genes are differentially expressed between the wild type and the *ap3.3* mutant in *Arabidopsis* at developmental stages that are similar to ours (Wuest et al., 2012).

To further investigate the conservation of the petal gene network, we took advantage of the knowledge of the AtAP3 gene network and the large amount of expression data available in *Arabidopsis*. Because the inactivation of *NdAP3-3* alone is sufficient to lose petal identity without affecting stamen identity in *N. damascena*, unlike the *AP3* mutation in *Arabidopsis*, we expected only partial conservation of the gene network between the two species. Among the most conserved set of genes between *Nigella* and *Arabidopsis* (11 NdH-BCG-DEG and 47 NdH-DEG, **Supplementary Table S6**) that are regulated by the *AP3* genes, almost half were homologs of direct targets of the AtAP3 protein, indicating an enrichment of AtAP3 target genes. Potential NdAP3-3 target genes included the three *NdAP3* paralogs, the *NdCRC* gene, as well as genes involved in hormone signaling and morphogenesis (**Supplementary Table S7**).

Early repression of carpel developmental genes could be a conserved function of *AP3* genes (Wuest et al., 2012).

The percentage of target genes of AP3-3 homologous to AtAP3 target genes are in the same range in *A. coerulea* (Jiang et al., 2020) and *N. damascena* (**Figure 4A**). Combining these results, we found a set of 18 potential target genes that were conserved between the three species. Because the developmental stage investigated in *A. coerulea* was quite late, part of early target genes that could be conserved between species could have been missed. Nevertheless, our analyses point to a core set of conserved genes between three species belonging to two divergent clades of eudicots with independently derived petals (Carrive et al., 2020). These genes might encode conserved protein functions and be targeted by the common ancestor protein of the AP3-III and euAP3 lineages. Among these conserved genes, we found again the homologs of *AP3* and other transcription factors, as well as enzymes involved in cell wall biosynthesis (**Supplementary Table S8**). Interestingly, when comparing *Arabidopsis* and the two Ranunculaceae species, we noticed that different paralogs of a gene family could be recruited as the direct target of the AP3 proteins to fulfill a similar function (6 out 18, **Supplementary Table S8**). To confirm these conserved genes as part of the AP3 gene network at an early stage, both additional ChIP- and RNA-seq analyses should be carried out in *A. coerulea*, as well as ChIP-sequence experiments in *N. damascena* when the genome sequence will become available.

The comparative analysis of the *Nigella* differentially expressed genes and the putative target genes of AcAP3-3 revealed a higher conservation of the petal gene network between the two Ranunculaceae species than between them and *Arabidopsis* (**Figure 4B**). This is expected, because petals in Ranunculaceae have been evolved once independently from those of core eudicots (Carrive et al., 2020), and Ranunculaceae and core eudicots diverged around 130 million years ago (Magallón et al., 2015). Interestingly, among these conserved Ranunculaceae putative target genes, we found 40 genes that have *Arabidopsis* homologs with a differential expression between the wild type and the *ap3.3* mutant, but no AP3-binding sites in their regulatory regions, suggesting that they are not direct target genes of the AtAP3 protein. One hypothesis would be that these genes would have a flexible position in the petal gene network and could shift from an AP3 direct-to-indirect target position, depending on the species. New plant models for flower development chosen across the angiosperm phylogeny, and advanced DNA sequencing and analyses methods, should help addressing these hypotheses in the near future.

DATA AVAILABILITY STATEMENT

The datasets presented in this study can be found in online repositories. The names of the repository/repositories and accession number(s) can be found at: https://www.ncbi.nlm.nih.gov/geo/, GSE159429.

AUTHOR CONTRIBUTIONS

YD, NC, CD, DM, and SN designed the study. MG and HC performed the molecular work. LS-T, SB, and JC produced the RNA-seq data. VB, HB, JJ, and ED performed the bioinformatic work. YD, NC, DM, and CD performed the analyses. All authors contributed to the article and approved the submitted version.

FUNDING

This project received financial support from the Institut Diversité, Ecologie et Evolution du Vivant (IDEEV; AAP2013 and AAP2015).

ACKNOWLEDGMENTS

The GQE-Le Moulon and Institute of Plant Sciences Paris-Saclay benefit from the support of the LabExSaclay Plant Sciences-SPS (ANR-10-LABX-0040-SPS). The authors acknowledge H Citerne for helpful comments, and M-L Martin-Magniette and G Rigaill for their advice on the statistical analyses of transcriptomic quantitative data.

SUPPLEMENTARY MATERIAL

The Supplementary Material for this article can be found online at: https://www.frontiersin.org/articles/10.3389/fpls.2021.660803/full#supplementary-material

REFERENCES

Altschul, S. F., Gish, W., Miller, W., Myers, E. W., and Lipman, D. J. (1990). Basic local alignment search tool. *J. Mol. Biol.* 215, 403–410. doi: 10.1016/S0022-2836(05)80360-2

Ambrose, B. A., Lerner, D. R., Ciceri, P., Padilla, C. M., Yanofsky, M. F., and Schmidt, R. J. (2000). Molecular and genetic analyses of the Silky1 gene reveal conservation in floral organ specification between eudicots and monocots. *Mol. Cell* 5, 569–579. doi: 10.1016/S1097-2765(00)80450-5

Ashburner, M., Ball, C. A., Blake, J. A., Botstein, D., Butler, H., Cherry, J. M., et al. (2000). Gene ontology: tool for the unification of biology. The gene ontology consortium. *Nat. Genet.* 25, 25–29. doi: 10.1038/75556

Benjamini, Y., and Hochberg, Y. (1995). Controlling the false discovery rate: a practical and powerful approach to multiple testing. *J. Roy. Soc.* 57, 289–300.

Bey, M., Stüber, K., Fellenberg, K., Schwarz-Sommer, Z., Sommer, H., Saedler, H., et al. (2004). Characterization of Antirrhinum petal development and identification of target genes of the class B MADS box gene DEFICIENS. *Plant Cell* 16, 3197–3215. doi: 10.1105/tpc.104.026724

Bolger, A. M., Lohse, M., and Usadel, B. (2014). Trimmomatic: a flexible trimmer for Illumina sequence data. *Bioinformatics* 30, 2114–2120. doi: 10.1093/bioinformatics/btu170

Carrive, L., Domenech, B., Sauquet, H., Jabbour, F., Damerval, C., and Nadot, S. (2020). Insights into the ancestral flowers of Ranunculales. *Bot. J. Linn. Soc.* 194, 23–46. doi: 10.1093/botlinnean/boaa031

Coen, E., and Meyerowitz, E. M. (1991). The war of the whorls: genetic interactions controlling flower development. *Nature* 353, 31–37. doi: 10.1038/353031a0

Damerval, C., Citerne, H. C., Conde e Silva, N., Deveaux, Y., Delannoy, E., Joets, J., et al. (2019). Unravelling the developmental and genetic mechanisms

underpinning floral architecture in proteaceae. *Front. Plant Sci.* 10:18. doi: 10.3389/fpls.2019.00018

Davila-Velderrain, J., Servin-Marquez, A., and Alvarez-Buylla, E. R. (2014). Molecular evolution constraints in the floral organ specification gene regulatory network module across 18 angiosperm genomes. *Mol. Biol. Evol.* 31, 560–573. doi: 10.1093/molbev/mst223

Di Stilio, V. S., Kramer, E. M., and Baum, D. A. (2005). Floral MADS box genes and homeotic gender dimorphism in *Thalictrum dioicum* (Ranunculaceae) – a new model for the study of dioecy. *Plant J.* 41, 755–766. doi: 10.1111/j.1365-313X.2005.02336.x

Drea, S., Hileman, L. C., de Martino, G., and Irish, V. F. (2007). Functional analyses of genetic pathways controlling petal specification in poppy. *Development* 134, 4157–4166. doi: 10.1242/dev.013136

Eddy, S. R., and Pearson, W. R. (2011). Accelerated profile HMM searches. *PLoS Comput. Biol.* 7:e1002195. doi: 10.1371/journal.pcbi.1002195

Edgar, R., Domrachev, M., and Lash, A. E. (2002). Gene expression omnibus: NCBI gene expression and hybridization array data repository. *Nucleic Acids Res.* 30, 207–210. doi: 10.1093/nar/30.1.207

Gagnot, S., Tamby, J.-P., Martin-Magniette, M.-L., Bitton, F., Taconnat, L., Balzergue, S., et al. (2007). CATdb: a public access to *Arabidopsis* transcriptome data from the URGV-CATMA platform. *Nucleic Acids Res.* 36, D986–D990. doi: 10.1093/nar/gkm757

Galimba, K. D., Martínez-Gómez, J., and Di Stilio, V. S. (2018). Gene duplication and transference of function in the paleoAP3 lineage of floral organ identity genes. *Front. Plant Sci.* 9:334. doi: 10.3389/fpls.2018.00334

Gonçalves, B., Nougué, O., Jabbour, F., Ridel, C., Morin, H., Laufs, P., et al. (2013). An Apetala3 homolog controls both petal identity and floral meristem patterning in *Nigella damascena* L. (Ranunculaceae). *Plant J.* 76, 223–235. doi: 10.1111/tpj.12284

Goto, K., and Meyerowitz, E. M. (1994). Function and regulation of the *Arabidopsis* floral homeotic gene *PISTILLATA*. *Genes Dev.* 8, 1548–1560. doi: 10.1101/gad.8.13.1548

Grabherr, M. G., Haas, B. J., Yassour, M., Levin, J. Z., Thompson, D. A., Amit, I., et al. (2011). Full-length transcriptome assembly from RNA-seq data without a reference genome. *Nat. Biotechnol.* 29, 644–652. doi: 10.1038/nbt.1883

Huala, E., Dickerman, A., Garcia-Hernandez, M., Weems, D., Reiser, L., LaFond, F., et al. (2001). The Arabidopsis information resource (TAIR): a comprehensive database and web-based information retrieval, analysis, and visualization system for a model plant. *Nucleic Acids Res.* 29, 102–105. doi: 10.1093/nar/29.1.102

Huang, T., and Irish, V. F. (2016). Gene networks controlling petal organogenesis. *J. Exp. Bot.* 67, 61–68. doi: 10.1093/jxb/erv444

Irish, V. F. (2009). Evolution of petal identity. *J. Exp. Bot.* 60, 2517–2527. doi: 10.1093/jxb/erp159

Jabbour, F., Udron, M., Le Guilloux, M., Gonçalves, B., Manicacci, D., Nadot, S., et al. (2015). Flower development schedule and AGAMOUS-like gene expression patterns in two morphs of *Nigella damascena* (Ranunculaceae) differing in floral architecture. *Bot. J. Linn. Soc.* 178, 608–619. doi: 10.1111/boj.12297

Jiang, Y., Wang, M., Zhang, R., Xie, J., Duan, X., Shan, H., et al. (2020). Identification of the target genes of AqAPETALA3-3 (AqAP3-3) in *Aquilegia coerulea* (Ranunculaceae) helps understand the molecular bases of the conserved and nonconserved features of petals. *New Phytol.* 227, 1235–1248. doi: 10.1111/nph.16601

Jones, P., Binns, D., Chang, H. Y., Fraser, M., Li, W., McAnulla, C., et al. (2014). InterProScan 5: genome-scale protein function classification. *Bioinformatics* 30, 1236–1240. doi: 10.1093/bioinformatics/btu031

Kaufmann, K., Muiño, J. M., Jauregui, R., Airoldi, C. A., Smaczniak, C., Krajewski, P., et al. (2009). Target genes of the MADS transcription factor SEPALLATA3: integration of developmental and hormonal pathways in the *Arabidopsis* flower. *PLoS Biol.* 7:e1000090. doi: 10.1371/journal.pbio.1000090

Kaufmann, K., Wellmer, F., Muiño, J. M., Ferrier, T., Wuest, S. E., Kumar, V., et al. (2010). Orchestration of floral initiation by APETALA1. *Science* 328, 85–89. doi: 10.1126/science.1185244

Kopylova, E., Noé, L., and Touzet, H. (2012). SortMeRNA: fast and accurate filtering of ribosomal RNAs in metatranscritomic data. *Bioinformatics* 28, 3211–3217. doi: 10.1093/bioinformatics/bts611

Kramer, E. M., Di Stilio, V. S., and Schlüter, P. M. (2003). Complex patterns of gene duplication in APETALA3 and PISTILLATA lineages of the Ranunculaceae. *Int. J. Plant Sci.* 164, 1–11. doi: 10.1086/344694

Kramer, E. M., Dorit, R. L., and Irish, V. F. (1998). Molecular evolution of genes controlling petal and stamen development: duplication and divergence within the APETALA3 and PISTILLATA MADS-box gene lineages. *Genetics* 149, 765–783. doi: 10.1093/genetics/149.2.765

Kramer, E. M., Holappa, L., Gould, B., Jaramillo, M. A., Setnikov, D., and Santiago, P. M. (2007). Elaboration of B gene function to include the identity of novel floral organs in the lower eudicot Aquilegia. *Plant Cell* 19, 750–766. doi: 10.1105/tpc.107.050385

Kramer, E. M., Su, H. J., Wu, C. C., and Hu, J. M. (2006). A simplified explanation for the frameshift mutation that created a novel C-terminal motif in the APETALA3 gene lineage. *BMC Evol. Biol.* 6:30. doi: 10.1186/1471-2148-6-30

Langmead, B., and Salzberg, S. (2012). Fast gapped-read alignment with Bowtie2. *Nat. Methods* 9, 357–359. doi: 10.1038/nmeth.1923

Lee, H. L., and Irish, V. F. (2011). Gene duplication and loss in a MADS box gene transcription factor circuit. *Mol. Biol. Evol.* 28, 3367–3380. doi: 10.1093/molbev/msr169

Magallón, S., Gómez-Acevedo, S., Sánchez-Reyes, L. L., and Hernández-Hernández, T. (2015). A metacalibrated time-tree documents the early rise of flowering plant phylogenetic diversity. *New Phytol.* 207, 437–453. doi: 10.1111/nph.13264

Mara, C. D., and Irish, V. F. (2008). Two GATA transcription factors are downstream effectors of floral homeotic gene action in *Arabidopsis*. *Plant Physiol.* 147, 707–718. doi: 10.1104/pp.107.115634

Mondragón-Palomino, M., and Theissen, G. (2008). MADS about the evolution of orchid flowers. *Trends Plant Sci.* 13, 51–59. doi: 10.1016/j.tplants.2007.11.007

Ó'Maoiléidigh, D. S., Wuest, S. E., Rae, L., Raganelli, A., Ryan, P. T., Kwasniewska, K., et al. (2013). Control of reproductive floral organ identity specification in *Arabidopsis* by the C function regulator AGAMOUS. *Plant Cell* 25, 2482–2503. doi: 10.1105/tpc.113.113209

Pajoro, A., Biewers, S., Dougali, E., Valentim, F. L., Mendes, M. A., Porri, A., et al. (2014). The (r)evolution of gene regulatory networks controlling *Arabidopsis* plant reproduction: a two decades history. *J. Exp. Bot.* 65, 4731–4745. doi: 10.1093/jxb/eru233

Pelaz, S., Tapia-Lopez, R., Alvarez-Buylla, E. R., and Yanofsky, M. F. (2001). Conversion of leaves into petals in *Arabidopsis*. *Curr. Biol.* 11, 182–184. doi: 10.1016/S0960-9822(01)00024-0

Perina, A., González-Tizón, A. M., Meilán, I. F., and Martínez-Lage, A. (2016). De novo transcriptome assembly of shrimp *Palaemon serratus*. *Genom. Data* 11, 89–91. doi: 10.1016/j.gdata.2016.12.009

Rasmussen, D. A., Kramer, E. M., and Zimmer, E. A. (2009). One size fits all? Molecular evidence for a commonly inherited petal identity program in Ranunculales. *Am. J. Bot.* 96, 96–109. doi: 10.3732/ajb.0800038

Rhee, S. Y., Beavis, W., Berardini, T. Z., Chen, G., Dixon, D., Doyle, A., et al. (2003). The Arabidopsis information resource (TAIR): a model organism database providing a centralized, curated gateway to *Arabidopsis* biology, research materials and community. *Nucleic Acids Res.* 31:224. doi: 10.1093/nar/gkg076

Robinson, M. D., McCarthy, D. J., and Smyth, G. K. (2010). EdgeR: a bioconductor package for differential expression analysis of digital gene expression data. *Bioinformatics* 26, 139–140. doi: 10.1093/bioinformatics/btp616

Ronse de Craene, L. P., and Brockington, S. F. (2013). Origin and evolution of petals in angiosperms. *Plant Ecol. Evol.* 146, 5–25. doi: 10.5091/plecevo.2013.738

Roy, N. S., Kim, J. A., Choi, A. Y., Ban, Y. W., Park, N. I., Park, K. C., et al. (2018). RNA-seq de novo assembly and differential transcriptome analysis of Korean medicinal herb *Cirsium japonicum* var. *spinossimum*. *Genomics Inform.* 16:e34. doi: 10.5808/GI.2018.16.4.e34

Sauquet, H., von Balthazar, M., Magallón, S., Doyle, J. A., Endress, P. K., Bailes, E. J., et al. (2017). The ancestral flower of angiosperms and its early diversification. *Nat. Commun.* 8:16047. doi: 10.1038/ncomms16047

Sharma, B., Guo, C., Kong, H., and Kramer, E. M. (2011). Petal-specific subfunctionalization of an APETALA3 paralog in the Ranunculales and its implications for petal evolution. *New Phytol.* 191, 870–883. doi: 10.1111/j.1469-8137.2011.03744.x

Sharma, B., and Kramer, E. M. (2013). Sub- and neo-functionalization of APETALA3 paralogs have contributed to the evolution of novel floral organ identity in *Aquilegia* (columbine, Ranunculaceae). *New Phytol.* 197, 949–957. doi: 10.1111/nph.12078

Suzek, B. E., Wang, Y., Huang, H., McGarvey, P. B., Wu, C. H., and the UniProt Consortium (2015). UniRef clusters: a comprehensive and scalable alternative for improving sequence similarity searches. *Bioinformatics* 31, 926–932. doi: 10.1093/bioinformatics/btu739

The Gene Ontology Consortium (2001). Creating the gene ontology resource: design and implementation. *Genome Res.* 11, 1425–1433. doi: 10.1101/gr.180801

Theißen, G., and Gramzow, L. (2016). "Structure and evolution of plant MADS domain transcription factors," in *Plant Transcription Factors: Evolutionary, Structural and Functional Aspects. Vol. 2016*. ed. D. H. Gonzalez (Philadelphia: Elsevier), 127–138.

Theißen, G., Melzer, R., and Rümpler, F. (2016). MADS-domain transcription factors and the floral quartet model of flower development: linking plant development and evolution. *Development* 143, 3259–3271. doi: 10.1242/dev.134080

Thomson, B., Zheng, B., and Wellmer, F. (2017). Floral organogenesis: when knowing your ABCs is not enough. *Plant Physiol.* 173, 56–64. doi: 10.1104/pp.16.01288

Toufighi, K., Brady, S. M., Austin, R., Ly, E., and Provart, N. J. (2005). The botany Array resource: e-northern, expression angling, and promoter analyses. *Plant J.* 43, 153–163. doi: 10.1111/j.1365-313X.2005.02437.x

Toxopéus, H. J. (1927). Erblichkeitsuntersuchungen an *Nigella damascena* L. *Genetica* 9, 341–440. doi: 10.1007/BF01508296

Wang, P., Liao, H., Zhang, W., Yu, X., Zhang, R., Shan, H., et al. (2016). Flexibility in the structure of spiral flowers and its underlying mechanisms. *Nat. Plants* 2:15188. doi: 10.1038/NPLANTS.2015.188

Wuest, S. E., O'Maoileidigh, D. S., Rae, L., Kwasniewska, K., Raganellia, A., Hanczaryk, K., et al. (2012). Molecular basis for the specification of floral organs by APETALA3 and PISTILLATA. *Proc. Natl. Acad. Sci. U. S. A.* 109, 13452–13457. doi: 10.1073/pnas.1207075109

Yan, W., Chen, D., and Kaufmann, K. (2016). Molecular mechanisms of floral organ specification by MADS domain proteins. *Curr. Opin. Plant Biol.* 29, 154–162. doi: 10.1016/j.pbi.2015.12.004

Zahn, L. M., Leebens-Mack, J., dePamphilis, C. W., Ma, H., and Theissen, G. (2005). To B or not to B a flower: the role of DEFICIENS and GLOBOSA Orthologs in the evolution of the angiosperms. *J. Hered.* 96, 225–240. doi: 10.1093/jhered/esi033

Zdobnov, E. M., and Apweiler, R. (2001). InterProScan - an integration platform for the signature-recognition methods in InterPro. *Bioinformatics* 17, 847–848. doi: 10.1093/bioinformatics/17.9.847

Zhang, R., Fu, X., Zhao, C., Cheng, J., Liao, H., Wang, P., et al. (2020). Identification of the key regulatory genes involved in elaborate petal development and specialized character formation in *Nigella damascena* (Ranunculaceae). *Plant Cell* 32, 3095–3311. doi: 10.1105/tpc.20.00330

Zhang, R., Guo, C., Zhang, W., Wang, P., Li, L., Duan, X., et al. (2013). Disruption of the petal identity gene APETALA3-3 is highly correlated with loss of petals within the buttercup family (Ranunculaceae). *Proc. Natl. Acad. Sci. U. S. A.* 13, 5077–5079. doi: 10.1073/pnas.1219690110

Zheng, Y., Zhao, L., Gao, J., and Fei, Z. (2011). iAssembler: a package for de novo assembly of Roche-454/sanger transcriptome sequences. *BMC Bioinform.* 12:453. doi: 10.1186/1471-2105-12-453

Conflict of Interest: The authors declare that the research was conducted in the absence of any commercial or financial relationships that could be construed as a potential conflict of interest.

frontiers in Plant Science

MINI REVIEW
published: 06 July 2021
doi: 10.3389/fpls.2021.709360

Do Epigenetic Timers Control Petal Development?

*Ruirui Huang[1], Tengbo Huang[2] and Vivian F. Irish[1,3]**

[1] Department of Molecular, Cellular and Developmental Biology, Yale University, New Haven, CT, United States, [2] Guangdong Provincial Key Laboratory for Plant Epigenetics, Longhua Bioindustry and Innovation Research Institute, College of Life Sciences and Oceanography, Shenzhen University, Shenzhen, China, [3] Department of Ecology and Evolutionary Biology, Yale University, New Haven, CT, United States

Epigenetic modifications include histone modifications and DNA methylation; such modifications can induce heritable changes in gene expression by altering DNA accessibility and chromatin structure. A number of studies have demonstrated that epigenetic factors regulate plant developmental timing in response to environmental changes. However, we still have an incomplete picture of how epigenetic factors can regulate developmental events such as organogenesis. The small number of cell types and the relatively simple developmental progression required to form the *Arabidopsis* petal makes it a good model to investigate the molecular mechanisms driving plant organogenesis. In this minireview, we summarize recent studies demonstrating the epigenetic control of gene expression during various developmental transitions, and how such regulatory mechanisms can potentially act in petal growth and differentiation.

Keywords: petal, organogenesis, *Arabidopsis*, epigenetic regulation, histones

OPEN ACCESS

Edited by:
Patrick Laufs,
Institut National de la Recherche Agronomique (INRA), France

Reviewed by:
Marcelo Carnier Dornelas, State University of Campinas, Brazil
Toshiro Ito, Nara Institute of Science and Technology (NAIST), Japan

***Correspondence:**
Vivian F. Irish
vivian.irish@yale.edu

Specialty section:
This article was submitted to Plant Development and EvoDevo, a section of the journal Frontiers in Plant Science

Received: *13 May 2021*
Accepted: *14 June 2021*
Published: *06 July 2021*

Citation:
Huang R, Huang T and Irish VF (2021) Do Epigenetic Timers Control Petal Development? Front. Plant Sci. 12:709360. doi: 10.3389/fpls.2021.709360

INTRODUCTION

The formation of petals, like plant organogenesis in general, occurs *via* a period of cell division followed by post-mitotic cell expansion (Powell and Lenhard, 2012) and entails precise spatiotemporal control of gene expression. The *Arabidopsis* petal is a well- studied simple laminar organ with few cell types, making it an excellent model for understanding the mechanisms underlying plant organogenesis (Irish, 2008). A number of gene regulatory networks have been identified that act early in petal development to promote cell proliferation, and a largely distinct set of genes have been shown to participate in the later phases of cell expansion (Li et al., 2016). This transition is undoubtedly regulated by a wide variety of gene products, with a number of TEOSINTE BRANCHED1/CYCLOIDEA/PCF (TCP) transcription factors likely playing a prominent role in the temporal control of cell proliferation arrest (Czesnick and Lenhard, 2015). Despite the identification of genes and regulatory pathways regulating different phases of petal growth, the mechanisms that control this developmental shift are still largely unknown. We will discuss the possibility that epigenetic mechanisms underlie the regulation of this temporal shift, particularly in the maintenance of expression of key genes controlling early petal development.

EPIGENETIC MODIFICATIONS AND GENE TRANSCRIPTION

"Epigenetic" refers to heritable changes in gene expression that are not due to changes in DNA sequence (Berger et al., 2009). In eukaryotes, DNA is packaged into chromatin, which is organized into nucleosomes that contain an octamer of histone proteins wrapped by 146 bp of DNA (Hollender and Liu, 2008). Alterations in the organization of chromatin, caused by

post-translational modifications of histone proteins or DNA methylation, can affect the accessibility of chromatin to the transcriptional machinery, resulting in changes of gene expression (Sims and Reinberg, 2008). Such epigenetic changes can impact DNA replication, cell proliferation and gene transcription (Suganuma and Workman, 2008). In particular, histone modifications can alter chromatin structure directly by altering chromatin accessibility or by influencing the recruitment of effector proteins (Strahl and Allis, 2000; Karlic et al., 2010).

The amino termini of the core histones in nucleosomes are substrates of covalent modifications including acetylation, methylation, ubiquitylation, phosphorylation and SUMOylation (Roguev et al., 2001). These various modifications constitute a specific "histone code" to regulate gene expression by instructing the chromatin configuration to be either "open" or "closed" (Iñiguez-Lluhí, 2006; Lee et al., 2010). For example, histone acetylation allows the chromatin to relax and provides transcription factors and RNA polymerases access to the DNA, whereas SUMOylation appears to repress gene expression through compacting the chromatin (Iñiguez-Lluhí, 2006). By contrast, the effects of methylation and ubiquitylation depend on the residues being modified and their contexts. For example, trimethylation of lysine 27 of histone H3 (H3K27me3) catalyzed by PcG (Polycomb-group) proteins is a repressive histone modification mark, whereas methylation of lysine 4 of histone H3 (H3K4me) is an active histone modification in plants (Zhang et al., 2009).

Histone acetylation is widely studied and of particular importance to plant development, defense and adaptation (Hollender and Liu, 2008). Histone acetyltransferases (HATs) and histone deacetylases (HDACs) are enzymes required to catalyze histone acetylation and deacetylation, respectively. Many of the HATs and HDACs are components of large multisubunit complexes, which are recruited to gene promoters by DNA-bound proteins (Howe et al., 2001). For example, HDA19, a member of the RPD3/HDA1 family of HDACs, interacts with the TOPLESS (TPL) co-repressor complex and is recruited by transcription factors to specific sites on the DNA to repress gene transcription (Krogan et al., 2012; Wang et al., 2013; Oh et al., 2014). Characterization of HDAC mutants in *Arabidopsis* has indicated that the members of the RPD3/HDA1 family of HDACs play a vital role in regulating gene expression in various biological processes (Liu et al., 2014). For instance, HDA19 was shown to repress the transcription of *AGAMOUS* in the outer whorl floral organs (Krogan et al., 2012), and to repress the expression of *CIRCADIAN CLOCK ASSOCIATED 1* (*CCA1*) in controlling the circadian period (Wang et al., 2013); both processes relying on the interaction of HDA19 with the TPL co-repressor.

EPIGENETIC MEMORY AND PLANT DEVELOPMENTAL TIMING

Plants can alter gene expression in response to environmental cues and such changes in gene expression can be maintained by epigenetic memory. Once the particular state of the cell is established, the epigenetic marks can act as codes to impart expression information from the mother cell to the daughter cell and even from generation to generation (D'Urso and Brickner, 2014). In *Arabidopsis*, cold exposure (vernalization) triggers epigenetic silencing of the floral repressor *FLOWERING LOCUS C (FLC)* and in turn makes the plants competent to flower (Angel et al., 2011). The silencing of *FLC* is achieved by the replacement of active histone modifications with repressive histone modifications across the *FLC* locus. Specifically, active histone modifications such as trimethylation of lysine 36 on histone H3 (H3K36me3) across the gene body are replaced by the repressive histone modification mark H3K27me3 (Berry and Dean, 2015; Tao et al., 2017). Upon returning to warmth, *FLC* repression is epigenetically maintained at the reproductive stage including in sperm and egg cells (Berry and Dean, 2015; **Figure 1**). Epigenetic marks that accumulate at the *FLC* locus during vernalization need to be reset to ensure proper development of the next generation (Feng et al., 2010; Moazed, 2011). The seed specific transcription factor LEAFY COTYLEDONI (LEC1) *de novo* activates gene expression of *FLC* in the pre-embryo stage by reversing the silenced chromatin inherited from gametes to an active state (Tao et al., 2017). Interestingly, the LEC1-induced active epigenetic memory on *FLC* can be transmitted to post-embryonic stages, even well after LEC1 expression dissipates (Tao et al., 2017; **Figure 1**). These observations indicate that the epigenetic memory of an initial transcriptional state can be maintained for some time during plant development.

Epigenetic modifiers also regulate the timing of floral meristem development. In floral meristems, the balance between the rates of stem cell proliferation and differentiation ensures a specific size and number of floral organs (sepals, petals, stamens and carpels) (Sun et al., 2009). In *Arabidopsis*, stem cell identity is maintained by *WUSCHEL (WUS)*, whereas the termination of stem cell identity is achieved by zinc-finger protein KNUCKLES (KNU) induced repression of *WUS* (Sun et al., 2009). *KNU* is transcriptionally activated by the floral homeotic protein AGAMOUS (AG) (**Figure 2A**). In turn, the timing of the initiation of AG expression depends on the upregulation of the LEAFY transcription factor, which is itself upregulated in response to environmental signals that induce a feedforward loop to maintain the floral transition (Parcy et al., 1998; Busch et al., 1999; Jaeger et al., 2013). The timing of this activation is key in balancing stem cell proliferation and differentiation during floral organogenesis. The action of AG in inducing *KNU* expression requires about 2 days during which the repressive histone modification mark H3K27me3 across the *KNU* locus is removed (Sun et al., 2009). Furthermore, AG binding to the *KNU* promoter displaces PcG proteins from the locus and lead to cell division-dependent induction of *KNU* expression and further repression of *WUS* (Sun et al., 2014; **Figure 2A**). In sum, environmental signals induce a cascade of molecular events that culminate in the precisely orchestrated temporal transition from indeterminate to determinate growth.

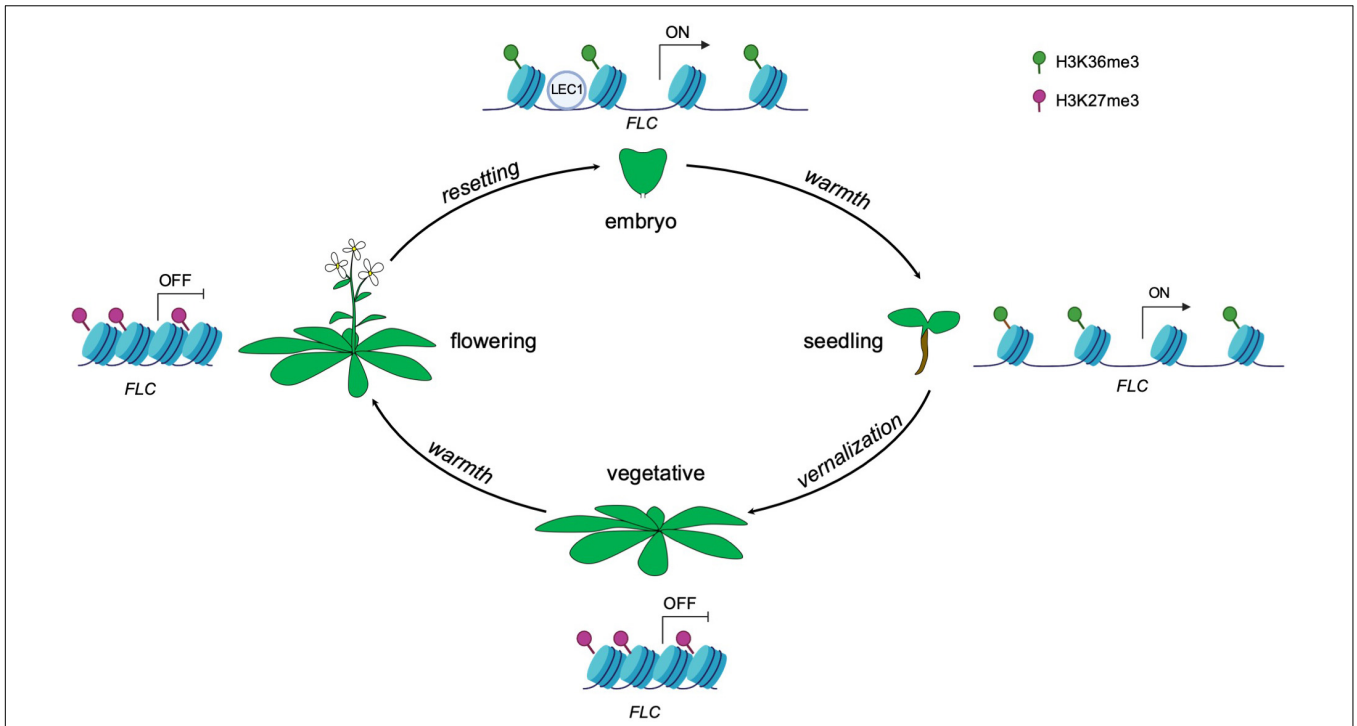

FIGURE 1 | Epigenetic control of *FLC* expression by the seed-specific LEC1 protein throughout the *Arabidopsis* life cycle. Vernalization induces the deposition of the repressive histone modification mark H3K27me3, resulting in a silenced state of *FLC*. The repressive state is maintained even upon returning to warmth. The transcriptional status of *FLC* is reset in each generation during embryogenesis, resulting in the activation of *FLC*. The seed specific transcription factor LEC1 initially activates *FLC* expression by establishment of active histone modification H3K36me3 in early embryogenesis and this active memory is maintained and passed on to post-embryonic stages (seedlings).

EPIGENETIC CONTROL OF PETAL ORGANOGENESIS

After petal primordia initiate, there is a period of cell division followed by a transition to cell expansion and cell differentiation to develop to mature petals (Krizek and Fletcher, 2005). The *RABBIT EARS* (*RBE*) gene encodes a C2H2 zinc finger transcription factor containing an EAR (ERF-associated amphiphilic repression) domain and regulates petal development in *Arabidopsis*. Loss of function *rbe* mutants exhibit underdeveloped petals and absence of petal initiation (Takeda et al., 2011). These strong petal defects make *rbe* an excellent genetic tool to disclose the molecular mechanisms underlying petal development. The *TCP5* gene is a major downstream target of RBE as *tcp5-1* largely rescues the petal defects of *rbe-1* and RBE directly binds to the *TCP5* regulatory region to repress its transcription (Huang and Irish, 2015). *RBE* transcripts are localized in the presumptive petal primordia from the stage 3 to stage 6 and act to promote cell division and establish enough cells with petal identity. This specific expression pattern of *RBE* implies that the alleviation of *TCP5* repression by *RBE* commences at stage 6 (Huang and Irish, 2015). However, *TCP5* transcription is only detectable from stage 11 on during petal development, which suggests a delay of approximately 6 days between alleviation of RBE-mediated repression and activation of *TCP5* expression.

It is possible that RBE represses *TCP5* by inducing chromatin-mediated silencing at that locus. The delay of transcriptional activation of *TCP5* can be explained by the gradual elimination of this chromatin-mediated silencing, which may accompany the transition from cell division to cell expansion during petal development. It has been demonstrated that EAR motif containing proteins such as RBE recruit the TPL-HDA19 co-repressor complex to regulate gene transcription (Kagale and Rozwadowski, 2011). For instance, the EAR-motif containing *APETALA2 (AP2)* gene product recruits both TPL and HDA19 to repress the expression of multiple floral organ identity genes (Krogan et al., 2012). Additionally, EAR motif containing proteins can also interact with PcG proteins. *SUPERMAN (SUP)*, encoding a similar C2H2 zinc finger protein to RBE, can interact with *CURLY LEAF (CLF)*, a PRC2 component, to regulate floral whorl boundaries by controlling the expression of auxin biosynthetic genes (Xu et al., 2018). Furthermore, recent reports indicate that the EAR motif could act as a docking point for the TPL-HDAC and PRC2 complexes which in turn can result in chromatin remodeling at a target locus by increasing H3K27me3 and decreasing H3ac levels (Baile et al., 2020; Pelayo et al., 2021). Thus, EAR motif containing transcription factors might employ multiple layers of epigenetic modifications to maintain long-term repression.

Based on these observations, it is likely that RBE physically interacts with the TOPLESS-HDA19 complex and/or PcG

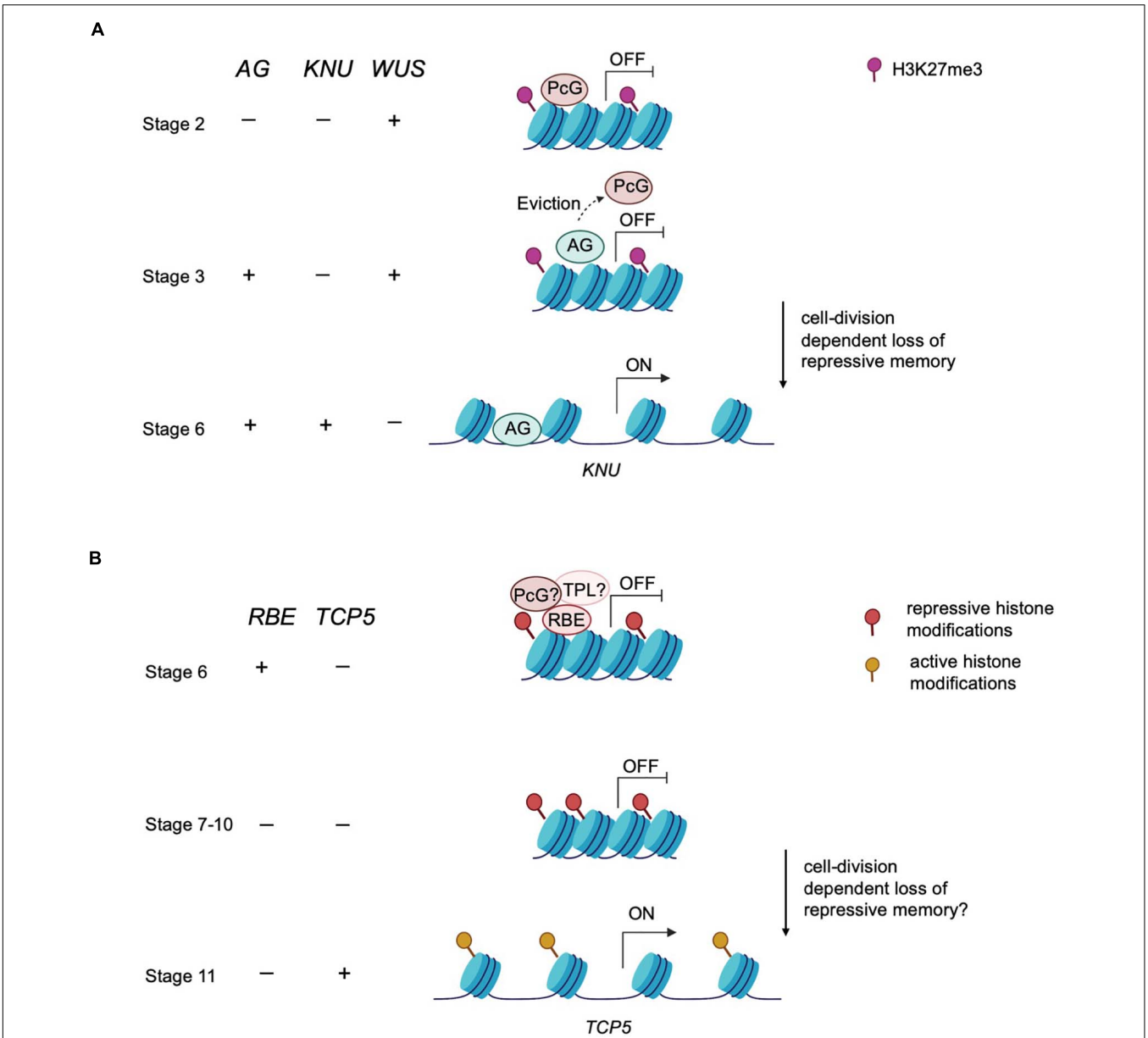

FIGURE 2 | An epigenetic timer regulates floral development. **(A)** Epigenetic control of meristem determinacy. Prior to and during stage 2, repressive H3K27me3 modification catalyzed by the PcG protein is deposited across the *KNU* locus to silence *KNU* expression. At these early stages, *WUS* is expressed and maintains floral meristem stem cell proliferation. At stage 3, AG binds to the *KNU* promoter, evicting the PcG protein from *KNU*. The eviction of PcG protein induces cell division-dependent loss of H3K27me3 on *KNU*, which takes about 2 days. By stage 6, *KNU* is expressed and acts to repress *WUS* transcription and stem cell activity is then terminated. **(B)** Postulated model of epigenetic control of petal development. RBE confers repression on *TCP5* to maintain cell proliferation at early stages of petal development. RBE could repress *TCP5* transcription by recruiting epigenetic modifiers such as TPL or PcG proteins to establish repressive histone modifications across the *TCP5* locus. This repressive memory is proposed to be maintained until about stage 10. By stage 11, *TCP5* transcription is initiated, which is presumed to result from accrual of active histone modifications.

proteins to temporally regulate the expression of *TCP5* during petal development. Furthermore, TOPLESS and HDA19 have been shown to act in maintaining the balance of cell division and cell differentiation. For instance, the product of the *WUSCHEL HOMEOBOX 5 (WOX5)* gene maintains the root meristem niche and prevents cell type differentiation by recruiting TOPLESS and HDA19 to repress *CYCLING DOF FACTOR 4* (*CDF4*) (Pi et al., 2015). Taken together, these results suggest RBE might orchestrate petal cell division and cell expansion by recruiting chromatin modifiers such as TPL or PcG proteins to temporally regulate *TCP5* transcription (**Figure 2B**). Given the role of RBE in orchestrating many aspects of petal development, this presumptive epigenetic timing mechanism could potentially

function to regulate the temporal control of expression of many downstream target genes involved in petal differentiation.

CONCLUSION AND PERSPECTIVE

To our knowledge, epigenetic control mechanisms that regulate aspects of plant development are triggered in response to external cues such as daylength or temperature. We propose here that developmental timing can also occur through a gating mechanism that depends on protein half-life. In other words, the decay of RBE protein over time could function as a timer to alter the epigenetic status of target genes such as *TCP5*, and potentially other target genes as well. It is also possible that other petal regulators containing the EAR motif, such as JAGGED (JAG), might also function by recruiting epigenetic factors to confer temporal control of petal organogenesis (Ohno, 2004; Schiessl et al., 2014). In summary, the temporal control of petal development, and more broadly organ development, may rely in part on the stochastic process of alleviating repressive epigenetic marks over time to control the transition from cell division to post-mitotic cell expansion.

AUTHOR CONTRIBUTIONS

RH, TH, and VFI were contributed to the writing of this review. All authors contributed to the article and approved the submitted version.

FUNDING

Our work on petal organogenesis has been supported by NSF grant IOS-1354389 to VFI, and awards from the Guangdong Basic and Applied Basic Research Foundation (2021A1515011035) and Guangdong Special Support Program for Young Talents in Innovation Research of Science and Technology (2019TQ05N940) to TH.

ACKNOWLEDGMENTS

We thank members of the Irish laboratory for discussions and comments during the course of writing this manuscript.

REFERENCES

Angel, A., Song, J., Dean, C., and Howard, M. (2011). A Polycomb-based switch underlying quantitative epigenetic memory. *Nature* 476, 105–108. doi: 10.1038/nature10241

Baile, F., Merini, W., Hidalgo, I., and Calonje, M. (2020). Dissection of PRC1 and PRC2 recruitment in *Arabidopsis* connects EAR repressome to PRC2 anchoring. *bioRxiv* [Preprint]. doi: 10.1101/2020.08.28.271999

Berger, S. L., Kouzarides, T., Shiekhattar, R., and Shilatifard, A. (2009). An operational definition of epigenetics. *Genes Dev.* 23, 781–783. doi: 10.1101/gad.1787609

Berry, S., and Dean, C. (2015). Environmental perception and epigenetic memory: mechanistic insight through FLC. *Plant J.* 83, 133–148. doi: 10.1111/tpj.12869

Busch, M. A., Bomblies, K., and Weigel, D. (1999). Activation of a floral homeotic gene in *Arabidopsis*. *Science* 285, 585–587. doi: 10.1126/science.285.5427.585

Czesnick, H., and Lenhard, M. (2015). Size control in plants–lessons from leaves and flowers. *Cold Spring Harb. Perspect. Biol.* 7:a019190. doi: 10.1101/cshperspect.a019190

D'Urso, A., and Brickner, J. H. (2014). Mechanisms of epigenetic memory. *Trends Genet.* 30, 230–236. doi: 10.1016/j.tig.2014.04.004

Feng, S., Jacobsen, S. E., and Reik, W. (2010). Epigenetic reprogramming in plant and animal development. *Science* 330, 622–627. doi: 10.1126/science.1190614

Hollender, C., and Liu, Z. (2008). Histone deacetylase genes in *Arabidopsis* development. *J. Integr. Plant Biol.* 50, 875–885. doi: 10.1111/j.1744-7909.2008.00704.x

Howe, L., Auston, D., Grant, P., John, S., Cook, R. G., Workman, J. L., et al. (2001). Histone H3 specific acetyltransferases are essential for cell cycle progression. *Genes Dev.* 15, 3144–3154. doi: 10.1101/gad.931401

Huang, T., and Irish, V. F. (2015). Temporal control of plant organ growth by TCP transcription factors. *Curr. Biol.* 25, 1765–1770. doi: 10.1016/j.cub.2015.05.024

Iñiguez-Lluhí, J. A. (2006). For a healthy histone code, a little SUMO in the tail keeps the acetyl away. *ACS Chem. Biol.* 1, 204–206. doi: 10.1021/cb600188m

Irish, V. F. (2008). The *Arabidopsis* petal: a model for plant organogenesis. *Trends Plant Sci.* 13, 430–436. doi: 10.1016/j.tplants.2008.05.006

Jaeger, K. E., Pullen, N., Lamzin, S., Morris, R. J., and Wigge, P. A. (2013). Interlocking feedback loops govern the dynamic behavior of the floral transition in *Arabidopsis*. *Plant Cell* 25, 820–833. doi: 10.1105/tpc.113.109355

Kagale, S., and Rozwadowski, K. (2011). EAR motif-mediated transcriptional repression in plants. *Epigenetics* 6, 141–146. doi: 10.4161/epi.6.2.13627

Karlic, R., Chung, H. R., Lasserre, J., Vlahovicek, K., and Vingron, M. (2010). Histone modification levels are predictive for gene expression. *Proc. Natl. Acad. Sci. U.S.A.* 107, 2926–2931. doi: 10.1073/pnas.0909344107

Krizek, B. A., and Fletcher, J. C. (2005). Molecular mechanisms of flower development: an armchair guide. *Nat. Rev. Genet.* 6, 688–698. doi: 10.1038/nrg1675

Krogan, N. T., Hogan, K., and Long, J. A. (2012). APETALA2 negatively regulates multiple floral organ identity genes in *Arabidopsis* by recruiting the co-repressor TOPLESS and the histone deacetylase HDA19. *Development* 139, 4180–4190. doi: 10.1242/dev.085407

Lee, J.-S., Smith, E., and Shilatifard, A. (2010). The language of histone crosstalk. *Cell* 142, 682–685. doi: 10.1016/j.cell.2010.08.011

Li, J., Wang, Y., Zhang, Y., Wang, W., Irish, V. F., and Huang, T. (2016). RABBIT EARS regulates the transcription of *TCP4* during petal development in *Arabidopsis*. *J. Exp. Bot.* 67, 6473–6480. doi: 10.1093/jxb/erw419

Liu, X., Yang, S., Zhao, M., Luo, M., Yu, C.-W., Chen, C.-Y., et al. (2014). Transcriptional repression by histone deacetylases in plants. *Mol. Plant* 7, 764–772. doi: 10.1093/mp/ssu033

Moazed, D. (2011). Mechanisms for the inheritance of chromatin states. *Cell* 146, 510–518. doi: 10.1016/j.cell.2011.07.013

Oh, E., Zhu, J.-Y., Ryu, H., Hwang, I., and Wang, Z.-Y. (2014). TOPLESS mediates brassinosteroid-induced transcriptional repression through interaction with BZR1. *Nat. Commun.* 5:4140. doi: 10.1038/ncomms5140

Ohno, C. K. (2004). The *Arabidopsis* JAGGED gene encodes a zinc finger protein that promotes leaf tissue development. *Development* 131, 1111–1122. doi: 10.1242/dev.00991

Parcy, F., Nilsson, O., Busch, M. A., Lee, I., and Weigel, D. (1998). A genetic framework for floral patterning. *Nature* 395, 561–566. doi: 10.1038/26903

Pelayo, M. A., Yamaguchi, N., and Ito, T. (2021). One factor, many systems: the floral homeotic protein AGAMOUS and its epigenetic regulatory mechanisms. *Curr. Opin. Plant Biol.* 61:102009. doi: 10.1016/j.pbi.2021.102009

Pi, L., Aichinger, E., van der Graaff, E., Llavata-Peris, C. I., Weijers, D., Hennig, L., et al. (2015). Organizer-derived WOX5 signal maintains root columella stem cells through chromatin-mediated repression of *CDF4* expression. *Dev. Cell* 33, 576–588. doi: 10.1016/j.devcel.2015.04.024

Powell, A. E., and Lenhard, M. (2012). Control of organ size in plants. *Curr. Biol.* 22, R360–R367. doi: 10.1016/j.cub.2012.02.010

Roguev, A., Schaft, D., Shevchenko, A., Pijnappel, W. W., Wilm, M., Aasland, R., et al. (2001). The *Saccharomyces cerevisiae* Set1 complex includes an Ash2 homologue and methylates histone 3 lysine 4. *EMBO J.* 20, 7137–7148. doi: 10.1093/emboj/20.24.7137

Schiessl, K., Muino, J. M., and Sablowski, R. (2014). *Arabidopsis* JAGGED links floral organ patterning to tissue growth by repressing Kip-related cell cycle inhibitors. *Proc. Natl. Acad. Sci. U.S.A.* 111, 2830–2835. doi: 10.1073/pnas.1320457111

Sims, R. J., and Reinberg, D. (2008). Is there a code embedded in proteins that is based on post-translational modifications? *Nat. Rev. Mol. Cell Biol.* 9, 815–820. doi: 10.1038/nrm2502

Strahl, B. D., and Allis, C. D. (2000). The language of covalent histone modifications. *Nature* 403, 41–45. doi: 10.1038/47412

Suganuma, T., and Workman, J. L. (2008). Crosstalk among histone modifications. *Cell* 135, 604–607. doi: 10.1016/j.cell.2008.10.036

Sun, B., Looi, L. S., Guo, S., He, Z., Gan, E. S., Huang, J., et al. (2014). Timing mechanism dependent on cell division is invoked by Polycomb eviction in plant stem cells. *Science* 343:1248559. doi: 10.1126/science.1248559

Sun, B., Xu, Y., Ng, K.-H., and Ito, T. (2009). A timing mechanism for stem cell maintenance and differentiation in the *Arabidopsis* floral meristem. *Genes Dev.* 23, 1791–1804. doi: 10.1101/gad.1800409

Takeda, S., Matsumoto, N., and Okada, K. (2011). RABBIT EARS, encoding a SUPERMAN-like zinc finger protein, regulates petal development in *Arabidopsis thaliana*. *Development* 138:3591. doi: 10.1242/dev.072058

Tao, Z., Shen, L., Gu, X., Wang, Y., Yu, H., and He, Y. (2017). Embryonic epigenetic reprogramming by a pioneer transcription factor in plants. *Nature* 551, 124–128. doi: 10.1038/nature24300

Wang, L., Kim, J., and Somers, D. E. (2013). Transcriptional corepressor TOPLESS complexes with pseudoresponse regulator proteins and histone deacetylases to regulate circadian transcription. *Proc. Natl. Acad. Sci. U.S.A.* 110, 761–766. doi: 10.1073/pnas.1215010110

Xu, Y., Prunet, N., Gan, E. S., Wang, Y., Stewart, D., Wellmer, F., et al. (2018). SUPERMAN regulates floral whorl boundaries through control of auxin biosynthesis. *EMBO J.* 37:e97414. doi: 10.15252/embj.201797499

Zhang, X., Bernatavichute, Y. V., Cokus, S., Pellegrini, M., and Jacobsen, S. E. (2009). Genome-wide analysis of mono-, di- and trimethylation of histone H3 lysine 4 in *Arabidopsis thaliana*. *Genome Biol.* 10:R62. doi: 10.1186/gb-2009-10-6-r6

Conflict of Interest: The authors declare that the research was conducted in the absence of any commercial or financial relationships that could be construed as a potential conflict of interest.

frontiers in Plant Science

ORIGINAL RESEARCH
published: 04 August 2021
doi: 10.3389/fpls.2021.718091

14-3-3 Proteins Are Involved in BR-Induced Ray Petal Elongation in *Gerbera hybrida*

Xiaohui Lin[1†], Shina Huang[1†], Gan Huang[1,2], Yanbo Chen[1], Xiaojing Wang[1] and Yaqin Wang[1]*

[1] Guangdong Provincial Key Laboratory of Biotechnology for Plant Development, School of Life Sciences, South China Normal University, Guangzhou, China, [2] College of Landscape Architecture and Art, Henan Agricultural University, Zhengzhou, China

14-3-3 proteins play a major role in the regulation of primary metabolism, protein transport, ion channel activity, signal transduction and biotic/abiotic stress responses. However, their involvement in petal growth and development is largely unknown. Here, we identified and characterized the expression patterns of seven genes of the 14-3-3 family in gerbera. While none of the genes showed any tissue or developmental specificity of spatiotemporal expression, all seven predicted proteins have the nine α-helices typical of 14-3-3 proteins. Following treatment with brassinolide, an endogenous brassinosteroid, the Gh14-3-3 genes displayed various response patterns; for example, *Gh14-3-3b* and *Gh14-3-3f* reached their highest expression level at early (2 h) and late (24 h) timepoints, respectively. Further study revealed that overexpression of *Gh14-3-3b* or *Gh14-3-3f* promoted cell elongation, leading to an increase in ray petal length. By contrast, silencing of *Gh14-3-3b* or *Gh14-3-3f* inhibited petal elongation, which was eliminated partly by brassinolide. Correspondingly, the expression of petal elongation-related and brassinosteroid signaling-related genes was modified in transgenic petals. Taken together, our research suggests that Gh14-3-3b and Gh14-3-3f are positive regulators of brassinosteroid-induced ray petal elongation and thus provides novel insights into the molecular mechanism of petal growth and development.

Keywords: 14-3-3 protein, ray petal elongation, cell elongation, BR, *Gerbera hybrida*

OPEN ACCESS

Edited by:
Elena M. Kramer, Harvard University, United States

Reviewed by:
Adam Saffer, Yale University, United States
Stephanie Conway, Harvard University, United States

***Correspondence:**
Yaqin Wang
wangyaqin@m.scnu.edu.cn

[†] These authors have contributed equally to this work

Specialty section:
This article was submitted to Plant Development and EvoDevo, a section of the journal Frontiers in Plant Science

Received: *31 May 2021*
Accepted: *12 July 2021*
Published: *04 August 2021*

Citation:
Lin X, Huang S, Huang G, Chen Y, Wang X and Wang Y (2021) 14-3-3 Proteins Are Involved in BR-Induced Ray Petal Elongation in Gerbera hybrida. Front. Plant Sci. 12:718091. doi: 10.3389/fpls.2021.718091

INTRODUCTION

14-3-3 proteins, with a molecular weight of 25∼32 kDa, are a class of highly conserved, acidic, soluble proteins that are present in almost all eukaryotes (Ferl, 1996; Mhawech, 2005). Each 14-3-3 isoform contains nine α-helices and shows a high degree of similarity to other 14-3-3 members (Aitken, 2006). As bridge proteins, they participate widely in the regulation of various physiological processes (including metabolism, hormone signaling and stress response) by interacting with numerous clients, such as metabolic enzymes, signaling proteins and transcription factors (Silva et al., 2001; Chevalier et al., 2009; Zhou et al., 2015; Li M. et al., 2016; Keicher et al., 2017; Camoni et al., 2018). Generally, 14-3-3 proteins, which are encoded by multiple genes in most species (Denison et al., 2011), bind to their clients via two sequence motifs (RSXpSXP and RXXXpSXP)

to activate or inhibit the activity of their target proteins (Sehnke et al., 2002). The first plant 14-3-3 protein identified was cloned from maize (de Vetten et al., 1992). In Arabidopsis, there are thirteen functionally expressed *14-3-3* genes (Chevalier et al., 2009), while tobacco has seventeen potential isoforms, rather more than the eight genes in rice and seven in cotton (Konagaya et al., 2004; Chen et al., 2006; Zhou et al., 2015). According to their gene structure, 14-3-3 proteins can be divided into two groups, termed ε and non-ε (DeLille et al., 2001; Konagaya et al., 2004; Chen et al., 2006; Chevalier et al., 2009).

Brassinosteroids (BRs) are plant steroid hormones that play key roles in regulating a variety of physiological processes, including leaf expansion, flowering, senescence, stress resistance and cell expansion and elongation (Clouse et al., 1996; Clouse and Sasse, 1998; Yang et al., 2011; Kim et al., 2012; Kaneko-Suzuki et al., 2018; Oh et al., 2020). BR signal cascades are well characterized in Arabidopsis, in which BZR1 is the key transcription factor, affecting plant growth and development by modulating thousands of BR target genes and interacting with other hormone signaling components (He et al., 2005; Wang et al., 2012; Qiao et al., 2017; Zheng et al., 2019; Zhang et al., 2020). 14-3-3 proteins are also important regulatory components of the BR signaling pathway: they regulate plant growth by anchoring BZR1 in the cytoplasm (Gampala et al., 2007; Ryu et al., 2007; Kim and Wang, 2010). Mutants of the 14-3-3-binding site of BZR1, with a phenotype similar to that of the *bzr1-1D* mutant, show a constitutive BR response and an increase in BZR1 nuclear retention (Gampala et al., 2007; Ryu et al., 2007).

The 14-3-3 proteins involved in BR signaling participate in plant growth and flowering processes by modulating cell differentiation and elongation (Pertl et al., 2010; Zhang et al., 2010; Taoka et al., 2011; Zhou et al., 2015; Kaneko-Suzuki et al., 2018; Minami et al., 2019). Analysis of multiple *14-3-3* mutants revealed their specificity and functional redundancy in primary root elongation under different environmental conditions, in which these genes are positive regulators under control conditions and negative regulators during abiotic stress (van Kleeff et al., 2014). In lily (*Lilium longiflorum*), 14-3-3 proteins were shown to play a role in the germination and elongation of pollen (Pertl et al., 2010). Minami et al. (2019) reported that, during BR-induced hypocotyl elongation, a 14-3-3 protein interacts with the phosphorylated C-terminus, and thereby enhances the catalytic activity, of plasma membrane H^+-ATPase. In addition, 14-3-3 proteins have a regulatory role in cotton fiber elongation (Zhou et al., 2015). Thus, overexpression of *14-3-3L* promotes fiber elongation in cotton, while gene silencing of *14-3-3L* results in a shortening of cotton fiber length (Zhou et al., 2015). Recently, Zuo et al. (2021) identified eighteen *14-3-3* genes in the apple genome and characterized their expression patterns, suggesting that some of them may participate in the regulation of the flowering process. These results all highlight the importance of 14-3-3 proteins in plant growth.

Gerbera hybrida, belonging to the Asteraceae family, is one of the mainstream cut flowers and its commercial and ornamental value depend on petal morphology and color (Bhatia et al., 2009; Mosqueda Frómeta et al., 2017). Thus, it is important to understand the regulatory mechanisms governing gerbera petal morphology. The research team of Prof. Elomaa has focused on the molecular mechanisms of flower development in Asteraceae, including *G. hybrida*, for many years (Kotilainen et al., 1999; Broholm et al., 2008; Tahtiharju et al., 2012; Juntheikki-Palovaara et al., 2014; Zhao et al., 2020; Zhang et al., 2021). Broholm et al. (2008) found that overexpression of *GhCYC2* in gerbera results in conversion of disc florets into ray-like florets with elongated petals, as well as disruption of stamen development. Functional analysis of GhCYC proteins revealed redundant functions of GhCYC2, GhCYC3 and GhCYC4 in regulating ray floret identity and in promoting petal development (Juntheikki-Palovaara et al., 2014). Various hormones (gibberellin, abscisic acid, ethylene, and BRs) are involved in the regulation of late-stage petal development in gerbera (Zhang et al., 2012; Li et al., 2015; Han et al., 2017; Huang et al., 2017, 2020; Ren et al., 2018). Li et al. (2015) found that GA_3 stimulates petal elongation in gerbera, while ABA inhibits it. Further research showed that GhWIP2, a WIP-type ZFP transcription factor, represses cell expansion during petal and leaf development by modulating crosstalk between gibberellin, abscisic acid and auxin (Ren et al., 2018). Another study found that exogenous brassinolide (BL) treatment can boost the elongation of ray floret petals, whereas BRZ (a BR synthesis inhibitor) reduces petal length (Huang et al., 2017). However, whether 14-3-3 proteins, as one of the BR signaling components, play a regulatory role in BR-induced petal elongation in gerbera, or indeed in any other flowering species, remains unknown.

Here, seven gerbera 14-3-3 genes were identified and their predicted proteins classified. The expression patterns of all seven genes were comprehensively investigated in various tissues and at different developmental stages. Overexpressing two of these genes, *Gh14-3-3b* and *Gh14-3-3f*, in ray florets increased petal length by promoting cell elongation, whereas gene silencing of *Gh14-3-3b* or *Gh14-3-3f* reduced petal growth. Further analysis found that several BR-related genes, such as BZR1 homologs (*GhBEH1* and *GhBEH2*) and petal elongation-associated genes (like *GhEXP1*, *GhEXP3*, *GhEXP10*, *GhXTH1*, and *GhXET*), were modified in transgenic petals. These results demonstrate a positive regulatory role of Gh14-3-3b and Gh14-3-3f in BR-induced ray petal elongation.

MATERIALS AND METHODS

Plant Materials and Growth Conditions

A variety of *G. hybrida* called "Shenzhen No. 5" was used in this work. The plants were cultured under greenhouse conditions at 26/18°C (day/night temperature) with a 16 h light/8 h dark photocycle and a relative humidity of 65∼80%. Three types of floret (ray floret, trans floret, and disc floret) at stage 6, as well as young leaf (leaf from plants transplanted into the soil for 10∼15 days), old leaf (basal leaf of plants transplanted into the soil for 3 months), young root (root of plants transplanted into the soil for 10∼15 days), old root (root of plants transplanted into the soil for 3 months), calyx, scape, and ray florets at different developmental stages, were sampled for quantitative real-time

PCR (qRT-PCR) analysis. The development stages of ray florets (S1∼S6, "S" represents "stage") are defined according to Meng and Wang (2004). Ray florets at stage 3 were used for transient transformation and hormone treatment assays.

Cloning and Sequence Analysis of *Gh14-3-3* Genes

Using the sequences of *14-3-3* genes in *Arabidopsis thaliana*, BLAST was performed against the transcriptome shotgun assembly database (Accession: PRJNA179026) of *G. hybrida* cultivar "Shenzhen No. 5" (taxid: 18101) (Kuang et al., 2013), and seven *Gh14-3-3* genes were identified. Seven full-length *Gh14-3-3* cDNA sequences were amplified from a gerbera cDNA library by PCR using PrimeSTAR Max Premix (Takara, Cat. No. R045) with specific primers. Alignment of the deduced amino acid sequences with Gh14-3-3 homolog from different species was performed using DNAMAN 6.0. Conserved domain analysis was executed in the Conserved Domain Database[1]. Protein structure prediction was performed with SWISS-MODEL[2]. Phylogenetic analysis was performed in MEGA 6.0 using a neighbor-joining algorithm with 1,000 bootstrap replicates. The primers for the constructs in each experiment and 14-3-3 protein information for various species are listed in **Supplementary Table 1**.

RNA Extraction and qRT-PCR Analysis

Total RNA was extracted from the samples using the Easystep® Super Total RNA Extraction Kit (Promega, Code No. LS1040) following the manufacturer's protocol. First-strand cDNA was synthesized from 1 μg total RNA using the ReverTra Ace qPCR RT Master Mix with gDNA Remover (Toyobo, Code No. FSQ-301). qRT-PCR was performed using RealStar Green Fast Mixture (GenStar, Code No. A301-01). 1 μL cDNA was added as a qPCR template in a total reaction volume of 20 μL. The samples were amplified using the CFX96 Touch™ Real-Time PCR Detection System (Bio-Rad Laboratories, Inc., United States) as follows: melting at 95°C for 2 min and amplification with 40 cycles of 95°C for 5 s and 60°C for 30 s. All analyses used a housekeeping gene (*GhACTIN*, AJ763915) as a normalization control (Kuang et al., 2013). The expression level was calculated according to the $2^{-\Delta\Delta Ct}$ method. The primers used for qRT-PCR are listed in **Supplementary Table 1**.

Transient Transformation of Ray Florets

Transient transformation of ray florets was performed as described by Han et al. (2017). Overexpression vectors (C17 and C17-Gh14-3-3b/f) and virus-induced gene silencing (VIGS) vectors (pTRV1, pTRV2, and pTRV2-Gh14-3-3b/f) were transformed into *Agrobacterium tumefaciens* strain C58C1. *A. tumefaciens* were cultured in Luria-Bertani medium containing 75 mg mL^{-1} kanamycin and 50 mg mL^{-1} rifampicin for 24 h at 28°C and then inoculated into 50 mL Luria-Bertani medium containing 20 μM acetosyringone (AS) and 10 mM 2-(N-morpholino) ethanesulfonic acid (MES) and shaken at 28°C overnight. When the absorbance (OD_{600}) of *A. tumefaciens* reached approximately 1.5, the cells were resuspended in infiltration buffer (200 μM AS, 10 mM MES, 10 mM $MgCl_2$, pH 5.6) to a final optical density at 600 nm (OD_{600}) of 1.5. *Agrobacterium tumefaciens* cultures carrying C17-Gh14-3-3b and C17-Gh14-3-3f, and the empty C17 vector as a mock treatment control, were stored at 28°C for 4 h in the dark at room temperature. *Agrobacterium tumefaciens* cultures carrying pTRV2-Gh14-3-3b/f and pTRV1 at a ratio of 1:1 (v/v), and a mixture containing pTRV2/pTRV1 as a mock treatment control, were also stored under the same conditions for 4 h.

Detached ray petals from fresh inflorescences at stage 3 were cleaned, and then immersed in the various resuspension buffers mentioned above under a vacuum of −0.09 MPa for 5 min. After 2 min, the vacuum was slowly released and the petals were rinsed with sterile distilled water (dH_2O) and placed in sterile Petri dishes with two layers of Whatman filter paper. After incubation at 4°C for 3 days, the transformed petals were grown at 23∼25°C for 9 days at 50∼60% humidity under long-day conditions (16 h light/8 h dark). At least 15 well-grown inflorescences were used for each treatment, and at least three biological replicates were used for each experiment.

Hormone Treatment of Ray Florets

Our previous study showed that detached petals can develop normally. The result of *in vitro* hormone and inhibitor experiments performed with detached petals were consistent with the result of *in vivo* experiments using intact inflorescences (Li et al., 2015; Huang et al., 2017). In this study, detached ray petals from inflorescences at stage 3 were used for BL treatments as described previously (Huang et al., 2017). Transiently transformed petals were placed in sterile Petri dishes with two layers of Whatman filter paper soaked in 10 μM BL or dH_2O as control. Subsequently, the petals were cultured at 24∼26°C for 2 days. At least 15 well-grown inflorescences were used for each treatment, and at least three biological replicates were used for each experiment.

Measurement of Ray Petal and Cell Length

A total of 45 petals were selected to measure their length as previously described (Li et al., 2015). Petals were imaged with a Nikon camera D7200 (Japan) and measured using ImageJ software. To measure the petal cell length and number, the top, middle and basal region of each petal were stained with propidium iodide (0.1 mg mL^{-1}) for 5 min. Next, images of adaxial epidermal cells were captured using a confocal laser scanning microscope (LSM710, Carl Zeiss, Germany) and more than 50 cells were analyzed using ImageJ software. At least three biological replicates were used for each observation. The elongation rate was calculated according Han et al. (2017).

Statistical Analysis

The data were analyzed with SPSS (version 13.0; IBM Corp., Armonk, NY, United States). Statistical significance between samples was investigated by Duncan's new multiple range

[1]https://www.ncbi.nlm.nih.gov/Structure/cdd/wrpsb.cgi

[2]https://swissmodel.expasy.org/interactive

test. The data are presented as mean ± standard error (SE). Different lowercase letters above the bars or line charts indicate significantly different groups: $^{*}P < 0.05$, $^{**}P < 0.01$.

RESULTS

Isolation and Characterization of *Gh14-3-3* Genes in Gerbera

To identify *14-3-3* genes in gerbera, we performed a tBLASTn search against the gerbera transcriptome data using 14-3-3 protein sequences from Arabidopsis as queries (Kuang et al., 2013). Seven putative *Gh14-3-3* genes (*Gh14-3-3a*, *Gh14-3-3b*, *Gh14-3-3c*, *Gh14-3-3d*, *Gh14-3-3e*, *Gh14-3-3f*, and *Gh14-3-3g*) were identified. As shown in **Figure 1**, sequence analysis predicted that the seven *Gh14-3-3* genes encode 258, 259, 257, 261, 336, 254, and 258 amino acids, respectively. Sequence alignment of the gerbera protein sequences showed a high degree of identity, >65%, with the 14-3-3 proteins of *Helianthus annuus*, *Lactuca sativa,* and *Cynara scolymus*. All seven gerbera sequences contained the nine antiparallel α-helices that are highly conserved among 14-3-3 proteins (**Figure 1A**). These results, together with the conserved domain analysis shown in **Supplementary Figure 1**, revealed that the seven gerbera genes belong to the 14-3-3 family. Phylogenetic tree analysis showed that these seven sequences could be divided into either the ε group or the non-ε group of 14-3-3 proteins (**Figure 1B**). Gh14-3-3c is located in the ε branch of the tree, while the other six Gh14-3-3 proteins belong to the non-ε group.

Dimerization Patterns of Gh14-3-3 Proteins

The 14-3-3 proteins usually exist as homo- or heterodimers (Mhawech, 2005). To investigate protein-protein interactions among the seven Gh14-3-3s, a yeast two-hybrid assay was performed. The results showed that only three proteins (Gh14-3-3b, Gh14-3-3c, and Gh14-3-3f) can form homodimers, while the other protein interaction patterns varied. For example, Gh14-3-3b formed heterodimers with the remaining six Gh14-3-3 proteins, while Gh14-3-3e only interacted with Gh14-3-3b. The other five Gh14-3-3 proteins showed a variety of different dimerization behaviors (**Figure 2** and **Supplementary Figure 2**). These results suggest that Gh14-3-3 protein interaction patterns vary according to isoform.

Spatiotemporal Expression Patterns and Response of *Gh14-3-3* Genes to BR

To explore the spatiotemporal expression patterns of the seven *Gh14-3-3* family members in gerbera, qRT-PCR was performed. We first analyzed their expression in different tissues and found that each gene was expressed in various organs or tissues (**Figure 3A**). The highest expression levels appeared in young root, young leaf, disc floret, calyx and old leaf, while the lowest expression levels were mostly observed in old root. The different expression profiles in different tissues imply functional diversity in the *Gh14-3-3* gene family.

We next evaluated the expression pattern of *Gh14-3-3* genes during ray floret developmental stages (S1∼S6, "S" represents "stage") in gerbera. As ray floret petals developed, the expression levels of these genes changed in different ways (**Figure 3B**). However, some patterns were comparable: for example, *Gh14-3-3b* and *Gh14-3-3f* showed a similar expression pattern, such that their transcription levels declined from the highest level in S1 to the lowest level in S3, followed by a gradual increase. Similarly, the transcript abundance of three genes (*Gh14-3-3a*, *Gh14-3-3c,* and *Gh14-3-3d*) dropped to the lowest level from S1 to S2, and then fluctuated in a related manner. In addition, *Gh14-3-3e* and *Gh14-3-3g* showed the highest expression levels in S2 and S1, and the lowest expression levels in S4 and S3, respectively. These results suggest that the expression of *Gh14-3-3* genes is developmentally regulated in petal cells of gerbera.

14-3-3 proteins play an essential role in the BR signaling pathway (Gampala et al., 2007; Ryu et al., 2007). To determine whether the expression of any of the seven *Gh14-3-3* genes responds to BR, the transcript levels of these genes were evaluated following BL treatment. As shown in **Figure 3C**, *Gh14-3-3a* and *Gh14-3-3b* shared the same expression profile: both genes began to respond at 1 h after BL treatment, rising to the highest expression level at 2 h, and then gradually decreasing to the lowest level at 24 h. Specifically, *Gh14-3-3b* had the highest peak value (225) among all seven members in response to BL. Three other genes (*Gh14-3-3d*, *Gh14-3-3e*, and *Gh14-3-3g*) had a similar response pattern to BR with two comparable response peaks (2.0∼2.5) at 0.5 h and 4 h. The expression level of *Gh14-3-3f* increased over the study period to a maximum at 24 h, while *Gh14-3-3c* expression varied slightly within a narrow range in response to BR. These results indicate that all members of the *Gh14-3-3* gene family responded to BR, with *Gh14-3-3a* and *Gh14-3-3b* both reaching the highest expression level at an early stage (2 h) after treatment and *Gh14-3-3f* at a late stage (24 h).

Gh14-3-3b and *Gh14-3-3f* Promote Ray Petal Elongation in Gerbera

Based on the above results, it is clear that *Gh14-3-3b* and *Gh14-3-3f* have the lowest expression level in S3 (the onset of cell elongation), compared to other developmental stages. The two genes reached their highest expression levels at early (2 h) and late stages (24 h) in response to BR, respectively. Thus, we chose to analyze the roles of *Gh14-3-3b* and *Gh14-3-3f* in ray petal elongation by transient overexpression and VIGS assays.

Overexpression of *Gh14-3-3b* significantly promoted petal length and elongation rate, while *Gh14-3-3f*-OE petals showed slightly increased petal length and elongation rate (**Figures 4A,D–F**). The elongation rate was 0.33 ± 0.01 in *Gh14-3-3b*-OE and 0.23 ± 0.01 in *Gh14-3-3f*-OE petals, which corresponds to increases of 57% and 10%, respectively, compared with an elongation rate of 0.21 ± 0.02 in the mock experiment (**Figure 4F**). To determine whether overexpression of *Gh14-3-3b* and *Gh14-3-3f* regulates petal length by promoting petal epidermal cell length, both cell length and number in the

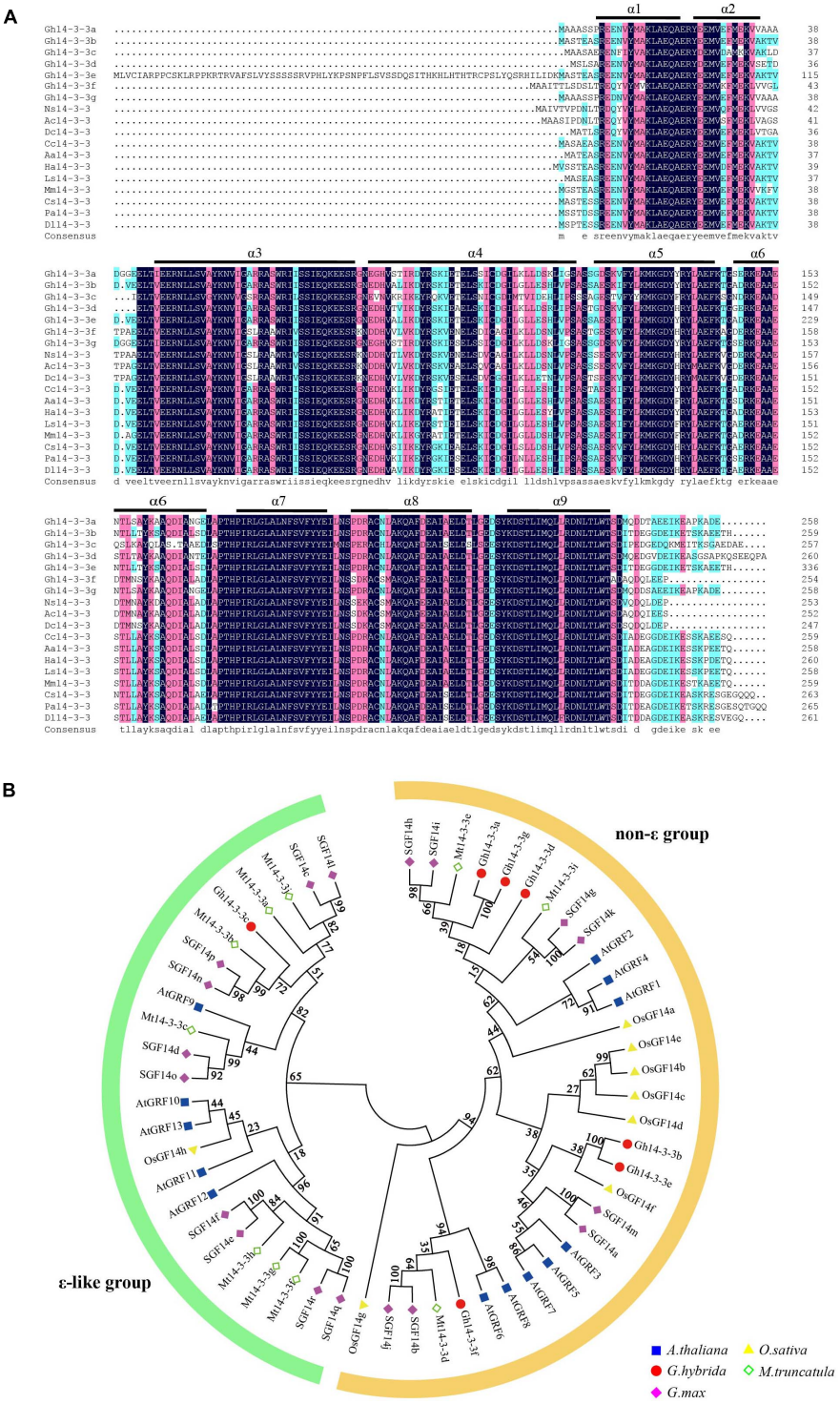

FIGURE 1 | Sequence analysis and phylogenetic tree of Gh14-3-3 proteins. **(A)** Amino acid alignment of Gh14-3-3 proteins with those from other plants. Ns14-3-3 (KAA8528342.1) *Nyssa sinensis*; Ac14-3-3 (PSR99833.1) *Actinidia chinensis*; Dc14-3-3 (XP_017252199.1) *Daucus carota*; Cc14-3-3 (XP_024978074.1) *Cynara cardunculus*; Aa14-3-3 (PWA87588.1) *Artemisia annua*; Ha14-3-3 (XP_022009462.1) *Helianthus annuus*; Ls14-3-3 (XP_023753461.1) *Lactuca sativa*; Mm14-3-3 (KAD2805724.1) *Mikania micrantha*; Cs14-3-3 (XP_028084704.1) *Camellia sinensis*; Pa14-3-3 (PON78199.1) *Parasponia andersonii*; Dl14-3-3 (ACK76233.1) *Dimocarpus longan*. The regions of the nine conserved antiparallel α-helices (α1∼α9) are underlined in black. **(B)** Phylogenetic relationship showing two groups of 14-3-3 proteins in the five species. The minimum evolution tree was constructed using MEGA 6.0 from 1,000 bootstrap replicates. Protein designations consist of the prefixes *Arabidopsis thaliana* (At, blue squares), *Oryza sativa* (Os, yellow triangles), *Gerbera hybrida* (Gh, Red circles), *Medicago truncatula* (Mt, green rhombus), and *Glycine max* (Gm, pink rhombus). Detailed information for 14-3-3s from these plant species are listed in **Supplementary Table 1**.

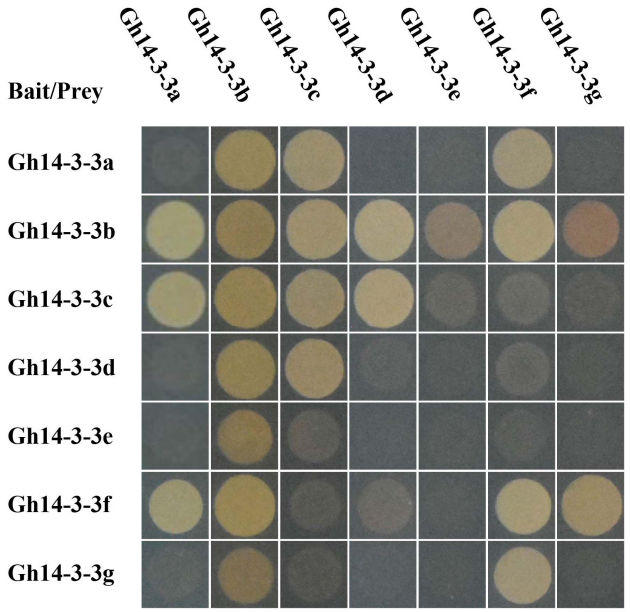

FIGURE 2 | Specific interactions among Gh14-3-3 proteins. pGADT7-largeT7/pGBKT7-53 and pGADT7-largeT7/pGBKT7-laminC were used as positive and negative controls, respectively. The original figure is shown in **Supplementary Figure 2**.

top, middle and basal regions of ray petals were measured (**Figures 4B,C**). The epidermal cell lengths of *Gh14-3-3b*-OE petals were markedly longer than in the mock controls in all three regions (**Figures 4C,G**). In addition, the epidermal cell numbers in *Gh14-3-3b*-OE petals were much smaller than in mock-treated equivalents (**Figure 4H**). For *Gh14-3-3f*-OE ray florets, epidermal cell lengths in the basal and middle regions were significantly longer than in the mock, while epidermal cell numbers in the basal and middle regions were lower. The results suggest that *Gh14-3-3b* and *Gh14-3-3f* promote ray petal elongation by regulating cell elongation.

We further confirmed the role of *Gh14-3-3b* and *Gh14-3-3f* in ray petal elongation using the VIGS system. As shown in **Figures 5A,E,F**, gene silencing of both *Gh14-3-3b* and *Gh14-3-3f* significantly shortened the length and elongation rate of ray petals, relative to the mock. However, exogenous BL treatment eliminated partly this repression (**Figures 5A,E**). Gene silencing of *Gh14-3-3b* and *Gh14-3-3f* also reduced the epidermal cell lengths and boosted cell numbers compared to the mock, while BR reversed this phenotype to some extent (**Figures 5B,G,H**). In addition, we analyzed the expression of *Gh14-3-3b* and *Gh14-3-3f* in *Gh14-3-3b*-VIGS and *Gh14-3-3f*-VIGS petals without and with BL treatment (**Figures 5C,D**). Surprisingly, BL induced the expression of both *Gh14-3-3b* and *Gh14-3-3f* to levels that were approximately 10-fold and 60-fold greater, respectively, than those of *Gh14-3-3b*-VIGS and *Gh14-3-3f*-VIGS petals. Taken together, these results suggest that *Gh14-3-3b* and *Gh14-3-3f* promote BR-induced ray petal elongation.

Expression of Genes Involved in BR Signaling and Petal Elongation Is Altered in *Gh14-3-3b* and *Gh14-3-3f* Transgenic Ray Petals

To investigate the mechanism by which *Gh14-3-3b* and *Gh14-3-3f* regulate ray petal elongation, the expression levels of genes involved in BR signaling and petal elongation were determined. As shown in **Figure 6A**, the expression of BR signaling genes (*GhBEH1*, *GhBEH2*, and *GhBIN2*) was significantly increased in *Gh14-3-3b*-OE petals, but only marginally upregulated in *Gh14-3-3f*-OE petals. The expression levels of genes involved in petal elongation (*GhEXP1*, *GhEXP2*, *GhEXP10*, *GhXTH1*, and *GhXET*) were markedly boosted in *Gh14-3-3b*-OE and *Gh14-3-3f*-OE petals, especially in the former (**Figure 6A**).

On the other hand, the expression levels of the above genes showed, in many cases, a declining trend in *Gh14-3-3b*-VIGS and *Gh14-3-3f*-VIGS petals. In the *Gh14-3-3f*-VIGS petals, the expression of all eight genes was significantly reduced, compared to the mock (**Figure 6B**), while in *Gh14-3-3b*-VIGS petals, the expression of six genes (*GhBEH1*, *GhEXP1*, *GhEXP2*, *GhEXP10*, *GhXTH1*, and *GhXET*) was markedly downregulated, with two genes, *GhBEH2* and *GhBIN2*, showing only a slightly decline. Notably, the expression of all eight genes was enhanced, albeit to different degrees, following BL treatment. These results suggest that *Gh14-3-3b* and *Gh14-3-3f* regulate BR-induced ray petal elongation by modulating genes associated with BR signaling and petal development.

DISCUSSION

Gh14-3-3 Proteins, Which Fall Into Two Groups, May Possess Functional Diversity

Since the first plant 14-3-3 protein was cloned from maize (de Vetten et al., 1992), researchers have identified eight 14-3-3 proteins in rice (Chen et al., 2006; Denison et al., 2011), 18 in apple (Zuo et al., 2021), nine in common bean (Li M. et al., 2016) and seven in cotton (Zhou et al., 2015). In the present study, seven 14-3-3 isoforms were identified in the gerbera transcriptome. Sequence analysis showed that all isoforms share the conserved nine α-helical regions typical of the 14-3-3 family and have 254∼336 amino acids (**Figure 1A**). Phylogenetics classified the seven gerbera 14-3-3 proteins into two groups, the ε and non-ε groups, consistent with similar groupings in Arabidopsis, rice, and banana (Yaffe et al., 1997; Chevalier et al., 2009; Li M. et al., 2016). Furthermore, they show a high degree of identity with 14-3-3 proteins in *Helianthus annuus* and *Lactuca sativa*, both of which belong to Asteraceae family, hinting that these proteins have similar functions across the Asteraceae (**Figure 1A**).

Previous studies revealed that 14-3-3 proteins can form homodimers or, instead, can form heterodimers with different isoforms, which promotes functional diversity (Liu et al., 1995; Xiao et al., 1995; Aghazadeh et al., 2015;

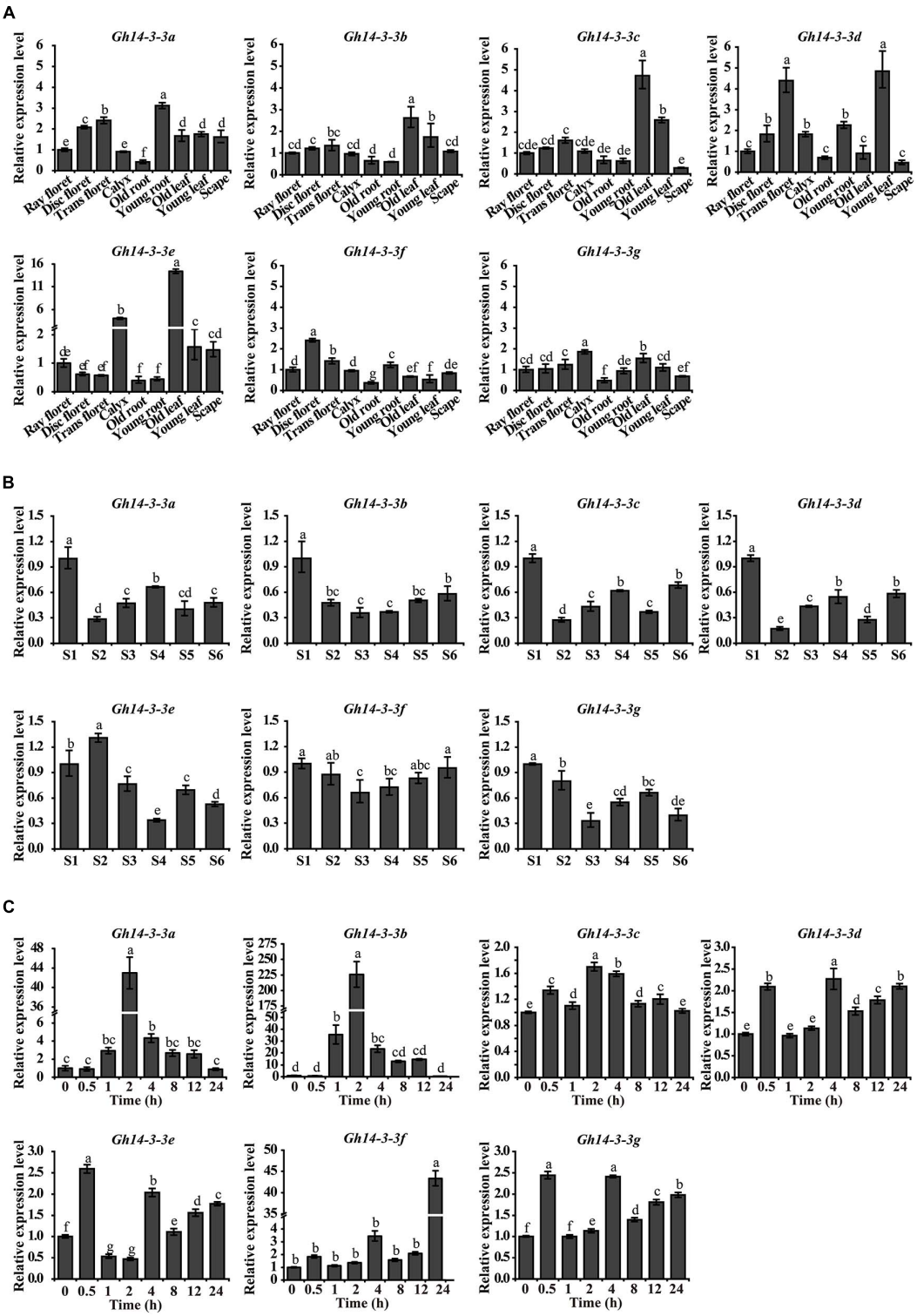

FIGURE 3 | The spatiotemporal expression pattern of *Gh14-3-3* genes. **(A)** The expression pattern of *Gh14-3-3* genes in gerbera tissues and organs. Relative mRNA level of the *Gh14-3-3* genes in gerbera tissues (ray floret, disc floret, trans floret, calyx, old root, young root, old leaf, young leaf, and scape) were detected by qRT-PCR. *GhACTIN* (AJ763915) is the reference gene (Kuang et al., 2013). Gene expression levels were set to 1 in ray floret. **(B)** The expression of *Gh14-3-3* genes during different growth stages (S1∼S6, "S" represents "stage") of ray floret in *G. bybrida*. The development stages of ray florets were defined according to Meng and Wang (2004). Gene expression levels were set to 1 in S1 ray floret petals. **(C)** The expression level of *Gh14-3-3* genes in ray floret of *G. bybrida* under BL treatments. The expression levels of *Gh14-3-3s* in the ray floret of gerbera were detected within 0∼24 h after BL treatment. Gene expression levels were set to 1 in "0 h" and were calculated using the $2^{-\Delta\Delta Ct}$ method. Values were the means ± SE from three biological replicates.

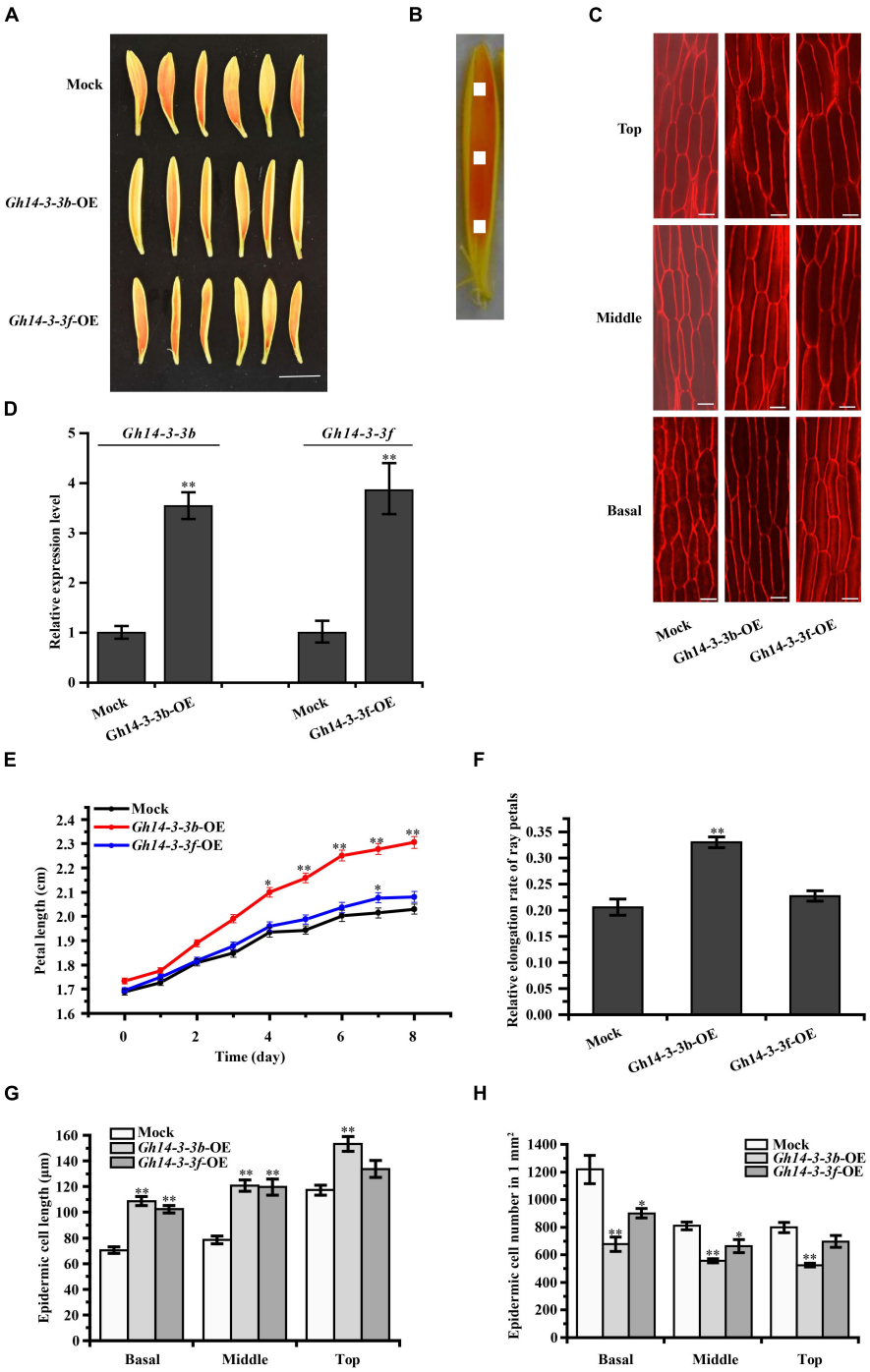

FIGURE 4 | Petal elongation of ray florets were promoted by the overexpression of *Gh14-3-3b* and *Gh14-3-3f*. **(A)** Petal phenotype of the *Gh14-3-3b*, *Gh14-3-3f* transient overexpression and Mock (*Gh14-3-3b*-OE, *Gh14-3-3f*-OE, Mock) after 8 days. Bar = 1 cm. **(B)** Schematic diagram of the petal. The picture shows basal, middle, top regions of ray floret petals. The white area (1 mm^2) shows the measured region for cell length. **(C)** The confocal microscope image of epidermal cells in top, middle and basal regions of petals. Bar = 20 μm. **(D)** The expression analysis of *Gh14-3-3b* and *Gh14-3-3f* in the Mock and transgenic ray petals by qRT-PCR. The length **(E)** and relative elongation rates **(F)** of mock, *Gh14-3-3b*-OE and *Gh14-3-3f*-OE petals (n = 45). The cell length **(G)** and cell number **(H)** in top, middle, and basal regions of transgenic ray petals. At least three biological replicates were used for each observation.

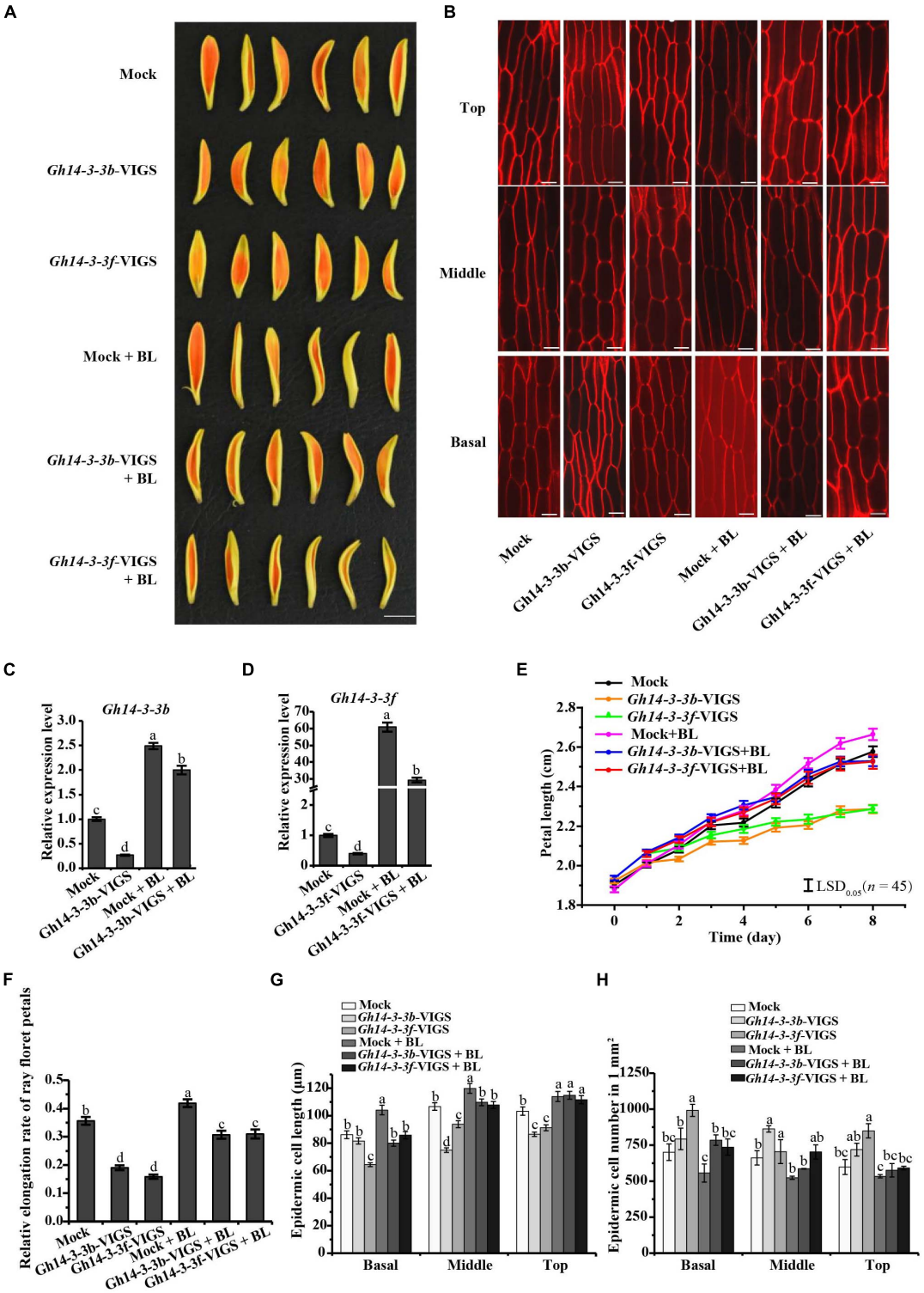

FIGURE 5 | Petal elongation of ray florets was inhibited by transient silencing of *Gh14-3-3b* and *Gh14-3-3f*. **(A)** Petal phenotype of Mock, *Gh14-3-3b* transient silencing, *Gh14-3-3f* transient silencing, and those treated with 10 μM BL (Mock, *Gh14-3-3b*-VIGS, *Gh14-3-3f*-VIGS, Mock + BL, *Gh14-3-3b*-VIGS + BL, *Gh14-3-3f*-VIGS + BL). Bar = 1 cm. **(B)** The confocal microscope image of epidermal cells in top, middle and basal regions of petals. Bar = 20 μm. **(C)** The relative expression level of *Gh14-3-3b* in Mock, *Gh14-3-3b*-OE, Mock + BL and *Gh14-3-3b*-VIGS + BL. **(D)** The relative expression level of *Gh14-3-3f* in Mock, *Gh14-3-3f*-OE, Mock + BL, and *Gh14-3-3f*-VIGS + BL. The length **(E)** and relative elongation rate **(F)** of Mock, *Gh14-3-3b*-VIGS, *Gh14-3-3f*-VIGS, Mock + BL, *Gh14-3-3b*-VIGS + BL, and *Gh14-3-3f*-VIGS + BL petals (n = 45). The elongation rate was calculated at day 8. The cell length **(G)** and cell number **(H)** in top, middle, and basal regions in transgenic ray petals. At least three biological replicates were used for each observation.

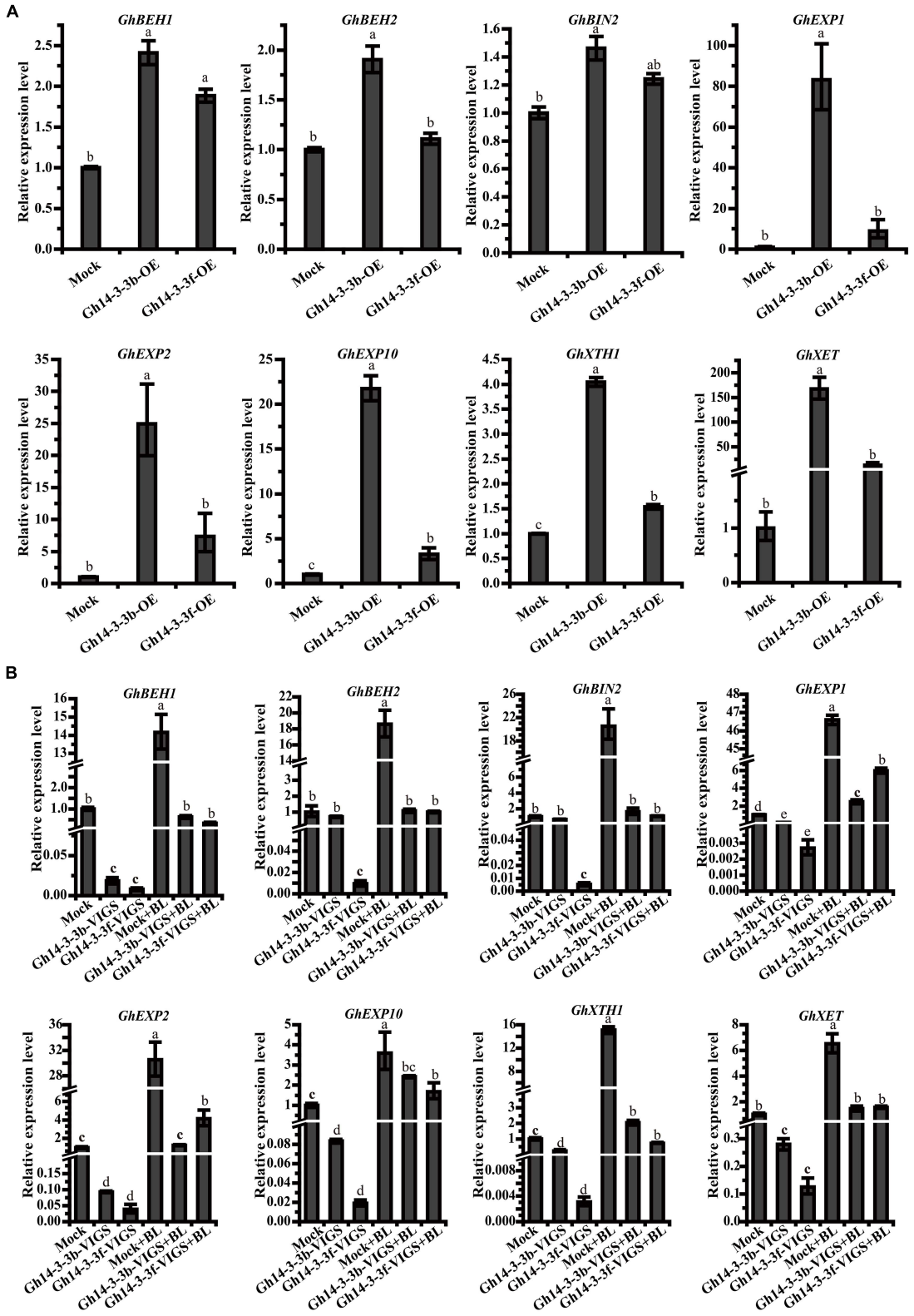

FIGURE 6 | The expression level of related genes in *Gh14-3-3b/f*-OE ray floret petals **(A)** and *Gh14-3-3b/f*-VIGS ray floret petals **(B)**. Gene expression levels were calculated using the $2^{-\Delta\Delta Ct}$ method. The accession numbers of related genes in GenBank are: *GhBEH1* (GACN01037487.1), *GhBEH2* (GACN01006390.1), *GhBIN2* (GACN01003499.1), *GhEXP1* (GACN01041978.1), *GhEXP2* (GACN01002748.1), *GhEXP10* (GACN01039741.1), *GhXTH1* (GACN01007419.1), and *GhXET* (GACN01007419.1).

Ormancey et al., 2017). Each isoform displays a different propensity to dimerize with others, depending on the highly variable amino acid sequences in their N-terminal helices (Liu et al., 1995; Xiao et al., 1995). Consistent with this, the sequences of the N-terminal helices of gerbera 14-3-3 proteins are less well conserved than their C-terminal helices (**Figure 1A**) and only three of the gerbera proteins (Gh14-3-3b, Gh14-3-3c, and Gh14-3-3f) form homodimers (**Figure 2** and **Supplementary Figure 2**). Among the seven Gh14-3-3 proteins, the number of heterodimers formed ranged from one for Gh14-3-3e to six for Gh14-3-3b, which demonstrates the selectivity of each isoform in protein-protein interactions.

Wilson et al. (2016) summarized the regulatory mechanisms of 14-3-3 proteins in several plants during the development of multiple organs, including seedling, leaf, root, flower, and developing seed. We found that the seven 14-3-3 isoforms are expressed in various organs in gerbera to different extents (**Figure 3A**). This implies a functional diversity among all seven members, similar to the 14-3-3 proteins of other species (Chen et al., 2006; Yao et al., 2007). In addition, we surveyed the expression patterns of the *Gh14-3-3* genes during ray floret developmental phases (S1∼S6) (**Figure 3B**). As development progresses through stages S1 to S6, the *Gh14-3-3* genes are expressed in various patterns. For example, *Gh14-3-3b* and *Gh14-3-3f* display a trend of earlier decrease and later increase from S1∼S6, and they both have the lowest expression level at S3 (**Figure 3B**). These genes also differ in their response to exogenous BL treatment (**Figure 3C**): *Gh14-3-3b* responds rapidly and reaches its highest expression level in the early phase of the experiment (2 h), while *Gh14-3-3f* shows a slow response pattern. These results suggest functional diversity of the *Gh14-3-3* genes during BR-induced gerbera growth and development (Chen et al., 2006; Zhou et al., 2015; Zuo et al., 2021).

Gh14-3-3b and Gh14-3-3f Play a Positive Regulatory Role in BR-Induced Ray Petal Elongation

The roles of 14-3-3 proteins in plant growth and development have been reported (Zhou et al., 2015; Huang et al., 2018). At14-3-3λ and At14-3-3K are involved in shade-induced hypocotyl elongation via PHYTOCHROME-INTERACTING FACTOR 7 (Huang et al., 2018). In cotton, 14-3-3 proteins are involved in cotton fiber elongation by regulating GhBZR1 protein, which binds to the promoters of genes involved in fiber development (Zhou et al., 2015). In the present study, overexpression of *Gh14-3-3b* and *Gh14-3-3f* in gerbera increased the length of ray petals, whereas gene silencing of *Gh14-3-3b* and *Gh14-3-3f* shortened petal length (**Figures 4E**, **5E**). Confocal images showed that this may be achieved by regulating epidermal cell length in petals (**Figures 4G**, **5G**). Moreover, the qRT-PCR results revealed that the expression of genes involved in BR signaling (*GhBEH1*, *GhBEH2,* and *GhBIN2*) is enhanced in *Gh14-3-3b*-OE and *Gh14-3-3f*-OE petals and inhibited in *Gh14-3-3b*-VIGS and *Gh14-3-3f*-VIGS petals (**Figures 6A,B**). BL treatment promotes petal length in *Gh14-3-3b*-VIGS and *Gh14-3-3f*-VIGS petals, and enhances the expression of *GhBEH1* in *Gh14-3-3b*-VIGS petals as well as the expressions of *GhBEH1*, *GhBEH2,* and *GhBIN2* in *Gh14-3-3f*-VIGS petals (**Figures 5E**, **6B**). These results suggest that Gh14-3-3b and Gh14-3-3f play a role in BR-induced ray petal elongation. In a previous study, BL was shown to promote ray petal elongation and *GhBEH1* expression in gerbera (Huang et al., 2017). In Arabidopsis, AtBZR1 is one of the most important transcription factors in BR signaling and promotes cell elongation in response to BR (Oh et al., 2012; Chaiwanon and Wang, 2015). Therefore, it is possible that Gh14-3-3b and Gh14-3-3f modulate ray petal elongation by regulating GhBEH1 and GhBEH2. The specific molecular mechanisms will be investigated further in future studies.

Expansins (EXPs), xyloglucan endotransglycosylases (XETs), and xylan transferases/hydrolases (XTHs) are involved in cell wall remodeling and cell elongation (Takeda et al., 2002; Harada et al., 2011; Che et al., 2016; Li Y. et al., 2016; Rao and Dixon, 2017; Ackerman-Lavert and Savaldi-Goldstein, 2020). Two *XTH* genes (*DcXTH2* and *DcXTH3*) and two expansin genes (*DcEXPA1* and *DcEXPA2*) are associated with petal growth and development during flower opening in carnation (Harada et al., 2011). *OsEXPA10* is expressed in the root tips and is necessary for cell elongation in rice (Che et al., 2016). Additionally, the expression of some *XTH* and *EXP* genes is markedly enhanced by BL treatment in Arabidopsis (Park et al., 2010) and soybean (Rao and Dixon, 2017). Our previous study also showed that BR promotes ray petal elongation and initiates the expression of a number of genes, including those encoding two putative cell wall proteins (Huang et al., 2017). In this study, the expression of a number of petal elongation-related genes (including *GhEXP1*, *GhEXP2*, *GhEXP10*, *GhXET,* and *GhXEH*) were altered in *Gh14-3-3b*-OE and *Gh14-3-3f*-OE, as well as *Gh14-3-3b*-VIGS and *Gh14-3-3f*-VIGS petals (**Figure 6B**). This suggests that Gh14-3-3b and Gh14-3-3f modulate petal elongation-related gene transcription, thereby mediating petal cell elongation and petal development.

As one of the mainstream cut flowers, gerbera has a high demand in the market. However, it has fewer flower types compared to chrysanthemum. Thus, obtaining a variety of flower types is one of the main goals of gerbera breeding, which requires an understanding of the regulatory mechanism of gerbera flower development. In this study, seven Gh14-3-3 protein genes were identified and their expression patterns were characterized. These genes share a conserved structure, but display different dimerization patterns, which implies they are functionally diverse. Transient transformation assays demonstrated that Gh14-3-3b and Gh14-3-3f play a positive regulatory role in BR-induced ray petal elongation. Thus, as well as providing novel insights into the role of 14-3-3 proteins in ray petal elongation, this study also highlights a number of candidate genes for flower type breeding of gerbera.

DATA AVAILABILITY STATEMENT

The original contributions presented in the study are included in the article/**Supplementary Material**, further inquiries can be directed to the corresponding author.

AUTHOR CONTRIBUTIONS

XL carried out the experiments, drafted the manuscript, and revised manuscript. SH conducted the experiments, analyzed the data, and prepared the figures. GH participated in part of the experiments. YC and XW revised the manuscript. YW conceived the study, participated in its design, and revised the manuscript. All authors read and approved the final manuscript.

FUNDING

This work was supported by the National Key R&D Program of China (2018YFD1000404), Research Team Project of Natural Science Foundation of Guangdong Province (2017A030312004), National Natural Science Foundation of China (31672188), and Natural Science Foundation of Guangdong Province (2021A1515012479, 2021A1515011315, and 201904010127).

ACKNOWLEDGMENTS

We thank Ling Li for providing the overexpression vector C17. We are grateful to Xiaoyan Tang and Cambridge Academic Manuscripts (www.CambridgeAcademicManuscripts.com) for manuscript editing.

SUPPLEMENTARY MATERIAL

The Supplementary Material for this article can be found online at: https://www.frontiersin.org/articles/10.3389/fpls.2021.718091/full#supplementary-material

Supplementary Figure 1 | Conserved domains analysis of seven Gh14-3-3s in the Conserved Domain Database.

Supplementary Figure 2 | The interactions among Gh14-3-3 proteins. *Gh14-3-3s* were introduced into pGADT7-AD and pGBKT7-BD. pGADT7-largeT7/pGBKT7-53 and pGADT7-largeT7/pGBKT7-laminC were used as positive and negative controls, respectively.

Supplementary Table 1 | Primers used in this study and amino acid sequences of 14-3-3s in different species.

REFERENCES

Ackerman-Lavert, M., and Savaldi-Goldstein, S. (2020). Growth models from a brassinosteroid perspective. *Curr. Opin. Plant Biol.* 53, 90–97. doi: 10.1016/j.pbi.2019.10.008

Aghazadeh, Y., Zirkin, B. R., and Papadopoulos, V. (2015). Pharmacological regulation of the cholesterol transport machinery in steroidogenic cells of the testis. *Vitam. Hormon.* 98, 189–227. doi: 10.1016/bs.vh.2014.12.006

Aitken, A. (2006). 14-3-3 proteins: a historic overview. *Semin. Cancer Biol.* 16, 162–172. doi: 10.1016/j.semcancer.2006.03.005

Bhatia, R., Singh, K. P., Jhang, T., and Sharma, T. R. (2009). Assessment of clonal fidelity of micropropagated gerbera plants by ISSR markers. *Sci. Hortic.* 119, 208–211. doi: 10.1016/j.scienta.2008.07.024

Broholm, S. K., Tähtiharju, S., Laitinen, R. A. E., Albert, V. A., Teeri, T. H., and Elomaa, P. (2008). A TCP domain transcription factor controls flower type specification along the radial axis of the gerbera (Asteraceae) inflorescence. *PNAS* 105, 9117–9122. doi: 10.1073/pnas.0801359105

Camoni, L., Visconti, S., Aducci, P., and Marra, M. (2018). 14-3-3 proteins in plant hormone signaling: doing several things at once. *Front. Plant Sci.* 9:297. doi: 10.3389/fpls.2018.00297

Chaiwanon, J., and Wang, Z. Y. (2015). Spatiotemporal brassinosteroid signaling and antagonism with auxin pattern stem cell dynamics in *Arabidopsis* roots. *Curr. Biol.* 25, 1031–1042. doi: 10.1016/j.cub.2015.02.046

Che, J., Yamaji, N., Shen, R. F., and Ma, J. F. (2016). An Al-inducible expansin gene, *OsEXPA10* is involved in root cell elongation of rice. *Plant J.* 88, 132–142. doi: 10.1111/tpj.13237

Chen, F., Li, Q., Sun, L., and He, Z. (2006). The rice 14-3-3 gene family and its involvement in responses to biotic and abiotic stress. *DNA Res.* 13, 53–63. doi: 10.1093/dnares/dsl001

Chevalier, D., Morris, E. R., and Walker, J. C. (2009). 14-3-3 and FHA domains mediate phosphoprotein interactions. *Annu. Rev. Plant Biol.* 60, 67–91. doi: 10.1146/annurev.arplant.59.032607.092844

Clouse, S. D., Langford, M., and McMorris, T. C. (1996). A brassinosteroid-insensitive mutant in *Arabidopsis thaliana* exhibits multiple defects in growth and development. *Plant Physiol.* 111, 671–678. doi: 10.1104/pp.111.3.671

Clouse, S. D., and Sasse, J. M. (1998). BRASSINOSTEROIDS: essential regulators of plant growth and development. *Annu. Rev. Plant Biol.* 49, 427–451. doi: 10.1146/annurev.arplant.49.1.427

de Vetten, N. C., Lu, G., and Feri, R. J. (1992). A maize protein associated with the G-box binding complex has homology to brain regulatory proteins. *Plant Cell* 4, 1295–1307. doi: 10.1105/tpc.4.10.1295

DeLille, J. M., Sehnke, P. C., and Ferl, R. J. (2001). The *Arabidopsis* 14-3-3 family of signaling regulators. *Plant Physiol.* 126, 35–38. doi: 10.1104/pp.126.1.35

Denison, F. C., Paul, A. L., Zupanska, A. K., and Ferl, R. J. (2011). 14-3-3 proteins in plant physiology. *Semin. Cell Dev. Biol.* 22, 720–727. doi: 10.1016/j.semcdb.2011.08.006

Ferl, R. J. (1996). 14-3-3 Proteins and signal transduction. *Annu. Rev. Plant. Physiol. Plant. Mol. Biol.* 47, 49–73. doi: 10.1146/annurev.arplant.47.1.49

Gampala, S. S., Kim, T. W., He, J., Tang, W., Deng, Z., Bai, M., et al. (2007). An essential role for 14-3-3 proteins in brassinosteroid signal transduction in arabidopsis. *Dev. Cell* 13, 177–189. doi: 10.1016/j.devcel.2007.06.009

Han, M., Jin, X., Yao, W., Kong, L., Huang, G., Tao, Y., et al. (2017). A mini zinc-finger protein (MIF) from *Gerbera hybrida* activates the GASA protein family gene, *GEG*, to inhibit ray petal elongation. *Front. Plant Sci.* 8:1649. doi: 10.3389/fpls.2017.01649

Harada, T., Torii, Y., Morita, S., Onodera, R., Hara, Y., Yokoyama, R., et al. (2011). Cloning, characterization, and expression of xyloglucan endotransglucosylase/hydrolase and expansin genes associated with petal growth and development during carnation flower opening. *J. Exp. Bot.* 62, 815–823. doi: 10.1093/jxb/erq319

He, J. X., Gendron, J. M., Sun, Y., Gampala, S. S. L., Gendron, N., Sun, C. Q., et al. (2005). BZR1 is a transcriptional repressor with dual roles in brassinosteroid homeostasis and growth responses. *Science* 307, 1634–1638. doi: 10.1126/science.1107580

Huang, G., Han, M., Jian, L., Chen, Y., Sun, S., Wang, X., et al. (2020). An ETHYLENE INSENSITIVE3-LIKE1 protein directly targets the *GEG* promoter and mediates ethylene-induced ray petal elongation in *Gerbera hybrida*. *Front. Plant Sci.* 10:1737. doi: 10.3389/fpls.2019.01737

Huang, G., Han, M., Yao, W., and Wang, Y. (2017). Transcriptome analysis reveals the regulation of brassinosteroids on petal growth in *Gerbera hybrida*. *PeerJ* 5:e3382. doi: 10.7717/peerj.3382

Huang, X., Zhang, Q., Jiang, Y., Yang, C., Wang, Q., and Li, L. (2018). Shade-induced nuclear localization of PIF7 is regulated by phosphorylation and 14-3-3 proteins in *Arabidopsis*. *Plant Biol.* 7:17. doi: 10.7554/eLife.31636

Juntheikki-Palovaara, I., Tähtiharju, S., Lan, T., Broholm, S. K., Rijpkema, A. S., Ruonala, R., et al. (2014). Functional diversification of duplicated *CYC2* clade genes in regulation of inflorescence development in *Gerbera hybrida* (Asteraceae). *Plant J.* 79, 783–796. doi: 10.1111/tpj.12583

Kaneko-Suzuki, M., Kurihara-Ishikawa, R., Okushita-Terakawa, C., Kojima, C., Nagano-Fujiwara, M., Ohki, I., et al. (2018). TFL1-Like proteins in rice antagonize rice FT-Like protein in inflorescence development by competition for complex formation with 14-3-3 and FD. *Plant Cell Physiol.* 59, 458–468. doi: 10.1093/pcp/pcy021

Keicher, J., Jaspert, N., Weckermann, K., Möller, C., Throm, C., Kintzi, A., et al. (2017). Arabidopsis 14-3-3 epsilon members contribute to polarity of PIN auxin carrier and auxin transport-related development. *eLife* 6:e24336. doi: 10.7554/eLife.24336

Kim, T. W., Michniewicz, M., Bergmann, D. C., and Wang, Z. (2012). Brassinosteroid regulates stomatal development by GSK3-mediated inhibition of a MAPK pathway. *Nature* 482, 419–422. doi: 10.1038/nature10794

Kim, T. W., and Wang, Z. (2010). Brassinosteroid signal transduction from receptor kinases to transcription factors. *Annu. Rev. Plant Biol.* 61, 681–704. doi: 10.1146/annurev.arplant.043008.092057

Konagaya, K., Matsushita, Y., Kasahara, M., and Nyunoya, H. (2004). Members of 14-3-3 protein isoforms interacting with the resistance gene product N and the elicitor of *Tobacco mosaic* virus. *J. Gen. Plant Pathol.* 70, 221–231. doi: 10.1007/s10327-003-0113-4

Kotilainen, M., Helariutta, Y., Mehto, M., Pöllänen, E., Albert, V. A., Elomaa, P., et al. (1999). *GEG* participates in the regulation of cell and organ shape during corolla and carpel development in *Gerbera hybrida*. *Plant Cell* 11, 1093–1104. doi: 10.1105/tpc.11.6.1093

Kuang, Q., Li, L., Peng, J., Sun, S., and Wang, X. (2013). Transcriptome analysis of *Gerbera hybrida* ray florets: putative genes associated with gibberellin metabolism and signal transduction. *PLoS One* 8:e57715. doi: 10.1371/journal.pone.0057715

Li, L., Zhang, W., Zhang, L., Li, N., Peng, J., Wang, Y., et al. (2015). Transcriptomic insights into antagonistic effects of gibberellin and abscisic acid on petal growth in *Gerbera hybrida*. *Front. Plant Sci.* 6:168. doi: 10.3389/fpls.2015.00168

Li, M., Ren, L., Xu, B., Yang, X., Xia, Q., He, P., et al. (2016). Genome-wide identification, phylogeny, and expression analyses of the 14-3-3 family reveal their involvement in the development, ripening, and abiotic stress response in banana. *Front. Plant Sci.* 7:1442. doi: 10.3389/fpls.2016.01442

Li, Y., Tu, L., Pettolino, F. A., Ji, S., Hao, J., Yuan, D., et al. (2016). *GbEXPATR*, a species-specific expansin, enhances cotton fiber elongation through cell wall restructuring. *Plant Biotechnol. J.* 14, 951–963. doi: 10.1111/pbi.12450

Liu, D., Bienkowska, J., Petosa, C., Collier, R. J., Fu, H., and Liddington, R. (1995). Crystal structure of the zeta isoform of the 14-3-3 protein. *Nature* 376, 191–194. doi: 10.1038/376191a0

Meng, X., and Wang, X. (2004). Regulation of flower development and anthocyanin accumulation in *Gerbera hybrida*. *J. Hortic. Sci. Biotechnol.* 79, 131–137. doi: 10.1080/14620316.2004.11511725

Mhawech, P. (2005). 14-3-3 proteins—an update. *Cell Res.* 15, 228–236. doi: 10.1038/sj.cr.7290291

Minami, A., Takahashi, K., Inoue, S., Tada, Y., and Kinoshita, T. (2019). Brassinosteroid induces phosphorylation of the plasma membrane H^+-ATPase during hypocotyl elongation in *Arabidopsis thaliana*. *Plant Cell Physiol.* 60, 935–944. doi: 10.1093/pcp/pcz005

Mosqueda Frómeta, O., Escalona Morgado, M. M., Teixeira da Silva, J. A., Pina Morgado, D. T., and Daquinta Gradaille, M. A. (2017). *In vitro* propagation of *Gerbera jamesonii* Bolus ex Hooker f. in a temporary immersion bioreactor. *Plant Cell Tissure Organ Cult.* 129, 543–551. doi: 10.1007/s11240-017-1186-7

Oh, E., Zhu, J. Y., and Wang, Z. Y. (2012). Interaction between BZR1 and PIF4 integrates brassinosteroid and environmental responses. *Nat. Cell Biol.* 14, 802–809. doi: 10.1038/ncb2545

Oh, M. H., Honey, S. H., and Tax, F. E. (2020). The control of cell expansion, cell division, and vascular development by brassinosteroids: a historical perspective. *Int. J. Mol. Sci.* 21:1743. doi: 10.3390/ijms21051743

Ormancey, M., Thuleau, P., Mazars, C., and Cotelle, V. (2017). CDPKs and 14-3-3 proteins: emerging duo in signaling. *Trends Plant Sci.* 22, 263–272. doi: 10.1016/j.tplants.2016.11.007

Park, C. H., Kim, T. W., Son, S. H., Hwang, J. Y., Lee, S. C., Chang, S. C., et al. (2010). Brassinosteroids control *AtEXPA5* gene expression in *Arabidopsis thaliana*. *Phytochemistry* 71, 380–387. doi: 10.1016/j.phytochem.2009.11.003

Pertl, H., Pöckl, M., Blaschke, C., and Obermeyer, G. (2010). Osmoregulation in lilium pollen grains occurs via modulation of the plasma membrane H^+ ATPase activity by 14-3-3 proteins. *Plant Physiol.* 154, 1921–1928. doi: 10.1104/pp.110.165696

Qiao, S., Sun, S., Wang, L., Wu, Z., Li, C., Li, X., et al. (2017). The RLA1/SMOS1 transcription factor functions with OsBZR1 to regulate brassinosteroid signaling and rice architecture. *Plant Cell* 29, 292–309. doi: 10.1105/tpc.16.00611

Rao, X., and Dixon, R. A. (2017). Brassinosteroid mediated cell wall remodeling in grasses under abiotic stress. *Front. Plant Sci.* 8:806. doi: 10.3389/fpls.2017.00806

Ren, G., Li, L., Huang, Y., Wang, Y., Zhang, W., Zheng, R., et al. (2018). GhWIP2, a WIP zinc finger protein, suppresses cell expansion in *Gerbera hybrida* by mediating crosstalk between gibberellin, abscisic acid, and auxin. *New Phytol.* 219, 728–742. doi: 10.1111/nph.15175

Ryu, H., Kim, K., Cho, H., Park, J., Choe, S., and Hwang, I. (2007). Nucleocytoplasmic shuttling of BZR1 mediated by phosphorylation is essential in *Arabidopsis* brassinosteroid signaling. *Plant Cell* 19, 2749–2762. doi: 10.1105/tpc.107.053728

Sehnke, P. C., DeLille, J. M., and Ferl, R. J. (2002). Consummating signal transduction: the role of 14-3-3 proteins in the completion of signal-induced transitions in protein activity. *Plant Cell* 14(Suppl.), S339–S354. doi: 10.1105/tpc.010430

Silva, N. F., Christie, L. N., Mazzurco, M., and Goring, D. R. (2001). Characterization of a novel *Brassica napus* kinase, BNK1. *Plant Sci.* 160, 611–620. doi: 10.1016/s0168-9452(00)00426-x

Tahtiharju, S., Rijpkema, A. S., Vetterli, A., Albert, V. A., Teeri, T. H., and Elomaa, P. (2012). Evolution and diversification of the *CYC/TB1* gene family in asteraceae—a comparative study in gerbera (Mutisieae) and sunflower (Heliantheae). *Mol. Biol. Evol.* 29, 1155–1166. doi: 10.1093/molbev/msr283

Takeda, T., Furuta, Y., Awano, T., Mizuno, K., Mitsuishi, Y., and Hayashi, T. (2002). Suppression and acceleration of cell elongation by integration of xyloglucans in pea stem segments. *PNAS* 99, 9055–9060. doi: 10.1073/pnas.132080299

Taoka, K., Ohki, I., Tsuji, H., Furuita, K., Hayashi, K., Yanase, T., et al. (2011). 14-3-3 proteins act as intracellular receptors for rice Hd3a florigen. *Nature* 476, 332–335. doi: 10.1038/nature10272

van Kleeff, P. J. M., Jaspert, N., Li, K. W., Rauch, S., Oecking, C., and de Boer, A. H. (2014). Higher order *Arabidopsis* 14-3-3 mutants show 14-3-3 involvement in primary root growth both under control and abiotic stress conditions. *J. Exp. Bot.* 65, 5877–5888. doi: 10.1093/jxb/eru338

Wang, Z.-Y., Bai, M. Y., Oh, E., and Zhu, J. Y. (2012). Brassinosteroid signaling network and regulation of photomorphogenesis. *Annu. Rev. Genet.* 46, 701–724. doi: 10.1146/annurev-genet-102209-163450

Wilson, R. S., Swatek, K. N., and Thelen, J. J. (2016). Regulation of the regulators: post-translational modifications, subcellular, and spatiotemporal distribution of plant 14-3-3 proteins. *Front. Plant Sci.* 7:611. doi: 10.3389/fpls.2016.00611

Xiao, B., Smerdon, S. J., Jones, D. H., Dodson, G. G., Soneji, Y., Aitken, A., et al. (1995). Structure of a 14-3-3 protein and implications for coordination of multiple signalling pathways. *Nature* 376, 188–191. doi: 10.1038/376188a0

Yaffe, M. B., Rittinger, K., Volinia, S., Caron, P. R., Aitken, A., Leffers, H., et al. (1997). The structural basis for 14-3-3: phosphopeptide binding specificity. *Cell* 91, 961–971. doi: 10.1016/S0092-8674(00)80487-0

Yang, C., Zhang, C., Lu, Y., Jin, J., and Wang, X. (2011). The mechanisms of brassinosteroids' action: from signal transduction to plant development. *Mol. Plant* 4, 588–600. doi: 10.1093/mp/ssr020

Yao, Y., Du, Y., Jiang, L., and Liu, J. (2007). Molecular analysis and expression patterns of the 14-3-3 gene family from *Oryza sativa*. *J. Biochem. Mol. Biol.* 40, 349–357. doi: 10.5483/bmbrep.2007.40.3.349

Zhang, L., Li, L., Wu, J., Peng, J., Zhang, L., and Wang, X. (2012). Cell expansion and microtubule behavior in ray floret petals of *Gerbera hybrida*: responses to light and gibberellic acid. *Photochem. Photobiol. Sci.* 11, 279–288. doi: 10.1039/C1PP05218G

Zhang, T., Cieslak, M., Owens, A., Wang, F., Broholm, S. K., Teeri, T. H., et al. (2021). Phyllotactic patterning of gerbera flower heads. *PNAS* 118:e2016304118. doi: 10.1073/pnas.2016304118

Zhang, X., Guo, W., Du, D., Pu, L., and Zhang, C. (2020). Overexpression of a maize BR transcription factor *ZmBZR1* in Arabidopsis enlarges organ and seed size of the transgenic plants. *Plant Sci.* 292:110378. doi: 10.1016/j.plantsci.2019.110378

Zhang, Z., Zhou, Y., Li, Y., Shao, S., Li, B., Shi, H., et al. (2010). Interactome analysis of the six cotton 14-3-3s that are preferentially expressed in fibres and involved in cell elongation. *J. Exp. Bot.* 61, 3331–3344. doi: 10.1093/jxb/erq155

Zhao, Y., Broholm, S. K., Wang, F., Rijpkema, A. S., Lan, T., Albert, V. A., et al. (2020). TCP and MADS-box transcription factor networks regulate heteromorphic flower. *Plant Physiol.* 184, 1455–1468. doi: 10.1104/pp.20.00702

Zheng, M., Hu, M., Yang, H., Tang, M., Zhang, L., Liu, H., et al. (2019). Three *BnaIAA7* homologs are involved in auxin/brassinosteroid-mediated plant morphogenesis in rapeseed (*Brassica napus* L.). *Plant Cell Rep.* 38, 883–897. doi: 10.1007/s00299-019-02410-4

Zhou, Y., Zhang, Z., Li, M., Wei, X., Li, X., Li, B., et al. (2015). Cotton (*Gossypium hirsutum*) 14-3-3 proteins participate in regulation of fibre initiation and elongation by modulating brassinosteroid signalling. *Plant Biotechnol. J.* 13, 269–280. doi: 10.1111/pbi.12275

Zuo, X., Wang, S., Xiang, W., Yang, H., Tahir, M. M., Zheng, S., et al. (2021). Genome-wide identification of the *14-3-3* gene family and its participation in floral transition by interacting with TFL1/FT in apple. *BMC Genom.* 22:41. doi: 10.1186/s12864-020-07330-2

Conflict of Interest: The authors declare that the research was conducted in the absence of any commercial or financial relationships that could be construed as a potential conflict of interest.

Publisher's Note: All claims expressed in this article are solely those of the authors and do not necessarily represent those of their affiliated organizations, or those of the publisher, the editors and the reviewers. Any product that may be evaluated in this article, or claim that may be made by its manufacturer, is not guaranteed or endorsed by the publisher.

frontiers in Plant Science

MINI REVIEW
published: 27 October 2021
doi: 10.3389/fpls.2021.745507

Petal Cellular Identities

*Quentin Cavallini-Speisser, Patrice Morel and Marie Monniaux**

Laboratoire de Reproduction et Développement des Plantes, Université de Lyon, ENS de Lyon, UCB Lyon 1, CNRS, INRAE, Lyon, France

Petals are typified by their conical epidermal cells that play a predominant role for the attraction and interaction with pollinators. However, cell identities in the petal can be very diverse, with different cell types in subdomains of the petal, in different cell layers, and depending on their adaxial-abaxial or proximo-distal position in the petal. In this mini-review, we give an overview of the main cell types that can be found in the petal and describe some of their functions. We review what is known about the genetic basis for the establishment of these cellular identities and their possible relation with petal identity and polarity specifiers expressed earlier during petal development, in an attempt to bridge the gap between organ identity and cell identity in the petal.

Keywords: petal, cell type, conical cell, mesophyll, epidermis, cell identity, petal polarities

OPEN ACCESS

Edited by:
Deshu Lin,
Fujian Agriculture and Forestry University, China

Reviewed by:
Tengbo Huang,
Shenzhen University, China
Amy Litt,
University of California, Riverside, United States

****Correspondence:***
Marie Monniaux
marie.monniaux@ens-lyon.fr

Specialty section:
This article was submitted to Plant Development and EvoDevo, a section of the journal Frontiers in Plant Science

Received: *22 July 2021*
Accepted: *04 October 2021*
Published: *27 October 2021*

Citation:
Cavallini-Speisser Q, Morel P and Monniaux M (2021) Petal Cellular Identities. Front. Plant Sci. 12:745507. doi: 10.3389/fpls.2021.745507

INTRODUCTION

Diversity in petal shape, size, color, and number is a key contributor to the dazzling variety of floral forms observed in the wild. The petal is often described as a very simple laminar structure, reminiscent of a leaf in its shape. The *Arabidopsis* petal could not be much simpler: a flat organ with a basal greenish claw and a distal white blade and only few different cell types (Irish, 2008). This simplicity makes it an excellent model to study plant organogenesis and cell type differentiation processes (Irish, 2008; Szécsi et al., 2014; Huang and Irish, 2016). However, *Arabidopsis* is only one among more than 350,000 flowering plant species (The Plant List, 2013), whose petal structures can be much more complex (Endress, 2001; Moyroud and Glover, 2017). Petals can display complex elaborations, such as lobes, fringes, nectary spurs, or hair pads (Endress and Matthews, 2006). In most asterid species, petals are fused together; therefore, the proximal (tube) and distal (limbs) parts of the fused petals can appear very different (Endress, 2001). Moreover, within a single flower, all petals are not the same, particularly in bilaterally symmetric flowers: Legume flowers develop distinct dorsal, lateral, and ventral petals (Ojeda et al., 2009). Petals also display an abaxial-adaxial polarity, the adaxial side of the petal being the upper/inner one (closest to the main stem), while the abaxial side is the lower/outer one. Finally, petal cells also have a layer identity, since petals generally derive from 2 (sometimes 3) layers from the shoot apical meristem that generates all aerial organs (Satina and Blakeslee, 1941; Jenik and Irish, 2000). Mature petals are thus typically composed of an adaxial epidermal layer (L1-derived), a few layers of mesophyll cells (L2-derived), and an abaxial epidermal layer (L1-derived).

In this mini-review, we will give an overview of the diversity of cell types that can be encountered on this apparently simple structure that is the petal. We will first focus on the two petal epidermises in which we find conical cells, together with many other cell types. We will next explore cell types and functions in the petal mesophyll, containing the petal vasculature surrounded by parenchyma cells. Finally, we will review the molecular mechanisms

involved in cell differentiation in the petal epidermis and their potential link with petal identity and polarity specifiers.

THE PETAL EPIDERMIS: CONICAL CELLS, STRIATIONS, TRICHOMES, AND STOMATA

Petal epidermal cells display striking differentiation features. The typical petal epidermal cell is conical (also called papillate), and this particular cell shape, readily observable by light microscopy or scanning electron microscopy, is often used as a marker for petal cell identity; indeed, it is found in 75–80% of angiosperm petals (Kay et al., 1981). Conical cells are generally found on the adaxial (upper) surface of the petal limb, and their shape and size can be extremely different among angiosperm species (Kay et al., 1981; Whitney et al., 2011a). They have been shown to increase petal color intensity and cause its sparkling appearance, increase pollinator's grip on the flower, affect overall petal shape, and decrease its wettability (Gorton and Vogelmann, 1996; Baumann et al., 2007; Whitney et al., 2009a, 2011a,b). They are also in most cases where pigments are produced (Kay et al., 1981) and frequently where scent is released (Baudino et al., 2007). All of the aforementioned traits potentially improve attraction and interaction with pollinators and therefore likely lead to a higher pollination success (Whitney et al., 2011a). Conical cells can thus be viewed as a key cellular innovation of flowering plants.

Other cell types are frequently found in the petal, and their distribution depends on their position in the petal. To explore this distribution along the petal proximo-distal axis, we chose the example of the petunia petal (*Petunia x hybrida*, **Figure 1A**). Petunia petals are fused, like petals from the vast majority of asterid flowers (Endress, 2001), and are organized in a tube and limbs (**Figure 1A**). In the limbs, cells are conical and smooth, and their density increases toward the center of the flower, which might influence petal color intensity and levels of emission of volatiles (Skaliter et al., 2021). At the most distal part of the tube, cells appear elongated and covered with striations (**Figure 1A**, tube 1). Striations are regular folds of the waxy cuticle of the outer epidermal cell wall and are frequently observed on petal epidermal cells (Antoniou Kourounioti et al., 2013). When regularly spaced and parallel oriented, these striations can cause light diffraction and iridescence of the petal, a visible cue for pollinators (Whitney et al., 2009b). Around the middle of the petunia petal tube, epidermal cells appear elongated with a small central papilla and still slightly striated (**Figure 1A**, tube 2). These striations progressively disappear as we progress toward the proximal part of the tube, and the central papilla becomes more and more pronounced (**Figure 1A**, tube 3). The function of this central papilla on tube cells is unknown.

Cell identity usually appears quite different on the two sides of the petal: Abaxial cells are flatter (lenticular) than adaxial conical cells, but they often contain pigments, and they can be a site of scent production (Kay et al., 1981; Baudino et al., 2007). Additionally, petal epidermal cells are often interspersed with trichomes, either glandular (for instance producing scent, nectar or defense compounds) or non-glandular ones, with various structures, shapes, and sizes. For instance in cotton flowers, both sides of the petals are covered in long non-glandular trichomes entangled together, resulting in the anchoring of adjacent petals together and their correct unfolding (Tan et al., 2016). In snapdragon flowers (*Antirrhinum majus*), glandular trichomes form very locally inside the corolla tube where they produce scent to attract pollinators and trap the pollen that they carry (Kolosova et al., 2001; Perez-Rodriguez et al., 2005). Finally, stomata are sometimes found on the petal epidermis, although their density is much more reduced than in leaves (Roddy et al., 2016; Zhang et al., 2018). They participate in gas exchange for photosynthesis in the petal (Zhang et al., 2018), and they might also be involved in maintenance of correct turgor pressure of the petal to avoid precocious wilting and have been proposed to play a role in flower opening in tulip (Azad et al., 2007).

This description of petal epidermal cell types is not exhaustive, and cell types in this tissue can be manifold. In elaborate petals, this diversity can be quite extreme. As an example, the *Nigella arvensis* flower forms highly elaborate petals of a complex shape with bifurcations and lobes, eyebrow-like stripes, long hairs, short trichomes, nectaries, and pseudo-nectaries (**Figure 1B**; Yao et al., 2019). Ten different subdomains can be defined in these petals, each displaying a distinct epidermal cell identity, among which conical cells, pavement cells, secretory cells, or polygonal cells, to cite just a few (Yao et al., 2019). One might argue that these petals are extremely derived and thus a particular case, but there is also strong variation in epidermal cell types on the petals of legume flowers, which are simple petals with a classical appearance (Dong et al., 2005; Ojeda et al., 2009).

THE PETAL MESOPHYLL: LIFE AND DEATH OF THE PETAL

In between the two epidermises stands the petal mesophyll, a spongy tissue whose thickness greatly varies between species: a single-cell layer in poppies (van der Kooi and Stavenga, 2019) but several dozens in the giant *Rafflesia* flower (Nikolov et al., 2013; Mursidawati et al., 2020). The petal mesophyll comprises the vascular bundles of the petal, surrounded by parenchyma cells that are roundish cells without any striking visual features.

One obvious role of the mesophyll is for petal nutrition. Vascular bundles embedded within the parenchyma supply the water and metabolites necessary for petal function. Additionally, in some species like petunia, mesophyll parenchyma cells contain chloroplasts, even in the mature petal (Weiss et al., 1988; Vainstein and Sharon, 1993). Coupled to the presence of stomata on the petal epidermis and lacunae in the mesophyll favoring gas exchange, conditions are gathered for active photosynthesis to take place in petunia petals, although it is not as intense nor as efficient as in leaves (Weiss et al., 1988, 1990).

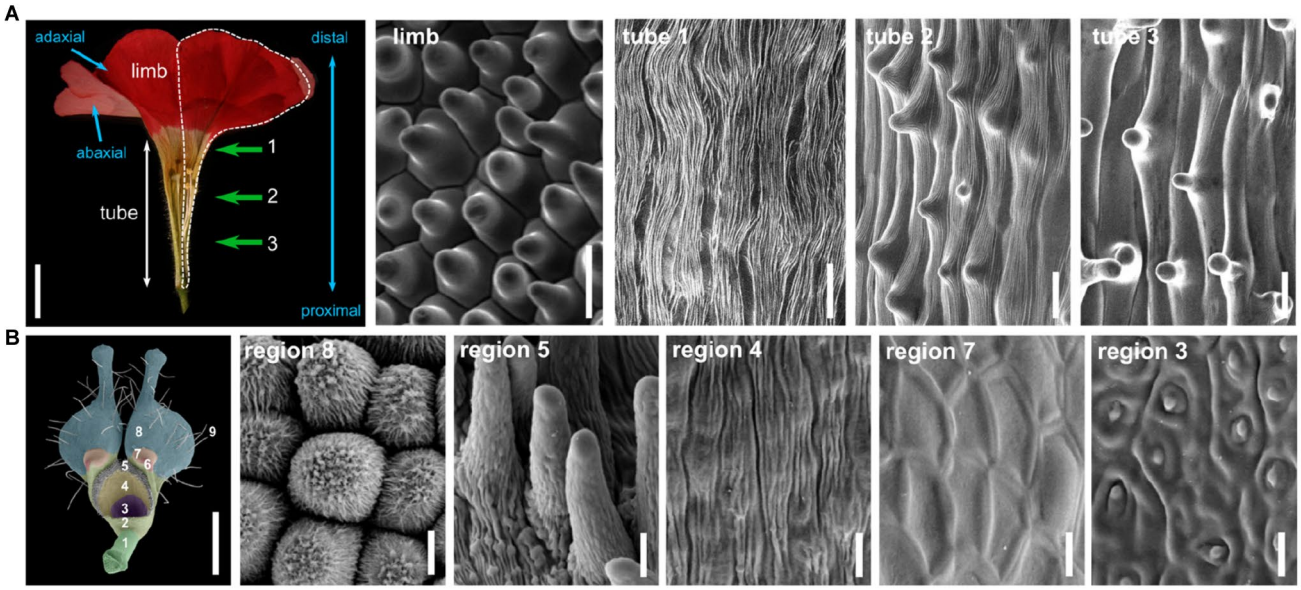

FIGURE 1 | Cellular identities in the petal epidermis. **(A)** Half-flower from *Petunia x hybrida*, cut open longitudinally to display the tube and limb regions (scale bar = 1 cm). The contour of one petal is shown with a white dotted line. Proximo/distal and adaxial/abaxial polarities of the petal are indicated with blue arrows. Scanning electron micrographs (scale bars = 20 μm) of the adaxial surface of petals in the limbs, and at three different regions from the tube, indicated by green arrows and numbers in the flower picture. These pictures were obtained with a HIROX SH-1500 bench top environmental scanning electron microscope equipped with a cooling stage (−10°C, 5 kV). **(B)** Petal from *Nigella arvensis* viewed from its adaxial side (scale bar = 1 mm), with nine regions with different cellular identities as identified in Yao et al. (2019). A 10th region is only visible on the abaxial side of the petal. Scanning electron micrographs of cells from five of these regions, giving an overview of cellular diversity in this organ (scale bars = 10 μm). Region 8: conical cells; region 5: short trichomes; region 4: oblong cells; region 7: polygonal cells with smooth surfaces; region 3: secretory cells. Pictures are reproduced from Yao et al. (2019) with permission from the authors.

This photosynthetic activity does not provide enough energy for the organ to be self-sustainable but, in particular, anthocyanin production appears to strongly depend on it (Weiss and Halevy, 1991).

The mesophyll is also involved in petal growth: In tulips, the mesophyll is considered to be the main driver of late petal growth by cell expansion (van Doorn and Van Meeteren, 2003), and in petunia, we recently showed that the mesophyll is the main driver for the growth of the petal tube (mainly by cell expansion), similarly to what had been previously observed in snapdragon flowers (Perbal et al., 1996; Efremova et al., 2001; Vincent et al., 2003; Chopy et al., 2021). In tulips and crocus flowers, temperature variation between lighted (outer) and shaded (inner) parts of the petal causes differential expansion of the parenchyma cell layers, resulting in flower opening (Wood, 1953). Similarly, in rose flowers, endoreduplication of parenchyma cells specifically on the adaxial side of the petal base, under the control of ethylene signaling, results in asymmetric growth of the petal mesophyll and flower opening (Cheng et al., 2021). Interestingly, only parenchyma cells toward the adaxial side of the petal respond to ethylene (Cheng et al., 2021), suggesting prior differentiation of mesophyll cells along the adaxial-abaxial axis.

The mesophyll also participates in petal pigmentation and therefore possibly in pollinator attraction. For instance in wallflowers petals (*Erysimum*), the epidermis is pigmented but the parenchyma cells also contain many chromoplasts and large pigmented cytoplasmic vesicles (Weston and Pyke, 1999). In the blue-flowered members of the *Boraginaceae* and *Liliaceae* families, the parenchyma cells contain anthocyanins and are the main contributor to petal pigmentation (Kay et al., 1981). The mesophyll can also influence the appearance of petals by reflecting or diffusing light. For example, buttercup petals (yellow-colored *Ranunculus*) have a reflective starch-containing parenchyma cell layer just underneath their epidermis, participating to the glossy and reflective petal surface (Parkin, 1928, 1931; Vignolini et al., 2012; van der Kooi et al., 2017). By a similar mechanism, the mesophyll of poppies and kingcup (*Caltha palustris*) petals contains large air cavities, creating a difference in refractive indices of the petal tissues and therefore strong light reflection and scattering, participating to the shiny appearance of the petals (Whatley, 1984; van der Kooi and Stavenga, 2019).

Finally, mesophyll cells are often the first site of petal senescence (van Doorn and Woltering, 2008). In petunia and lilies, this process begins in the petal parenchyma as early as 2 days after pollination, as evidenced by signs of autophagy (granules formation, loss of membrane integrity or expression of programmed cell death markers; Shibuya et al., 2013; Mochizuki-Kawai et al., 2015). This suggests that resource relocation after pollination, from the petal to the ovary, first relies on mesophyll degradation. In Iris flowers, mesophyll cell death begins at the apical part of the petal and progresses toward the base (van Doorn et al., 2003), suggesting that the mesophyll is not entirely homogeneous in this respect and that the process is influenced by petal polarity.

In summary, mesophyll cells play various specific roles over the course of petal development. Although parenchyma cells display only subtle differentiation features and therefore might not be classified into different cell types within this tissue, there can be a zonation of their activity and function along the different petal axes.

FROM ORGAN IDENTITY TO CELL IDENTITY

As proposed in the ABCE model of floral organ identity, petal identity is specified in a region of the floral meristem by expression of B-class genes in a floral context, defined by A- and E-class genes, most of them being MADS-box genes (Schwarz-Sommer et al., 1990; Coen and Meyerowitz, 1991; Pelaz et al., 2000; Causier et al., 2010; Thomson and Wellmer, 2019). This is generally well conserved within all angiosperms (Soltis et al., 2007; Irish, 2009). The question then arises as to how expression of a small number of MADS-box genes results in the specification of the different petal cell types that we have described in the previous paragraphs. To our knowledge, in the petal mesophyll, nothing specific is known about the molecular players downstream of MADS-box genes that could define cell identity. In contrast, the acquisition of cell identity in the petal epidermis has been well characterized at the molecular level, specifically for conical cells and trichomes. Interestingly, and although these two cell types can appear quite different, it might be relatively simple to switch from one to the other.

Major molecular players in conical cell formation are MIXTA and MIXTA-like proteins, belonging to the large group of R2R3-MYB (MYB proteins with two repeats of the MYB DNA-binding domain) transcription factors (TFs). *MIXTA* was first identified in snapdragon petals; it is sufficient to drive both conical cell and trichome differentiation when overexpressed in tobacco leaves, but since its endogenous expression pattern is only late during petal development, it only directs conical cell differentiation *in vivo* (Glover et al., 1998; Martin et al., 2002). Indeed, another *MIXTA*-like gene, *AmMYBML1*, is expressed early in the ventral petal, and because of this early expression, it directs both conical cell and trichome differentiation (Perez-Rodriguez et al., 2005). This suggests that conical cell and trichome specification processes are closely related to the molecular level, and that shifts in the spatio-temporal pattern of *MIXTA*-like genes expression are sufficient to drive conical cell and/or trichome specification, and therefore the patterning of these cell types at the petal scale.

More generally, the identities of various plant epidermal cell types are determined by MBW protein complexes, composed of one MYB TF, one bHLH TF, and one WD40 repeat protein (Ramsay and Glover, 2005; Robinson and Roeder, 2015). In the different species (mainly *Arabidopsis*, snapdragon, maize, and petunia) and tissues (root, leaf, seed, and flower) where these complexes have been studied, they can trigger the formation of different cell types (trichomes, stomata, pavement cells, or root hairs), the production of pigmentation (in the whole plant, the seed coat or the petal), or of other epidermal features (seed mucilage). The WD40 protein appears to have a general scaffolding role, and there has been only one WD40 protein identified per species, while there are few bHLH proteins and many different MYB proteins, thereby resulting in a combination of specific MBW complexes (Ramsay and Glover, 2005). In petals, the specific role of these complexes has been elucidated in particular when exploring the petal pigmentation patterns in different petunia lines. Production of anthocyanins in petunia petals is controlled by MBW complexes composed of the WD40 protein ANTHOCYANIN11 (AN11), the bHLH protein AN1, and an R2R3-MYB protein that can be any among AN2, AN4, DEEP PURPLE (DPL), or PURPLE HAZE (PHZ), which will, respectively, result in pigmentation in the limbs (AN2), in the tube and anthers (AN4), in the petal veins (DPL), or during blushing of the petal under high light (PHZ; Quattrocchio et al., 1993, 1999; de Vetten et al., 1997; Spelt et al., 2000; Albert et al., 2011). These complexes regulate the expression of several structural genes in the anthocyanin pathway (Quattrocchio et al., 1993; Huits et al., 1994). The diversity and specificity of action of each MYB protein grant high modularity to the petal pigmentation system and the potential to evolve subtle changes in pigmentation patterns while avoiding to loose anthocyanin production entirely (Ramsay and Glover, 2005). Cell identity and pigmentation are thus specified by similar protein complexes in the petal epidermis.

Additionally, the petal appears to be pre-patterned to specify particular cell fates when the right regulators are expressed at the right time and place (**Figure 2**). For instance, as seen previously, *MIXTA-like* genes do not direct the development of the same cell fates when expressed at a different time and place. What could this petal pre-patterning be? Briefly, markers of layer identity, such as the *HD-ZIP class IV* genes *MERISTEM L1 LAYER* (*ATML1*) or *PROTODERMAL FACTOR2* (*PDF2*) in *Arabidopsis* (Lu et al., 1996; Abe et al., 2003), specify epidermal identity from the embryonic stage onwards. Later, as floral organs initiate, their adaxial/abaxial polarity is established by genes, such as the *KANADI* and *YABBY* genes (abaxial side) and *HD-ZIP class III* genes (adaxial side; Siegfried et al., 1999; Kerstetter et al., 2001; Emery et al., 2003; Manuela and Xu, 2020), and their proximo-distal polarity is established by genes, such as *BLADE ON PETIOLE1* (*BOP1*) and *BOP2*, *TCP* genes or *JAGGED* (Hepworth et al., 2005; Norberg et al., 2005; Sauret-Gueto et al., 2013; Huang and Irish, 2015). More or less simultaneously, the B-class MADS-box genes specify petal identity, in a floral context specified by A- and E-class genes. Their initial expression appears quite homogeneous in all layers of the petal primordia (Urbanus et al., 2009; Prunet et al., 2017), but these genes are expressed throughout organ development and their expression pattern can be quite dynamic (Dornelas et al., 2011; Wuest et al., 2012). For instance in *Arabidopsis*, the E-class SEP3 protein is mostly expressed in the epidermis of the developing petal and more strongly on its adaxial side; similarly, the A-class AP1 protein accumulates more at the tip of developing sepals than at their base

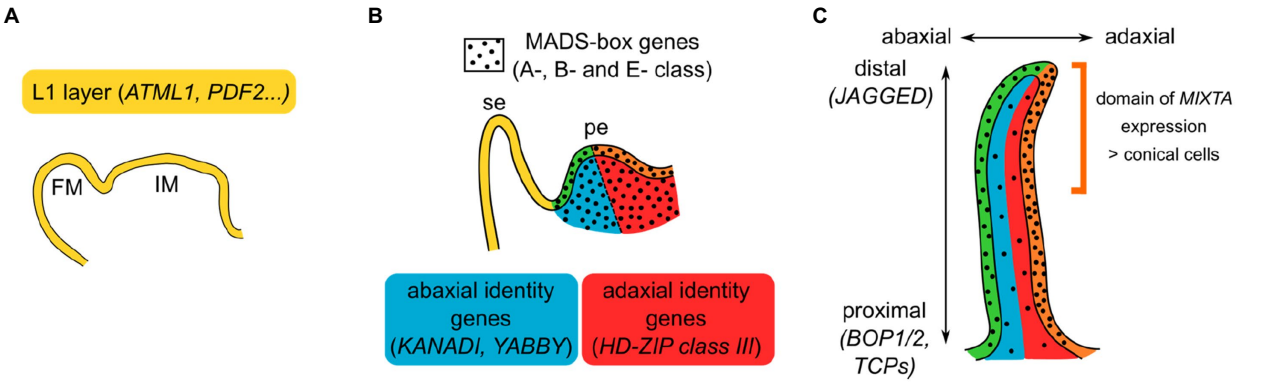

FIGURE 2 | Model for the combinatorial specification of petal identity and polarities. **(A)** In the inflorescence and flower meristems (IM and FM, respectively), layer identity is already specified. In particular, the meristematic L1 layer and the epidermis that derives from it express a specific set of genes. **(B)** Initiating sepal (se) and petal (pe). Petal identity is defined by the expression of B-class MADS-box genes, in a floral context defined by A- and E-class genes, in all layers of the petal primordia (black dots). Abaxial (blue) and adaxial (red) sides of the petal are specified by a set of genes. Intersection of epidermal identity with abaxial or adaxial identity results in petal subdomains represented in green and orange, respectively. **(C)** Developing petal. Layer identity and abaxial/adaxial polarity are still maintained, and proximo-distal polarity establishes as the petal grows. MADS-box genes expression is not necessarily homogeneous in the developing petal: here is depicted the case of *Arabidopsis* SEP3 protein, enriched in the petal epidermis and particularly on its adaxial side. The combination of these different positional signals can result in the specification of distinct cell fates: In snapdragon, *MIXTA* is only expressed in the epidermal, adaxial, and distal part of the petal, driving there the formation of conical cells.

(Urbanus et al., 2009; Dornelas et al., 2011). Interestingly, mutations in epidermal specifier genes from the *PDF2* family result in alterations of petal identity with reduced expression of the B-class gene *APETALA3* (*AP3*), suggesting that *AP3* might be a particularly prominent target of these epidermal specifiers (Kamata et al., 2013a,b). MADS-box gene expression and/or protein localization might thus depend on layer identity, abaxial/adaxial, and proximal/distal polarity specifiers, through molecular mechanisms unknown so far. *Vice versa*, members from the *HD-ZIP class IV*, *KANADI, YABBY, HD-ZIP class III,* or *TCP* gene families, as well as *BOP1*, are found within the direct regulatory targets of B-class proteins in *Arabidopsis* (Wuest et al., 2012), suggesting a feedback loop between petal identity and positional signals within the petal.

How could these different positional signals relate to the different cell identities observed in the petal? Quite similarly to the combinatorial ABCE model proposed for floral organ identity, we propose that the combination of positional signals in the petal specifies the patterning of different cell types at the petal scale (**Figure 2**). The example of *MIXTA-like* genes, the main specifiers of conical cell fate, can illustrate this idea: In snapdragon, *MIXTA* is specifically expressed in the adaxial epidermis of the petal, particularly at the distal part where conical cells develop (Glover et al., 1998). This specific expression pattern can be interpreted as the result of the presence of petal and epidermal markers, together with distal and adaxial polarity specifiers. Indeed, pieces of genetic or molecular evidence support a link between *MIXTA-like* genes expression or function and positional signals: *MIXTA-like* gene expression is genetically downstream of petal identity, proximo/distal, and adaxial/abaxial specifiers (Eshed et al., 2001; Perez-Rodriguez et al., 2005; van Es et al., 2018), and MIXTA-like proteins can directly interact with HD-Zip class IV and TCP proteins (Yan et al., 2018; Camoirano et al., 2021). Therefore, one can imagine that petal positional signals activate *MIXTA-like* genes expression in the right time and place, driving cell differentiation toward the conical cell fate, later reinforced by the direct interaction of MIXTA-like proteins with proteins specifying position in the petal.

Downstream this layer of regulatory genes, effector genes act to modify the cytoskeleton arrangement and the cell wall, to give the petal cells their final shape and function, participating to their identity. Most of the knowledge on this topic comes from *Arabidopsis* conical cells, in which it was found that a circumferential arrangement of cortical microtubules, controlled by proteins such as KATANIN1, SPIKE1, or ROPs, supports cellulose deposition and cone formation (Ren et al., 2016, 2017). Other players, such as RHAMNOSE BIOSYNTHESIS 1, control cell wall composition in conical cells and thus correct cell and petal shape (Saffer et al., 2017), while striations on the surface of petal epidermal cells depend on enzymes from the cutin synthesis pathway (Li-Beisson et al., 2009). The direct link between those various effector genes and the upstream regulatory genes is not established yet, but a glimpse of the whole regulatory network is beginning to emerge (Irish, 2008; Huang and Irish, 2016). Additional molecular evidence is needed to understand how cell types are specified in the petal and surely, the processes of interest here are complex, continuous, and overlapping with each other, with extensive cross-talk involved throughout petal development.

CONCLUSION AND FUTURE DIRECTIONS

Although the petal is a simple laminar structure, it contains several different cell types whose identity is specified by a wide range of signals. How these signals are integrated at the

molecular level and result in a specific gene expression profile and cellular function is mostly unknown. Today, the petal should not be viewed as an organ with a single identity, but rather as a population of cells in a petal specification context, each with a slightly different combination of lineage and positional signals (Xu et al., 2021). Single-cell technologies (transcriptome, proteome, interactome, chromatin accessibility, metabolome…) will surely lead to breakthroughs in the understanding of cell type specification in the petal and the molecular basis for its variation between species.

AUTHOR CONTRIBUTIONS

PM performed the electron micrographs. QC-S and MM wrote the article. All authors contributed to the article and approved the submitted version.

FUNDING

This work is supported by grants to QC-S and MM from the Agence Nationale de la Recherche (grant ANR-19-CE13-0019, FLOWER LAYER).

ACKNOWLEDGMENTS

We thank the PLATIM platform (SFR BioSciences Lyon, UAR3444/CNRS, US8/Inserm, ENS de Lyon, UCBL) for electron microscopy technical support, Mathilde Chopy for kindly providing us with the petunia limb electron micrograph, and Clément Verez for his help in electron microscopy. We also thank Hongzi Kong and colleagues for agreeing that we reproduce their pictures from *Nigella arvensis* petals. We also thank Michiel Vandenbussche for critical reading of the manuscript.

REFERENCES

Abe, M., Katsumata, H., Komeda, Y., and Takahashi, T. (2003). Regulation of shoot epidermal cell differentiation by a pair of homeodomain proteins in *Arabidopsis*. *Development* 130, 635–643. doi: 10.1242/dev.00292

Albert, N. W., Lewis, D. H., Zhang, H., Schwinn, K. E., Jameson, P. E., and Davies, K. M. (2011). Members of an R2R3-MYB transcription factor family in petunia are developmentally and environmentally regulated to control complex floral and vegetative pigmentation patterning. *Plant J.* 65, 771–784. doi: 10.1111/j.1365-313X.2010.04465.x

Antoniou Kourounioti, R. L., Band, L. R., Fozard, J. A., Hampstead, A., Lovrics, A., Moyroud, E., et al. (2013). Buckling as an origin of ordered cuticular patterns in flower petals. *J. R. Soc. Interface* 10:20120847. doi: 10.1098/rsif.2012.0847

Azad, A. K., Sawa, Y., Ishikawa, T., and Shibata, H. (2007). Temperature-dependent stomatal movement in tulip petals controls water transpiration during flower opening and closing. *Ann. Appl. Biol.* 150, 81–87. doi: 10.1111/j.1744-7348.2006.00111.x

Baudino, S., Caissard, J.-C., Bergougnoux, V., Jullien, F., Magnard, J.-L., Scalliet, G., et al. (2007). Production and emission of volatile compounds by petal cells. *Plant Signal. Behav.* 2, 525–526. doi: 10.4161/psb.2.6.4659

Baumann, K., Perez-Rodriguez, M., Bradley, D., Venail, J., Bailey, P., Jin, H., et al. (2007). Control of cell and petal morphogenesis by R2R3 MYB transcription factors. *Development* 134, 1691–1701. doi: 10.1242/dev.02836

Camoirano, A., Alem, A. L., Gonzalez, D. H., and Viola, I. L. (2021). *Arabidopsis thaliana* TCP15 interacts with the MIXTA-like transcription factor MYB106/NOECK. *Plant Signal. Behav.* 16:1938432. doi: 10.1080/15592324.2021.1938432

Causier, B., Schwarz-Sommer, Z., and Davies, B. (2010). Floral organ identity: 20 years of ABCs. *Semin. Cell Dev. Biol.* 21, 73–79. doi: 10.1016/j.semcdb.2009.10.005

Cheng, C., Yu, Q., Wang, Y., Wang, H., Dong, Y., Ji, Y., et al. (2021). Ethylene-regulated asymmetric growth of the petal base promotes flower opening in rose (*Rosa hybrida*). *Plant Cell* 33, 1229–1251. doi: 10.1093/plcell/koab031

Chopy, M., Cavallini-Speisser, Q., Chambrier, P., Morel, P., Just, J., Hugouvieux, V., et al. (2021). Cell layer-specific expression of the B-class MADS-box gene PhDEF drives petal tube or limb development in petunia flowers. bioRxiv [Preprint]. doi: 10.1101/2021.04.03.438311

Coen, E. S., and Meyerowitz, E. M. (1991). The war of the whorls: genetic interactions controlling flower development. *Nature* 353, 31–37. doi: 10.1038/353031a0

de Vetten, N., Quattrocchio, F., Mol, J., and Koes, R. (1997). The an11 locus controlling flower pigmentation in petunia encodes a novel WD-repeat protein conserved in yeast, plants, and animals. *Genes Dev.* 11, 1422–1434. doi: 10.1101/gad.11.11.1422

Dong, Z., Zhao, Z., Liu, C., Luo, J., Yang, J., Huang, W., et al. (2005). Floral patterning in *Lotus japonicus*. *Plant Physiol.* 137, 1272–1282. doi: 10.1104/pp.104.054288

Dornelas, M. C., Patreze, C. M., Angenent, G. C., and Immink, R. G. H. (2011). MADS: the missing link between identity and growth? *Trends Plant Sci.* 16, 89–97. doi: 10.1016/j.tplants.2010.11.003

Efremova, N., Perbal, M. C., Yephremov, A., Hofmann, W. A., Saedler, H., and Schwarz-Sommer, Z. (2001). Epidermal control of floral organ identity by class B homeotic genes in *Antirrhinum* and *Arabidopsis*. *Development* 128, 2661–2671. doi: 10.1242/dev.128.14.2661

Emery, J. F., Floyd, S. K., Alvarez, J., Eshed, Y., Hawker, N. P., Izhaki, A., et al. (2003). Radial patterning of *Arabidopsis* shoots by class III HD-ZIP and KANADI genes. *Curr. Biol.* 13, 1768–1774. doi: 10.1016/j.cub.2003.09.035

Endress, P. K. (2001). Origins of flower morphology. *J. Exp. Zool.* 291, 105–115. doi: 10.1002/jez.1063

Endress, P. K., and Matthews, M. L. (2006). Elaborate petals and staminodes in eudicots: diversity, function, and evolution. *Org. Divers. Evol.* 6, 257–293. doi: 10.1016/j.ode.2005.09.005

Eshed, Y., Baum, S. F., Perea, J. V., and Bowman, J. L. (2001). Establishment of polarity in lateral organs of plants. *Curr. Biol.* 11, 1251–1260. doi: 10.1016/S0960-9822(01)00392-X

Glover, B. J., Perez-Rodriguez, M., and Martin, C. (1998). Development of several epidermal cell types can be specified by the same MYB-related plant transcription factor. *Development* 125, 3497–3508. doi: 10.1242/dev.125.17.3497

Gorton, H. L., and Vogelmann, T. C. (1996). Effects of epidermal cell shape and pigmentation on optical properties of *Antirrhinum* petals at visible and ultraviolet wavelengths. *Plant Physiol.* 112, 879–888. doi: 10.1104/pp.112.3.879

Hepworth, S. R., Zhang, Y., McKim, S., Li, X., and Haughn, G. W. (2005). BLADE-ON-PETIOLE-dependent signaling controls leaf and floral patterning in *Arabidopsis*. *Plant Cell* 17, 1434–1448. doi: 10.1105/tpc.104.030536

Huang, T., and Irish, V. F. (2015). Temporal control of plant organ growth by TCP transcription factors. *Curr. Biol.* 25, 1765–1770. doi: 10.1016/j.cub.2015.05.024

Huang, T., and Irish, V. F. (2016). Gene networks controlling petal organogenesis. *J. Exp. Bot.* 67, 61–68. doi: 10.1093/jxb/erv444

Huits, H. S., Gerats, A. G., Kreike, M. M., Mol, J. N., and Koes, R. E. (1994). Genetic control of dihydroflavonol 4-reductase gene expression in *Petunia hybrida*. *Plant J.* 6, 295–310. doi: 10.1046/j.1365-313X.1994.06030295.x

Irish, V. F. (2008). The *Arabidopsis* petal: a model for plant organogenesis. *Trends Plant Sci.* 13, 430–436. doi: 10.1016/j.tplants.2008.05.006

Irish, V. F. (2009). Evolution of petal identity. *J. Exp. Bot.* 60, 2517–2527. doi: 10.1093/jxb/erp159

Jenik, P. D., and Irish, V. F. (2000). Regulation of cell proliferation patterns by homeotic genes during *Arabidopsis* floral development. *Development* 127, 1267–1276. doi: 10.1242/dev.127.6.1267

Kamata, N., Okada, H., Komeda, Y., and Takahashi, T. (2013a). Mutations in epidermis-specific HD-ZIP IV genes affect floral organ identity in *Arabidopsis thaliana*. *Plant J.* 75, 430–440. doi: 10.1111/tpj.12211

Kamata, N., Sugihara, A., Komeda, Y., and Takahashi, T. (2013b). Allele-specific effects of PDF2 on floral morphology in *Arabidopsis thaliana*. *Plant Signal. Behav.* 8:e27417. doi: 10.4161/psb.27417

Kay, Q. O. N., Daoud, H. S., and Stirton, C. H. (1981). Pigment distribution, light reflection and cell structure in petals. *Bot. J. Linn. Soc.* 83, 57–83. doi: 10.1111/j.1095-8339.1981.tb00129.x

Kerstetter, R. A., Bollman, K., Taylor, R. A., Bomblies, K., and Poethig, R. S. (2001). KANADI regulates organ polarity in *Arabidopsis*. *Nature* 411, 706–709. doi: 10.1038/35079629

Kolosova, N., Sherman, D., Karlson, D., and Dudareva, N. (2001). Cellular and subcellular localization of *S*-adenosyl-l-methionine:benzoic acid carboxyl methyltransferase, the enzyme responsible for biosynthesis of the volatile ester methylbenzoate in snapdragon flowers. *Plant Physiol.* 126, 956–964. doi: 10.1104/pp.126.3.956

Li-Beisson, Y., Pollard, M., Sauveplane, V., Pinot, F., Ohlrogge, J., and Beisson, F. (2009). Nanoridges that characterize the surface morphology of flowers require the synthesis of cutin polyester. *Proc. Natl. Acad. Sci. U. S. A.* 106, 22008–22013. doi: 10.1073/pnas.0909090106

Lu, P., Porat, R., Nadeau, J. A., and O'Neill, S. D. (1996). Identification of a meristem L1 layer-specific gene in *Arabidopsis* that is expressed during embryonic pattern formation and defines a new class of homeobox genes. *Plant Cell* 8, 2155–2168. doi: 10.1105/tpc.8.12.2155

Manuela, D., and Xu, M. (2020). Patterning a leaf by establishing polarities. *Front. Plant Sci.* 11:568730. doi: 10.3389/fpls.2020.568730

Martin, C., Bhatt, K., Baumann, K., Jin, H., Zachgo, S., Roberts, K., et al. (2002). The mechanics of cell fate determination in petals. *Philos. Trans. R. Soc. Lond. Ser. B Biol. Sci.* 357, 809–813. doi: 10.1098/rstb.2002.1089

Mochizuki-Kawai, H., Niki, T., Shibuya, K., and Ichimura, K. (2015). Programmed cell death progresses differentially in epidermal and mesophyll cells of lily petals. *PLoS One* 10:e0143502. doi: 10.1371/journal.pone.0143502

Moyroud, E., and Glover, B. J. (2017). The evolution of diverse floral morphologies. *Curr. Biol.* 27, R941–R951. doi: 10.1016/j.cub.2017.06.053

Mursidawati, S., Wicaksono, A., and Teixeira da Silva, J. A. (2020). *Rafflesia patma* Blume flower organs: histology of the epidermis and vascular structures, and a search for stomata. *Planta* 251:112. doi: 10.1007/s00425-020-03402-5

Nikolov, L. A., Endress, P. K., Sugumaran, M., Sasirat, S., Vessabutr, S., Kramer, E. M., et al. (2013). Developmental origins of the world's largest flowers, Rafflesiaceae. *Proc. Natl. Acad. Sci. U. S. A.* 110, 18578–18583. doi: 10.1073/pnas.1310356110

Norberg, M., Holmlund, M., and Nilsson, O. (2005). The BLADE ON PETIOLE genes act redundantly to control the growth and development of lateral organs. *Development* 132, 2203–2213. doi: 10.1242/dev.01815

Ojeda, I., Francisco-Ortega, J., and Cronk, Q. C. B. (2009). Evolution of petal epidermal micromorphology in Leguminosae and its use as a marker of petal identity. *Ann. Bot.* 104, 1099–1110. doi: 10.1093/aob/mcp211

Parkin, J. (1928). The glossy petal of ranunculus. *Ann. Bot.* os-42, 739–755. doi: 10.1093/oxfordjournals.aob.a090138

Parkin, J. (1931). The structure of the starch layer in the glossy petal of ranunculus. *Ann. Bot.* os-45, 201–205. doi: 10.1093/oxfordjournals.aob.a090266

Pelaz, S., Ditta, G. S., Baumann, E., Wisman, E., and Yanofsky, M. F. (2000). B and C floral organ identity functions require SEPALLATA MADS-box genes. *Nature* 405, 200–203. doi: 10.1038/35012103

Perbal, M. C., Haughn, G., Saedler, H., and Schwarz-Sommer, Z. (1996). Non-cell-autonomous function of the *Antirrhinum* floral homeotic proteins DEFICIENS and GLOBOSA is exerted by their polar cell-to-cell trafficking. *Development* 122, 3433–3441. doi: 10.1242/dev.122.11.3433

Perez-Rodriguez, M., Jaffe, F. W., Butelli, E., Glover, B. J., and Martin, C. (2005). Development of three different cell types is associated with the activity of a specific MYB transcription factor in the ventral petal of *Antirrhinum majus* flowers. *Development* 132, 359–370. doi: 10.1242/dev.01584

Prunet, N., Yang, W., Das, P., Meyerowitz, E. M., and Jack, T. P. (2017). SUPERMAN prevents class B gene expression and promotes stem cell termination in the fourth whorl of *Arabidopsis thaliana* flowers. *Proc. Natl. Acad. Sci. U. S. A.* 114, 7166–7171. doi: 10.1073/pnas.1705977114

Quattrocchio, F., Wing, J. F., Leppen, H. T. C., Mol, J. N. M., and Koes, R. E. (1993). Regulatory genes controlling anthocyanin pigmentation are functionally conserved among plant species and have distinct sets of target genes. *Plant Cell* 5, 1497–1512. doi: 10.2307/3869734

Quattrocchio, F., Wing, J., van der Woude, K., Souer, E., de Vetten, N., Mol, J., et al. (1999). Molecular analysis of the anthocyanin2 gene of petunia and its role in the evolution of flower color. *Plant Cell* 11, 1433–1444. doi: 10.1105/tpc.11.8.1433

Ramsay, N. A., and Glover, B. J. (2005). MYB–bHLH–WD40 protein complex and the evolution of cellular diversity. *Trends Plant Sci.* 10, 63–70. doi: 10.1016/j.tplants.2004.12.011

Ren, H., Dang, X., Cai, X., Yu, P., Li, Y., Zhang, S., et al. (2017). Spatio-temporal orientation of microtubules controls conical cell shape in *Arabidopsis thaliana* petals. *PLoS Genet.* 13:e1006851. doi: 10.1371/journal.pgen.1006851

Ren, H., Dang, X., Yang, Y., Huang, D., Liu, M., Gao, X., et al. (2016). SPIKE1 activates ROP GTPase to modulate petal growth and shape. *Plant Physiol.* 172, 358–371. doi: 10.1104/pp.16.00788

Robinson, D. O., and Roeder, A. H. K. (2015). Themes and variations in cell type patterning in the plant epidermis. *Curr. Opin. Genet. Dev.* 32, 55–65. doi: 10.1016/j.gde.2015.01.008

Roddy, A. B., Brodersen, C. R., and Dawson, T. E. (2016). Hydraulic conductance and the maintenance of water balance in flowers: hydraulic structure-function of flowers. *Plant Cell Environ.* 39, 2123–2132. doi: 10.1111/pce.12761

Saffer, A. M., Carpita, N. C., and Irish, V. F. (2017). Rhamnose-containing cell wall polymers suppress helical plant growth independently of microtubule orientation. *Curr. Biol.* 27, 2248.e4–2259.e4. doi: 10.1016/j.cub.2017.06.032

Satina, S., and Blakeslee, A. F. (1941). Periclinal chimeras in datura stramonium in relation to development of leaf and flower. *Am. J. Bot.* 28, 862–871. doi: 10.1002/j.1537-2197.1941.tb11017.x

Sauret-Gueto, S., Schiessl, K., Bangham, A., Sablowski, R., and Coen, E. (2013). JAGGED controls *Arabidopsis* petal growth and shape by interacting with a divergent polarity field. *PLoS Biol.* 11:e1001550. doi: 10.1371/journal.pbio.1001550

Schwarz-Sommer, Z., Huijser, P., Nacken, W., Saedler, H., and Sommer, H. (1990). Genetic control of flower development by homeotic genes in *Antirrhinum majus*. *Science* 250, 931–936. doi: 10.1126/science.250.4983.931

Shibuya, K., Niki, T., and Ichimura, K. (2013). Pollination induces autophagy in petunia petals via ethylene. *J. Exp. Bot.* 64, 1111–1120. doi: 10.1093/jxb/ers395

Siegfried, K. R., Eshed, Y., Baum, S. F., Otsuga, D., Drews, G. N., and Bowman, J. L. (1999). Members of the YABBY gene family specify abaxial cell fate in *Arabidopsis*. *Development* 126, 4117–4128. doi: 10.1242/dev.126.18.4117

Skaliter, O., Kitsberg, Y., Sharon, E., Shklarman, E., Shor, E., Masci, T., et al. (2021). Spatial patterning of scent in *Petunia corolla* is discriminated by bees and involves the ABCG1 transporter. *Plant J.* 106, 1746–1758. doi: 10.1111/tpj.15269

Soltis, D. E., Chanderbali, A. S., Kim, S., Buzgo, M., and Soltis, P. S. (2007). The ABC model and its applicability to basal angiosperms. *Ann. Bot.* 100, 155–163. doi: 10.1093/aob/mcm117

Spelt, C., Quattrocchio, F., Mol, J. N. M., and Koes, R. (2000). anthocyanin1 of petunia encodes a basic helix-loop-helix protein that directly activates transcription of structural anthocyanin genes. *Plant Cell* 12, 1619–1631. doi: 10.1105/tpc.12.9.1619

Szécsi, J., Wippermann, B., and Bendahmane, M. (2014). Genetic and phenotypic analyses of petal development in *Arabidopsis*. *Methods Mol. Biol.* 1110, 191–202. doi: 10.1007/978-1-4614-9408-9_8

Tan, J., Walford, S.-A., Dennis, E. S., and Llewellyn, D. (2016). Trichomes control flower bud shape by linking together young petals. *Nat. Plants* 2:16093. doi: 10.1038/nplants.2016.93

The Plant List (2013). Version 1.1. Published on the Internet. Available at: http://www.theplantlist.org/ (Accessed October 22, 2021).

Thomson, B., and Wellmer, F. (2019). Molecular regulation of flower development. *Curr. Top. Dev. Biol.* 131, 185–210. doi: 10.1016/bs.ctdb.2018.11.007

Urbanus, S. L., de Folter, S., Shchennikova, A. V., Kaufmann, K., Immink, R. G., and Angenent, G. C. (2009). In planta localisation patterns of MADS domain proteins during floral development in *Arabidopsis thaliana*. *BMC Plant Biol.* 9:5. doi: 10.1186/1471-2229-9-5

Vainstein, A., and Sharon, R. (1993). Biogenesis of petunia and carnation corolla chloroplasts: changes in the abundance of nuclear and plastid-encoded photosynthesis-specific gene products during flower development. *Physiol. Plant.* 89, 192–198. doi: 10.1111/j.1399-3054.1993.tb01805.x

van der Kooi, C. J., Elzenga, J. T. M., Dijksterhuis, J., and Stavenga, D. G. (2017). Functional optics of glossy buttercup flowers. *J. R. Soc. Interface* 14:20160933. doi: 10.1098/rsif.2016.0933

van der Kooi, C. J., and Stavenga, D. G. (2019). Vividly coloured poppy flowers due to dense pigmentation and strong scattering in thin petals. *J. Comp. Physiol. A Neuroethol. Sens. Neural Behav. Physiol.* 205, 363–372. doi: 10.1007/s00359-018-01313-1

van Doorn, W. G., Balk, P. A., van Houwelingen, A. M., Hoeberichts, F. A., Hall, R. D., Vorst, O., et al. (2003). Gene expression during anthesis and senescence in iris flowers. *Plant Mol. Biol.* 53, 845–863. doi: 10.1023/B:PLAN.0000023670.61059.1d

van Doorn, W. G., and Van Meeteren, U. (2003). Flower opening and closure: a review. *J. Exp. Bot.* 54, 1801–1812. doi: 10.1093/jxb/erg213

van Doorn, W. G., and Woltering, E. J. (2008). Physiology and molecular biology of petal senescence. *J. Exp. Bot.* 59, 453–480. doi: 10.1093/jxb/erm356

van Es, S. W., Silveira, S. R., Rocha, D. I., Bimbo, A., Martinelli, A. P., Dornelas, M. C., et al. (2018). Novel functions of the *Arabidopsis* transcription factor TCP5 in petal development and ethylene biosynthesis. *Plant J.* 94, 867–879. doi: 10.1111/tpj.13904

Vignolini, S., Thomas, M. M., Kolle, M., Wenzel, T., Rowland, A., Rudall, P. J., et al. (2012). Directional scattering from the glossy flower of *ranunculus*: how the buttercup lights up your chin. *J. R. Soc. Interface* 9, 1295–1301. doi: 10.1098/rsif.2011.0759

Vincent, C. A., Carpenter, R., and Coen, E. S. (2003). Interactions between gene activity and cell layers during floral development. *Plant J.* 33, 765–774. doi: 10.1046/j.1365-313X.2003.01666.x

Weiss, D., and Halevy, A. H. (1991). The role of light reactions in the regulation of anthocyanin synthesis in *Petunia corollas*. *Physiol. Plant.* 81, 127–133. doi: 10.1111/j.1399-3054.1991.tb01724.x

Weiss, D., Schönfeld, M., and Halevy, A. H. (1988). Photosynthetic activities in the *Petunia corolla*. *Plant Physiol.* 87, 666–670. doi: 10.1104/pp.87.3.666

Weiss, D., Shomer-Ilan, A., Vainstein, A., and Halevy, A. H. (1990). Photosynthetic carbon fixation in the corollas of *Petunia hybrida*. *Physiol. Plant.* 78, 345–350. doi: 10.1111/j.1399-3054.1990.tb09046.x

Weston, E. L., and Pyke, K. A. (1999). Developmental ultrastructure of cells and plastids in the petals of wallflower (*Erysimum cheiri*). *Ann. Bot.* 84, 763–769. doi: 10.1006/anbo.1999.0981

Whatley, J. M. (1984). The ultrastructure of plastids in the petals of *Caltha palustris* L. *New Phytol.* 97, 227–231. doi: 10.1111/j.1469-8137.1984.tb04126.x

Whitney, H. M., Bennett, K. M. V., Dorling, M., Sandbach, L., Prince, D., Chittka, L., et al. (2011a). Why do so many petals have conical epidermal cells? *Ann. Bot.* 108, 609–616. doi: 10.1093/aob/mcr065

Whitney, H. M., Chittka, L., Bruce, T. J. A., and Glover, B. J. (2009a). Conical epidermal cells allow bees to grip flowers and increase foraging efficiency. *Curr. Biol.* 19, 948–953. doi: 10.1016/j.cub.2009.04.051

Whitney, H. M., Kolle, M., Andrew, P., Chittka, L., Steiner, U., and Glover, B. J. (2009b). Floral iridescence, produced by diffractive optics, acts as a cue for animal pollinators. *Science* 323, 130–133. doi: 10.1126/science.1166256

Whitney, H. M., Poetes, R., Steiner, U., Chittka, L., and Glover, B. J. (2011b). Determining the contribution of epidermal cell shape to petal wettability using isogenic *Antirrhinum* lines. *PLoS One* 6:e17576. doi: 10.1371/journal.pone.0017576

Wood, W. M. L. (1953). Thermonasty in tulip and crocus flowers. *J. Exp. Bot.* 4, 65–77. doi: 10.1093/jxb/4.1.65

Wuest, S. E., O'Maoileidigh, D. S., Rae, L., Kwasniewska, K., Raganelli, A., Hanczaryk, K., et al. (2012). Molecular basis for the specification of floral organs by APETALA3 and PISTILLATA. *Proc. Natl. Acad. Sci. U. S. A.* 109, 13452–13457. doi: 10.1073/pnas.1207075109

Xu, X., Smaczniak, C., Muino, J. M., and Kaufmann, K. (2021). Cell identity specification in plants: lessons from flower development. *J. Exp. Bot.* 72, 4202–4217. doi: 10.1093/jxb/erab110

Yan, T., Li, L., Xie, L., Chen, M., Shen, Q., Pan, Q., et al. (2018). A novel HD-ZIP IV/MIXTA complex promotes glandular trichome initiation and cuticle development in *Artemisia annua*. *New Phytol.* 218, 567–578. doi: 10.1111/nph.15005

Yao, X., Zhang, W., Duan, X., Yuan, Y., Zhang, R., Shan, H., et al. (2019). The making of elaborate petals in *Nigella* through sdevelopmental repatterning. *New Phytol.* 223, 385–396. doi: 10.1111/nph.15799

Zhang, F.-P., Murphy, M. R. C., Cardoso, A. A., Jordan, G. J., and Brodribb, T. J. (2018). Similar geometric rules govern the distribution of veins and stomata in petals, sepals and leaves. *New Phytol.* 219, 1224–1234. doi: 10.1111/nph.15210

Conflict of Interest: The authors declare that the research was conducted in the absence of any commercial or financial relationships that could be construed as a potential conflict of interest.

Publisher's Note: All claims expressed in this article are solely those of the authors and do not necessarily represent those of their affiliated organizations, or those of the publisher, the editors and the reviewers. Any product that may be evaluated in this article, or claim that may be made by its manufacturer, is not guaranteed or endorsed by the publisher.

frontiers in Plant Science

ORIGINAL RESEARCH
published: 19 November 2021
doi: 10.3389/fpls.2021.769246

Micro- and Macroscale Patterns of Petal Morphogenesis in *Nigella damascena* (Ranunculaceae) Revealed by Geometric Morphometrics and Cellular Analyses

Pierre Galipot[1,2], Sylvain Gerber[1], Martine Le Guilloux[2], Florian Jabbour[1] and Catherine Damerval[2]**

[1] Institut de Systématique, Evolution, Biodiversité (ISYEB), Muséum National d'Histoire Naturelle, CNRS, Sorbonne Université, EPHE, Université des Antilles, Paris, France, [2] Génétique Quantitative et Evolution-Le Moulon, Université Paris-Saclay, INRAE, CNRS, AgroParisTech, Gif-sur-Yvette, France

Petals, the inner organs in a differentiated perianth, generally play an important role in pollinator attraction. As such they exhibit an extraordinary diversity of shapes, sizes, and colors. Being involved in pollinator attraction and reward, they are privileged targets of evolution. The corolla of the Ranunculaceae species *Nigella damascena* consists of elaborate nectariferous petals, made of a stalk, upper, and lower lips forming a nectar pouch, shiny pseudonectaries, and pilose ears. While the main events of petal development are properly described, a few is known about the pattern of organ size and shape covariation and the cellular dynamics during development. In this study, we investigated the relationships between morphogenesis and growth of *N. damascena* petals using geometric morphometrics coupled with the study of cell characteristics. First, we found that petal shape and size dynamics are allometric during development and that their covariation suggests that petal shape change dynamics are exponentially slower than growth. We then found that cell proliferation is the major driver of shape patterning during development, while petal size dynamics are mostly driven by cell expansion. Our analyses provide a quantitative basis to characterize the relationships between shape, size, and cell characteristics during the development of an elaborate floral structure. Such studies lay the ground for future evo-devo investigations of the large morphological diversity observed in nectariferous structures, in Ranunculaceae and beyond.

Keywords: ***Nigella damascena*, petal, allometry, geometric morphometrics, morphogenesis, Ranunculaceae, development**

OPEN ACCESS

Edited by:
Elena M. Kramer,
Harvard University, United States

Reviewed by:
Bharti Sharma,
California State Polytechnic University, Pomona, United States
Rui Zhang,
Northwest A&F University, China

***Correspondence:**
Florian Jabbour
fjabbour@mnhn.fr
Catherine Damerval
catherine.damerval@universite-paris-saclay.fr

Specialty section:
This article was submitted to Plant Development and EvoDevo, a section of the journal Frontiers in Plant Science

Received: *01 September 2021*
Accepted: *12 October 2021*
Published: *19 November 2021*

Citation:
Galipot P, Gerber S, Le Guilloux M, Jabbour F and Damerval C (2021) Micro- and Macroscale Patterns of Petal Morphogenesis in Nigella damascena (Ranunculaceae) Revealed by Geometric Morphometrics and Cellular Analyses. Front. Plant Sci. 12:769246. doi: 10.3389/fpls.2021.769246

INTRODUCTION

In the flowers of most angiosperms, sterile structures, collectively called the perianth, surround fertile organs and are organized in two functionally and morphologically differentiated organ types. While the most external organs, i.e., the sepals, play a protective role for the developing stamens and carpels, the innermost perianth organs, i.e., the petals, generally carry an attractive role for pollinators, based on a particular shape, size, color, and sometimes fragrance. Elaborate petals, as opposed to simple petals, have been described in various eudicot groups. They have evolved a variety of patterns, such as lobes, spurs, and specialized trichomes (Endress and Matthews, 2006).

In the early-diverging eudicot family Ranunculaceae, a large diversity of petal forms is found, from simple laminas with a tiny nectariferous scale, as in *Ranunculus*, to highly elaborate nectariferous spurred organs, as in *Aquilegia*. Floral development and, to a lesser extent, petal development have already been described qualitatively using the classical microscopy techniques (Erbar et al., 1999; Tucker and Hodges, 2005; Jabbour et al., 2009, 2015; Ren et al., 2009; Zhao et al., 2011). A detailed investigation of the development of the elaborate petal has been conducted in the genus *Nigella* using histology and micro-CT (Yao et al., 2019). It has been shown that petal complexity is progressively acquired during development, as different elaborated features appear sequentially, giving rise to a mature petal that comprises a stalk, upper, and lower lips, a nectar pouch, lobes, pseudonectaries (Liao et al., 2020), trichomes, and color patterns. Although some of these features are present in all *Nigella* species, others are shared by few species only (Yao et al., 2019). Nevertheless, the precise quantification of petal shape transformation, as well as the covariation of petal shape with petal growth, during development, is still lacking.

From a developmental perspective, petals are lateral organs initiated as groups of cells on the flank of the floral meristem. After polarity establishment, the transitions from the period of cell proliferation to expansion and differentiation in space and time are key to shape acquisition. The shape is altered during development due to variation in local growth rates and anisotropy (for review, Whitewoods and Coen, 2017). In model species such as *Arabidopsis thaliana* and *Antirrhinum majus*, clonal cell analysis has provided information on the growth processes at play, opening the way to mathematical modeling (Rolland-Lagan et al., 2003; Sauret-Güeto et al., 2013). When the study species is not amenable to such cell lineage marking, the analyses of cell proliferation, cell counting, and measurements can give clues about the processes directing shape variation, as demonstrated in the spurred petals of *Aquilegia*, *Centranthus*, and *Linaria* (Puzey et al., 2012; Mack and Davis, 2015; Cullen et al., 2018). Still, at a more integrated level, the quantification of allometry during development with the geometric morphometric methods provides invaluable information on form transformation (Gerber, 2014; Klingenberg, 2016).

As in other *Nigella* species, the mature petal of *Nigella damascena* is composed of several differentiated domains (**Figure 1**). These domains differentiate progressively during development from a simple lamina (Jabbour et al., 2015). Their respective contribution to the overall petal shape and size during development is still to be described. Shape and size are two characteristics that may theoretically change independently during development. While shape and size are often treated conceptually and analytically as distinct components of form, their dynamics are, in fact, often governed by common processes (e.g., cell proliferation or cell expansion). Nevertheless, other processes seem to preferentially affect shape (e.g., cell rearrangements) or size (e.g., homogeneous cell expansion). For these reasons, there is no universal rule governing shape and size dynamics during development (Klingenberg, 2016).

In this study, we conducted a geometric morphometric study coupled to cellular investigations to assess the pattern of shape and size variation and covariation during the development of *N. damascena* petal. We found that covariation between shape and size is linearized when considering the log of size, suggesting an exponential allometric relationship between these variables. By repeating the study with different domains of the petal (stalk and nectar pouch) with distinct geometries, we found that this relationship seems to hold at these subscales, suggesting that this exponential relationship is based on general mechanisms. As cell expansion and cell division are the two main processes that influence petal size and shape, we followed their dynamics during petal development through the cell map analysis. We then managed to measure their relative contributions to petal size and shape changes. Focusing on the petal dorsal view, corresponding to the lower lip of the nectar pouch, we found that cell proliferation is prevalent in the first stages, which correspond to the period when most of the mature shapes are achieved. We then found that, in late stages, cell expansion takes over and controls the final growth of the petal but without leading to major shape changes.

MATERIALS AND METHODS

Scanning Electron Microscopy

A total of 121 terminal flower buds were sampled from *N. damascena* plants grown in a growth chamber or in a greenhouse, from 8 days after floral transition to preanthetic flowers, for a time period of about 3 weeks. The sampling was designed to cover the time period of petal development and shape acquisition after the lag time following petal initiation (Jabbour et al., 2015). Floral buds were fixed in FAA (90% ethanol 70%, 5% formalin, 5% acetic acid) and then dissected under a stereoscope (Nikon, Tokyo, Japan SMZ 745T). Petals were then dehydrated in an ethanol series (70%, 80%, absolute alcohol) and dried using an Emitech K850 critical-point dryer (Quorum Technologies, Laughton, United Kingdom). Samples were mounted on the aluminum stubs with colloidal graphite, sputter-coated with platinum using an EM ACE600 fine coater (Leica, Wetzlar, Germany), and observed using a SU3500 scanning electron microscope (SEM, Hitachi, Tokyo, Japan).

Four different views (i.e., dorsal, ventral, medial-sagittal, and lateral-sagittal; **Figure 1**) were used to satisfactorily capture the three-dimensional (3D) form of *N. damascena* petal throughout

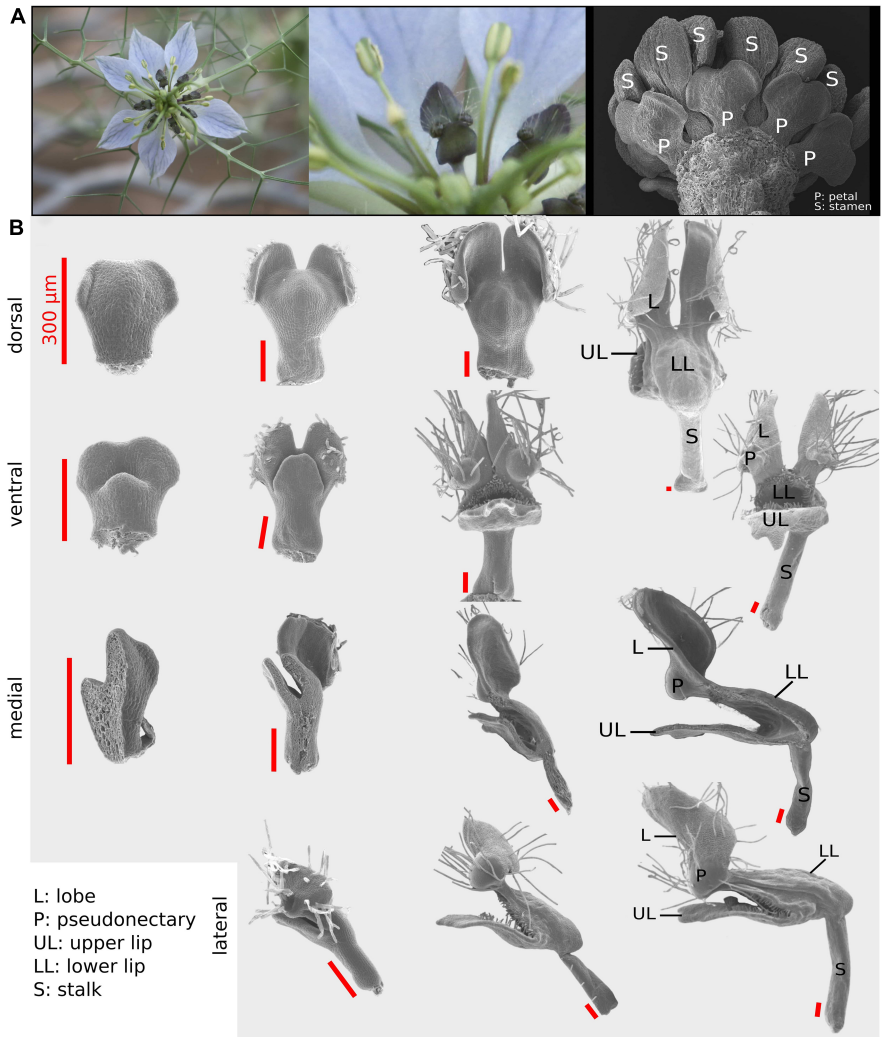

FIGURE 1 | The *Nigella damascena* petal and its developmental sequence. **(A)** Wild-type flowers of *N. damascena* comprise 7–9 petals. **(B)** Four views have been used to recapitulate petal morphogenesis: dorsal, ventral, medial, and lateral. On every column, petals are approximately at the same developmental stage. First column petals are taken after the restart of petal development (which undergoes a stasis after petal primordia formation). In the last column, petal morphogenesis is almost complete and all elaborations are present.

development. Among the 121 dissected petals, 32 were mounted for dorsal view observation, 33 for ventral view, 36 for sagittal section observed from the medial side (hereafter "medial"), and 20 for sagittal section observed from the lateral side (hereafter "lateral") (**Figure 1**). The medial and lateral views were informative regarding the shape of both the nectar pouch and the lobes.

Geometric Morphometrics

Both shape and size of the growing petal were characterized morphometrically from the 2D configurations of landmarks defined for each of the four views. These configurations were chosen to ensure that the landmarks could be unambiguously identified and digitized on all specimens across the entire developmental phase studied. Consequently, some structures that were not yet present at the early stages, such as pseudonectaries, had to be ignored from our morphometric scheme. We also chose not to consider the lobed structures (except for their radial ridge), since they start to fold precociously in development, thereby precluding the definition of reliable landmarks.

We used 12, 10, 8, and 7 landmarks (for ventral, dorsal, medial, and lateral, respectively) and 1, 3, and 1 series of 25 semi-landmarks (for ventral, medial side, and lateral side, respectively) to capture the homologous curved outlines of the lower lip (ventral and sagittal sides) and the petal lobes (sagittal sides) (**Figure 2**).

Landmark coordinates were manually recorded using tpsDig2 (Rohlf, 2015) and processed following standard procedures with tpsRelw (Rohlf, 2015). Landmark configurations were optimally aligned by generalized Procrustes analysis (Dryden and Mardia, 2016), which extract shape data by filtering out differences in scale, location, and orientation among raw

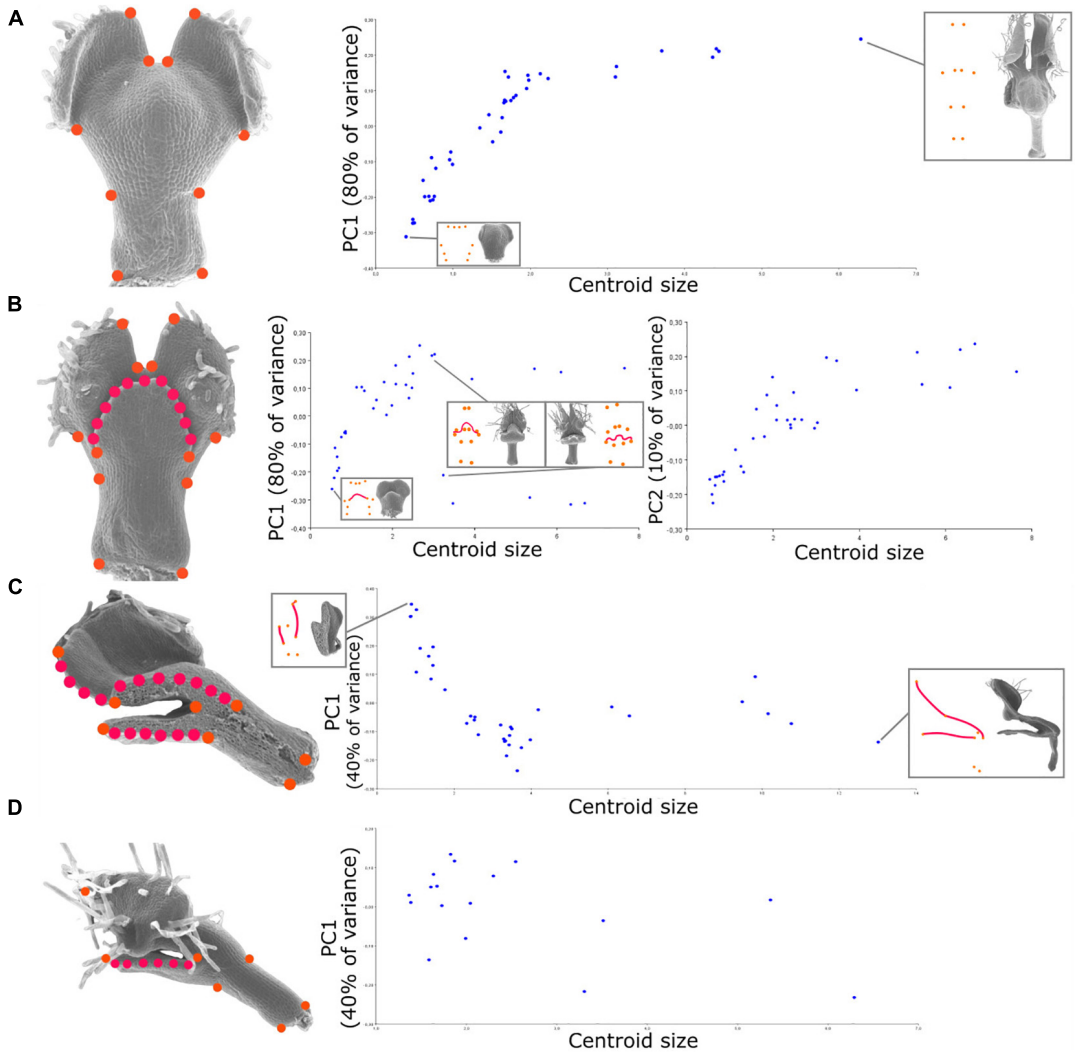

FIGURE 2 | Relationship between shape and size during petal development revealed by geometric morphometrics of the developing *N. damascena* petal in the four views (i.e., dorsal, ventral, medial, and lateral). On the left side of **(A–D)** panels, landmark sets are indicated and superimposed to the corresponding petal scanning electron microscopy (SEM) pictures (orange dots are landmarks, and red dots are semi-landmarks). For the four views, the Procrustes analyses are followed by the principal component analysis (PCA), and its first axis (and also the second axis for ventral view) is plotted against centroid size (proxy of petal size). The first axis explains 80% of the variance for dorsal and ventral views and 40% of the variance for medial and lateral views. The percentage of variance explained by an axis corresponds to the ratio between the variance of that principal component and the total variance.

landmark configurations. The minimum bending energy was used as a criterion to slide the semi-landmarks. The statistical analyses of shape variation were then carried out from the shape tangent coordinates. Notably, the landmark configurations for the ventral and dorsal views are the instances of configurations exhibiting bilateral object symmetry. Landmarks have been digitized on both sides, but only the symmetric component of shape variation was considered in subsequent analyses by averaging each specimen with its reflected copy. The patterns of shape variation were explored using the principal component analysis (PCA) (Jolliffe, 1986), and the patterns of ontogenetic allometry were investigated with multivariate regression of shape on size (i.e., centroid size).

We applied the same protocol on the subsets of landmarks corresponding to petal subdomains. Both stalk and nectar pouch were the only domains of the petal that could be identified at every stage of development. They were separately analyzed to examine their particular growth dynamics and possible contributions to the overall shape changes (**Figures 3C,D**).

Cell Characteristics in the Nectar Pouch Domain

We investigated cell characteristics in the nectar pouch domain using the area delimited by six landmarks in the dorsal view. We took advantage of the fact that cell boundaries are visible on SEM images to (i) count cells and measure the total surface

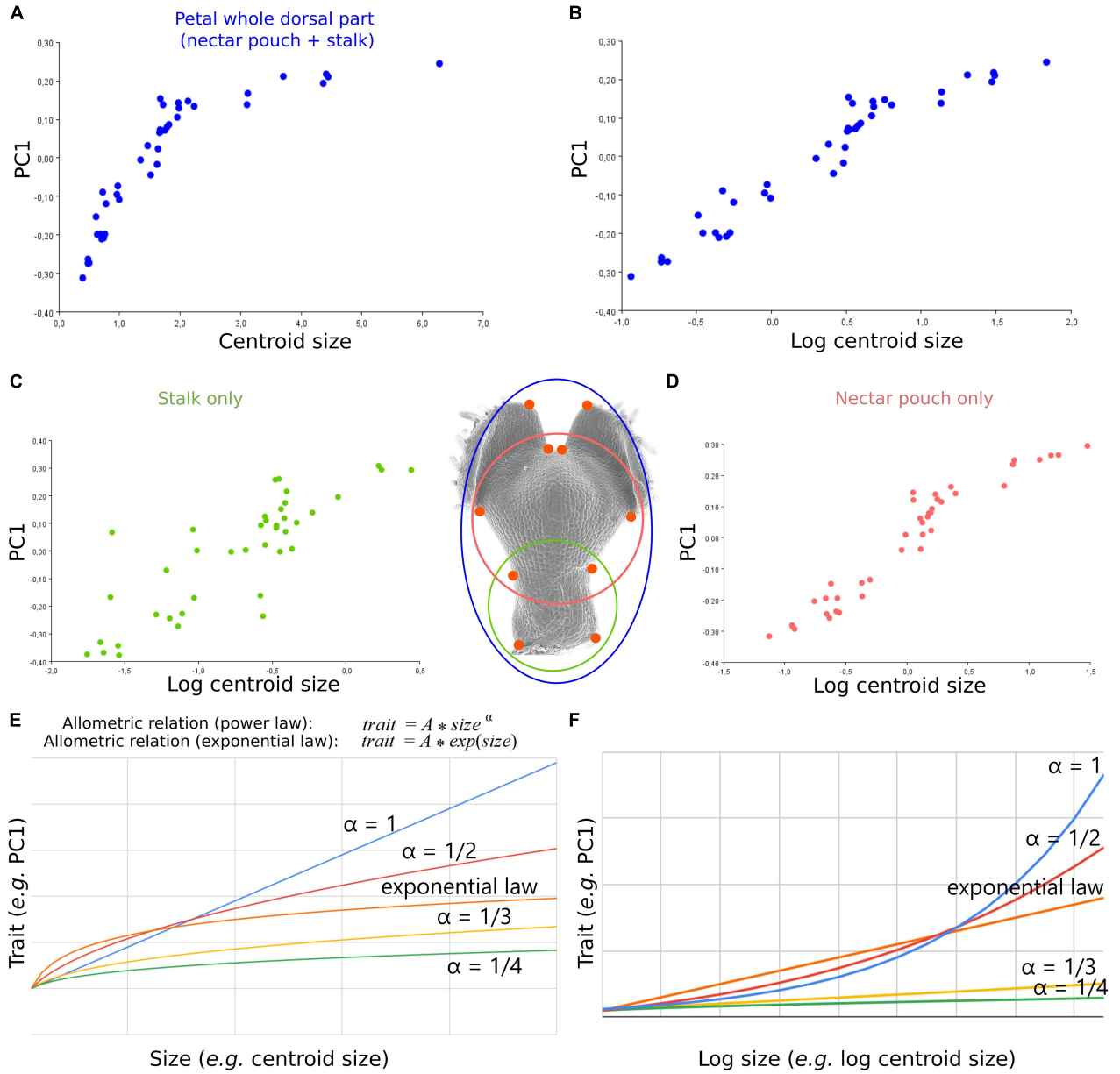

FIGURE 3 | An allometric relation, potentially exponential, links shape and size dynamics of *N. damascena* whole petal from dorsal view and its subdomains (stalk and nectar pouch) during morphogenesis. **(A)** The first axis of PCA of dorsal view plotted against centroid size (proxy of petal size) and log of centroid size, and **(B)** shows that their covariation is well approximated by an exponential law. The same analysis was performed on the subsets of landmarks delimiting stalk only **(C)** and nectar pouch only **(D)**. Comparison between exponential and power-law allometric relations of a trait (PC1 in this study) and size **(E)** or log size **(F)**.

of the domain, making it possible to calculate the mean cell surface for each sample; (ii) transform the nectar pouch domain into a tessellating network using Fiji software (Schindelin et al., 2012), in order to visualize cell populations that may differ by shape, size, and number during development. All the SEM pictures where cell boundaries were clearly visible have been used, which corresponds to 17 petals, covering the same developmental sequence as in the geometric morphometric analyses.

Cell area and elongation analyses and color representations were performed with Fiji MorphoLibJ plugins (Legland et al., 2016). Violin plots were produced with R (version 4.0.5) and ggplot2 library (version 3.3.2).

We used a unique cell color coding for all petals in order to be able to visually compare the stages (i.e., all cell area and cell elongation maps are available in **Supplementary Figure 1**). We then extracted cell area and elongation distribution using violin plots, the latter being plotted against the total cell number for each specimen.

Since the petals are not planar objects, the deviations from a perfect plane model were estimated by angle measurements

on medial and lateral views in Fiji software, and they were shown to be an order of magnitude smaller than the apparent size differences among cells. This implies that the observed differences cannot be explained only by an effect of focal length distortion and angle of view effect.

Relative Contributions of Cell Proliferation and Cell Expansion to Shape Transformation

Geometric morphometrics is based on the coordinates of landmarks optimally aligned through a series of steps, one of which removing the effect of scale. This implies that any shape variation can be viewed as a differential evolution of the distances between pairs of landmarks. Consequently, we used this assumption to investigate the number and size of cells that are located between every pair of landmarks corresponding, in dorsal view, to the nectar pouch (**Figure 4A**). We defined three stages (i.e., early, mid, and late plus adult stages; **Figure 4B**), and for each stage, we calculated cell number and absolute length between every pair of landmarks. Three individuals for each stage were used for averaging purposes, and a left/right average was also performed to match the geometric morphometric analyses, which use only the symmetric component. We then calculated what we called the cell proliferation contribution (*Cp*) and the cell expansion contribution (*Ce*) as follows:

$$Cp^{i,j}(stage\ 2 - stage\ 1) = \left(\frac{N^{i,j}(stage\ 2) - N^{i,j}(stage\ 1)}{N^{i,j}(stage\ 1)}\right) / \left(\frac{D^{i,j}(stage\ 2) - D^{i,j}(stage\ 1)}{D^{i,j}(stage\ 1)}\right) \times 100$$

$$Ce^{i,j}(stage\ 2 - stage\ 1) = 100 - Cp^{i,j}\ (stage\ 2 - stage\ 1)$$

where $N^{i,j}$ is the cell number between landmarks i and j at a given stage, and $D^{i,j}$ is the distance between landmarks i and j at a given stage, which measure, for a given pair of landmarks and between two stages, what percentage of the increase in absolute distance between these two landmarks can be attributed to cell proliferation or expansion, respectively (**Figures 4B,C**). More precisely, *Cp* is equal to proliferation rate (i.e., the number of supplementary cells compared with the initial amount, in percentage) divided by the expansion rate (i.e., the supplementary length compared with the initial distance, in percentage). *Ce* is equal to 100−*Cp*. We did not observe any decrease in the length or number of cells between two landmarks, from a young stage to an older stage, resulting in exclusively positive values for *Cp* and *Ce*.

Some landmark pairs target regions that contribute more than others to the shape variation during development, but the identification of these regions can be obscured by the Procrustes fit. We, therefore, used an alternative way to classify their contributions by attributing a "growth score" to each pair of landmarks, i.e., calculated as the ratio of the distance between them at the oldest stage divided by the length at the youngest stage.

RESULTS

Geometric Morphometrics of the Developing *Nigella damascena* Petal: An Allometric Law Governs the Covariation of Petal Shape and Size Dynamics During Development

To depict the allometric patterns of covariation between shape and size, we used a bivariate representation of their proxies (i.e., the first principal component of shape variation and centroid size, respectively). For the dorsal view, shape follows a fairly clear developmental path from the youngest to the oldest stages (**Figure 2A**). The variation of shape of the ventral view globally shows a pattern similar to that of the dorsal view, with the exception that late stages exhibit a bifurcation along the first axis (**Figure 2B**). This is explained by the positioning of the upper lip in either an open or closed position (the second component shows a trend closer to the dorsal one). For the medial view, we observed a similar trend for early to intermediate stages, as later stages show a plateau in terms of shape variation (**Figure 2C**). For the lateral view, the first two principal components of shape capture less shape variation (40 and 30%) than for the other views, and no clear developmental trajectory emerges from their pattern of covariation with size.

Covariation between size and global shape variations is well approximated by a mathematical relation at least for dorsal view, which, at a first approximation, seems exponential as it is linearized by applying log to size (**Figure 3B**). In other words, during overall petal development, dorsal shape (but also ventral and sagittal, although to a lesser degree) shows a shape acquisition exponentially slower than size. The morphometric analyses of the subsets of landmarks, corresponding to the stalk (**Figure 3C**, 4 landmarks) or the nectar pouch (**Figure 3D**, 6 landmarks), compared with overall petal analysis (**Figure 3A**, 10 landmarks), suggest that each substructure of the organ seems to behave similarly to the overall petal (in the sense that, to a given increase of size, the corresponding increment of shape change is lower and lower as the size increase). In particular, applying log to size partially linearizes the covariation between shape and size for only either stalk or nectar pouch (**Figures 3C,D**, respectively); however, it is much less clear than for the entire petal. The real relationship between size and shape is probably more subtle than a simple exponential law.

Disparities in Cell Characteristics on the Dorsal Part of the Nectar Pouch During Development

The dorsal part of the nectar pouch can be clearly delimited from the neighboring domains (i.e., lobes and stalk) from early to late stages, and as seen earlier, its shape acquisition follows a clear developmental trend. The relationship between its shape and size follows the same allometric relation as the overall petal. Together, these characteristics make the dorsal part of the nectar pouch a key model to study cellular processes (**Figure 5A**).

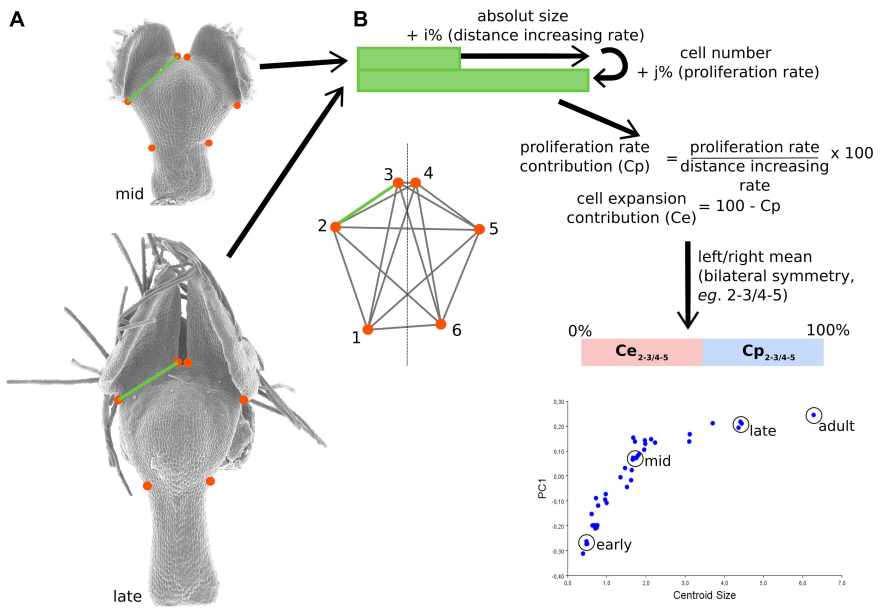

FIGURE 4 | The relative contribution of cell proliferation and cell expansion during nectar pouch development. Distances between every pair of landmarks recapitulate shape information as much as landmark coordinates **(A)**. The calculation of proliferation rate and cell expansion contributions to landmark inter-distance dynamics is presented **(B)**. Three triplets of petals corresponding to early, mid, and late stages and one adult petal have been used to study the contributions. For each individual, pairs of landmarks that are left-right symmetric have been averaged, and the measures of each triplet have also been averaged. The relative contributions of cell proliferation (light blue) and expansion (pink) are summarized in **(C)**. For each comparison (early to mid, mid to late, and early to late), landmarks have been ordered according to increasing inter-distance values between the two stages. Green bars correspond to the average rate of the increase in inter-landmark distance between consecutive stages.

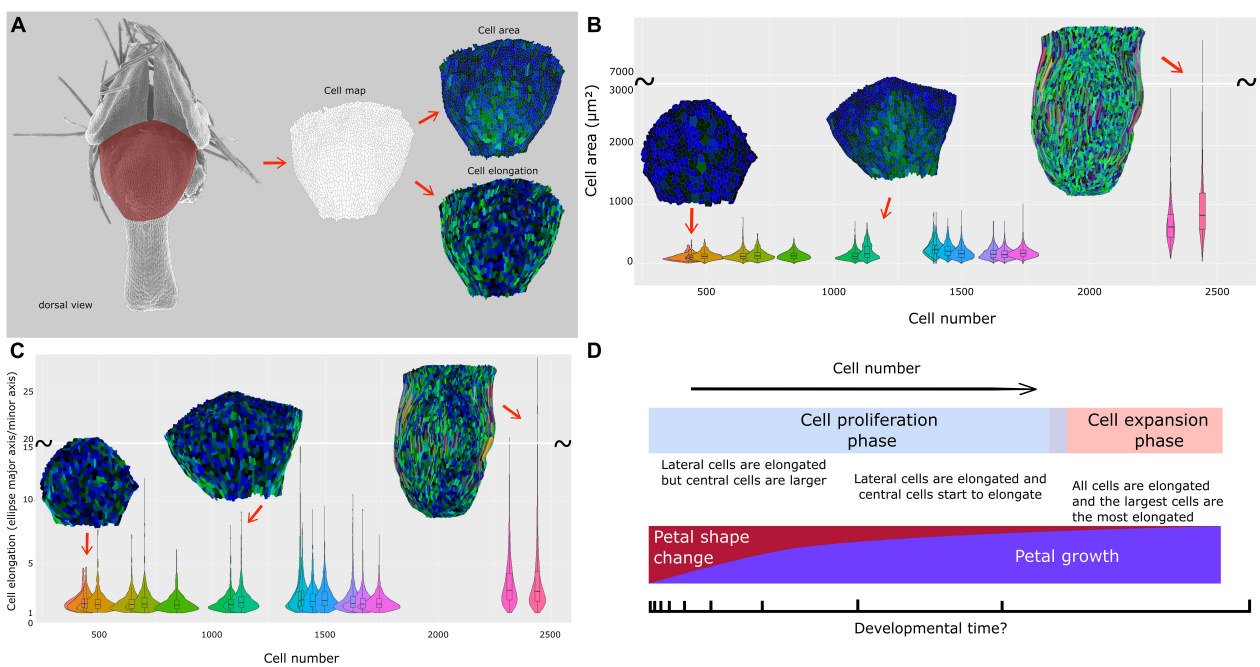

FIGURE 5 | Cell dynamics during petal morphogenesis with focus on a dorsal view of the nectar pouch. **(A)** The petal dorsal view of the nectar pouch has been transformed into cell maps to measure and visualize cell area (up) and cell expansion (down) dynamics. Color code is detailed in **Supplementary Figure 1**. Dynamics and distribution of cell area **(B)** and elongation (major axis/minor axis of the equivalent ellipse) **(C)** are visualized through violin plots, themselves plotted against total cell number. **(D)** Summary of macroscopic and cellular characteristics of *N. damascena* petal during development.

Cell number and mean cell surface were computed on the dorsal views of the nectar pouch. Despite a lack of resolution for older stages, the mean cell surface is globally constant, around 20 μm^2, from early to late stages, when suddenly mean cell size strongly increases to reach about 80 μm^2 (**Supplementary Figure 3A**). In parallel, in the first phase, cell number increases proportionally faster than petal size, but then it increases much slower when cells undergo cell growth (**Supplementary Figure 3B**).

The cell maps drawn from the dorsal views of the nectar pouch during development allowed us to highlight the diversity of cell behaviors in terms of shape and size changes, depending on their localization on the tissue. In the earliest stages, all cells have approximately the same size, but variance progressively tends to increase, and while the largest cells are located in the middle of the pouch, the most elongated ones are distributed on the lateral sides (**Figures 5B,C** and **Supplementary Figure 1**). Finally, as the pouch grows, the largest cells are also the most elongated ones, suggesting anisotropic expansion. Most of them are localized on the lateral sides, but central cells are also affected by elongation. Cells at the boundary between lobes and nectar pouch (i.e., the topmost cells in these maps) are characterized by small size and relatively limited elongation, even in the latest stages.

Disentangling the Contribution of Cell Proliferation and Cell Expansion in the Acquisition of the Final Shape and Size of the Nectar Pouch

If cell proliferation and cell expansion are the two major cell events that influence petal shape acquisition and growth, their respective contributions may vary during the petal development and remain to be determined.

The pairs of landmarks are arranged by increasing growth scores, measured as the ratio of the distances between consecutive stages (**Figure 4C**). Pairs whose score is higher or lower than the average can be considered as the ones contributing the most to the evolution of the overall shape. This permits to highlight a great difference in cell proliferation and growth contributions depending on the pairs of landmarks. In particular, it is interesting to note that between the early and intermediate stages, which is the most important interval in terms of shape patterning, cell proliferation is predominant for landmark pairs that undergo the largest expansion (with a high growth score, located at the right of **Figure 4C**) and almost absent for landmark pairs that undergo the smallest expansion [with a low growth score, located at the left of the graph (**Figure 4C**)]. Between intermediate and late stages, cell expansion becomes predominant (>80% for all pairs of landmarks).

DISCUSSION

Complex petal shape elaborations have been qualitatively described in many taxa. They are very common and diverse in some of them, such as Ranunculaceae or Rosids, and rarer in other taxa such as Asterids (Endress and Matthews, 2006). How these elaborations are acquired during development can also be found from numerous developmental studies (Kosuge and Tamura, 1988; Erbar et al., 1999; Tucker and Hodges, 2005; Sauret-Güeto et al., 2013; Sharma et al., 2014). However, the covariation of shape and size entailed by the progressive acquisition of the various elaborations contributing to a complex shape has been rarely studied. This study is the first attempt at this characterization using the Ranunculaceae species *N. damascena* and combining the analyses of geometric morphometrics and cell characteristics. We found that shape changes more rapidly than size increases at early stages, marking a nonlinear allometric relationship between them. In other words, the different domains constituting the mature petal differentiate quite early during development, well before the final size is reached. We also found that cell proliferation plays a major role in shape transformation, contrary to cell expansion, which rather contributes to petal growth. This strongly suggests that morphogenetic cues, whatever their nature, preferentially act through the spatial and temporal control of cell proliferation, while petal size establishment is controlled by cell expansion.

Developmental Patterns of Petal Shape and Size Dynamics

Size increases as development proceeds. To capture the complex shape of petals across their developmental range of size variation, each of the four views (i.e., dorsal, ventral, medial, and lateral) allows a focus on specific regions and transects, which give information not available in the other views (e.g., upper lip for ventral view or the bottom of the nectar pouch for medial view). At the exception of most of the shape of the lobes (including the pseudonectaries), every petal domain has been documented in this analysis, which was important considering that all these domains, as well as, in particular, their shape and arrangements, contribute in one way or another to the final shape of the petal as a biologically functional unit. For example, due to the location of the nectar at the bottom of the pouch, the stalk (and, in particular, its length) defines the position of the insect when it feeds. In the same way, nectar pouch size and shapes are crucial for nectar storage and reward access.

For a given view, we might have missed petal shape information because (i) SEM pictures are the 2D projections of a 3D shape, and (ii) the number of landmarks summarizing the overall shape is limited. These limitations impact the multidimensional analysis of shape. Nevertheless, several clues suggest that the PCA first axes are good proxies to follow petal shape variation during development, as long as the real ontogenetic trajectory is linear. First, 80% of the variation is carried by the first axis for dorsal and ventral views. Second, plots against centroid size show a clear developmental trend for three of the four views (i.e., distributions are sparsely dispersed). Among the four views, the dorsal view presents the clearest trend. The ventral view exhibits a bifurcation in large petals, explained by the presence of the upper lip, which is long enough in late stages to be either in an opened or closed position according to the sample, hence affecting the landmark positions and so the global shape. Many factors, such

as specimen preparation, could explain why the upper lip is in one or the other position for a given petal. However, if it strongly affects the global shape analysis, it is less relevant from a biological perspective. Nevertheless, the second principal component, while capturing only 10% of the total variation, does not discriminate the petals according to this "opening" criterion and presents a distribution close to that of the first component for the dorsal view. The sagittal medial view shows a clear trend for the young-to-medium individuals and then probably exhibits a plateau, although studying additional mature specimens would be needed to confirm it. Nevertheless, as this plateau is also observed for the second and third axes, it suggests that the final sagittal shape is reached earlier than the final size. Finally, the lateral view does not show any clear developmental trend (i.e., shape variation between two different developmental stages was not higher than that between two organs at the same stage), probably due to the lack of a sufficient sample of the early-stage petals and a very-large inter-individual variation.

Origin of the Allometric Relation, Which Links Petal Pouch Shape and Size Dynamics

The first axis of PCA coordinates variation, and the relative distance between two individuals on the axis can be interpreted not only qualitatively but also quantitatively and therefore constitutes a proxy for studying the dynamics of the variation in petal shape.

In this study and particularly for the dorsal view, the allometric relation observed between the dynamics of shape and the dynamics of size seems to be fairly approximated by an exponential law. Similar trends are also found for subdomains such as stalk or nectar pouch. To exclude an effect due to the unequal sampling of different stages in terms of size distribution, the Procrustes analysis and the PCAs were repeated using a subsampling procedure (**Supplementary Figure 2**). For all subsamplings, an exponential law is found again, which leads it to a more robust biological interpretation.

Nevertheless, more replicates would be needed to distinguish from an exponential law to a power law or another relationship (**Figures 3E,F**).

Several scenarios can explain this relationship between shape and size dynamics. In particular, such tight covariation may imply that there is a control of one parameter over the other, which in turn causes this quantitative relationship between them. On the contrary, as correlation is not causation, petal shape and size may not be linked causally but to a third parameter (e.g., developmental time), which could also cause such covariation.

In fact, the cell counts we performed suggest this last scenario. The relationship between cell number and petal surface seems globally linear in the early-to-mid stages (**Supplementary Figure 3B**), or, equivalently, the average surface of a cell is globally constant (around 20 μm^2, **Supplementary Figure 3A**) during the first part of the development.

If cell proliferation rate is assumed to be constant through developmental time (at least during this first part of development), it entails that the dorsal part of the petal nectar pouch follows an exponential growth. Consequently, every biological process that has a constant dynamic through developmental time will be automatically linked to the size of the dorsal part of the petal nectar pouch exponentially, even if there is no biological link between them. We assumed that it may be the case for shape changes and that the allometric relationship between shape and size is not causal for *N. damascena* petal nectar pouch. Although all of these assumptions concerned the early-mid "proliferation phase," which is also the phase where the shape changes the most, the "expansion" phase that follows may accentuate the shape of the distribution by stretching it at its tail. This probably explains why the distribution of shape against size does not clearly appear under two distinct phases, yet observed and measured on cellular parameters.

A complete and definitive confirmation of these assumptions (summarized in **Figure 5D**) would, however, require additional studies, such as real-time tracking of cell division during petal development.

Differential Contributions to Petal Size and Shape of Both Cell Division and Cell Expansion

External tissue shape derives from the four primary characteristics of cell features (Guillot and Lecuit, 2013): not only cell number and size but also cell shape and arrangements. These characteristics originate from growth processes, mainly cell proliferation and expansion, and from their local variation in rates and orientation (Rolland-Lagan et al., 2003). The distances between all pairs of landmarks carry equivalent information to shape coordinates and, therefore, recapitulates the shape, as coordinates do. This is the reason why we chose to measure the number and size of cells along transects between every pair of landmarks and compare them among the developmental stages. Contrary to many animal tissues, cell rearrangements (and cell death) are rare in plant epidermis (Dickman et al., 2017), but if they happened, they would be indistinguishable from cells produced by mitosis, and the real-time tracking of cell division would be needed to distinguish between the two phenomena. Nevertheless, if a cell moved and got inserted into the transect between two landmarks, this event would be considered as cell proliferation as it would affect the number of cells. Alternatively, cell shape variation affecting cells between two landmarks would be considered as cell expansion events (including cell size decrease) as they can affect cell width on this line. The four primary characteristics could hence be considered as two main cell characteristics, which are easily measurable between two landmarks. On the one hand, counting the number of cells between two landmarks and comparing this number between two stages will give access to a mean value of proliferation. Dividing the absolute distance between the two landmarks by the number of cells gives, on the other hand, the mean cell size and so the mean value of cell expansion through comparison between two stages.

Even if cell number and cell size can be characterized, it is not trivial to deduce their relative contributions to shape dynamics because the shape is reflected by the relative distances between landmarks and not directly the distances themselves. Even if the Procrustes analysis does not give access to this information, we managed to build some bridges between cell characteristics (i.e., microscopic level) and shape changes as reconstructed by geometric morphometrics (i.e., macroscopic level). We considered that pairs of landmarks that undergo extreme variations (i.e., the farthest from the mean) in terms of the relative distance between two stages are the ones that participate the most to shape variation. Thereby, we found that the lengths of the external ridges of the pouch (1–2, with its symmetric 5–6, **Figure 4C**) and, at the other extreme, the between lobe sinus width (3–4) are the major contributors to shape dynamics. Pairs of landmarks concerning petal length tend to undergo higher increases than those concerning petal width. This is coherent with the major axis of cell elongation visualized on cellular maps (**Figure 5** and **Supplementary Figure 1**).

The comparison between early-mid and mid-late graphs shows that cell proliferation has a preponderant role in the youngest stages, especially for the pouch width and overall length, which coincides with the phase where the shape changes the most. In later phases, cell expansion takes over, which supports the development in two phases, namely, first mainly proliferation and then mainly expansion, as has been reported for many plant organs (Rolland-Lagan et al., 2003; Puzey et al., 2012; Walcher-Chevillet and Kramer, 2016).

Finally, in the early-mid graph, corresponding to the crucial period in terms of shape changes, the pairs of landmarks that know the highest differential growths are governed at 50% or more by cell proliferation. On the contrary, in the pairs of landmarks that know the lowest differential growths (i.e., 3–4 and 1–6 pairs, corresponding between lobe sinus width and stalk width), cell proliferation is absent or almost absent, contrary to cell expansion. As a result, cell proliferation seems to be the predominant factor in shape dynamics and could therefore be the preferential cellular process controlled by the morphogenetic actors.

What Are the Potential Contributions of This Study to the Understanding of Petal Diversity in *Nigella* and Other Genera of Ranunculaceae?

Petal shape and elaborations are quite diverse in the genus *Nigella* (Yao et al., 2019). The authors have focused on the timing of elaborations during development in a comparative framework. They have shown that most cellular elaborations and species-specific elaborations such as upper lip tail, ridges, pseudonectaries, begin to appear at the S7 stage, which is comparable to our mid-stage. If the bi-phasic development of the petal shape that we observed in *N. damascena* is conserved among species, this means that elaborations take place at different stages at the end of the proliferation phase and during the expansion phase. In contrast, the overall outline of the petal shape could be acquired during the first developmental phase governed by cell proliferation, with species-specific local differential growth rates. Expanding our approach to species with contrasting shapes such as *Nigella integrifolia*, *Nigella orientalis*, and *Nigella arvensis*, for example, would help to understand the developmental bases of shape diversification in the genus.

One of the elaborations of the *Nigella* petal is the nectar pouch. While we did not directly examine the contributions of cell proliferation and cell expansion to the deepening of the pouch, the cell maps and the growth scores of the distances between landmarks (e.g., 1–5/2–6, 1–4/3–6) support also a bi-phasic developmental process. In Ranunculaceae, spurred petals are encountered in the genus *Aquilegia* and in the tribe Delphinieae. In *Aquilegia*, the spur is established through an early phase of localized cell proliferation, followed by a phase of anisotropic cell elongation. Interestingly, cell expansion and more specifically its duration account for 99% of the differences in spur elongation among species (Puzey et al., 2012). Because the ancestor of the Ranunculaceae is devoid of petal nectar spur, and *Aquilegia* and *Nigella* belong to different subfamilies (Cossard et al., 2016; Zhai et al., 2019), the spur in *Aquilegia* and the pouch in *Nigella* cannot be considered as homologous structures. However, hollow petals appear to originate according to similar two-phase developmental processes. The Delphinieae tribe that encompasses all other Ranunculaceae species with spurred petals is the sister group of Nigelleae, raising the possibility of homology between the pouch and the spurs in these tribes. The hollow part of the petal spurs in these species has very diverse shapes (Zalko et al., 2021), including different lengths, and it is much deeper than the *Nigella* petal pouch. From an evolutionary perspective, it would be interesting to compare the dynamics of spur and pouch development in Delphinieae species and in *Nigella*, to establish whether a bi-phasic developmental process is also at play in Delphinieae and, if so, if the spur/pouch morphological differences could be accounted for by differences in the duration of cell proliferation and/or expansion phases.

DATA AVAILABILITY STATEMENT

The raw data supporting the conclusions of this article will be made available by the authors, without undue reservation.

AUTHOR CONTRIBUTIONS

PG, FJ, and CD designed the experiments. ML, FJ, and CD grew, collected, and sampled the material. PG designed and performed the morphometric analyses and wrote the manuscript. SG contributed to the morphometric analyses. PG and CD designed and performed the cell map analyses. All authors contributed to the article and approved the submitted version.

FUNDING

This study was financially supported by the Institut de Systématique Évolution Biodiversité (ISYEB) and the Muséum National d'Histoire Naturelle (MNHN). CD benefits from the support of the Saclay Plant Sciences (SPS; ANR-10-LABX-0040-SPS, LabEx SPS, and ANR-17-EUR-0007, EUR SPS-GSR). PG was supported by a fellowship from ENS de Lyon.

ACKNOWLEDGMENTS

We acknowledge the Institut de Systématique Évolution Biodiversité (ISYEB) and the Muséum National d'Histoire Naturelle (MNHN) for their financial support. We thank the Plateau Technique de Microscopie Électronique (UMR 7245 CNRS/MNHN; Géraldine Toutirais) where the SEM study was conducted. We warmly thank Philippe Andrey for his useful comments and advice, notably on cell map analyses.

SUPPLEMENTARY MATERIAL

The Supplementary Material for this article can be found online at: https://www.frontiersin.org/articles/10.3389/fpls.2021.769246/full#supplementary-material

Supplementary Figure 1 | The sequence of cell maps colored by cell area or cell elongation values. Cell maps for cell area **(A)** and cell elongation **(B)** are ordered from top left to bottom right in increasing total surface. For every individual, a common color code has been used to make easier comparisons between stages.

Supplementary Figure 2 | Resamplings confirm the presence of an allometric law between shape and size during nectar pouch development. PC1 plots against centroid size **(A,C,E)** or log centroid size **(B,D,F)** after original sampling (characterized by an oversampling of smallest petals), equilibrate resampling (i.e., individuals regularly spaced on the size scale), and oversampling of largest petals. An exponential relation is found for every case, excluding a sampling bias and consolidating its biological origin.

Supplementary Figure 3 | Cell characteristics (mean size and number) during development. **(A)** Cell number plotted against nectar pouch surface (mm^2). **(B)** Mean cell size (μm^2) plotted against cell number shows a stasis phase of mean cell size (compatible with a proliferation phase), which ends with a sharp increase in cell mean size (compatible with an expansion phase).

REFERENCES

Cossard, G. G., Sannier, J., Sauquet, H., Damerval, C., Craene, L. R., Jabbour, F., et al. (2016). Subfamilial and tribal relationships of Ranunculaceae: evidence from eight molecular markers. *Plant Syst. Evol.* 302, 419–431. doi: 10.1007/s00606-015-1270-6

Cullen, E., Fernández-Mazuecos, M., and Glover, B. J. (2018). Evolution of nectar spur length in a clade of *Linaria* reflects changes in cell division rather than in cell expansion. *Ann. Bot.* 122, 801–809. doi: 10.1093/aob/mcx213

Dickman, M., Williams, B., Li, Y., de Figueiredo, P., and Wolpert, T. (2017). Reassessing apoptosis in plants. *Nat. Plants* 3, 773–779. doi: 10.1038/s41477-017-0020-x

Dryden, I. L., and Mardia, K. V. (2016). *Statistical Shape Analysis: With Applications in R*. Hoboken, NJ: John Wiley & Sons.

Endress, P. K., and Matthews, M. L. (2006). Elaborate petals and staminodes in eudicots: diversity, function, and evolution. *Org. Divers. Evol.* 6, 257–293. doi: 10.1016/j.ode.2005.09.005

Erbar, C., Kusma, S., and Leins, P. (1999). Development and interpretation of nectary organs in Ranunculaceae (May 16, 1998). *Flora* 194, 317–332. doi: 10.1016/S0367-2530(17)30920-9

Gerber, S. (2014). Not all roads can be taken: development induces anisotropic accessibility in morphospace. *Evol. Dev.* 16, 373–381. doi: 10.1111/ede.12098

Guillot, C., and Lecuit, T. (2013). Mechanics of epithelial tissue homeostasis and morphogenesis. *Science* 340, 1185–1189. doi: 10.1126/science.1235249

Jabbour, F., Ronse De Craene, L. P., Nadot, S., and Damerval, C. (2009). Establishment of zygomorphy on an ontogenic spiral and evolution of perianth in the tribe Delphinieae (Ranunculaceae). *Ann. Bot.* 104, 809–822. doi: 10.1093/aob/mcp162

Jabbour, F., Udron, M., Le Guilloux, M., Gonçalves, B., Manicacci, D., Nadot, S., et al. (2015). Flower development schedule and AGAMOUS-like gene expression patterns in two morphs of *Nigella damascena* (Ranunculaceae) differing in floral architecture. *Bot. J. Linn. Soc.* 178, 608–619. doi: 10.1111/boj.12297

Jolliffe, I. T. (1986). "Principal components in regression analysis," in *Principal Component Analysis. Springer Series in Statistics*, ed. I. T. Jolliffe (New York, NY: Springer), 129–155. doi: 10.1007/978-1-4757-1904-8_8

Klingenberg, C. P. (2016). Size, shape, and form: concepts of allometry in geometric morphometrics. *Dev. Genes Evol.* 226, 113–137. doi: 10.1007/s00427-016-0539-2

Kosuge, K., and Tamura, M. (1988). Morphology of the petal in *Aconitum*. *Bot. Mag. Shokubutsu Gaku Zasshi* 101, 223–237. doi: 10.1007/BF02488601

Legland, D., Arganda-Carreras, I., and Andrey, P. (2016). MorphoLibJ: integrated library and plugins for mathematical morphology with imageJ. *Bioinformatics* 32, 3532–3534. doi: 10.1093/bioinformatics/btw413

Liao, H., Fu, X., Zhao, H., Cheng, J., Zhang, R., Yao, X., et al. (2020). The morphology, molecular development and ecological function of pseudonectaries on *Nigella damascena* (Ranunculaceae) petals. *Nat. Commun.* 11:1777. doi: 10.1038/s41467-020-15658-2

Mack, J.-L. K., and Davis, A. R. (2015). The relationship between cell division and elongation during development of the nectar-yielding petal spur in *Centranthus ruber* (Valerianaceae). *Ann. Bot.* 115, 641–649. doi: 10.1093/aob/mcu261

Puzey, J. R., Gerbode, S. J., Hodges, S. A., Kramer, E. M., and Mahadevan, L. (2012). Evolution of spur-length diversity in *Aquilegia* petals is achieved solely through cell-shape anisotropy. *Proc. R. Soc. B Biol. Sci.* 279, 1640–1645. doi: 10.1098/rspb.2011.1873

Ren, Y., Chang, H.-L., Tian, X.-H., Song, P., and Endress, P. K. (2009). Floral development in *Adonideae* (Ranunculaceae). *Flora Morphol. Distrib. Funct. Ecol. Plants* 204, 506–517. doi: 10.1016/j.flora.2008.07.002

Rohlf, F. (2015). The Tps series of software. *Hystrix* 26, 1–4. doi: 10.4404/hystrix-26.1-11264

Rolland-Lagan, A.-G., Andrew Bangham, J., and Coen, E. (2003). Growth dynamics underlying petal shape and asymmetry. *Nature* 422, 161–163. doi: 10.1038/nature01443

Sauret-Güeto, S., Schiessl, K., Bangham, A., Sablowski, R., and Coen, E. (2013). JAGGED controls *Arabidopsis* petal growth and shape by interacting with a divergent polarity field. *PLoS Biol.* 11:e1001550. doi: 10.1371/journal.pbio.1001550

Schindelin, J., Arganda-Carreras, I., Frise, E., Kaynig, V., Longair, M., Pietzsch, T., et al. (2012). Fiji: an open-source platform for biological-image analysis. *Nat. Methods* 9, 676–682. doi: 10.1038/nmeth.2019

Sharma, B., Yant, L., Hodges, S. A., and Kramer, E. M. (2014). Understanding the development and evolution of novel floral form in *Aquilegia*. *Curr. Opin. Plant Biol. Growth Dev.* 17, 22–27. doi: 10.1016/j.pbi.2013.10.006

Tucker, S. C., and Hodges, S. A. (2005). Floral ontogeny of *Aquilegia*, *Semiaquilegia* and *Enemion* (Ranunculaceae). *Int. J. Plant Sci.* 166, 557–574. doi: 10.1086/429848

Walcher-Chevillet, C. L., and Kramer, E. M. (2016). Breaking the mold: understanding the evolution and development of lateral organs in diverse plant models. *Curr. Opin. Genet. Dev. Dev. Mech. Patterning Evol.* 39, 79–84. doi: 10.1016/j.gde.2016.06.005

Whitewoods, C. D., and Coen, E. (2017). Growth and development of three-dimensional plant form. *Curr. Biol.* 27, R910–R918. doi: 10.1016/j.cub.2017.05.079

Yao, X., Zhang, W., Duan, X., Yuan, Y., Zhang, R., Shan, H., et al. (2019). The making of elaborate petals in *Nigella* through developmental repatterning. *N. Phytol.* 223, 385–396. doi: 10.1111/nph.15799

Zalko, J., Frachon, S., Morel, A., Deroin, T., Espinosa, F., Xiang, K.-L., et al. (2021). Floral organogenesis and morphogenesis of *Staphisagria* (Ranunculaceae): implications for the evolution of synorganized floral structures in Delphinieae. *Int. J. Plant Sci.* 182, 59–70. doi: 10.1086/711471

Zhai, W., Duan, X., Zhang, R., Guo, C., Li, L., Xu, G., et al. (2019). Chloroplast genomic data provide new and robust insights into the phylogeny and evolution of the Ranunculaceae. *Mol. Phylogenet. Evol.* 135, 12–21. doi: 10.1016/j.ympev.2019.02.024

Zhao, L., Liu, P., Che, X.-F., Wang, W., and Ren, Y. (2011). Floral organogenesis of *Helleborus thibetanus* and *Nigella damascena* (Ranunculaceae) and its systematic significance. *Bot. J. Linn. Soc.* 166, 431–443. doi: 10.1111/j.1095-8339.2011.01142.x

Conflict of Interest: The authors declare that the research was conducted in the absence of any commercial or financial relationships that could be construed as a potential conflict of interest.

frontiers in Plant Science

ORIGINAL RESEARCH
published: 16 December 2021
doi: 10.3389/fpls.2021.793516

Genome Size and Labellum Epidermal Cell Size Are Evolutionarily Correlated With Floral Longevity in *Paphiopedilum* Species

Feng-Ping Zhang[1] *and Shi-Bao Zhang*[2]*

[1] College of Traditional Chinese Medicine, Yunnan University of Chinese Medicine, Kunming, China, [2] Key Laboratory of Economic Plants and Biotechnology, Yunnan Key Laboratory for Wild Plant Resources, Kunming Institute of Botany, Chinese Academy of Sciences, Kunming, China

Genome size is known to influence phenotypic traits in leaves and seeds. Although genome size is closely related to cellular and developmental traits across biological kingdoms, floral longevity is a floral trait with important fitness consequence, but less is known about the link between floral longevity and sizes of genomes and cells. In this study, we examined evolutionary coordination between genome size, floral longevity, and epidermal cell size in flowers and leaves in 13 *Paphiopedilum* species. We found that, across all the study species, the genome size was positively correlated with floral longevity but negatively associated with labellum epidermal cell size, and a negative relationship was found between floral longevity and labellum epidermal cell size. This suggested that genome size is potentially correlated with floral longevity, and genome size has an important impact on life-history trait. In addition, genome size was positively correlated with leaf epidermal cell size, which was different from the relationship in flower due to different selective pressures they experienced or different functions they performed. Therefore, genome size constraints floral longevity, and it is a strong predictor of cell size. The impact of genome size on reproduction might have more implications for the evolution of flowering plants and pollination ecology.

Keywords: genome size, floral longevity, cell size, flower, leaf, slipper orchids

OPEN ACCESS

Edited by:
Elena M. Kramer,
Harvard University, United States

Reviewed by:
Philipp M. Schlüter,
University of Hohenheim, Germany
Xiaohua Jin,
Institute of Botany, Chinese Academy of Sciences (CAS), China

***Correspondence:**
Shi-Bao Zhang
sbzhang@mail.kib.ac.cn

Specialty section:
This article was submitted to Plant Development and EvoDevo, a section of the journal Frontiers in Plant Science

Received: *12 October 2021*
Accepted: *19 November 2021*
Published: *16 December 2021*

Citation:
Zhang F-P and Zhang S-B (2021) Genome Size and Labellum Epidermal Cell Size Are Evolutionarily Correlated With Floral Longevity in Paphiopedilum Species. Front. Plant Sci. 12:793516. doi: 10.3389/fpls.2021.793516

INTRODUCTION

It is well known that genome size varies significantly within plants, even in very closely related plant species (Šmarda and Bureš, 2010; Pellicer et al., 2018). However, the ecological adaptation and evolutionary significance of genome size remains unclear. Phylogenetic studies have revealed that increases and decreases of genome size have taken place many times within lineages (Soltis et al., 2003; Leitch et al., 2005; Simonin and Roddy, 2018). Genome size variation may suffer from strong selection pressures (Petrov, 2002), which suggests that some cost may exist to associate large genomes, or benefits from small genome size (Knight et al., 2005; Beaulieu et al., 2007). Therefore, there has been a growing interest in identifying the phenotypic consequences from species with different genome sizes (Knight et al., 2005; Beaulieu et al., 2007; Simonin and Roddy, 2018; Théroux-Rancourt et al., 2021).

Variations in genome sizes may be closely related to cell sizes across biological kingdoms (Cavalier-Smith, 2005; Simonin and Roddy, 2018; Théroux-Rancourt et al., 2021). Such coordination is indirectly and/or directly linked with whole-organism fitness characters (Jockusch, 1997). Previous studies have found that the cell size is positively correlated with genome size (Bennett, 1972; Edwards and Endrizzi, 1975; Sugiyama, 2005). In addition, there is a positive relationship between genome size and cell cycle duration (Rees et al., 1966; Baetcke et al., 1967; Bennett et al., 1983; Lawrence, 1985). In view of these cellular associations, it is assumed that many physiological and functional traits may link with genome size.

Observations have shown that there are positive and negative relationships between genome size and the structural characteristics in leaves, such as cell size, densities of veins and stomata, stomatal size, leaf mass per unit area, and leaf specific area (Beaulieu et al., 2007; Simonin and Roddy, 2018). In addition, changes in genome size are also associated with variation in many functional physiological traits, such as maximum rate of photosynthesis, minimum generation time, seed mass, flower size, and environmental variables (Bennett, 1972; Knight and Ackerly, 2002; Knight et al., 2005; Meagher et al., 2005; Beaulieu et al., 2007; Simonin and Roddy, 2018; Roddy et al., 2020; Faizulah et al., 2021; Théroux-Rancourt et al., 2021). In turn, the variation of plant traits may impact the evolution of genome size (Simonin and Roddy, 2018; Roddy et al., 2020; Théroux-Rancourt et al., 2021). It has been proposed that genome size is a predictor of cell sizes and photosynthetic rates in terrestrial vascular plants (Roddy et al., 2020). In addition, seed mass is strongly positively correlated with genome size (Beaulieu et al., 2008). Environmentally, genome size has been reported to vary with latitude, precipitation, altitude, and temperature (Sims and Price, 1985; Wakamiya et al., 1993; Knight and Ackerly, 2002; Knight et al., 2005). These suggest that variations in genome size may be adaptive.

Flower is a sexual reproductive organ of flowering plants, which has an important impact on its reproduction success (Rosas-Guerrero et al., 2014). Floral longevity is the length of duration that flowers remain open and functional, which is a key floral characteristic that impacts the reproductive fitness of plants (Primack, 1985). Floral longevity varies considerably from a day or less (e.g., *Ipomoea purpurea*) up to 2 months (e.g., some species from *Orchidaceae*) among flowering plants (Kerner von Marilaum, 1895; Gori, 1983; Primack, 1985; Ashman and Schoen, 1994; Zhang et al., 2017, 2021). Some studies have indicated that the duration of the life history in leaves was correlated with genome size within vascular plants (Finch, 1990; Morgan and Westoby, 2005; Beaulieu et al., 2007, 2008; Théroux-Rancourt et al., 2021). However, a previous study found a weak positive correlation between leaf lifespan, leaf mass per area, and genome size, suggesting that among angiosperms, genome size and leaf strategy are not related (Morgan and Westoby, 2005). Variation of floral longevity may imply different ecological strategies (Zhang et al., 2021). Therefore, understanding the genetic basis of variation in floral longevity is of great value. However, the potential link between floral longevity and the sizes of genome and cell is still lacking. We speculated that genome size may be related to floral longevity through cell size effect on physiological function within floral organs. Species with larger genome and longer floral longevity might need longer developmental duration (Feng et al., 2021).

The family *Orchidaceae* is an important group of flowering plants with great values in ornamental, medical, conservation, and evolutionary research (Zhang et al., 2018). The high diversity in morphology, floral longevity, growth form, habitat, and genome size mean that orchid species exhibit various biological and ecological consequences (Cox et al., 1998; Chase, 2005; Leitch et al., 2009; Zhang et al., 2017, 2018, 2021). The genus *Paphiopedilum* species are commonly named as "Lady's or Venus's Slipper" orchids, and these species are among the most cultivated and horticulturally important plants (Liu et al., 2009; Parveen et al., 2012). This genus *Paphiopedilum* was divided into three subgenera as follows: *Parvisepalum*, *Brachypetalum*, and *Paphiopedilum* (Guo et al., 2015; Tsai et al., 2020). Species of this genus are characterized by their exotic flowers with a deep shoe-shaped labellum, a structure unique to orchids that is a strongly modified petal, which is the main classification characteristics and pollination channel (Liu et al., 2009), and the droop and wilting of labellum were regarded as the end of floral longevity (Sugiura et al., 2001). Their flowers have long life span, and they can remain on the plant for 62 days (Zhang et al., 2017). However, there are few studies on factors influencing floral longevity of *Paphiopedilum* species (Zhang et al., 2017, 2021). In this study, we examined the potential link between floral longevity, sizes of genomes, and cells in 13 *Paphiopedilum* species. Specifically, we hypothesized that floral longevity is positively correlated with genome size, such that species with longer floral longevity may have larger genome. We also examined whether the scaling of genome size and cell size is similar between flower and leaf, or such relationship is different as a result of distinct selective pressures they experienced.

MATERIALS AND METHODS

Plant Materials

A total of 13 *Paphiopedilum* species from three subgenera, namely, *Parvisepalum*, *Brachypetalum*, and *Paphiopedilum* were used in this study (**Supplementary Figure 1**). These plants are grown and kept in the greenhouse at Kunming Institute of Botany, Chinese Academy of Sciences (102°41′ 25°10′ N; elevation 1,990 m). It is helpful to eliminate the effect of environmental divergence on their growth by applying similar culturing conditions. Therefore, variations may mirror the effect of a genetic consequence.

Genome Size

Genome size (1C, pg) (the DNA content of cells in the unreplicated phase from leaf tissue) was measured by flow cytometry in Kunming Institute of Botany, Chinese Academy of Sciences. Three heart leaves of the studied plant tops of species have not been expanded, which were collected and fixed in precooled mGb dissociation solution (45 mM $MgCl_2 \cdot 6H_2O$, 20 mM MOPS, 30 mM sodium citrate, 1% (W/V) PVP 40, 0.2% (v/v) Triton X-100, 10 mM Na_2EDTA, 20μl/ml β-mercaptoethanol, pH 7.5). The tissues immediately are chopped in the buffer with a new razor blade, and then mixed

the homogenate by pipetting up and down for several times. The homogenate was filtered using the 42-μm nylon mesh and incubated with DNA fluorochrome propidium iodide (PI). PI is used at 50 mg/ml simultaneously with RNase (Dolezel and Bartos, 2005; Dolezel et al., 2007; Tian et al., 2011).

The stained nuclear suspension samples were detected by BD FACScalibur^{TM} flow cytometry (Becton, Dickinson and Company, San Jose, CA 95131, USA). The cytometer was equipped with an argon ion laser operating at 488 nm. The PI fluorescence was collected using the 620 nm fluorescence-2 (FL2) filter. The sample flow rate was set at ∼100 nuclei/s, and at least 6,000 nuclei were acquired for each sample. The results were analyzed using BD CellQuest^{TM} Pro software (BD, USA). The results with coefficient of variation values (CV) < 5% were considered as reliable (**Supplementary Figure 2**). The emitted light fluorescence intensity of PI was detected by 488 nm blue light excitation.

By observing the fluorescence peaks of PI-DNA complex of the tested sample and the internal standard (*Zea mays*, 1C = 2.41 pg; Schnable et al., 2009), the ratio of DNA content of the two individuals can be obtained, and then multiplied by the *C* value of internal standard plant, the *C* value of the tested plant can be tested and calculated by the following equation: DNA content of tested the sample = internal standard DNA content × fluorescence intensity of tested/fluorescence intensity of internal standard (Tian et al., 2011). Orchids are known to differ in cellular ploidy levels (endopolyploidy) in different tissues (Teixeira da Silva et al., 2014; Bateman et al., 2018; Li et al., 2020). In this study, to test the differences of genome size between leaves and other tissues, tissues from labellum and root of *Paphiopedilum villosum* were used to measure the genome size. We have found that values of genome sizes between leaf and labellum and root tissues are insignificantly different (**Supplementary Figure 3**). The measure method of genome size (1C, pg) from labellum (the even central part of labellum, **Supplementary Figure 4**) and root (root tip) was the same as leaf.

Cell Size

Six labellum from newly opened flowers from six plants of each species were fixed in a formalin acetic acid-alcohol solution (37% formaldehyde, glacial acetic acid, 95% ethanol, and deionized water in a 10:5:50:35 mixture) for microscopic analysis. The even central part of labellum was cut into a section to ensure they are flattened, which was used to measure the cell size of labellum (**Supplementary Figure 4**), and the sampled part of labellum in all plants was the same. Six mature leaves from six different plants per species were sampled. Abaxial epidermis from the middle part of a mature leaf was coated with a thin layer without color, transparent nail polish. These films were gently torn away from the leaf surface with tweezers. These films were mounted on a microscope slide, and images were taken using the light microscope. All samples were obtained to observe epidermal cell and measured using the ImageJ software (National Institutes of Health, Bethesda, MD, USA). Epidermal cell size was subsequently calculated as suggested by Carins Murphy et al. (2016) using the following equation: Epidermal cell size = [1 – (mean stomatal size × stomatal density)]/epidermal cell density.

Floral Longevity

The 10–20 newly emerged floral buds from different plants per species were marked. An individual flower was regarded as "opening" when the dorsal sepal upward and any floral visitor could enter labellum. A flower was identified as "wilting" when perianth was discolored or when labellum began to wilt, thereby ending its function (Sugiura et al., 2001).

Statistical Analysis

Correlations between variables were analyzed using both Pearson's correlation and phylogenetically independent contrasts (PIC). The evolutionary correlations were tested with PIC analysis by using the "ape" package, combining molecular phylogenetic relationships (Cox et al., 1997; Guo et al., 2015). Statistical analyses were performed using R v.4.0.0 (R Core Team, 2020).

RESULTS

Across all studied species, the genome size from the leaf tissue, floral longevity, and epidermal cell size of labellum and leaf varied considerably (**Figure 1**; **Table 1**). Specially, genome size (mean genome size ranging from 17.83 to 29.41 pg in the largest species) and floral longevity (mean floral longevity ranging from 26 to 62.13 days in the longest species) varied by up to 1.65 and 2.60 times, respectively. The epidermal cell size of labellum and leaf also varied substantially between species, with a 1.90-fold and a 2.35-fold range, respectively (**Table 1**).

Genome size had a significant positive correlation with floral longevity among all species whether or not phylogeny was considered (**Figure 2**). The epidermal cell size in labellum had a significant negative correlation with genome size and floral longevity even after phylogeny was considered (**Figure 2**). In addition, genome size was positively correlated with leaf epidermal cell size in both non-phylogenetic and phylogenetic analyses (**Figure 3**).

DISCUSSION

To determine whether floral longevity was driven by genome size and cell size, we obtained data for genome size, floral longevity, and the epidermal cell size of flower and leaf for 13 *Paphiopedilum* species. We first tested whether floral longevity is associated with the sizes of genomes and epidermal cells. Our results showed that coordinated changes in genome size and cell size to potentially constraint floral longevity in flower (labellum) and leaf of *Paphiopedilum*. Our results provide new insights into the significance of genome size variation in maintaining floral longevity and evolution of floral traits in orchid plants.

Variation in genome size has aroused studies for seeking evidences as to its phenotypic consequences in plants and animals (Chung et al., 1998; Monaghan and Metcalfe, 2000; Morgan and Westoby, 2005; Beaulieu et al., 2006, 2007; Faizulah et al., 2021; Théroux-Rancourt et al., 2021). Genome size may be closely linked to cell size in biological kingdoms (Cavalier-Smith, 2005). The results may indirectly and/or directly link with

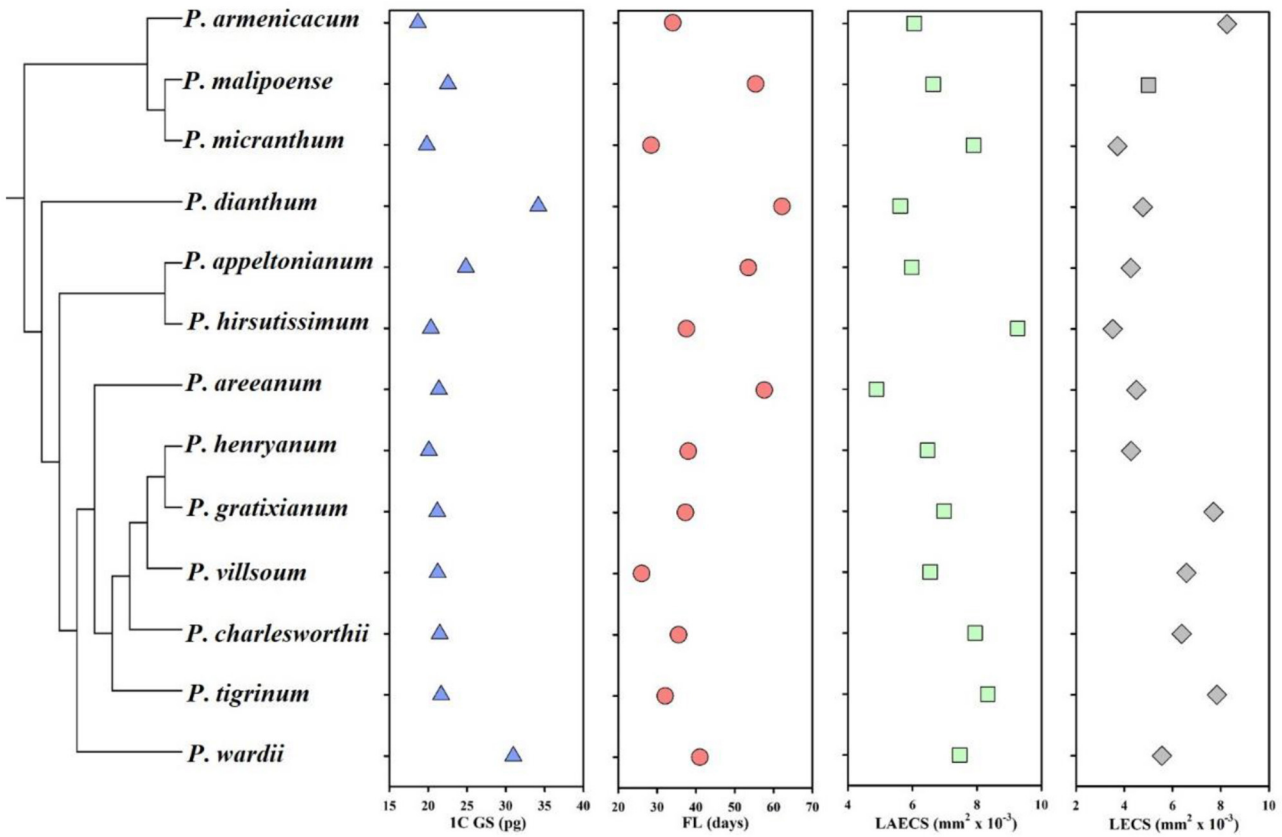

FIGURE 1 | Mean of raw values in genome size, floral longevity, and epidermal cell size of labellum and leaf from 13 *Paphiopedilum* species. GS, genome size; FL, floral longevity; LAECS, labellum epidermal cell size; LECS, leaf epidermal cell size. The phylogenetic relationships of the studied *Paphiopedilum* species in this study are obtained from the study by Cox et al. (1997) and Guo et al. (2015).

TABLE 1 | Mean values of genome size from leaf tissue ($n = 3$), floral longevity (10–20 flowers from different plants), epidermal cell size of labellum ($n = 6$), and leaf ($n = 6$) from 13 *Paphiopedilum* species.

Species	1C genome size (pg)	Floral longevity (days)	Labellum epidermal cell size ($mm^2 \times 10^{-3}$)	Leaf epidermal cell size ($mm^2 \times 10^{-3}$)
P. appletonianum (Gower) Rolfe	24.84 ± 0.13	53.47 ± 1.31	5.98 ± 0.32	7.70 ± 0.73
P. areeanum Gruss	21.37 ± 0.14	38.00 ± 0.33	6.47 ± 0.33	4.50 ± 0.05
P. armeniacum S. C. Chen and F. Y. Liu	18.67 ± 0.03	34.00 ± 0.63	6.05 ± 0.38	5.56 ± 0.04
P. charlesworthii (Rolfe) Pfitzer	21.48 ± 0.02	26.00 ± 0.74	6.55 ±0.46	3.72 ± 0.05
P. dianthum Tang and F. T. Wang	34.17 ± 0.07	62.13 ± 1.10	5.62 ±0.11	6.58 ± 0.06
P. gratrixianum Rolfe	21.17 ± 0.05	41.00 ± 0.56	7.46 ±0.31	4.27 ± 0.10
P. henryanum Braem	20.08 ± 0.08	32.07 ± 0.66	8.33 ±0.41	3.52 ± 0.15
P. hirsutissimum (Lindley ex Hooker) Stein	20.34 ± 0.16	37.53 ± 0.51	9.26 ±1.48	4.28 ± 0.13
P. malipoense S. C. Chen and Z. H. Tsi	22.54 ± 0.09	55.33 ± 1.09	6.64 ±0.18	7.84 ± 0.04
P. micranthum Tang and F. T. Wang	19.82 ± 0.02	28.45 ± 0.55	7.89 ±0.48	6.38 ± 0.11
P. tigrinum Koop. and N. Haseg	21.66 ± 0.13	37.27 ± 0.67	6.98 ±0.06	5.00 ± 0.05
P. villosum (Lindley) Stein	21.22 ± 0.13	35.50 ± 0.81	7.94 ±0.17	4.77 ± 0.17
P. wardii Summerh	30.96 ± 0.21	57.60 ± 0.49	4.88 ±0.16	8.26 ± 0.04

Values shown are mean ± SE.

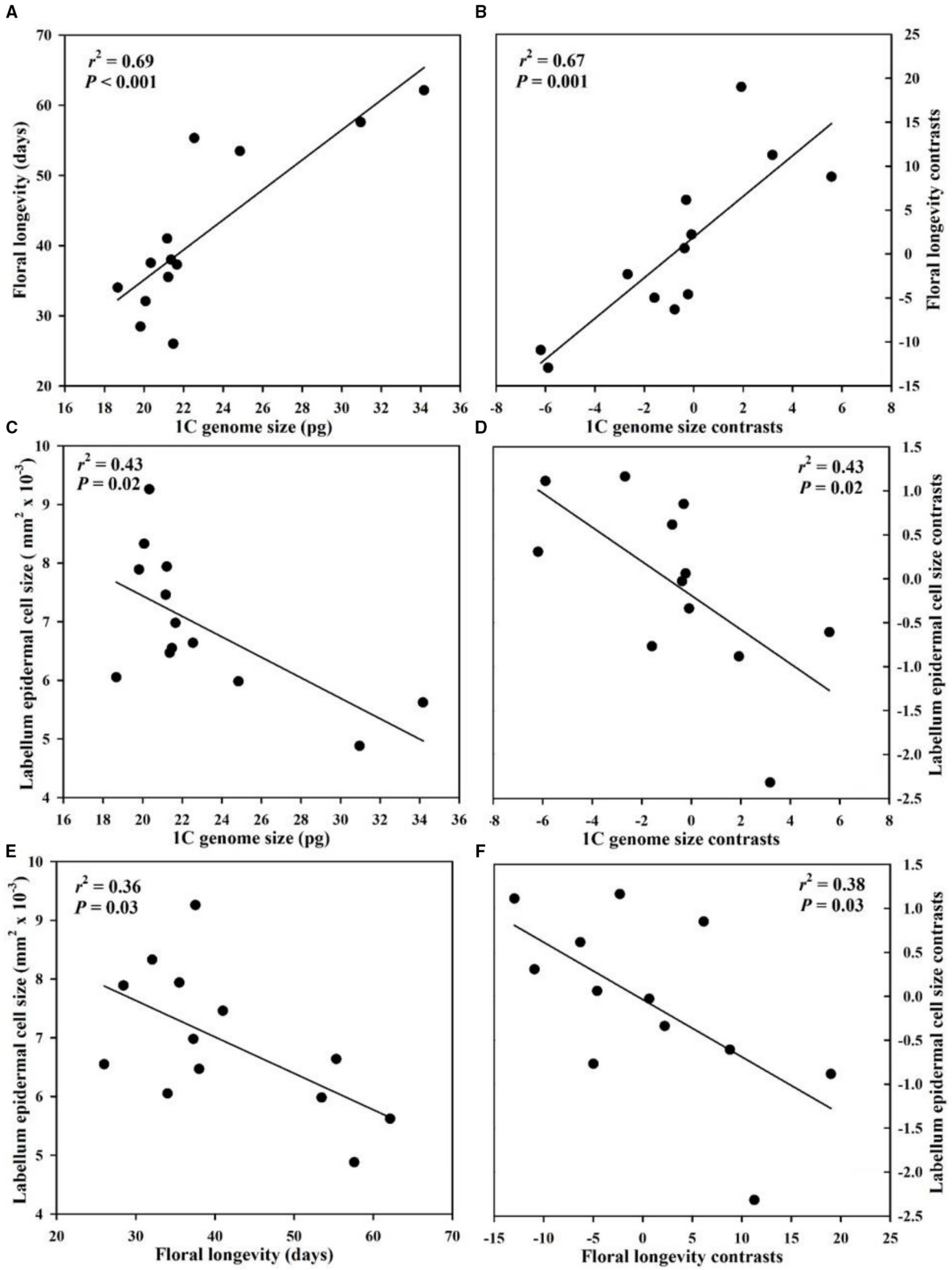

FIGURE 2 | Correlations among genome size, floral longevity, and labellum epidermal cell size from 13 *Paphiopedilum* species. **(A,C,E)** Pearson's regressions; **(B,D,F)** phylogenetically independent contrast correlations.

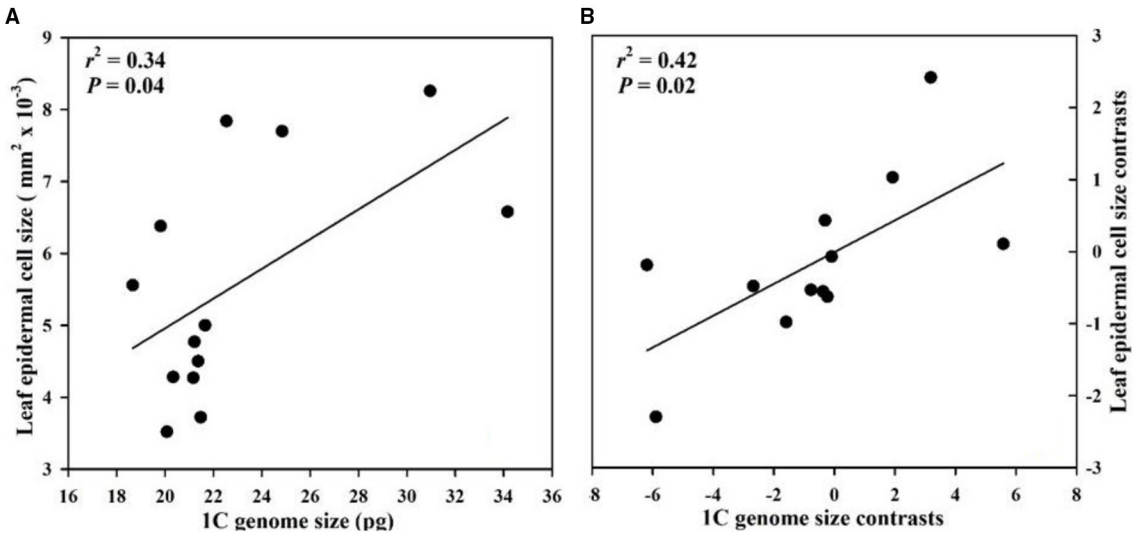

FIGURE 3 | Correlations between genome size and leaf epidermal cell size from 13 *Paphiopedilum* species. **(A)** Pearson's regressions; **(B)** phylogenetically independent contrast correlations.

whole-organism fitness values (Jockusch, 1997). Longevity is a biological trait with important fitness consequences (Monaghan and Metcalfe, 2000). Differences of longevity between species are likely to be linked to divergences in genome sizes and tissue maintenances (Kirkwood, 1985; Monaghan and Metcalfe, 2000). Our results showed that floral longevity was evolutionarily correlated with genome size and floral epidermal cell size (labellum). Species with longer floral longevity had a large genome and a small labellum cell. Our findings implied that the sizes of genome and cell played an important role in regulating floral longevity. The correlation between genome size and floral longevity that we have shown is very interesting. Whether it may be a causal link and what mechanisms might underlie it remain to be further studied. Endopolyploidy is regarded as the simultaneous existence of multiple ploidy nuclei in adjacent somatic cells of the same individual, tissue, or organ, and it is caused by normal DNA replication without cell division (Barlow, 1978). Recent studies showed that endopolyploidization commonly appeared, and levels from different tissues were different in *Orchidaceae* (Yang and Loh, 2004; Teixeira da Silva et al., 2014; Bateman et al., 2018; Li et al., 2020). For example, in *Ophyrys*, the endoreplication was frequent and (Bateman et al., 2018), while there was no evidence of endoreplication in *Dactylorhiza* (Bateman et al., 2018). In *Spathoglottis plicata*, the pedicel at the development stage showed the high level of endoploidy, but no endoploidy was found in calyx, petals, and ovary (Yang and Loh, 2004). However, the polyploidy from floral tissues of *Paphiopedilum delenatii* Guillaumin has not been demonstrated (Teixeira da Silva et al., 2014). In our study, we tried to avoid the interference of internal polyploidy by selecting young leaves. Moreover, we have measured genome sizes from labellum and root tissues, and our results showed that genome sizes from leaves and from other tissues were consistent (**Supplementary Figure 3**).

Floral longevity can influence the visiting frequency of pollinators, thus affecting plant reproductive rate. Meanwhile, the length of floral longevity is likely to reflect a trade-off between maintenance costs and plant fitness consequences (Kerner von Marilaum, 1895). Therefore, a trade-off should exist between investment and return in flowering plants. Time taken for DNA synthesis, and developmental duration in organs, is longer with larger genomes (Finch, 1990; Monaghan and Metcalfe, 2000; Feng et al., 2021). Within the angiosperms, the genome size of the orchids is relatively large (Leitch et al., 2009), and the reason for this is not clear. But a significant negative correlation between metabolic rate (photosynthetic rate, A_{mass}) and genome size was found (Beaulieu et al., 2007), and the sizes of genomes and cells constraint photosynthetic rate (Roddy et al., 2020). The large genome is thought to be correlated with the low metabolic rate (Beaulieu et al., 2007).

The floral longevity in orchids is generally much longer than other flowering plant. Thus, large genome size would be possibly correlated with floral longevity. Probably, exceeding a certain value, increases of genome size may need to pay a phenotypic cost in biological function. The cell division duration in organs may be an important life history traits (e.g., floral longevity), and *Paphiopedilum dianthum* with longer floral longevity has longer duration of floral bud differentiation than that of *P. micrantum* and *P. henryanum* with shorter floral longevity (Feng et al., 2021). In this study, the strong positive correlation is between floral longevity and genome size in 13 *Paphiopedilum* species. This result contradicts previous studies showing insignificant relationship between leaf longevity and genome size (Morgan and Westoby, 2005), which suggests that flower and leaf traits *of Paphiopedilum* have evolved independently, and this possible explanation is that different selective pressures flower and leaf experienced and they acted as different functions (Roddy et al., 2013; Zhang et al., 2017).

In this study, genome size was a strong predictor of leaf epidermal cell size whether or not phylogenetic relatedness of species was considered. Genome size constrains cell size in leaves, so that cell size varies widely as cell grow and differentiate to influence its structure and function in the context of various factors, and then define phenotype (Bennett, 1987; Franks et al., 2012; Simova and Herben, 2012; Théroux-Rancourt et al., 2021), which potentially affect rates of leaf water loss (transpiration) and photosynthetic rate (Beaulieu et al., 2007; Théroux-Rancourt et al., 2021). In our study, we found that the correlation between genome size and cell size from flowers and leaves was different, implying that selective pressures they experienced may be different due to their structures and functions.

CONCLUSION

We uncovered significant evolutionary correlations between floral longevity and sizes of genomes and cells in *Paphiopedilum* using a phylogenetic comparative method. These relationships between the sizes of genomes and cell and floral longevity perhaps represent a genotype and phenotype selection relationships. In addition, our results showed that genome size is a strong predictor of cell size. These findings provide novels insights into floral physiological and developmental traits and genome sizes of evolutionary correlations among flowering plant species. Therefore, sampling more species with different genome sizes in orchids and/or angiosperms should be necessary. Further investigation should pay close attention to test for a more direct influence of genome size on floral functional traits. Besides, answering the primary questions needs a continued effort to combine floral functional trait studies with the evolution of plant genome size studies. The endeavor of joining results is critical to reveal evolutionary relationships between genome sizes with floral functional traits in flowering plants.

DATA AVAILABILITY STATEMENT

The raw data supporting the conclusions of this article will be made available by the authors, without undue reservation.

AUTHOR CONTRIBUTIONS

F-PZ and S-BZ designed the study and wrote and revised the manuscript. F-PZ collected the samples and data, carried out the experiments, and analyzed the data. All authors contributed to the article and approved the submitted version.

FUNDING

This study was supported by the National Natural Science Foundation of China (31960224), the Young Top Talents of the Ten Thousand Talents Plan in Yunnan Province (YNWR-QNBJ-2018-337), the Project for Innovation Team of Yunnan Province (202105AE160012), the Yunnan Provincial Science and Technology Department-Applied Basic Research Joint Special Funds of Yunnan University of Chinese Medicine (202001AZ070001-041).

ACKNOWLEDGMENTS

The authors thank Jing-Qiu Feng, Wei Zhang, and Xue-Wei Fu for providing the images of *Paphiopedilum* species. They also thank the editors and reviewers for valuable suggestions that greatly improve the quality of the manuscript.

SUPPLEMENTARY MATERIAL

The Supplementary Material for this article can be found online at: https://www.frontiersin.org/articles/10.3389/fpls.2021.793516/full#supplementary-material

REFERENCES

Ashman, T. L., and Schoen, D. J. (1994). How long should flowers live? *Nature* 371, 788–791. doi: 10.1038/371788a0

Baetcke, K., Sparrow, A., Nauman, C., and Schwemmer, S. S. (1967). The relationship of DNA content to nuclear and chromosome volumes and to radiosensitivity (LD50). *Proc. Natl. Acad. Sci. USA* 58, 533–540. doi: 10.1073/pnas.58.2.533

Barlow, P. W. (1978). Endopolyploidy: Towards an understanding of its biological significance. *Acta Biotheoretica*. 27, 1–18. doi: 10.1007/BF00048400

Bateman, M. R., Guy, J. J., Rudall, P. J., Leitch, I. J., Pellicer, J., and Leitch, A. R. (2018). Evolutionary and functional potential of ploidy increase within individual plants: somatic ploidy mapping of the complex labellum of sexually deceptive bee orchids. *Ann. Bot*. 122, 133–150. doi: 10.1093/aob/mcy048

Beaulieu, J. M., Leitch, I. J., and Knight, C. A. (2007). Genome size evolution in relation to leaf strategy and metabolic rates revisited. *Ann. Bot*. 99, 495–505. doi: 10.1093/aob/mcl271

Beaulieu, J. M., Leitch, I. J., Patel, S., Pendharkar, A., and Knight, C. A. (2008). Genome size is a strong predictor of cell size and stomatal density in angiosperms. *New Phytol*. 179, 975–986. doi: 10.1111/j.1469-8137.2008.02528.x

Beaulieu, J. M., Moles, A. T., Leitch, I. J., Bennett, M. D., Dickie, J. B., and Knight, C. A. (2006). Correlated evolution of genome size and seed mass. *New Phytol*. 173, 422–437. doi: 10.1111/j.1469-8137.2006.01919.x

Bennett, M. D. (1972). Nuclear DNA content and minimum generation time in herbaceous plants. *Proc. R. Soc. B* 181, 109–135. doi: 10.1098/rspb.1972.0042

Bennett, M. D. (1987). Variation in genomic form in plants and its ecological implications. *New Phytol*. 106, 177–200. doi: 10.1111/j.1469-8137.1987.tb04689.x

Bennett, M. D., Heslop-Harrison, J. S., Smith, J. B., and Ward, J. P. (1983). DNA density in mitotic and meiotic metaphase chromosomes of plants and animals. *J. Cell Sci*. 63, 173–179. doi: 10.1242/jcs.63.1.173

Carins Murphy, M. R., Jordan, G. J., and Brodribb, T. J. (2016). Cell expansion not cell differentiation predominantly co-ordinates veins and stomata within and among herbs and woody angiosperms grown under sun and shade. *Ann. Bot*. 118, 1127–1138. doi: 10.1093/aob/mcw167

Cavalier-Smith, T. (2005). Economy, speed and size matter: evolutionary forces driving nuclear genome miniaturization and expansion. *Ann. Bot*. 95, 147–175. doi: 10.1093/aob/mci010

Chase, M. W. (2005). Classification of Orchidaceae in the age of DNA data. *Curtis's Bot. Mag*. 22, 2–7. doi: 10.1111/j.1355-4905.2005.00466.x

Chung, J., Lee, J. H., Arumuganathan, K., Graef, G. L., and Specht, J. E. (1998). Relationships between nuclear DNA content and seed and leaf size in soybean. *Theor. Appl. Genet*. 96, 1064–1068. doi: 10.1007/s001220050840

Cox, A. V., Abdelnour, G. J., Bennett, M. D., and Leitch, I. J. (1998). Genome size and karyotype evolution in the slipper orchids (Cypripedioideae: Orchidaceae). *Am. J. Bot*. 85, 681–687. doi: 10.2307/2446538

Cox, A. V., Pridgeon, A. M., Albert, V. A., and Chase, M. W. (1997). Phylogenetics of the slipper orchids (Cypripedioideae, Orchidaceae): nuclear rDNA ITS sequences. *Plant Syst. Evol*. 208, 197–223. doi: 10.1007/BF00985442

Dolezel, J., and Bartos, J. (2005). Plant DNA flow cytometry and estimation of nuclear genome size. *Ann. Bot*. 95, 99–110. doi: 10.1093/aob/mci005

Dolezel, J., Greilhuber, J., and Suda, J. (2007). Estimation of nuclear DNA content in plants using flow cytometry. *Nat. Protoc*. 2, 2233–2244. doi: 10.1038/nprot.2007.310

Edwards, G. A., and Endrizzi, J. L. (1975). Cell size nuclear size and DNA content relationships in Gossypium. *Can. J. Genet. Cytol*. 17, 181–186. doi: 10.1139/g75-024

Faizulah, L., Morton, J., Hersch-Green, E. I., Walczyk, A. M., Leitch, A. R., and Leitch, I. J. (2021). Exploring environmental selection on genome size in angiosperms. *Trends Plant Sci*. 26, 1039–1049. doi: 10.1016/j.tplants.2021.06.001

Feng, J. Q., Xia, Q., Zhang, F. P., Wang, J. W., and Zhang, S. B. (2021). Is seasonal flowering time of *Paphiopedilum* species caused by differences in initial time of floral bud differentiation? *AoB Plants* 13: *plab*053. doi: 10.1093/aobpla/plab053

Finch, C. E. (1990). *Longevity, Senescence, and the Genome University of Chicago Press*. Chicago, IL: University of Chicago Press

Franks, P. J., Leitch, I. J., Ruszala, E. M., Hetherington, A. M., and Beerling, D. J. (2012). Physiological framework for adaptation of stomata to CO_2 from glacial to future concentrations. *Philos. T. R. Soc. B* 367, 537–546. doi: 10.1098/rstb.2011.0270

Gori, D. F. (1983). "Post-pollination phenomena and adaptive floral changes," in *Handbook of Experimental Pollination Biology*, eds Jones, C.E., Little, R.J. (New York, NY: Scientific and Academic), 31–49.

Guo, Y. Y., Luo, Y. B., Liu, Z. J., and Wang, X. Q. (2015). Reticulate evolution and sea-level fluctuations together drove species diversification of slipper orchids in South-East Asia. *Mol. Ecol*. 24, 2838–2855. doi: 10.1111/mec.13189

Jockusch, E. L. (1997). An evolutionary correlate of genome size change in plethodontid salamanders. *Proc. R. Soc. B* 264, 597–604. doi: 10.1098/rspb.1997.0085

Kerner von Marilaum, A. (1895). *The Natural History of Plants, Their Forms, Growth, Reproduction and Distribution*. New York, NY: Henry Holt.

Kirkwood, T. B. L. (1985). "Comparative aspects of longevity," in *Handbook of the Biology of Aging*, eds Finch, C. E. and Schneider, E. L. New York, NY: Van Nostrand Reinhold, 27–45.

Knight, C. A., and Ackerly, D. D. (2002). Variation in nuclear DNA content across environmental gradients: a quantile regression analysis. *Ecol. Lett*. 5, 66–76. doi: 10.1046/j.1461-0248.2002.00283.x

Knight, C. A., Molinari, N. A., and Petrov, D. A. (2005). The large genome constraint hypothesis: evolution, ecology and phenotype. *Ann. Bot*. 95, 177–190. doi: 10.1093/aob/mci011

Lawrence, M. E. (1985). *Senecio* L. *(Asteraceae)* in Australia: nuclear DNA amounts. *Aust. J. Bot*. 33, 221–232. doi: 10.1071/BT9850221

Leitch, I. J., Kahandawala, I., Suda, J., Hanson, L., Ingrouille, M. J., Chase, M. W., et al. (2009). Genome size diversity in orchids: consequences and evolution. *Ann. Bot*. 104, 469–481. doi: 10.1093/aob/mcp003

Leitch, I. J., Soltis, D. E., Soltis, P. S., and Bennett, M. D. (2005). Evolution of DNA amounts across land plants (Embryophyta). *Ann. Bot*. 95, 207–217. doi: 10.1093/aob/mci014

Li, C. N., Fu, Q. J., Shen, G. Z., Zhao, F. K., Zhang, X. Y., and Ruan, R. X. (2020). Applications of flow cytometry in orchidaceae. *J. Nucl. Agricult. Sci.* 34, 0973–0981. doi: 10.11869/j.issn.100-8551.2020.05.0973

Liu, Z. J., Chen, X. Q., Chen, L. J., and Lei, S. P. (2009). *The Genus Paphiopedilum in China*. Beijing: Science Press.

Meagher, T. R., Gillies, A. C. M., and Costich, D. E. (2005). Genome size, quantitative genetics and the genomic basis for flower size evolution in *Silene latifolia*. *Ann. Bot*. 95, 247–254. doi: 10.1093/aob/mci018

Monaghan, P., Metcalfe, N.B. (2000). Genome size and longevity. *Trends Genet*. 16, 331–332. doi: 10.1016/S0168-9525(00)02051-5

Morgan, H. M., and Westoby, M. (2005). The relationship between Nuclear DNA content and leaf strategy in seed plant. *Ann. Bot*. 96, 1321–1330. doi: 10.1093/aob/mci284

Parveen, I., Singh, H. K., Raghuvanshi, S., and Pradhan, U. C. (2012). DNA barcoding of endangered Indian *Paphiopedilum* species. *Mol. Ecol*. 12, 82–90. doi: 10.1111/j.1755-0998.2011.03071.x

Pellicer, J., Hidalgo, O., Dodsworth, S., and Leitch, I. J. (2018). Genome size diversity and its impact on the evolution of land plants. *Genes* 9:88. doi: 10.3390/genes9020088

Petrov, D. A. (2002). Mutational equilibrium model of genome size evolution. *Theor. Popul. Biol*. 61, 531–543. doi: 10.1006/tpbi.2002.1605

Primack, R. B. (1985). Longevity of individual of flowers. *Annu. Rev. Ecol. Syst*. 16, 15–37. doi: 10.1146/annurev.es.16.110185.000311

R Core Team (2020). *R: A Language and Environment for Statistical Computing*. R Foundation for Statistical Computing, Vienna, Austria. Available online at: www.R-project.org/

Rees, H., Cameron, F. M., Hararika, M. H., and Jones, G. H. (1966). Nuclear variation between diploid angiosperms. *Nature* 211, 828–830. doi: 10.1038/211828a0

Roddy, A. B., Guilliams, C. M., Lilittham, T., Farmer, J., Wormser, V., Pham, T., et al. (2013). Uncorrelated evolution of leaf and petal venation patterns across the angiosperm phylogeny. *J. Exp. Bot*. 64, 4081–4088. doi: 10.1093/jxb/ert247

Roddy, A. B., Theroux-Rancourt, G., Abbo, T., Brodersen, C. R., and Simonin, K. A. (2020). The scaling of genome size and cell size limits maximum rates of photosynthesis with implications for ecological strategies. *Int. J. Plant Sci*. 181, 75–87. doi: 10.1086/706186

Rosas-Guerrero, V., Aguila, R., Martén-Rodríguez, S., Ashworth, L., Lopezaraiza-Mikel, M., Bastida, J. M., et al. (2014). A quantitative review of pollination syndromes: do floral traits predict effective pollinators? *Ecol. Lett*. 17, 388–400. doi: 10.1111/ele.12224

Schnable, P. S., Ware, D., Fulton, R. S., Stein, J. C., Wei, F. S., Pasternak, S., et al. (2009). The B73 Maize genome: complexity, diversity, and dynamics. *Science* 326:1112. doi: 10.1126/science.1178534

Simonin, K. A., and Roddy, A. B. (2018). Genome downsizing, physiological novelty, and the global dominance of flowering plants. *PLoS Biol*. 16:e2003706. doi: 10.1371/journal.pbio.2003706

Simova, I., and Herben, T. (2012). Geometrical constraints in the scaling relationships between genome size, cell size and cell cycle length in herbaceous plants. *Proc. R. Soc. B* 279, 867–875. doi: 10.1098/rspb.2011.1284

Sims, L. E., and Price, H. J. (1985). Nuclear DNA content variation in *Helianthus* (Asteraceae). *Am. J. Bot*. 72, 1213–1219. doi: 10.1002/j.1537-2197.1985.tb08374.x

Šmarda, P., and Bureš, P. (2010). Understanding intraspecific variation in genome size in plants. *Preslia* 82, 41–61. doi: 10.1055/s-0029-1240632

Soltis, D. E., Soltis, P. S., Bennett, M. D., and Leitch, I. J. (2003). Evolution of genome size in the angiosperms. *Am. J. Bot*. 90, 1596–1603. doi: 10.3732/ajb.90.11.1596

Sugiura, N., Fujie, T., Inoue, K., and Kitamura, K. (2001). Flowering phenology, pollination, and fruit set of *Cypripedium macranthos* var. *rebunense, a threatened lady's slipper (Orchidaceae). J. Plant Res*. 114, 171–178. doi: 10.1007/PL00013980

Sugiyama, S. (2005). Developmental basis of interspecific differences in leaf size and specific leaf area among C_3 grass species. *Funct. Ecol*. 19, 916–924. doi: 10.1111/j.1365-2435.2005.01044.x

Teixeira da Silva, J., Giang, D., Dobránszki, J., Zeng, S., and Tanaka, M. (2014). Ploidy analysis of *Cymbidium*, *Phalaenopsis*, *Dendrobium* and *Paphiopedillum* (Orchidaceae), and *Spathiphyllum* and *Syngonium* (Araceae). *Biologia* 69, 750–755. doi: 10.2478/s11756-014-0370-z

Théroux-Rancourt, G., Roddy, A. B., Earles, M. J., Gilbert, M. E., Maciej, A., Zwieniecki, M. A., et al. (2021). Maximum CO_2 diffusion inside leaves is limited by the scaling of cell size and genome size. *Proc. R. Soc. B* 288:20203145. doi: 10.1098/rspb.2020.3145

Tian, X. M., Zhou, X. Y., and Gong, N. (2011). Application of flow cytometry in plant research—analysis of nuclear DNA content and ploidy level in plant cells. *Chinese Agricult. Sci. Bull*. 9, 21–27. doi: 10.1093/mp/ssq070

Tsai, C. C., Liao, P. C., Ko, Y. Z., Chen, C. H., and Chiang, Y. C. (2020). Phylogeny and Historical Biogeography of *Paphiopedilum* Pfitzer (Orchidaceae) Based on Nuclear and Plastid DNA. *Front. Plant Sci*. 11:126. doi: 10.3389/fpls.2020.00126

Wakamiya, I., Newton, R. J., Johnston, S. J., and Price, J. H. (1993). Genome size and environmental factors in the genus *Pinus*. *Am. J. Bot*. 80, 1235–1241. doi: 10.1002/j.1537-2197.1993.tb15360.x

Yang, M., and Loh, C. S. (2004). Systemic endopolyploidy in *Spathoglottis plicata* (orchidaceae) development. *BMC Cell Biol*. 5:33. doi: 10.1186/1471-2121-5-33

Zhang, F. P., Feng, J. Q., Huang, J. L., Huang, W., Fu, X. W., Hu, H., et al. (2021). Floral Longevity of *Paphiopedilum* and *Cypripedium* is associated with floral morphology. *Front. Plant Sci.* 12:637236. doi: 10.3389/fpls.2021.637236

Zhang, F. P., Yang, Y. J., Yang, Q. Y., Zhang, W., Brodribb, T. J., Hao, G. Y., et al. (2017). Floral mass per area and water maintenance traits are correlated with floral longevity in *Paphiopedilum* (Orchidaceae). *Front. Plant Sci.* 8:501. doi: 10.3389/fpls.2017.00501

Zhang, S. B., Yang, Y. G., Li, J. W., Qin, J., Zhang, W., Huang, W., et al. (2018). Physiological diversity of orchids. *Plant Divers.* 40, 196–208. doi: 10.1016/j.pld.2018.06.003

Conflict of Interest: The authors declare that the research was conducted in the absence of any commercial or financial relationships that could be construed as a potential conflict of interest.

Publisher's Note: All claims expressed in this article are solely those of the authors and do not necessarily represent those of their affiliated organizations, or those of the publisher, the editors and the reviewers. Any product that may be evaluated in this article, or claim that may be made by its manufacturer, is not guaranteed or endorsed by the publisher.

frontiers in Plant Science

ORIGINAL RESEARCH
published: 10 February 2022
doi: 10.3389/fpls.2021.764843

Investigating Host and Parasitic Plant Interaction by Tissue-Specific Gene Analyses on Tomato and *Cuscuta campestris* Interface at Three Haustorial Developmental Stages

*Min-Yao Jhu[1,2], Moran Farhi[1,3], Li Wang[1,4], Kristina Zumstein[1] and Neelima R. Sinha[1]**

[1] Department of Plant Biology, University of California, Davis, CA, United States, [2] Crop Science Centre, Department of Plant Sciences, University of Cambridge, Cambridge, United Kingdom, [3] The Better Meat Co., West Sacramento, CA, United States, [4] College of Life Sciences, Nanjing Normal University, Nanjing, China

OPEN ACCESS

Edited by:
Elena M. Kramer,
Harvard University, United States

Reviewed by:
Charles Melnyk,
Swedish University of Agricultural Sciences, Sweden
Senjuti Sinharoy,
National Institute of Plant Genome Research (NIPGR), India

***Correspondence:**
Neelima R. Sinha
nrsinha@ucdavis.edu

Specialty section:
This article was submitted to Plant Development and EvoDevo, a section of the journal Frontiers in Plant Science

Received: 26 August 2021
Accepted: 28 December 2021
Published: 10 February 2022

Citation:
Jhu M-Y, Farhi M, Wang L, Zumstein K and Sinha NR (2022) Investigating Host and Parasitic Plant Interaction by Tissue-Specific Gene Analyses on Tomato and Cuscuta campestris Interface at Three Haustorial Developmental Stages. Front. Plant Sci. 12:764843. doi: 10.3389/fpls.2021.764843

Parasitic weeds cause billions of dollars in agricultural losses each year worldwide. *Cuscuta campestris* (*C. campestris*), one of the most widespread and destructive parasitic plants in the United States, severely reduces yield in tomato plants. Reducing the spread of parasitic weeds requires understanding the interaction between parasites and hosts. Several studies have identified factors needed for parasitic plant germination and haustorium induction, and genes involved in host defense responses. However, knowledge of the mechanisms underlying the interactions between host and parasitic plants, specifically at the interface between the two organisms, is relatively limited. A detailed investigation of the crosstalk between the host and parasite at the tissue-specific level would enable development of effective parasite control strategies. To focus on the haustorial interface, we used laser-capture microdissection (LCM) with RNA-seq on early, intermediate and mature haustorial stages. In addition, the tomato host tissue that immediately surround the haustoria was collected to obtain tissue- resolution RNA-Seq profiles for *C. campestris* and tomato at the parasitism interface. After conducting RNA-Seq analysis and constructing gene coexpression networks (GCNs), we identified *CcHB7*, *CcPMEI*, and *CcERF1* as putative key regulators involved in *C. campestris* haustorium organogenesis, and three potential regulators, *SlPR1*, *SlCuRe1-like*, and *SlNLR*, in tomatoes that are involved in perceiving signals from the parasite. We used host-induced gene silencing (HIGS) transgenic tomatoes to knock-down the candidate genes in *C. campestris* and produced CRISPR transgenic tomatoes to knock out candidate genes in tomatoes. The interactions of *C. campestris* with these transgenic lines were tested and compared with that in wild-type tomatoes. The results of this study reveal the tissue-resolution gene regulatory mechanisms at the parasitic plant-host interface and provide the potential of developing a parasite-resistant system in tomatoes.

Keywords: parasitic plants, *Cuscuta campestris*, laser-capture microdissection, host-induced gene silencing, CRISPR, haustoria, Solanum lycopersicum

INTRODUCTION

Parasitic angiosperms are among the worst agricultural pests, reducing the yields of agricultural crops each year by billions of dollars worldwide (Agrios, 2005; Yoder and Scholes, 2010). Parasitic plants directly attach to host plants using specialized organs known as haustoria to extract nutrients and water from their hosts. Most standard herbicides and control techniques have not been effective or are too costly in managing parasitic plant infestations because of this tight physiological link between host plants and parasites. A better understanding of the mechanisms of parasitic signaling and haustorium development will allow us to develop more robust biocontrol approaches to eliminate the agricultural damage caused by parasitic plants.

Cuscuta species (dodders) lack functional roots and leaves and coil their stems counterclockwise as they grow on their host (Furuhashi et al., 2011; Alakonya et al., 2012). About 75% of *Cuscuta* species are found in the Americas (Furuhashi et al., 2011; García et al., 2014), including *Cuscuta campestris* (*C. campestris*). Many crop species are susceptible to *C. campestris* attack, including domesticated tomatoes (*Solanum lycopersicum*), leading to 50–72% yield reductions (Yaakov et al., 2001). In California, over 12,000 hectares of land are affected by *Cuscuta* (Lanini and Kogan, 2005). Tomato is one of the most consumed fruit crops in the world, and the United States is one of the world's leading producers of tomatoes (Kimura and Sinha, 2008). In the United States, more than $2 billion in annual farm cash receipts are from fresh and processed tomatoes. Therefore, a detailed investigation of the haustorial development process in the interactions between tomato and *Cuscuta* is essential to developing effective strategies to prevent agricultural losses that are caused by *Cuscuta* species.

However, the signals involved in haustorium development at specific developmental stages and the tissue-specific communication between host and parasite during the haustorium penetration process remain largely unknown. This is especially true for stem parasitic plant systems. Several studies have indicated that haustoria can transport not only water and nutrients, but also mRNA, miRNA, and small peptides (Kim et al., 2014; Johnson et al., 2019; Shen et al., 2020). These bidirectional communications create a tight physiological connection between host and parasite. During the haustorium development process, parasitic plants change their host morphologically and physiologically by secreting hormones or effectors to help them establish haustorial connections (Shimizu and Aoki, 2019; Su et al., 2020). On the other hand, host plants deploy various defense strategies to counteract this infestation and prevent vascular connections (Fishman and Shirasu, 2021). Understanding what parasitism-related genes have been explicitly activated at the interface between host and parasite could help develop a more efficient parasite-resistant system in crop plants.

Therefore, in this study, we used laser-capture microdissection (LCM) coupled with RNA-seq to zoom in on the interface between the host and parasite and to investigate the tissue-specific gene expression changes. We identified *CcHB7*, *CcPMEI*, and *CcERF1* as key regulators involved in haustorium organogenesis, and the functions of these candidate genes were validated by HIGS transgenic plants. We also identified three potential key regulators, *SlPR1*, *SlCuRe1-like*, and *SlNLR*, in tomatoes that may be involved in perceiving signals from the parasites, and two of them were further characterized with CRISPR knockout mutants.

RESULTS

Transcriptomes at the Host-Parasite Interface Using Laser-Capture Microdissection

To investigate specific gene expression changes in penetrating haustoria, we used LCM with RNA-seq to analyze haustorial tissues from three different developmental stages. We defined three time points: early - the haustorium has just contacted the host, intermediate - the haustorium has developed searching hyphae, which are elongated tip-growing cells on haustoria, but has not formed vascular connections, and mature - a haustorium with continuous vascular tissue between host and parasite (**Figures 1A-C**).

We collected both parasite haustorial tissues and host tissues at the interface at these three-time points from *C. campestris* attached on *S. lycopersicum* cv. Heinz 1706 (H1706). To identify genes involved in *C. campestris* haustorial development during the penetration process, the protruding regions of haustoria were specifically collected from paraffin sections using LCM (**Figures 1D,E**). To capture the earliest host responses or defense mechanisms to combat *C. campestris* parasitism, we choose the same three developmental time points, early, intermediate, and mature stages of parasitism, to specifically collect the few layers of tomato cells that surround the penetrating *C. campestris* haustoria (**Figure 1F**). These host cells are most likely to exhibit the initial host defense response upon attacks by the parasite. These collected tomato and *C. campestris* tissues were processed for RNA extraction and library preparation for RNA-Seq and subsequent transcriptome analysis.

RNA-Seq Analyses and Gene Coexpression Networks Across Three Developmental Stages of *Cuscuta campestris* Haustoria

We analyzed the transcriptome of LCM *C. campestris* haustorial tissues by mapping reads to the genome of *C. campestris* (Vogel et al., 2018). With multidimensional scaling analysis, the gene expression patterns among different samples showed that the early and intermediate stages are distinct from the mature stage (**Supplementary Figure 1**). We conducted a principal component analysis (PCA) and coupled it with clustering analysis using self-organizing maps (SOM) to visualize the expression profile of each gene (**Supplementary Table 1** and **Supplementary Figure 2**). To identify potential key regulators that are involved in *C. campestris* haustorium development at different stages, we conducted further gene coexpression analysis on specific SOM clusters (**Figure 2** and **Supplementary Figure 3**).

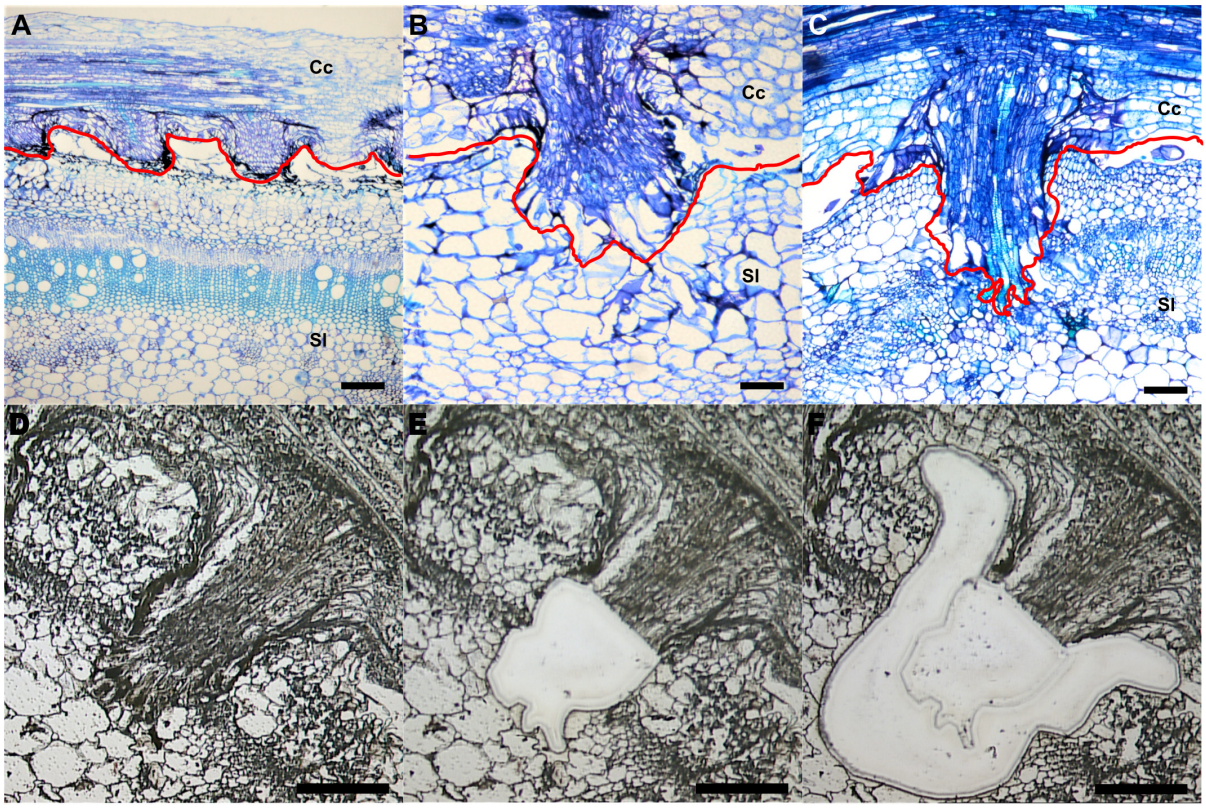

FIGURE 1 | Laser-capture microdissection (LCM) of *C. campestris* haustoria penetrating tomato stems at three developmental stages. **(A–C)** Toluidine blue O stained paraffin sections of tomato stem with *C. campestris* early **(A)**, intermediate **(B)**, and mature stage **(C)** haustoria. Red line indicates the interface between *C. campestris* and host tomato. Cc indicates *C. campestris*; Sl indicates *S. lycopersicum*. **(D–F)** *C. campestris* haustorial tissues and host tissues were collected using LCM. A paraffin section of an intermediate stage haustorium before collection **(D)**, after haustorial tissue collection **(E)**, and after host tissue collection **(F)**. **(A)** and **(C)**, scale bars = 250 μm. **(B)**, **(D)**, **(E)**, and **(F)**, scale bars = 100 μm. Part of this figure **(A–C)** is modified from one in a previously published paper Jhu et al., 2021 with new information added.

First, we hypothesized that the genes highly up-regulated at the early stage of parasitism are most likely to be involved in the haustorium initiation and attachment process. Therefore, we focused on genes in SOM5, which is a cluster enriched with genes that are highly expressed in the early haustorial stage. Among these SOM5 genes, we constructed a gene coexpression network (GCN) to generate an overview of the potential molecular regulatory machinery and to identify central hub genes, which are genes with high degree of centrality in the coexpression network, that could be the regulators of the initiation and attachment mechanisms. Visualizing the network using Cytoscape (Cline et al., 2007), the SOM5 GCN is composed of four major modules (**Figures 2A–C** and **Supplementary Table 2**) based on the fast greedy modularity optimization algorithm (Clauset et al., 2004). Using our previously published combined annotation profile, we conducted GO enrichment analysis using the matched TAIR ID for each *C. campestris* gene in the network to identify the major GO terms (FDR-values < 0.05) for the target modules. We find the SOM5 module 1 enriched in biological process GO terms including "response to abiotic and biotic stimulus, response to stress, response to hormone, and response to far-red light" (**Supplementary Table 5**). This result indicates the genes contained in module 1 are likely involved in the haustorium initiation process, which is responding to physical contact with the host and high far-red light environments, which are both important signals for haustorium induction in *Cuscuta* species.

To identify the key regulators in the haustorium initiation, we focused on genes in module 1 and calculated the degree centrality and betweenness centrality scores of each gene within this group because these gene are the potential master regulators. Many central hub genes in module 1 are protein kinases or enzymes involved in cell signaling. We focused on genes that are annotated as transcription factors to identify the potential master upstream key regulators of this developmental stage. Among these central hub transcription factors, a homeobox-leucine zipper protein (Cc014209) that is similar to transcription factor homeobox 7 (HB7) in *Arabidopsis* was identified (**Figure 2B**). Based on previous reports, *AtHB7* is a negative regulator of ABA response (Pehlivan, 2019) and modulates abscisic acid (ABA) signaling by controlling the activity of protein phosphatases type 2C (PP2C) and ABA receptors (Valdés et al., 2012). Intriguingly, a recent study showed that ABA levels regulate haustoria formation in the root parasitic plant *Phtheirospermum japonicum* (Kokla et al., 2021). In *P. japonicum*, lowering ABA biosynthesis

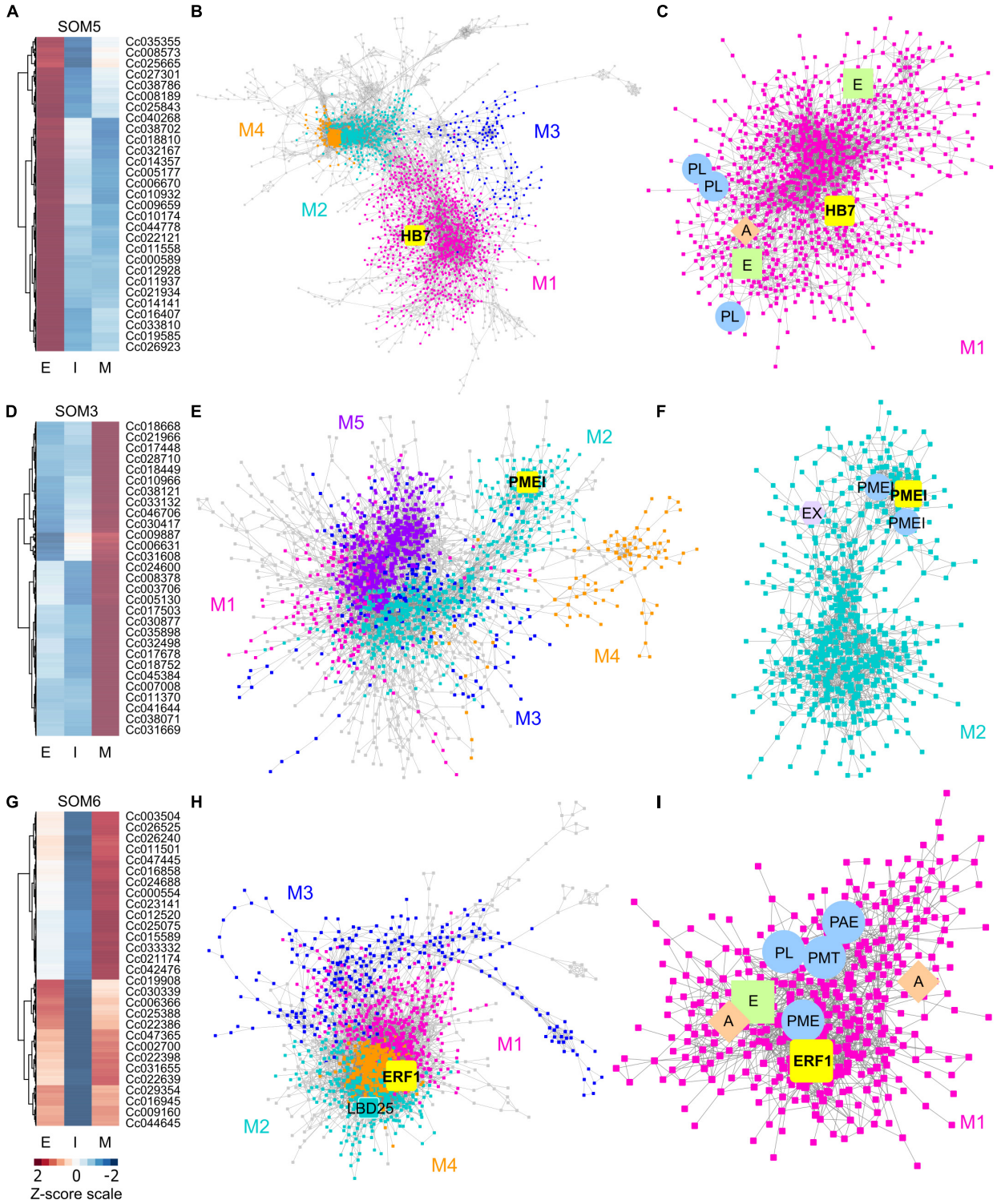

FIGURE 2 | Heatmaps and gene-coexpression networks (GCNs) of *C. campestris* haustorial tissues across three developmental stages. **(A)** A heatmap of gene expression profiles in z-scores for SOM5, which includes genes that are highly expressed in the early stage. **(B)** A GCN of genes in SOM5. This SOM5 GCN is composed of four major modules. Magenta indicates genes in Module 1, which has enriched biological process GO term including "response to abiotic and biotic stimulus, stress, hormone, far-red light." The transcription factor HB7 is enlarged and labeled in yellow. **(C)** GCN of genes that are classified in SOM5 Module 1. PL, pectin lyase-like superfamily protein. A, auxin response factor 1. E, ethylene signaling-related genes. **(D)** A heatmap of gene expression profiles in z-scores for SOM3, which includes genes that are highly expressed in the mature stage. **(E)** A GCN of genes that are in SOM3. The SOM3 GCN is composed of five major modules.

(Continued)

FIGURE 2 | Cyan indicates genes in Module 2, which has enriched biological process GO term including "root radial pattern formation." Selected pectin methyl-esterase inhibitor (PMEI) is enlarged and labeled in yellow. **(F)** GCN of genes that are classified in SOM3 Module 2. PMEI, pectin methyl-esterase inhibitor. EX, expansin. **(G)** A heatmap of gene expression profiles in z-scores for SOM6, which includes genes that are relatively highly expressed in the early and mature stage. **(H)** A GCN of genes in SOM6. This SOM6 GCN is composed of four major modules. Magenta indicates genes in Module 1, which has enriched biological process GO term including "response to stimulus, hormone, organic substance." Ethylene responsive element binding factor 1 (ERF1) is enlarged and labeled in yellow. The transcription factor LBD25 is enlarged and labeled in cyan as other genes in Module 2. **(I)** GCN of genes that are classified in SOM6 Module 1. PL, pectin lyase-like superfamily protein. A, auxin transporter or auxin-responsive protein; E, ethylene signaling-related genes; PL, pectin lyase-like superfamily protein; PME, pectin methylesterase; PMT, pectin methyltransferase-like; PAE, pectin acetylesterase family protein. The complete gene lists for all SOM units with SOM distances and PCA principal component values are included in **Supplementary Table 1**. The selected SOM gene lists were used for constructing the GCN based on the expression profiles in *C. campestris* LCM data with the following normal quantile cutoffs. The SOM5 GCN cutoff = 0.97. The SOM3 GCN cutoff = 0.98. The SOM6 GCN cutoff = 0.95.

enabled haustoria to form in the presence of nitrates. Based on these pieces of evidence, we focus on *CcHB7* for further functional analysis.

Second, the genes highly up-regulated at the mature stage are most likely to be involved in establishment of vascular connection between host and parasite. Therefore, we also focused on genes in SOM3, which is a cluster enriched with genes that are highly expressed in the mature haustorial stage (**Figure 2D**). Using these SOM3 genes, we constructed a GCN to generate an overview of the potential molecular regulatory machinery. This SOM3 GCN is composed of five major modules based on the GCN community structure (**Figure 2E** and **Supplementary Table 3**). Using GO enrichment analysis, we noticed that the SOM3 module 2 has enriched biological process GO terms including "root radial pattern formation" (**Supplementary Table 5**). This result matches our recent discovery that *C. campestris* also utilizes the root developmental program during haustorium organogenesis (Jhu et al., 2021). Therefore, we focused on SOM3 module 2 for further analysis. Based on the degree centrality and betweenness centrality scores, we noticed that many central hub genes in SOM3 module 2 are involved in cell wall modification, including expansins and several pectin methyl-esterase inhibitors (PMEIs) (**Figure 2F**). *CcPMEI* (Cc038093) is one of the central hub genes and has strong co-expression connection with other PMEIs. Thus, we focused on this *CcPMEI* for further functional analysis.

Last but not least, the previously identified key regulator in *C. campestris* haustorium development, transcription factor *LATERAL ORGAN BOUNDARIES DOMAIN 25* (*CcLBD25*) (Jhu et al., 2021) is classified in SOM6, which is enriched with genes that are highly expressed in the early and mature haustorial stage (**Figure 2G**). The SOM6 GCN is composed of four major modules based on the GCN community structure (**Figure 2H** and **Supplementary Table 4**). *CcLBD25* is located in module 2, which does not have any significantly enriched biological process GO terms (**Supplementary Table 5**). On the other hand, we noticed module 1 has enriched biological process GO term including "response to stimulus, response to hormone, response to organic substance." Based on previous studies, auxin (Tomilov et al., 2005; Ishida et al., 2016) and ethylene (Cui et al., 2020) signaling play essential roles in parasitic plant haustorium development. Appropriate tactile stimuli, which come from the pressure coiling on the host, are also crucial for haustorium induction (Tada et al., 1996). Therefore, we zoomed in on SOM6 module 1 for further GCN analysis.

Many genes in SOM6 module 1 are enzymes that catalyze the degradation or modification of pectin, including pectin lyase (PL), pectin methyl esterase (PME), pectin methyltransferase (PMT), and pectin acetyl esterase (PAE) (**Figure 2I**). These findings coincide with several previous studies that cell wall modification, especially pectin structural dynamic and integrity, plays an important role in haustorium development (Vaughn, 2002; Johnsen et al., 2015; Hozumi et al., 2017). Besides cell wall remodeling, auxin and ethylene signaling also seem to play a role in the early and mature developmental stages. An auxin efflux carrier (Cc034373) and an auxin-responsive protein (Cc038909) were also located in SOM6 module 1 (**Figure 2I**). Furthermore, among the central hub genes in SOM6 module 1, the top central hub transcription factor is an ethylene responsive element binding factor 1 (*ERF1*, Cc002541), which is in the ERF/AP2 domain-containing transcription factor family. Intriguingly, a recent study showed that the root parasitic plant *Phtheirospermum japonicum* uses ethylene as a signal for host recognition and to tweak the haustorium development and penetration process (Cui et al., 2020). Our gene coexpression analysis suggests that this ethylene-mediated haustorial development regulatory pathway might be shared by both root and stem parasitic plants. Therefore, we focused on this *CcERF1* for further functional analysis.

Functional Characterization of Candidate *Cuscuta campestris* Genes by Host-Induced Gene Silencing

Since an efficient transformation system for *C. campestris* is currently not available, to further validate the function of these candidate *C. campestris* genes, *CcHB7*, *CcPMEI*, and *CcERF1*, we used host-induced gene silencing (HIGS) to knock-down the candidate genes in *C. campestris.* Based on previous studies, cross-species transport of mRNAs, miRNAs and siRNAs between *C. campestris* and their hosts through haustoria vascular connections is common (Kim et al., 2014; Johnson et al., 2019). These transported siRNAs can successfully down-regulate target gene transcription in *C. campestris*, *via* HIGS. Therefore, we generated transgenic tomatoes with hairpin RNAi constructs that target and down-regulate the candidate *C. campestris* genes, *CcHB7*, *CcPMEI*, and *CcERF1*, after the first successful attachment. If these genes are important in haustorium development, down-regulating these genes should influence haustorium penetration and parasitism. We collected *C. campestris* haustorium and prehaustorium tissues next to the

attachment sites and validated by qPCR that *CcHB7*, *CcPMEI*, and *CcERF1* are successfully knocked down in *C. campestris* tissues grown on HIGS transgenic tomatoes (**Supplementary Figures 4A,C,D**).

To determine if these genes impact haustorium structure or the parasitism process, we grew *C. campestris* strands on the HIGS transgenic tomato. We collected tomato stem sections with *C. campestris* strands successfully attached on them and used vibratome sectioning to prepare 100 μm-thick fresh haustorium sections and subsequently stained them with Toluidine Blue O (O'Brien et al., 1964). We observed searching hyphae that entered the host cortex successfully and converted into xylic hyphae, which create the xylem bridge between host and parasite, or phloic hyphae, which mimic sieve elements and establish phloem-to-phloem connections, as they linked to the host xylem and phloem in sections of the haustoria growing on wild-type H1706 tomato plants (**Figures 3A–C**). However, we observed that many haustoria growing on *CcHB7* RNAi (**Figures 3D–F**), *CcPMEI* RNAi (**Figures 3G–I**), and *CcERF1* RNAi (**Figures 3J–L**) transgenic tomatoes seems to stop their penetration process at the cortex region. Furthermore, they also all shared a common phenotype that the host cortex cells that are surrounding the haustoria seem to enlarge and have a very loose cell wall structure, appearing degraded (**Figures 3D–L**). These *C. campestris* haustoria were not able to form vascular connections with their hosts and easily detached from their host stems.

This structural phenotype also corresponds well with our GCN results, especially the GCN for SOM3 and SOM6 (**Figure 2**). Several previous studies indicate that the interaction between pectin methyl esterase (PME) and pectin methyl esterase inhibitor (PMEI) is a determinant factor in pectin degradation, cell wall loosening, strengthening, and organogenesis. Pectin acetyl esterases (PAEs) are involved in the enzymatic deacetylation of pectin and are used by plant pathogens to infect their hosts (Kong et al., 2019). However, the balance between different pectin enzyme functions might be precisely regulated by many key regulators. The down-regulation of these key regulators might disrupt the dynamic balance between enzymes and cause an out-of-control cell wall degradation, which lead to haustorium detachment from its host (**Figures 3D–L**).

Notably, since these plants are in a HIGS system, the first successful haustorial connection is necessary for the small interfering RNAs to transfer from the host to the parasite. Therefore, we often observed a successfully connected haustorium followed by several abnormal haustorium attachments, including the phenotype of overly degraded host cortex cell walls (**Figure 3I**). The overall plant phenotypes of *C. campestris* growing on the HIGS transgenic plants also showed very few haustorial connections and the inability to continue to form more attachments with the hosts compared to those growing on wild-type H1706 tomato plants (**Figures 4A–C**). In addition, our preliminary biomass measurements also showed that the *C. campestris* plants growing on RNAi transgenic plants have reduced biomass compared with those growing on wild-type tomato plants (**Figure 4D**). All of these results indicate that the down-regulation of these candidate gene expression levels by HIGS interfered with haustorium development and hampered *C. campestris* parasitism.

RNA-Seq Analyses and Gene Coexpression Networks Across Three Developmental Stages of Host Tissues Surrounding *Cuscuta campestris* Haustoria

On the other side of this host-parasite interface is the tomato host. We analyzed the LCM RNA-Seq data from the host tomato tissues surrounding *C. campestris* haustoria by mapping reads to the tomato genome ITAG4.0 (Sato et al., 2012). Using multidimensional scaling analysis, the gene expression patterns in control host cell types (the regular tomato cortex cells that are not next to haustorium) are distinct from the cortex tissues surrounding *C. campestris* haustoria (**Supplementary Figure 5**). We also conducted a PCA coupled with SOM clustering analysis to visualize the expression profile of each gene (**Figure 5** and **Supplementary Table 6**). To identify potential key regulators of the interaction between host and parasite at different haustorium penetration stages, we conducted further gene coexpression analysis on specific SOM clusters (**Figure 6** and **Supplementary Figure 6**).

First, the host genes that are highly up-regulated at the early stage are most likely to be involved in perceiving parasite signals, triggering pattern-triggered immunity (PTI) and effector-triggered immunity (ETI) to help the host repel *C. campestris* attacks. Based on previous reports, the changes in the levels of salicylic acid (SA) and jasmonic acid (JA) in hosts are most obvious in the early stage [4 days post attachment (DPA)] (Runyon et al., 2010). So, we hypothesized that the most pronounced gene expression changes of key regulators would be at the initial stage of infestation. Therefore, we focused on genes in SOM8, which is a cluster enriched with host genes that are highly expressed in the early haustorial stage (**Figure 6A**). Among the genes in SOM8, we noticed inclusion of *SlWRKY16* (Solyc07g056280), a negative regulator of the lignin-based resistance response (Jhu et al., 2020). The SOM8 GCN is composed of four major modules based on the GCN community structure (**Figure 6B** and **Supplementary Table 7**). *SlWRKY16* is located in module 2. Based on our GO enrichment analysis, there are some genes that matched the GO term "regulation of defense response, and defense response to fungus," but none of the GO terms were statistically significantly enriched in this module (**Supplementary Table 9**). However, one of the previously identified CuRe1 homologs (*CuRe1-like*, Solyc08g016210) (Fürst et al., 2016), which is a leucine-rich repeat (LRR) receptor-like serine/threonine-protein kinase, is also located in module 2 (**Figure 6B**). Therefore, we zoomed in on the SOM8 module 2 for further GCN analysis.

Many other genes in SOM8 module 2 are involved in ethylene signaling (**Figure 6C**). Ethylene is known to play a vital role in activating plant defenses against various biotic stresses, including microbial pathogens and herbivores (Broekgaarden et al., 2015). Previous studies also used the emission of ethylene in *N. benthamiana* and *S. lycopersicum* as an indicator that

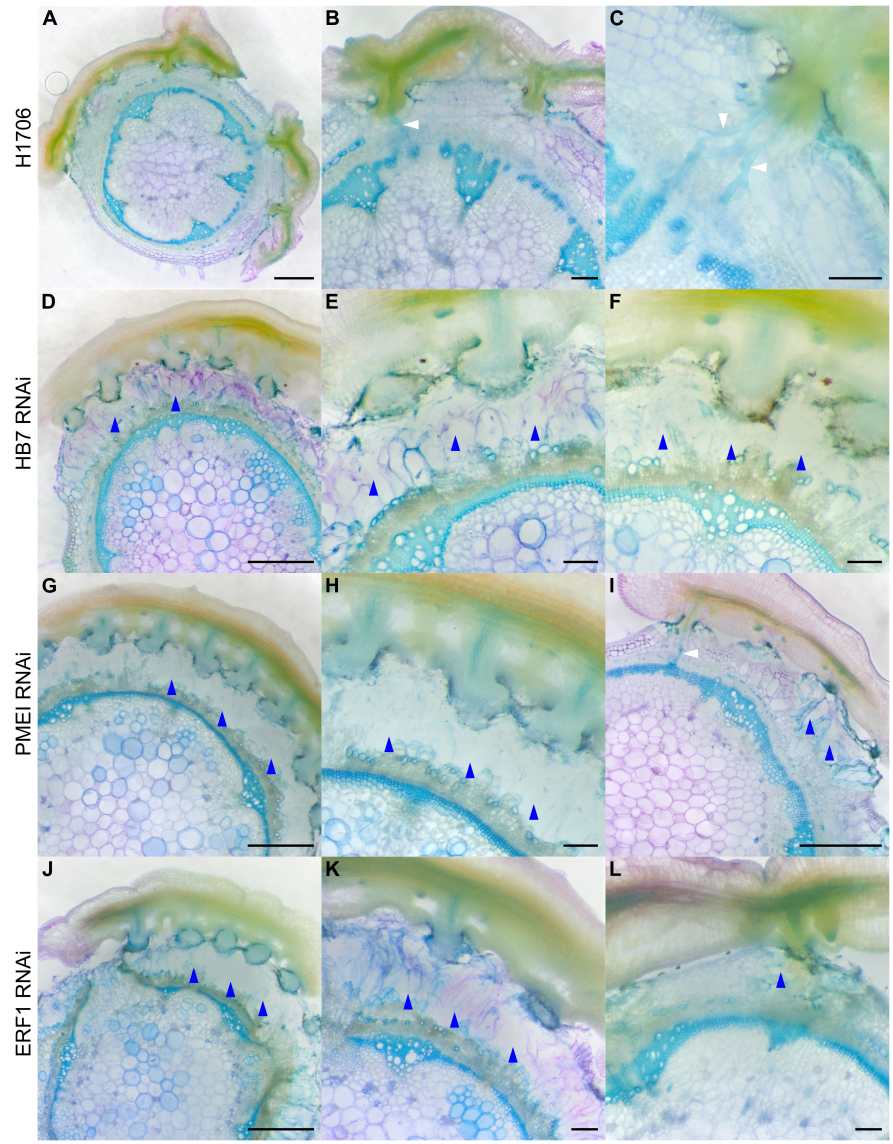

FIGURE 3 | Haustorium phenotypes of *C. campestris* growing on Heinz tomato wild-types and HIGS RNAi transgenic plants. *C. campestris* haustoria that were growing on wild-type H1706 tomato hosts **(A–C)**, on HB7 RNAi transgenic tomato plants **(D–F)**, on PMEI RNAi transgenic tomato plants **(G–I)**, on ERF1 RNAi transgenic tomato plants **(J–L)**. **(A,D,G,I,J)** Scale bars = 1 mm. **(B,C,E,F,H,K,L)** Scale bars = 200 μm. **(A–L)** 100 μm thick vibratome sections of fresh haustorium stained with Toluidine Blue O. White arrowhead indicates normal haustorial vascular connections. Blue arrowhead indicates the phenotype of overly degraded host cortex cell walls.

the defense response was successfully triggered upon *Cuscuta reflexa* infestation *(Hegenauer et al., 2016, 2020)*. In addition to the CuRe1-like homolog, several LRR receptor-like protein kinases are also identified in SOM8 module 2 (**Figure 6C**). This result matches our hypothesis that the host genes that are highly up-regulated at the early stage are most likely to be involved in perceiving parasite signals. We suspect that *CuRe1-like* might play a role in sensing unknown *Cuscuta* signals, so we generated CRISPR-Cas9 edited *Cure1-like* mutant plants for further analysis.

Among the central hub genes in SOM8 module 2, *Pathogenesis-Related protein 1* (*PR1*, Solyc01g106600) was one of the top central hubs (*PR1* degree centrality = 64; median degree centrality in SOM8 = 13) (**Figure 6C**). PR1 proteins are known to be highly produced upon plant pathogen infection and have often been used as a marker for SA-mediated disease resistance (Breen et al., 2017). However, the role of PR1 in host plant responses upon parasitic plant attack is currently unknown. Therefore, we also focused on PR1 for further functional analysis using CRISPR-Cas9 gene editing.

Other than the host genes that are specifically only highly expressed at the early stage, another group of host genes are up-regulated at the early stage and gradually decrease their expression throughout parasitism. Genes with this expression

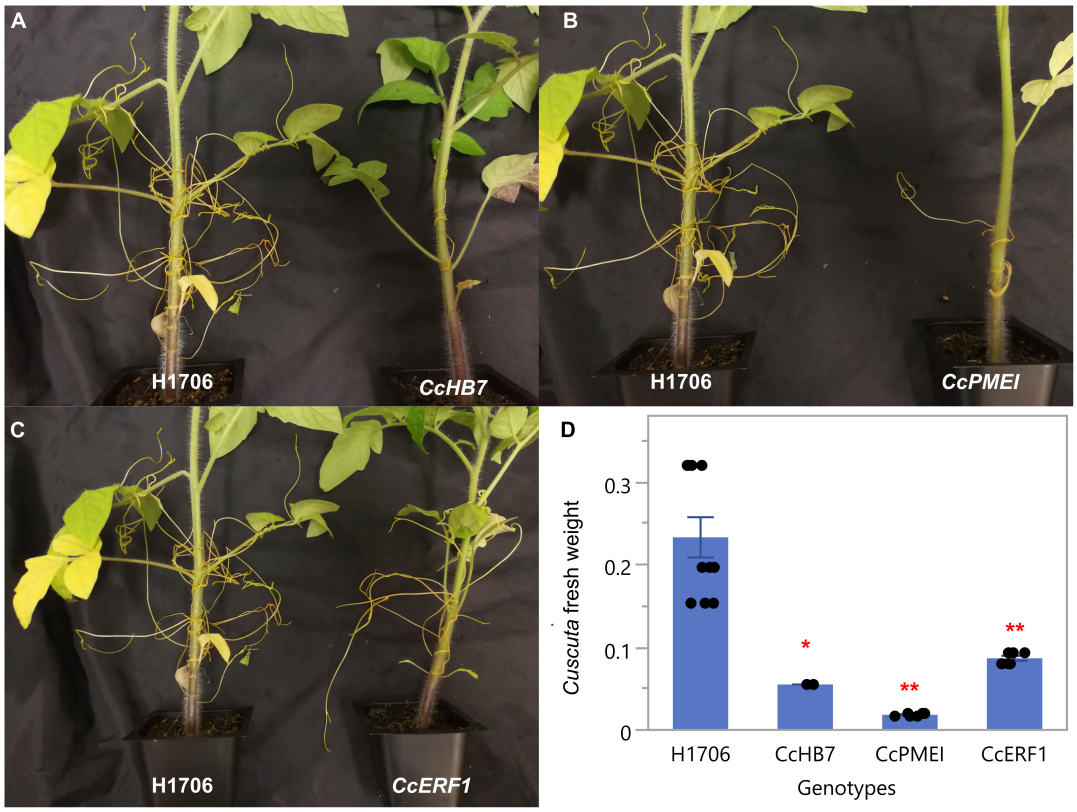

FIGURE 4 | Phenotypes of *C. campestris* growing on Host-Induced Gene Silencing (HIGS) RNAi transgenic plants. **(A)** *C. campestris* growing on wild-type H1706 tomatoes and T1 *CcHB7* RNAi transgenic plants. **(B)** *C. campestris* growing on wild-type H1706 tomatoes and T1 *CcPMEI* RNAi transgenic plants. **(C)** *C. campestris* growing on wild-type H1706 tomatoes and T1 *CcERF1* RNAi transgenic plants. **(D)** Averaged biomass of *C. campestris* growing on wild-type H1706 tomatoes and T1 *CcHB7*, *CcPMEI*, and *CcERF1*RNAi transgenic plants. Fresh net weights of *C. campestris* were measured in grams (g). Each data point represents one tomato plant (biological replicate). Data presented are assessed using Dunnett's test with wild-type H1706 as control. "*" p-value < 0.0005. "**" p-value < 0.0001.

pattern are found in SOM3 (**Figure 6D**). We suspected that these genes might also be involved in the parasite signal perceiving process. Hence, we focus on SOM3 for further GCN analysis. The SOM3 GCN is composed of four major modules based on the GCN community structure (**Figure 6E** and **Supplementary Table 8**). Based on our GO enrichment analysis, there are some genes in module 3 that matched the GO term "response to hormone," but none of the GO terms were statistically significantly enriched in this module (**Supplementary Table 9**). However, many genes in SOM3 module 3 are LRR receptor-like kinases or nucleotide-binding site–leucine-rich repeat (NBS-LRR, or NLR) proteins. Therefore, we focused on SOM3 module 3 for further analysis.

Among the genes in SOM3 module 3, four genes involved in ethylene signaling were identified, including an ethylene-responsive transcription factor, an ethylene-responsive proteinase inhibitor and an ethylene-inducing xylanase receptor. This result provides further support for the hypothesis that ethylene might also play an important role in plant resistance responses against parasitic plants. In addition to the ethylene signaling pathway, potential transcription factors or receptors are also enriched in SOM3 module 3. Three LRR proteins and two NLRs are identified in module 3. NLRs are common disease resistance genes (R genes) and are known to be involved in biotic stress detection, including various plant pathogens and herbivores (McHale et al., 2006; Van Ghelder et al., 2019). Therefore, we suspected that these NLRs are potentially involved in the process of detecting parasitic plants signals and choose the NLR with the highest degree centrality (Solyc07g056200 degree centrality = 7; median degree centrality of NLRs in SOM3 module 3 = 6.5) in SOM3 module 3 as our candidate genes for further functional analysis.

Functional Characterization of Tomato Host Genes by CRISPR-Cas9 Gene Editing

Since CRISPR knockout techniques (Pan et al., 2016) and tomato transformation systems are readily available, we designed and cloned synthetic guide RNAs (sgRNA) targeting our candidate genes, *SlPR1*, *SlCuRe1-like*, *SlNLR*, and then produced transgenic tomato plants in the M82 background with CRISPR/Cas9 targeted candidate gene knockout mutations. We selected the T0 transgenic plants that had biallelic insertion or

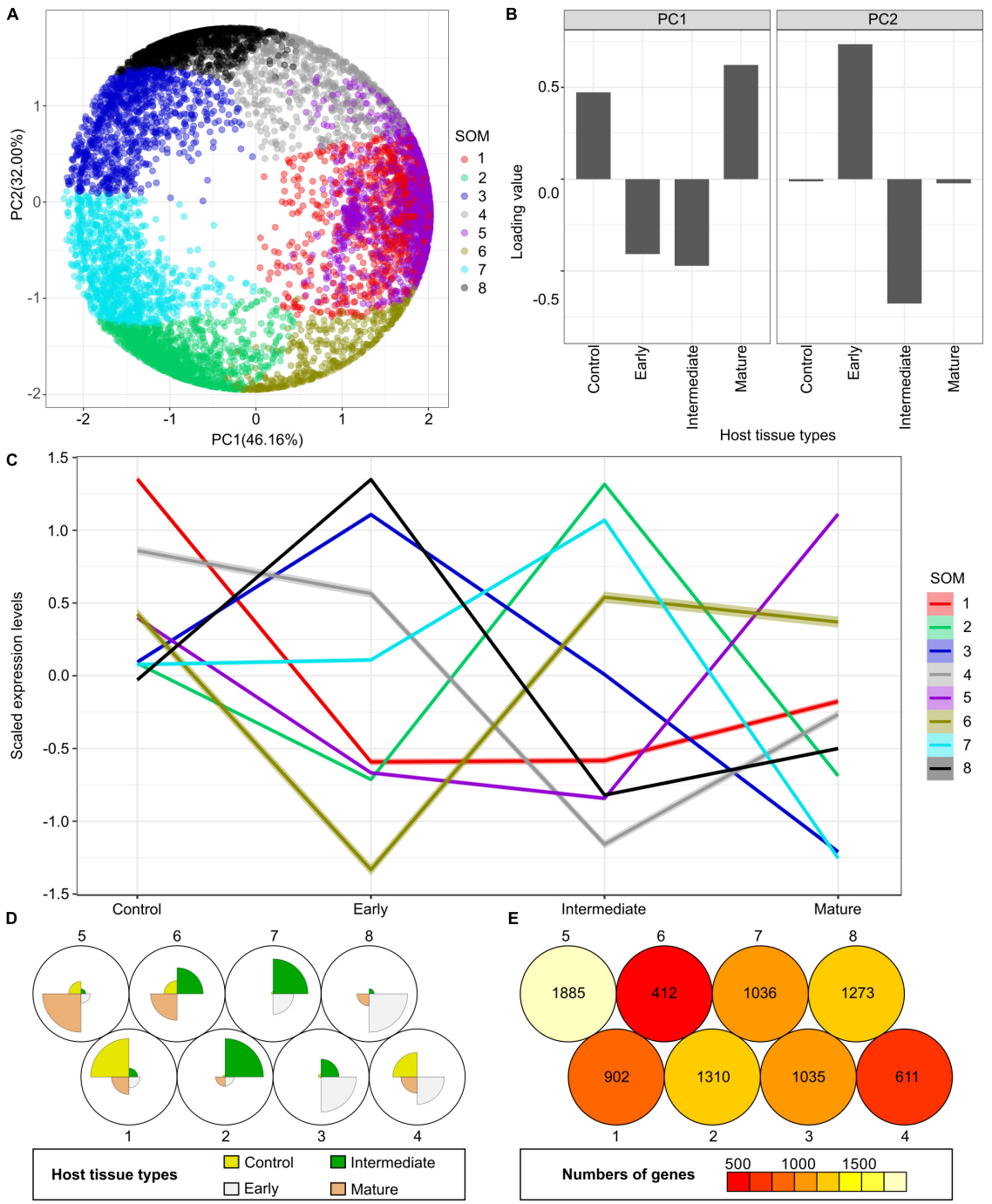

FIGURE 5 | Principal component analysis (PCA) and self-organizing maps (SOM) clustering of LCM RNA-Seq data from the host tomato tissues surrounding *C. campestris* haustoria. **(A)** PCA plot of the first and second principal components (PC1 and PC2) and colored indicate their corresponding SOM groups. Each dot represents a gene. **(B)** Loading values of PC1 and PC2. "Control" means the tomato stem cortex tissue samples that are not next to *C. campestris* haustoria, which serve as negative controls in this experiment. PC1 separates the genes specifically expressed in host tissues sounding the early and intermediate-stage haustoria from those specifically expressed in other stages. PC2 separates the genes specifically expressed in host tissues surrounding the intermediate-stage haustoria from those expressed explicitly at the mature stage. **(C)** A plot of each SOM group's scaled expression levels at four types of host tomato tissue surrounding *C. campestris* haustoria at different developmental stages. The color of each line represents the SOM group it belongs to. The shaded area around the lines indicates the 95 percent confidence interval. **(D)** A code plot of SOM clustering showing which developmental stage predominantly expresses genes of each SOM group based on sector size. Each sector represents the host tissues surrounding *C. campestris* haustoria at a specific developmental stage and is colored according to the tissue types it represents in figure legends. The number 1-8 next to each circle represents the corresponding SOM group. **(E)** A count plot of SOM clustering represents how many genes showed differential expression in each SOM group. The numbers of genes are labeled inside each circle representing SOM. **(D,E)** The number 1–8 next to each circle represents the corresponding SOM group.

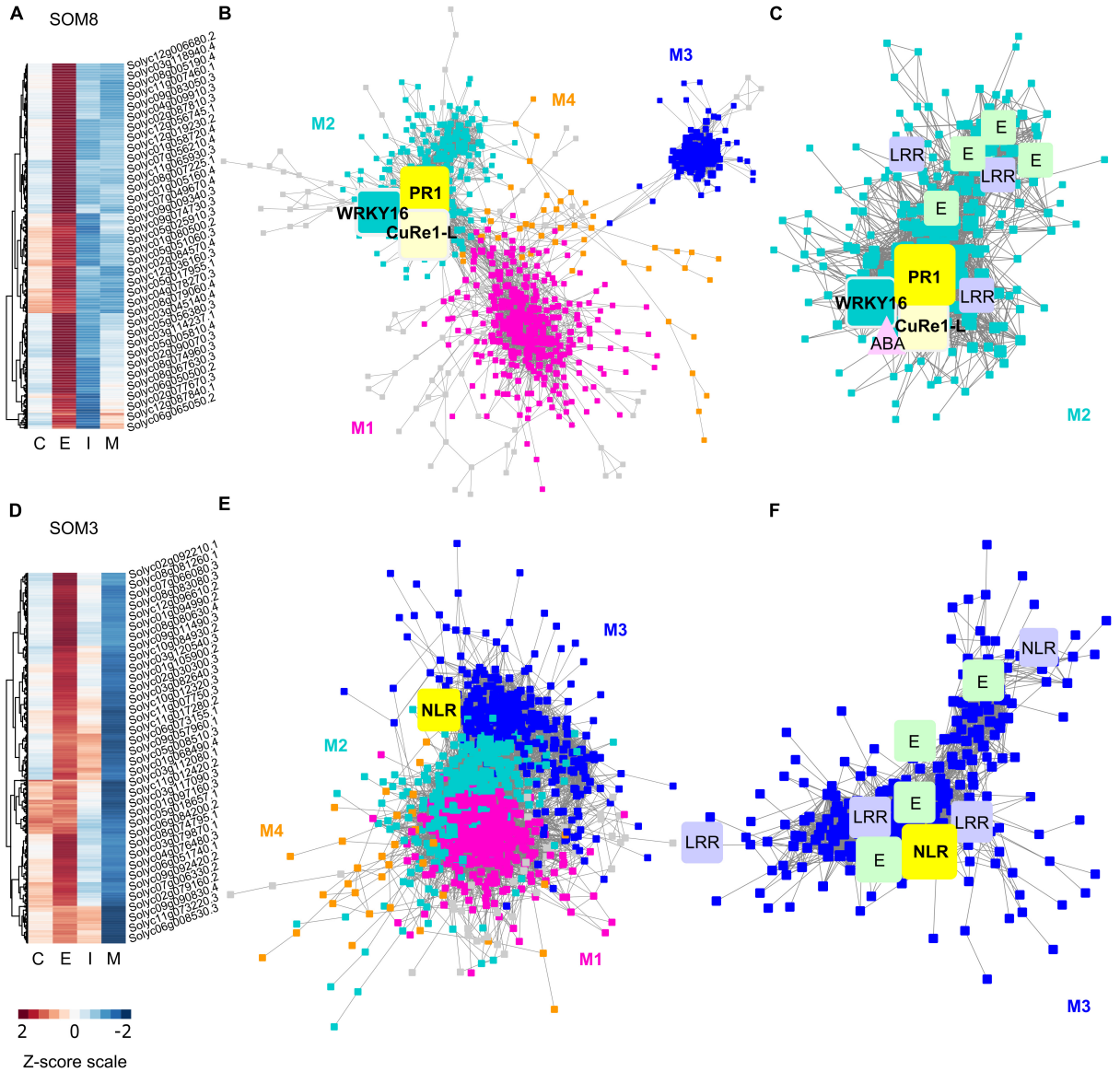

FIGURE 6 | Heatmaps and gene-coexpression networks (GCNs) of LCM RNA-Seq data from the host tomato tissues surrounding *C. campestris* haustoria. **(A)** A heatmap of gene expression profiles in *z*-scores for SOM8, which includes genes specifically highly expressed in the early stage. **(B)** A GCN of genes in SOM8. This SOM8 GCN is composed of four major modules. Cyan indicates genes in Module 2. The transcription factor WRKY16 is enlarged and labeled in cyan as other genes in Module 2. PR1 is enlarged and labeled in yellow. CuRe1-like receptor (CuRe1-L) is enlarged and labeled in light yellow. **(C)** GCN of genes that are classified in SOM8 Module 2. CuRe1-L, CuRe1-like receptor. LRR, Leucine-rich repeat receptor-like protein kinase. ABA, Abscisic acid stress ripening 5. E, ethylene-responsive transcription factor. **(D)** A heatmap of gene expression profiles in z-scores for SOM3, including genes that have high expression levels in the early stage and moderate expression levels in the intermediate stage. **(E)** A GCN of genes in SOM3. This SOM3 GCN is composed of four major modules. Blue indicates genes in Module 3. NBS is enlarged and labeled in yellow. **(F)** GCN of genes that are classified in SOM3 Module 3. LRR, Leucine-rich repeat receptor-like protein kinase. E, ethylene-responsive transcription factor. NLR, NBS-LRR protein. The complete gene lists for all SOM units with SOM distances and PCA principal component values are included in **Supplementary Table 6**. The selected SOM gene lists were used for constructing the GCN based on the expression profiles in tomato LCM data with the following normal quantile cutoffs. The SOM8 GCN cutoff = 0.90. The SOM3 GCN cutoff = 0.80.

deletion or substitution mutations for further T1 plants analysis (**Supplementary Figure 6**). After obtaining these CRISPR transgenic tomato lines, we tested the interactions of *C. campestris* with these engineered tomato lines and compared their *C. campestris*-host interactions with those seen in wild-type M82 tomatoes by phenotyping the haustorium attachment sites.

Interestingly, the *SlCuRe1-like* CRISPR T0 transgenic tomato lines were very vulnerable to pathogens and insect herbivores, did not grow well in our greenhouse conditions and only produced very few seeds. This indicates that *SlCuRe1-like* might play a role in the plant defense responses to other pathogens and herbivores in addition to any possible role in plant parasitism. As a result,

due to low seed set we were unable to phenotype these CRISPR tomato lines, so *SlCuRe1-like* phenotyping is excluded from our current analysis.

When compared with wild-type M82 tomato plants (**Figures 7A,B**), *SlPR1* CRISPR T1 tomato plants (**Figures 7E,F**) and *SlNLR* CRISPR T1 tomato plants (**Figures 7I,J**) did not have an obvious difference in their overall plant or tissue phenotypes without *C. campestris* infestation, based on the fresh vibratome sections. However, the differences were apparent when these CRISPR tomato plants were infested by *C. campestris*. On wild-type M82 tomato plants, we observed that searching hyphae entered the host cortex and linked to the host xylem and phloem, but *C. campestris* did not change the overall host stem structure much, other than penetrating and forming vascular connections (**Figures 7C,D**).

In contrast, *SlPR1* CRISPR tomato plants seem to be more susceptible to *C. campestris* attack and have hypertrophy symptoms, which is abnormal plant outgrowth caused by cell enlargement, at the haustorium attachment sites (**Figures 7G,H**). The vascular connections between host and parasite, especially the xylem bridges, were enlarged. Based on previous reports, hypertrophy improves the efficiency of root parasitic plant *Phtheirospermum japonicum* parasitism (Spallek et al., 2017). This parasite-derived modification can change host tissue morphology and help with parasite fitness. Similarly, *C. campestris* haustoria not only penetrated and formed vascular connections with *SlNLR* CRISPR tomato vascular tissue, but also changed the overall host stem vascular tissue arrangement, causing a reduction in the secondary xylem in the region of haustorium penetration (**Figures 7K,L**). This phenotype also indicates that *SlNLR* CRISPR tomato plants are more vulnerable to *C. campestris*.

The overall plant phenotypes of wild-type M82 tomatoes and CRISPR transgenic plants with *C. campestris* infestation also showed that the *SlPR1* and *SlNLR* CRISPR transgenic plants have stunted growth after being parasitized by *C. campestris* (**Figure 8**). The CRISPR transgenic plants with *C. campestris* infestation are much shorter than wild-type M82 with *C. campestris* infestation. Notably, the *SlPR1* and *SlNLR* CRISPR transgenic plants without *C. campestris* infestation have no significant height difference comparing to wild-type M82 (**Figure 8C**). This result indicates that the CRISPR-mediated mutations do not lead to the stunted growth phenotype directly; however, the *SlPR1* and *SlNLR* knockout mutations cause a growth penalty in the presence of *C. campestris*. These results also suggest that the knockout of candidate genes might interfere with the host defense response and make these CRISPR plants more susceptible to *C. campestris* parasitism.

DISCUSSION

In this study, we use LCM captured *C. campestris* haustorial tissues and tomato host tissues surrounding haustoria, coupled with RNA-seq analysis to reveal the potential tissue-resolution molecular regulatory machinery and the complexity of gene coexpression networks involved in haustorium organogenesis and host defense responses. We identified three potential key regulators in *C. campestris* that are involved in the early or/and mature stage of haustorium development, and all three of them were validated by using HIGS transgenic plants. We also identified three potential key regulators in tomato plants that are involved in perceiving signals from the parasite, and two of them were further verified with CRISPR knockout mutants.

Pectin Dynamic Regulation in *Cuscuta parasitism* and Haustorium Development

The chemical structure and mechanical properties of plant cell walls play an important role in organogenesis (Chebli and Geitmann, 2017). Several reports indicate that the physical interactions between pectins and other cell wall components regulate many vital aspects of plant development (Saffer, 2018). Pectin composition and mechanical characteristics have also been found to control the parasitism process and the development of haustorium in *Cuscuta* species. For example, a previous study discovered that *Cuscuta pentagona* secretes de-esterified pectins at the host and parasite interface (Vaughn, 2002). These low-esterified pectins function as a cement to help adhesion to their hosts during the early stage of the *Cuscuta* parasitism process. Similar de-esterified pectin accumulation phenomena have also been reported in *Cuscuta reflexa, Cuscuta campestris*, and *Cuscuta japonica* to facilitate the formation of strong adhesion (Johnsen et al., 2015; Hozumi et al., 2017). De-esterified pectin is a good substrate for pectate lyases, which are also found to be highly expressed at haustoria in *C. reflexa* (Johnsen et al., 2015). High levels of pectate lyases suggest that *Cuscuta* utilizes these enzymes to remodel their host cell walls to achieve successful penetration. The SOM5 and SOM6 GCNs of *C. campestris* genes also identified several highly expressed pectate lyases and pectin methyl-esterases at early and/or mature stages (**Figures 2A–C,G–I**). Our GCN analysis is not only consistent with previous findings but also provides a more comprehensive potential gene regulatory machinery at specific haustorial developmental stages.

The interplay between PME and PMEI is also known to regulate the chemical and physical characteristics of the cell wall, including cell wall porosity and elasticity (Wormit and Usadel, 2018). Although cell wall loosening is a necessary step for haustorium penetration, an out-of-control cell wall degradation could lead to haustorium detachment from its host (**Figure 3**). The balance between different pectin enzyme functions might be precisely regulated by many key regulators. The down-regulation of these key regulators might disrupt the dynamic balance between enzymes and lead to abnormal cell wall degradation. Therefore, regulation of the enzymes that likely help with the haustorium penetration process may be disrupted, leading to over-degradation of the host cell wall, resulting in haustorium detachment (**Figures 3D–L**). Therefore, loosening the host plant cell wall should be precisely regulated during the parasitism process. Several highly expressed PMEIs are found in the SOM3 GCN at the mature stage, verifying this hypothesis (**Figures 2D–F**). Furthermore, in SOM6 module 1 (**Figures 2G–I**), tight connections between

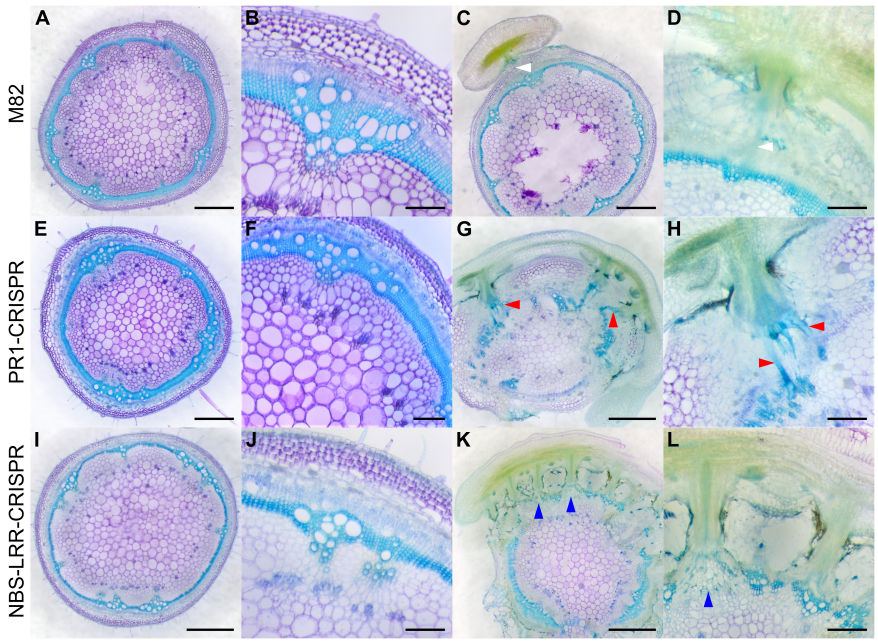

FIGURE 7 | Haustorium phenotypes of *C. campestris* growing on M82 tomato wild-types and candidate genes-CRISPR transgenic plants. *C. campestris* haustoria that were growing on wild-type M82 tomato hosts **(A–D)**, on PR1-CRISPR T1 transgenic tomato plants **(E–H)**, on NBS-LRR-CRISPR T1 transgenic tomato plants **(I–L)**. **(G–H)** Vibratome sections of *C. campestris* growing on PR1-CRISPR T1 plant #6. **(K,L)** Vibratome sections of *C. campestris* growing on NBS-LRR-CRISPR T1 plant #4. **(A,C,E,G,I,K)** Scale bars = 1 mm. **(B,D,F,H,J,L)** Scale bars = 200 μm. **(A–L)** 100 μm thick vibratome sections of fresh haustorium stained with Toluidine Blue O. White arrowhead indicates normal haustorial vascular connections. Red arrowhead indicates the hypertrophy symptom with enlarged xylem bridges. Blue arrowhead indicates the phenotype of disrupted host stem vascular tissue arrangement.

several enzymes that catalyze the modification of pectin, including PLs, PME, PMT, and PAE, reveal the complexity of dynamic pectin regulation in the haustorium penetration process and the importance of balancing various aspects of cell wall modification.

Auxin and Ethylene in Haustorium Development

Regulating auxin transport and distribution is a pivotal factor in plant organogenesis (Benková et al., 2003). Regional auxin accumulation is commonly seen in root development, lateral root initiation, and root hair formation. Previous studies also indicate that spatial and temporal auxin accumulation play an important role in the early stage of haustorium organogenesis in root parasitic plants, like *Phtheirospermum japonicum* and *Triphysaria versicolor* (Tomilov et al., 2005; Ishida et al., 2016), which adopted the root morphogenesis program into haustorium development (Yoshida et al., 2016). Our SOM5 and SOM6 GCNs also included several genes that are auxin transporters or auxin-responsive proteins at the early stage of haustorium development (**Figure 2**). This suggests that auxin-mediated regulation of haustorium initiation might be shared by both root and stem parasitic plants, and also further validates our hypothesis that stem parasites also co-opted the root parasite program into haustorium development.

Other than auxin regulation, ethylene accumulation has also been observed in the early stage of haustorium development in *T. versicolor* (Tomilov et al., 2005). A recent study further discovered that ethylene signaling plays an important role in regulating cell proliferation and differentiation in the haustorial development process of *P. japonicum* (Cui et al., 2020). This root parasitic plant utilizes host-produced ethylene as a signal for host recognition to help with the haustorium penetration process (Cui et al., 2020). However, whether ethylene is also involved in haustorium development in stem parasitic plant remains an open question. The identification of ethylene signaling-related genes in SOM5 GCN (**Figure 2C**) and *ERF1* as one of the central hub genes in our SOM6 GCN (**Figure 2I**) provides some clues that ethylene signaling might also play a vital role in regulating haustorium initiation at the early haustorium initiation stage, and later cell differentiation at the mature haustorium stage in *C. campestris*.

Ethylene and Abscisic Acid in Host Responses Upon *Cuscuta campestris* Infestation

Besides regulating cell wall modification and organogenesis, ethylene is also known as a key hormone involved in plant defense response against various biotic stresses, including pathogens and herbivores (Adie et al., 2007; Liu et al., 2013; Tintor et al., 2013; Böhm et al., 2014). The production of ethylene has often been observed in host plants upon parasitic plant infestation. For example, an ethylene biosynthesis gene (Dos Santos et al., 2003) and an ethylene-responsive element-binding factor (Vieira

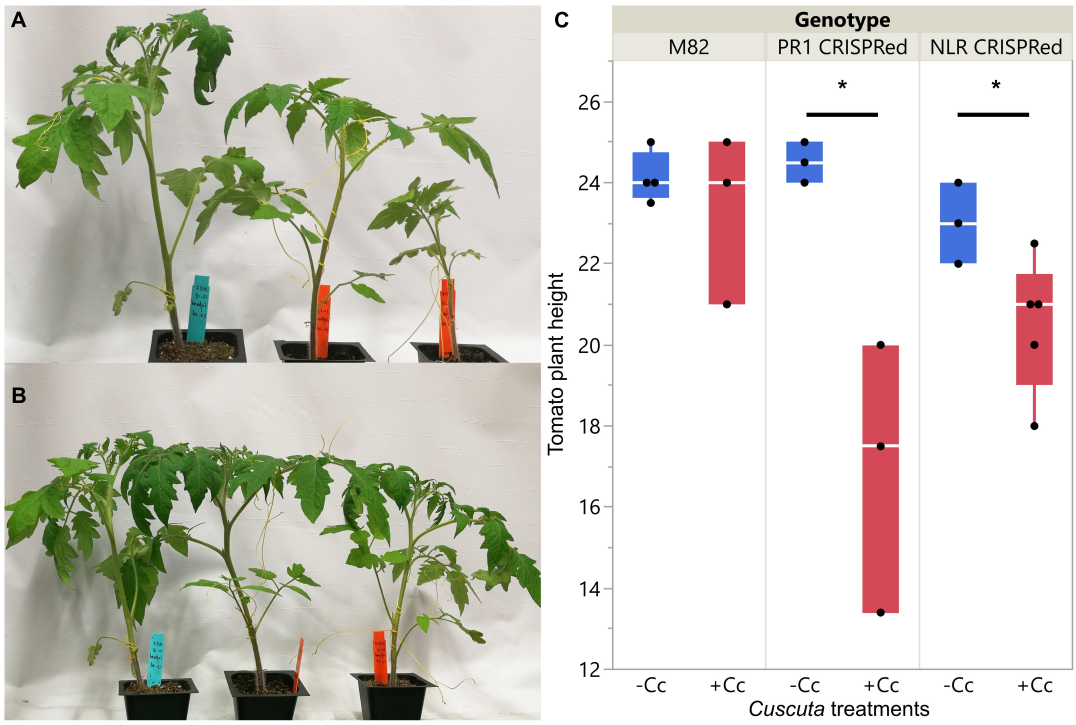

FIGURE 8 | Phenotypes of wild-types and CRISPR transgenic plants with *C. campestris* infestation. **(A)** Wild-type M82 tomatoes and T1 *SlPR1* CRISPR transgenic plants with *C. campestris* infestation. **(B)** Wild-type M82 tomatoes and T1 *SlNLR* CRISPR transgenic plants with *C. campestris* infestation. **(C)** Plant height of wild-type H1706 tomatoes and CRISPR transgenic plants with *C. campestris* infestation. The plant height of host tomato plants was measured in centimeters (cm). Data presented are assessed using one-tailed t-test with wild-type M82 as control. "*" p-value < 0.05. *SlPR1* CRISPR transgenic T1 plants #1-3 were used for control (-Cc) and T1 plants #4-6 were used for *Cuscuta* infestation treatments (+ Cc). *SlNLR* CRISPR transgenic T1 plants #1, 5, 9 were used for control (–Cc) and T1 plants #2, 4, 6, 8, 10 were used for *Cuscuta* infestation treatments (+ Cc). Detailed genotyping results of the T1 CRISPR transgenic plants are listed in **Supplementary Table 12**.

Dos Santos et al., 2003) were activated in *A. thaliana* upon *O. ramosa* infestation. Similarly, ethylene emission was induced in *N. benthamiana* and *S. lycopersicum* upon *Cuscuta reflexa* infestation *(Hegenauer et al., 2016, 2020)*. The identification of many ethylene-responsive transcription factors in our tomato SOM8 and SOM3 GCNs and their tight connections with many LRR and NLR genes (**Figure 6**) suggest that ethylene may also play a key role in host defense against *C. campestris* by triggering and regulating local and systemic immune responses.

Many previous studies also indicate that ethylene has complex crosstalk with other hormone pathways, including ABA, which is another major phytohormone regulating stress responses (Veselov et al., 2003; Ku et al., 2018; Berens et al., 2019). Although ABA is often known to be involved in responses to abiotic stress (Ku et al., 2018; Berens et al., 2019), induction of ABA biosynthesis and signaling were also observed in the interaction between host and parasitic plants. For example, ABA levels increased in both leaves and roots of tomatoes upon the infestation of root parasitic plant *Phelipanche ramose* (Cheng et al., 2017). ABA concentrations also increased in maize leaves upon *Striga hermonthica* infestation (Taylor et al., 1996). The induction of ABA was also observed in tomatoes at 36 h after *C. pentagona* infestation and continued to accumulate through 120 h (Runyon et al., 2010). Furthermore, in the early stage of *P. ramosa* infestation, elevated gene expression levels of ABA-responsive and biosynthesis genes were also reported. An ABA signaling-related gene has also been included in SOM8 module 2 (**Figure 6C**) suggests that ABA might play a role in host defense response at the early stage of perceiving *C. campestris* attack.

Parasitic Plant-Induced Hypertrophy

Hypertrophy, abnormal plant outgrowth caused by cell enlargement, is also a common plant symptom that can be induced by various pathogens, herbivores, or parasites (Bowman, 2019). Hyperplasia is abnormal plant outgrowth caused by excessive cell division, leading to increased cell numbers, resulting in the formation of plant galls that can be induced by viruses, pathogens, parasites, or insects (Bowman, 2019). Parasitic plant-induced hypertrophy and hyperplasia have also been reported in several different systems (Heide-Jørgensen, 2008). For example, hypertrophy has also been observed on crabapple trees, *Malus toringoides,* induced by the stem parasitic plant European mistletoe, *Viscum album (Spallek et al., 2017)*. Similarly, the root parasitic plant *Phtheirospermum japonicum* induced hypertrophy at the haustorial attachment site in both *A. thaliana* and tomato roots (Spallek et al., 2017). This hypertrophy phenotype enlarged the width of xylem tissues in the host root right above haustoria attachment sites, which could

help the parasites uptake more water and nutrients from the host. The induction of cytokinin and ethylene might be one reason for the hypertrophy phenotype (Spallek et al., 2017; Mignolli et al., 2020; Greifenhagen et al., 2021). However, the detailed mechanism underlying parasitic plant-induced hypertrophy remains unknown.

In this study, our fresh sections showed that *C. campestris* induced xylem bridge cell enlargement in *PR1*-CRISPR transgenic tomato plants (**Figure 7**). This might allow *C. campestris* to obtain water and nutrients more efficiently from host plants and help with the fitness of the parasite. At the same time, this result also suggests that wild-type tomatoes might originally have a PR1-mediated defense mechanism to prevent hypertrophy upon parasitism. The removal of PR1 makes these transgenic plants more vulnerable to *C. campestris* and these plants have obviously stunted growth upon *C. campestris* infestation (**Figures 7**, **8**). Investigating the connection between PR1 and hypertrophy would be of interest for future research because this could help us to not only understand a potential new defense mechanism against parasitic plants but also know how parasites and host plants influence each other physiologically and morphologically.

Potential Receptors and Factors Involved in Detecting *Cuscuta campestris* Signals

Detecting pathogens or herbivores is the essential first step in triggering plant innate immunity and the following defense responses. Many plant immune receptors have the leucine-rich repeat (LRR) domain (Padmanabhan et al., 2009). More recent studies have indicated that host plants can identify stem and root parasitic plants by utilizing the mechanisms that are similar to the systems for recognizing bacterial and fungal pathogens. For example, the previously identified *CUSCUTA RECEPTOR 1* (*CuRe1*) encodes a leucine-rich repeat receptor-like protein (LRR-RLP) in tomatoes (Hegenauer et al., 2016). This cell surface receptor-like protein bind with a Cuscuta factor, glycine-rich protein (GRP), or its minimal peptide epitope Crip21 to trigger resistance responses, including hypersensitive responses (HRs) and induced ethylene synthesis (Hegenauer et al., 2016, 2020).

However, the host plants that lack CuRe1 are still fully resistant to *C. reflexa*, indicating that CuRe1 is not the only receptor involved in defense responses against parasitic plants (Hegenauer et al., 2016). Recent studies indicate that multilayered resistance mechanisms are deployed by plants to ensure efficient defense against pathogens and parasites (Jhu et al., 2020). Therefore, investigating other potential receptors is important for identifying other potential layers of defense mechanisms and could help with developing parasitic plant resistant systems in crops. In our LCM RNA-Seq analysis results, many LRR genes, including a CuRe1-like gene, are highly expressed in tomato hosts at the early stage of haustorium penetration and are included in SOM8 module 2 and SOM3 module 3 GCNs (**Figure 6**). These discoveries not only provide some evidence for the multilayered resistance hypothesis but also identify potential receptors that might be able to perceive different unknown *Cuscuta* signals.

In addition to LRRs, many NLRs encoded by R genes also have been identified to detect parasitic plants. For example, the *RSG3-301* gene encodes a coiled-coil nucleotide-binding site leucine-rich repeat protein (CC-NBS-LRR) protein in the resistant cowpea, which can trigger the hypersensitive response upon *S. gesnerioides* attack (Li and Timko, 2009). Similarly, *Cuscuta R-gene for Lignin-based Resistance 1* (*CuRLR1*) encodes an N-terminal CC-NBS-LRR, which can induce lignin-based resistance responses in the stem cortex of specific resistant Heinz tomato upon *C. campestris* infestation (Jhu et al., 2020). The two NLRs (Solyc07g056200, Solyc12g006040) that are identified in SOM3 module 3 suggest that other NLRs might also be involved in the defense response against *C. campestris*. The tight gene co-expression connection between NLRs and LRRs indicates either that there is potential crosstalk among different layers of resistance mechanisms, or that these receptors might be regulated by common master regulators.

The results of this study reveal the detailed tissue-resolution gene regulatory mechanisms at the parasitic plant and host interface and identifies key regulators of parasitism in both the parasitic plant *C. campestris* and its tomato host. These findings will not only shed light on the field of plant parasitism and haustorium development but also help to develop a parasite-resistant system in tomatoes to reduce economic losses in agriculture. Parasitic weeds-resistant crops will be effective approaches for regulating parasitic plant infestations, reduce the usage of herbicides, and help with developing sustainable agriculture.

MATERIALS AND METHODS

Cuscuta campestris Materials

The *C. campestris* plant materials used in this study were generous gifts from W. Thomas Lanini, who collected *C. campestris* seeds from tomato fields in California. By using molecular phylogenetics of plastid DNA, and nuclear large-subunit ribosomal DNA (*nrLSU*) sequences (Stefanović et al., 2007; García et al., 2014; Costea et al., 2015), we have verified that this *Cuscuta* isolate is the same as *Cuscuta campestris* 201, Rose 46281 (WTU) from United States, CA (Jhu et al., 2020) by comparing with published sequences (Costea et al., 2015).

Haustorium Section Preparation

To capture specific tissues at the host and parasitic plant interface, we prepared haustorium paraffin sections for further analysis. About four-leaf-stage Heinz 1706 tomato (*Solanum lycopersicum*) plants were infested with 10–15 cm long *C. campestris* strands. First, sections of tomato stem with haustoria, about 0.75 cm long, were collected for histology. Second, these stem sections were fixed in formaldehyde – acetic acid – alcohol (FAA). Third, these samples were dehydrated by the ethanol series for one hour at each step (75, 85, 95, 100, 100, and 100% ethanol) and proceeded through xylene in ethanol series for two hours each (25, 50, 75, 100, and 100% xylene). Fourth, these stem sections were then incubated at 42°C in paraffin and xylene solution series and kept in 100% paraffin and changed twice daily for

three days at 55°C. Finally, these stem sections were embedded in paraffin (Paraplast X-TRA, Thermo Fisher Scientific). 10 μm thick paraffin sections were prepared using a Leica RM2125RT rotary microtome. These paraffin section strips were placed on polyethylene naphthalate (PEN)-coated membrane slides (Leica), dried at room temperature, and deparaffinized with 100% xylene.

Laser-Capture Microdissection Sample Collection

Comparing with our previous transcriptome that used the whole tomato stem tissues near the haustorial attachments (Jhu et al., 2020) or the whole *Cuscuta* strands with haustoria (Ranjan et al., 2014) for RNA library construction, to zoom in on the interface between the host and parasite, laser-capture microdissection (LCM) was used for tissue sample collection in this project. With this method, the tissue of *C. campestris* haustorium protruding region and the tomato host tissue that were surrounding the haustoria from paraffin sections were specifically captured for RNA library construction. Targeted haustorial and host tissues were dissected on a Leica LMD6000 Laser Microdissection System (**Figure 1**). Based on the haustorial structures, we classified haustoria into three different developmental stages. "Early" indicates that the haustorium has just penetrated the tomato stem cortex region. "Intermediate" indicates that the haustorium has penetrated the tomato stem cortex and formed searching hyphae, but has not formed vascular connections with the host vascular system. "Mature" indicates that the haustorium has formed continuous vasculatures with the host (**Figure 1**). Both haustorial tissues and tomato host tissues were microdissected from each of the three developmental stages. These tissues were collected in lysis buffer from RNAqueous®-Micro Total RNA Isolation Kit (Ambion) and stored at −80°C. Collected tissues were processed within one month of fixation to ensure RNA quality. Approximately 30 regions of 10 μm thickness each were cut from each slide, and three to four slides were used per library preparation.

Laser-Capture Microdissection RNA-Seq Library Preparation and Sequencing

RNAs of these collected tissues were extracted using RNAqueous-Micro Total RNA Isolation Kit (Ambion) and amplified using WT-Ovation Pico RNA Amplification System (ver. 1.0, NuGEN Technologies Inc.) following manufacturer instructions. RNA-seq libraries for Illumina sequencing were constructed following a previously published method (Kumar et al., 2012) with slight modifications. Libraries were quantified, pooled to equal amounts, and their quality was checked on a Bioanalyzer 2100 (Agilent). Libraries were sequenced on a HiSeq2000 Illumina Sequencer at the Vincent J Coates Genomics Sequencing Laboratory at UC Berkeley.

RNA-Seq Data Mapping and Processing

After receiving raw reads data for these LCM libraries, we separated them into two groups based on tissue origin, *C. campestris* (dodder) and *S. lycopersicum* (tomato). For the LCM RNA-Seq data from *C. campestris*, these raw reads were mapped to the published genome of *C. campestris* (Vogel et al., 2018) with Bowtie 2 (Langmead and Salzberg, 2012). For the LCM RNA-Seq data from tomato, these raw reads were mapped to the published current tomato genome version ITAG4.0 (Sato et al., 2012) with Bowtie 2 (Langmead and Salzberg, 2012). Both data were then analyzed by using EdgeR (Robinson et al., 2009) to get normalized trimmed means of *M*-values (TMM) for further analysis.

Multidimensional Scaling and Principal Component Analysis With Self-Organizing Maps Clustering

After the normalization steps, to visualize the overall expression profiles of each library, the function "cmdscale" in the R stats package was used to create multidimensional scaling (MDS) data matrix and then generate MDS plots. For both *C. campestris* and tomato LCM RNA-Seq data, genes in the upper 50% quartile of coefficient of variation were selected for further analysis. For principal component analysis (PCA), principal component (PC) values were calculated using the "prcomp" function in the R stats package. The expression profiles of selected genes were visualized in a two-dimensional (2D) plot for PC1 and PC2.

These selected genes were then clustered for multilevel three-by-two hexagonal SOM using the som function in the "kohonen" package (Wehrens and Buydens, 2007). The SOM clustering results were then visualized in PCA plots. The complete gene lists for all SOM units in *C. campestris* and tomato LCM RNA-Seq data with SOM distances and PCA principal component values are included in **Supplementary Tables 1**, **2**, respectively. For both *C. campestris* and tomato LCM RNA-Seq data, we specifically focused on the SOM groups with genes that are highly expressed in the early developmental stage (4 DPA). From *C. campestris* libraries, these genes are likely involved in the mechanisms of haustorium early development and penetration process. From tomato libraries, these genes are likely regulating the early host responses or defense mechanism upon parasitic plant attacks.

Construction of Gene Co-expression Networks

To identify potential key regulators, we use the genes that are classified in selected SOM groups to build GCNs. The R script is modified from our previously published method (Ichihashi et al., 2014), and the updated script is uploaded to GitHub and included in code availability. For the GCN of *C. campestris* LCM data, we used the selected SOM gene list and constructed the GCN of these genes based on the expression profiles in *C. campestris* LCM data with the following normal quantile cutoffs. The SOM5 GCN cutoff = 0.97. The SOM3 GCN cutoff = 0.98. The SOM6 GCN cutoff = 0.95. For the GCN of tomato LCM data, we used the selected SOM gene list and constructed the GCN of these genes based on the expression profiles in tomato LCM data with the following normal quantile cutoffs. The SOM3 GCN cutoff = 0.80. The SOM8 GCN cutoff = 0.90. These networks were then

visualized using Cytoscape version 3.8.0. Based on the number of connections, we identified the central hub genes with the highest connections as our candidate genes (**Supplementary Tables 2**, **3**, **4**, **7**, **8**).

Functional Annotation and GO Enrichment Analysis of RNA-Seq Data

For tomato genes, the current published tomato genome ITAG4.0 is well-annotated, so the gene name and functional annotation that is currently available on the Sol Genomics Network website (https://solgenomics.net/) were used in this study. For *C. campestris* genes, since many genes are not functionally annotated in the current published *C. campestris* genome (Vogel et al., 2018), we used our previously published master list for annotated *C. campestris* transcriptome (Ranjan et al., 2014) combined with *C. campestris* genome gene IDs to create a more complete functional annotation (Jhu et al., 2021). TAIR ID hits were used for GO Enrichment Analysis on http://geneontology.org/for gene clusters and modules. After obtaining these functional annotations, we specifically focused on our candidate genes that are annotated as transcription factors (TFs) or receptors for further analysis.

Host-Induced Gene Silencing RNAi and CRISPR Transgenic Plants

For HIGS RNAi constructs for *C. campestris* candidate genes, we used the previously published destination vector pTKO2 vector (Snowden et al., 2005; Brendolise et al., 2017). This pTKOS2 vector contains two GATEWAY cassettes positioned at opposite directions that are separated by an Arabidopsis ACT2 intron, and the whole construct is under the control of the constitutive 35S promoter. To avoid off-target effects on influencing potential homologs in tomatoes, we used BLAST to identify a sequence fragment that is specific to each *C. campestris* candidate gene. We conducted BLASTN analysis with the currently most up-to-date tomato genome ITAG4.0. We were not able to find similar sequences or potential off-target sequences in the tomato genome for our *CcHB7*, *CcPMEI*, and *CcERF1* RNAi constructs. We also conducted BLASTN analysis with the currently available *Cuscuta campestris* genome to ensure no other known genes in the same gene family would be off-target of our RNAi constructs. This was indeed the case except one hit of *CcHB7* RNAi sequence on Cc037848, which is a gene with unknown function. Based on the Blastn results using NCBI database, Cc037848 might be a *HB7-like* gene. However, this gene is only partially similar to *CcHB7* (query coverage percentage is less than 43%) and this *HB7-like* gene was not knocked down by the *CcHB7* RNAi construct (**Supplementary Figure 4B**).

However, we are also aware that the current *Cuscuta campestris* genome is not as well annotated as the tomato genome. The sequences that are used in HIGS RNAi constructs are listed in **Supplementary Table 10**. This RNAi fragment was amplified from *C. campestris* genomic DNA and cloned into pCR8/GW-TOPO (Life Technologies), and then *in vitro* recombined with the destination vector pTKO2 to generate a final expression clone. The final plasmids were verified by Sanger sequencing and introduced into *A. tumefaciens* EHA105. Among these RNAi tomato transgenic lines, we did not observe any abnormal growth phenotypes in these RNAi tomato plants grown without *Cuscuta campestris*. Therefore, with all of this information and evidence, we believe that no targets in the host might be affected.

For CRISPR constructs of candidate genes, we identified guide RNA (gRNA) sequences that were specific to the target genes using CCTop - CRISPR/Cas9 target predictor (Stemmer et al., 2015; Labuhn et al., 2017). Among CCTop provided candidates, we identified two sequences that are 50∼150 bp apart at the 5′ of the coding sequence and that are scored highly by the CRISPRscan software (Moreno-Mateos et al., 2015). The gRNA sequences that were used in CRISPR constructs are listed in **Supplementary Table 11**. One of these two gRNAs was cloned into pDONR_L1R5_U6gRNA and another was cloned into pDONR_L5L2_AtU6-26gRNA. Both plasmids were digested with *Bbs*I, which places gRNAs under a U6 promoter. Using the *in vitro* CRISPR assay, we verified that the selected gRNAs are functional by expressing gRNAs from a T7 promoter (NEB HiScribe T7 High Yield RNA Synthesis Kit E2040S), generating targets by PCR with gene specific primers, and then mixing them with commercial Cas9 protein (NEB *Streptococcus pyogenes* Cas9, M0641S). Next, both gRNA expression cassettes were recombined by multi-site GATEWAY LR cloning into binary plant transformation vector pMR290, in which an Arabidopsis codon-optimized *Streptococcus pyogenes Cas9* is placed under the control of 2 × 35S constitutive promoter. The final plasmids were verified by Sanger sequencing and transformed into *A. tumefaciens* EHA105.

All of these HIGS RNAi and CRISPR constructs were sent to the Ralph M. Parsons Plant Transformation Facility at the University of California Davis to generate transgenic tomato plants. HIGS RNAi transgenic tomato plants are in Heinz 1706 background. To verify that these transgenic plants contained HIGS RNAi constructs, all T0 transgenic plants were selected for kanamycin resistance, and their genomic DNAs were extracted and tested by PCR. CRISPR transgenic tomato plants are in the M82 background. To verify that transgenic plants contained CRISPR mutations in the target gene, a region spanning and extending the regions between the two gRNAs targets were amplified by PCR and sequenced. The sequence results and the mutations generated by CRISPR in T1 plants are shown in **Supplementary Figure 7** for each candidate gene.

CODE AVAILABILITY STATEMENT

The code that are used for RNA-Seq analysis in this study can be found on https://github.com/MinYaoJhu/Cuscuta_LCM_project.

DATA AVAILABILITY STATEMENT

The datasets presented in this study can be found in online repositories. The names of the repository/repositories and

accession number(s) can be found below: https://www.ncbi.nlm.nih.gov/, PRJNA687611 and PRJNA756681.

AUTHOR CONTRIBUTIONS

MF conducted LCM to capture tissues and prepared libraries for RNA-Seq and made CRISPR and RNAi constructs and used the UC Davis transformation facility to generate transgenic plants and genotyped T0 transgenic plants. M-YJ mapped the LCM RNA-Seq data to *C. campestris* and tomato genome and performed MDS, PCA, SOM clustering and GO term analysis respectively, constructed gene coexpression networks for selected *C. campestris* and tomato SOM cluster gene lists, analyzed T1 CRISPR and RNAi transgenic plants genotyping and phenotyping data, and wrote the initial manuscript and organized all data to make figures and tables with primary editing from NS. LW performed genotyping and phenotyping on T1 CRISPR and RNAi transgenic plants. KZ conducted qPCR experiments, maintained transgenic tomato seed stocks, and analyzed T1 CRISPR genotyping results. NS supervised this project and serves as the author responsible for contact and communication. All authors contributed to the article and approved the submitted version.

FUNDING

This work was funded by USDA-NIFA (2013-02345). M-YJ was supported by Yen Chuang Taiwan Fellowship, Taiwan Government Scholarship (GSSA), Elsie Taylor Stocking Memorial Fellowship, Katherine Esau Summer Graduate Fellowship, Loomis Robert S. and Lois Ann Graduate Fellowship in Agronomy, and the UCD Graduate Research Award. MF was supported by United States-Israel Binational Agricultural Research and Development Fund (postdoctoral fellowship no. FI–463–12).

ACKNOWLEDGMENTS

We are grateful to the UC Davis Plant Transformation Facility for generating CRISPR and RNAi transgenic tomato plants. We thank Richard Philbrook for helping in genotyping CRISPR plants. We also thank Mily Ron for providing CRISPR vectors.

SUPPLEMENTARY MATERIAL

The Supplementary Material for this article can be found online at: https://www.frontiersin.org/articles/10.3389/fpls.2021.764843/full#supplementary-material

Supplementary Figure 1 | Multidimensional scaling (MDS) plot of RNA expression profile in all libraries from LCM of three different *C. campestris* developmental stages mapped to *C. campestris* genome. The early stage has five libraries. The intermediate stage has three libraries. The mature stage has two libraries. This figure is modified from one of the supplemental figures in our previously published paper Jhu et al. (2021).

Supplementary Figure 2 | Principal component analysis (PCA) analysis results coupled with self-organizing maps (SOM) clustering in *C. campestris* haustoria across three developmental stages from LCM RNA-Seq data. **(A)** PCA plot of the first and second principal components (PC1 and PC2) and colored to indicate their corresponding SOM groups. Each dot represents a gene. **(B)** Loading values of PC1 and PC2. PC1 separate the mature stage-specific genes from the early and intermediate stage-specific genes. PC2 separates the genes specifically expressed in the early stage from those specifically expressed in the intermediate stage. **(C)** A plot of each SOM group's scaled expression levels at three *C. campestris* haustorial developmental stages. The color of each line represents the SOM group it belongs to. The 95% confidence interval is indicated by the shaded area around the lines. **(D)** A code plot of SOM clustering showing which developmental phase expressed genes are dominant in each SOM group based on sector size. Each sector represents a developmental stage and is colored according to the stage it represents. **(D,E)** The number 1–6 next to each circle represents the corresponding SOM group. This figure is modified from one of the figures and supplemental figures in our previously published manuscript Jhu et al., 2021 with new information added.

Supplementary Figure 3 | Heatmaps and gene-coexpression networks (GCNs) of *C. campestris* haustorial tissues across three developmental stages. **(A)** A heatmap of gene expression profiles in z-scores for SOM1, which includes genes that are highly expressed in the intermediate stage. **(B)** A GCN of genes in SOM1. This SOM1 GCN is composed of five major modules. **(C)** A heatmap of gene expression profiles in z-scores for SOM2, which includes genes that are highly expressed in the intermediate and mature stage. **(D)** A GCN of genes that are in SOM2. The SOM2 GCN is composed of five major modules. **(E)** A heatmap of gene expression profiles in z-scores for SOM4, which includes genes that are relatively highly expressed in the early and intermediate stage. **(F)** A GCN of genes that are in SOM4. The SOM4 GCN is composed of five major modules. The complete gene lists for all SOM units with SOM distances and PCA principal component values are included in **Supplementary Table 1**. The selected SOM gene lists were used for constructing the GCN based on the expression profiles in *C. campestris* LCM data with the following normal quantile cutoffs. The SOM1 GCN cutoff = 0.97. The SOM2 GCN cutoff = 0.95. The SOM4 GCN cutoff = 0.98.

Supplementary Figure 4 | *CcHB7*, *CcHB7-like*, *CcPMEI*, and *CcERF1* expression levels in *C. campestris* haustorium and prehaustorium tissues grown on HIGS transgenic tomatoes. **(A)** Normalized *CcHB7* expression level from qPCR data in *HB7* RNAi transgenic tomatoes. H1706, biological replicates: $n_b = 1$, technical replicates for each biological replicate: $n_t = 4$; *HB7* RNAi, biological replicates: $n_b = 4$, technical replicates for each biological replicate: $n_t = 4$. **(B)** Normalized *CcHB7-like* expression level from qPCR data in *HB7* RNAi transgenic tomatoes. H1706, biological replicates: $n_b = 1$, technical replicates for each biological replicate: $n_t = 3$; *HB7* RNAi, biological replicates: $n_b = 4$, technical replicates for each biological replicate: $n_t = 3$ or 4. **(C)** Normalized *CcPMEI* expression level from qPCR data in *PMEI* RNAi transgenic tomatoes. H1706, biological replicates: $n_b = 3$, technical replicates for each biological replicate: $n_t = 4$; *PMEI* RNAi, biological replicates: $n_b = 5$; technical replicates for each biological replicate: $n_t = 4$. **(D)** Normalized *CcERF1* expression level from qPCR data in *ERF1* RNAi transgenic tomatoes. H1706, biological replicates: $n_b = 3$, technical replicates for each biological replicate: $n_t = 4$; *ERF1* RNAi, biological replicates: $n_b = 5$; technical replicates for each biological replicate: $n_t = 4$. Data presented are assessed using two-tailed Student's *t*-test. "*" p-value < 0.05. "n.s." p-value > 0.05.

Supplementary Figure 5 | Multidimensional scaling (MDS) plot of LCM RNA-Seq data from the host tomato tissues surrounding *C. campestris* haustoria. "Control" means the tomato stem cortex tissue samples that are not next to *C. campestris* haustoria, which serve as negative controls in this experiment. The control has eight libraries. The early stage has eight libraries. The intermediate stage has four libraries. The mature stage has three libraries.

Supplementary Figure 6 | Heatmaps and gene-coexpression networks (GCNs) of LCM RNA-Seq data from the host tomato tissues surrounding *C. campestris* haustoria. **(A)** A heatmap of gene expression profiles in z-scores for SOM1, which

includes genes specifically highly expressed in the control stage. **(B)** A GCN of genes in SOM1. This SOM1 GCN is composed of five major modules. **(C)** A heatmap of gene expression profiles in z-scores for SOM2, which includes genes specifically highly expressed in the intermediate stage. **(D)** A GCN of genes in SOM2. This SOM2 GCN is composed of five major modules. **(E)** A heatmap of gene expression profiles in *z*-scores for SOM4, which includes genes specifically highly expressed in the control and early stage. **(F)** A GCN of genes in SOM4. This SOM4 GCN is composed of five major modules. **(G)** A heatmap of gene expression profiles in z-scores for SOM5, which includes genes specifically highly expressed in the control and mature stage. **(H)** A GCN of genes in SOM5. This SOM5 GCN is composed of five major modules. **(I)** A heatmap of gene expression profiles in z-scores for SOM6, which includes genes specifically repressed expression in the early stage. **(J)** A GCN of genes in SOM6. This SOM6 GCN is composed of five major modules. **(K)** A heatmap of gene expression profiles in *z*-scores for SOM7, which includes genes specifically repressed expression in the mature stage. **(L)** A GCN of genes in SOM7. This SOM7 GCN is composed of five major modules. The complete gene lists for all SOM units with SOM distances and PCA principal component values are included in **Supplementary Table 6**. The selected SOM gene lists were used for constructing the GCN based on the expression profiles in tomato LCM data with the following normal quantile cutoffs. The SOM1 GCN cutoff = 0.95. The SOM2 GCN cutoff = 0.93. The SOM4 GCN cutoff = 0.93. The SOM5 GCN cutoff = 0.96. The SOM6 GCN cutoff = 0.94. The SOM7 GCN cutoff = 0.92.

Supplementary Figure 7 | Genotyping results of the T1 CRISPR transgenic plants that are used in this study. **(A)** Genomic DNA PCR product sequencing result of PR1 T1 CRISPR plants. T1 plant #1-3 have similar mixed peaks were present next to the sgRNA1, indicating a biallelic or heterozygous mutation. **(B)** Genomic DNA PCR product sequencing result of NLR T1 CRISPR plants. T1 plant #1, 2, 6 have similar mixed peaks were present next to the sgRNA1, indicating a biallelic or heterozygous mutation. T1 plant #4 might have a large section of deletion (> 150 bp) next to the two gRNAs, so it has a large section of mismatch and mixed peaks. **(A,B)** The dark red line indicates the sequencing result. The number next to each dark red line indicates the T1 plant ID number (T1 plant #). The section filled with dark red color indicates regions of perfect sequence match; the empty boxes indicate regions of sequence mismatch. The dark red arrowhead above each sequence indicates a section of insertion. The dark red line above each sequence indicates a single base pair insertion. The gRNAs are labeled as blue arrows. The gRNA sequences that were used in these CRISPR constructs are listed in **Supplementary Table 11**. The protospacer adjacent motif (PAM) sites are labeled as small red boxes that are right next to gRNAs. Detailed genotyping results of the T1 CRISPR transgenic plants are listed in **Supplementary Table 12**.

REFERENCES

Adie, B., Chico, J. M., Rubio-Somoza, I., and Solano, R. (2007). Modulation of Plant Defenses by Ethylene. *J. Plant Growth Regul.* 26, 160–177.

Agrios, G. N. (2005). *Chapter Thirteen - Plant Diseases Caused by Parasitic Higher Plants, Invasive Climbing Plants, and Parasitic Green Algae*. San Diego: Academic Press. 705–722.

Alakonya, A., Kumar, R., Koenig, D., Kimura, S., Townsley, B., Runo, S., et al. (2012). Interspecific RNA Interference of SHOOT MERISTEMLESS-Like Disrupts Cuscuta pentagona Plant Parasitism. *Plant Cell* 24, 3153–3166. doi: 10.1105/tpc.112.099994

Benková, E., Michniewicz, M., Sauer, M., Teichmann, T., Seifertová, D., Jürgens, G., et al. (2003). Local, efflux-dependent auxin gradients as a common module for plant organ formation. *Cell* 115, 591–602. doi: 10.1016/s0092-8674(03)00924-3

Berens, M. L., Wolinska, K. W., Spaepen, S., Ziegler, J., Nobori, T., Nair, A., et al. (2019). Balancing trade-offs between biotic and abiotic stress responses through leaf age-dependent variation in stress hormone cross-talk. *Proc. Natl. Acad. Sci.* 116, 2364–2373. doi: 10.1073/pnas.1817233116

Böhm, H., Albert, I., Fan, L., Reinhard, A., and Nürnberger, T. (2014). Immune receptor complexes at the plant cell surface. *Curr. Opin. Plant Biol.* 20, 47–54. doi: 10.1016/j.pbi.2014.04.007

Bowman, C. (2019). *Plant Virology*. United Kingdom: Edtech.

Breen, S., Williams, S. J., Outram, M., Kobe, B., and Solomon, P. S. (2017). Emerging Insights into the Functions of Pathogenesis-Related Protein 1. *Trends Plant Sci.* 22, 871–879. doi: 10.1016/j.tplants.2017.06.013

Brendolise, C., Montefiori, M., Dinis, R., Peeters, N., Storey, R. D., and Rikkerink, E. H. (2017). A novel hairpin library-based approach to identify NBS-LRR genes required for effector-triggered hypersensitive response in *Nicotiana benthamiana*. *Plant Methods*. 13:32.

Broekgaarden, C., Caarls, L., Vos, I. A., Pieterse, C. M. J., and Van Wees, S. C. M. (2015). Ethylene: traffic Controller on Hormonal Crossroads to Defense. *Plant Physiol.* 169, 2371–2379. doi: 10.1104/pp.15.01020

Chebli, Y., and Geitmann, A. (2017). Cellular growth in plants requires regulation of cell wall biochemistry. *Curr. Opin. Cell Biol.* 44, 28–35. doi: 10.1016/j.ceb.2017.01.002

Cheng, X., Floková, K., Bouwmeester, H., and Ruyter-Spira, C. (2017). The Role of Endogenous Strigolactones and Their Interaction with ABA during the Infection Process of the Parasitic Weed Phelipanche ramosa in Tomato Plants. *Front. Plant Sci.* 8:392. doi: 10.3389/fpls.2017.00392

Clauset, A., Newman, M. E. J., and Moore, C. (2004). Finding community structure in very large networks. *Phys. Rev. E* 70:066111. doi: 10.1103/PhysRevE.70.066111

Cline, M. S., Smoot, M., Cerami, E., Kuchinsky, A., Landys, N., Workman, C., et al. (2007). Integration of biological networks and gene expression data using Cytoscape. *Nat. Protocols* 2, 2366–2382. doi: 10.1038/nprot.2007.324

Costea, M., García, M. A., Baute, K., and Stefanović, S. (2015). Entangled evolutionary history of Cuscuta pentagona clade: a story involving hybridization and Darwin in the Galapagos. *TAXON* 64, 1225–1242.

Cui, S., Kubota, T., Nishiyama, T., Ishida, J. K., Shigenobu, S., Shibata, T. F., et al. (2020). Ethylene signaling mediates host invasion by parasitic plants. *Sci. Adv.* 6:eabc2385. doi: 10.1126/sciadv.abc2385

Dos Santos, C. V., Letousey, P., Delavault, P., and Thalouarn, P. (2003). Defense Gene Expression Analysis of Arabidopsis thaliana Parasitized by Orobanche ramosa. *Phytopathology* 93, 451–457. doi: 10.1094/PHYTO.2003.93.4.451

Fishman, M. R., and Shirasu, K. (2021). How to resist parasitic plants: pre- and post-attachment strategies. *Curr. Opin. Plant Biol.* 62:102004. doi: 10.1016/j.pbi.2021.102004

Fürst, U., Hegenauer, V., Kaiser, B., Körner, M., Welz, M., and Albert, M. (2016). Parasitic Cuscuta factor(s) and the detection by tomato initiates plant defense. *Commun. Integr. Biol.* 9:e1244590. doi: 10.1080/19420889.2016.1244590

Furuhashi, T., Furuhashi, K., and Weckwerth, W. (2011). The parasitic mechanism of the holostemparasitic plant Cuscuta. *J. Plant Interact.* 6, 207–219.

García, M. A., Costea, M., Kuzmina, M., and Stefanović, S. (2014). Phylogeny, character evolution, and biogeography of Cuscuta (dodders; Convolvulaceae) inferred from coding plastid and nuclear sequences. *Am. J. Bot.* 101, 670–690. doi: 10.3732/ajb.1300449

Greifenhagen, A., Braunstein, I., Pfannstiel, J., Yoshida, S., Shirasu, K., Schaller, A., et al. (2021). The Phtheirospermum japonicum isopentenyltransferase PjIPT1a regulates host cytokinin responses in Arabidopsis. *New Phytol.* 232, 1582–1590. doi: 10.1111/nph.17615

Hegenauer, V., Fürst, U., Kaiser, B., Smoker, M., Zipfel, C., Felix, G., et al. (2016). Detection of the plant parasite Cuscuta reflexa by a tomato cell surface receptor. *Science* 353, 478–481. doi: 10.1126/science.aaf3919

Hegenauer, V., Slaby, P., Körner, M., Bruckmüller, J.-A., Burggraf, R., Albert, I., et al. (2020). The tomato receptor CuRe1 senses a cell wall protein to identify Cuscuta as a pathogen. *Nat. Commun.* 11:5299. doi: 10.1038/s41467-020-19147-4

Heide-Jørgensen, H. (2008). *Parasitic Flowering Plants*. Netherlands: Brill.

Hozumi, A., Bera, S., Fujiwara, D., Obayashi, T., Yokoyama, R., Nishitani, K., et al. (2017). Arabinogalactan Proteins Accumulate in the Cell Walls of Searching Hyphae of the Stem Parasitic Plants, Cuscuta campestris and Cuscuta japonica. *Plant Cell Physiol.* 58, 1868–1877. doi: 10.1093/pcp/pcx121

Ichihashi, Y., Aguilar-Martínez, J. A., Farhi, M., Chitwood, D. H., Kumar, R., Millon, L. V., et al. (2014). Evolutionary developmental transcriptomics reveals a gene network module regulating interspecific diversity in plant

leaf shape. *Proc. Natl. Acad. Sci.* 111, E2616–E2621. doi: 10.1073/pnas.1402835111

Ishida, J. K., Wakatake, T., Yoshida, S., Takebayashi, Y., Kasahara, H., Wafula, E., et al. (2016). Local Auxin Biosynthesis Mediated by a YUCCA Flavin Monooxygenase Regulates Haustorium Development in the Parasitic Plant Phtheirospermum japonicum. *Plant Cell* 28, 1795–1814. doi: 10.1105/tpc.16.00310

Jhu, M.-Y., Farhi, M., Wang, L., Philbrook, R. N., Belcher, M. S., Nakayama, H., et al. (2020). Lignin-based resistance to Cuscuta campestris parasitism in Heinz resistant tomato cultivars. *bioRxiv* 706861. doi: 10.1101/706861

Jhu, M.-Y., Ichihashi, Y., Farhi, M., Wong, C., and Sinha, N. R. (2021). LATERAL ORGAN BOUNDARIES DOMAIN 25 functions as a key regulator of haustorium development in dodders. *Plant Physiol.* 186, 2093–2110. doi: 10.1093/plphys/kiab231

Johnsen, H. R., Striberny, B., Olsen, S., Vidal-Melgosa, S., Fangel, J. U., Willats, W. G. T., et al. (2015). Cell wall composition profiling of parasitic giant dodder (Cuscuta reflexa) and its hosts: a priori differences and induced changes. *New Phytol.* 207, 805–816. doi: 10.1111/nph.13378

Johnson, N. R., Depamphilis, C. W., and Axtell, M. J. (2019). Compensatory sequence variation between trans-species small RNAs and their target sites. *Elife* 8:e49750. doi: 10.7554/eLife.49750

Kim, G., Leblanc, M. L., Wafula, E. K., Depamphilis, C. W., and Westwood, J. H. (2014). Genomic-scale exchange of mRNA between a parasitic plant and its hosts. *Science* 345, 808–811. doi: 10.1126/science.1253122

Kimura, S., and Sinha, N. (2008). Tomato (Solanum lycopersicum): a Model Fruit-Bearing Crop. *Cold Spring Harbor Protocols* 2008:db.emo105. doi: 10.1101/pdb.emo105

Kokla, A., Leso, M., Zhang, X., Simura, J., Cui, S., Ljung, K., et al. (2021). Nitrates increase abscisic acid levels to regulate haustoria formation in the parasitic plant Phtheirospermum japonicum. *Biorxiv* 2021. doi: 10.1101/2021.06.15.448499

Kong, G., Wan, L., Deng, Y. Z., Yang, W., Li, W., Jiang, L., et al. (2019). Pectin acetylesterase PAE5 is associated with the virulence of plant pathogenic oomycete Peronophythora litchii. *Physiol. Mol. Plant Pathol.* 106, 16–22.

Ku, Y.-S., Sintaha, M., Cheung, M.-Y., and Lam, H.-M. (2018). Plant Hormone Signaling Crosstalks between Biotic and Abiotic Stress Responses. *Int. J. Mol. Sci.* 19:3206. doi: 10.3390/ijms19103206

Kumar, R., Ichihashi, Y., Kimura, S., Chitwood, D., Headland, L., Peng, J., et al. (2012). A High-Throughput Method for Illumina RNA-Seq Library Preparation. *Front. Plant Sci.* 3:202. doi: 10.3389/fpls.2012.00202

Labuhn, M., Adams, F. F., Ng, M., Knoess, S., Schambach, A., Charpentier, E. M., et al. (2017). Refined sgRNA efficacy prediction improves large- and small-scale CRISPR–Cas9 applications. *Nucleic Acids Res.* 46, 1375–1385. doi: 10.1093/nar/gkx1268

Langmead, B., and Salzberg, S. L. (2012). Fast gapped-read alignment with Bowtie 2. *Nat. Methods* 9, 357–359. doi: 10.1038/nmeth.1923

Lanini, W., and Kogan, M. (2005). Biology and Management of Cuscuta in Crops. *Ciencia Investig. Agrar.* 32, 127–141. doi: 10.1371/journal.pone.0081389

Li, J., and Timko, M. P. (2009). Gene-for-Gene Resistance in Striga-Cowpea Associations. *Science* 325, 1094–1094. doi: 10.1126/science.1174754

Liu, Z., Wu, Y., Yang, F., Zhang, Y., Chen, S., Xie, Q., et al. (2013). BIK1 interacts with PEPRs to mediate ethylene-induced immunity. *Proc. Natl. Acad. Sci.* 110, 6205–6210. doi: 10.1073/pnas.1215543110

McHale, L., Tan, X., Koehl, P., and Michelmore, R. W. (2006). Plant NBS-LRR proteins: adaptable guards. *Genome Biol.* 7:212. doi: 10.1186/gb-2006-7-4-212

Mignolli, F., Todaro, J. S., and Vidoz, M. L. (2020). Internal aeration and respiration of submerged tomato hypocotyls are enhanced by ethylene-mediated aerenchyma formation and hypertrophy. *Physiol. Plantarum* 169, 49–63. doi: 10.1111/ppl.13044

Moreno-Mateos, M. A., Vejnar, C. E., Beaudoin, J.-D., Fernandez, J. P., Mis, E. K., Khokha, M. K., et al. (2015). CRISPRscan: designing highly efficient sgRNAs for CRISPR-Cas9 targeting *in vivo*. *Nat. Methods* 12, 982–988. doi: 10.1038/nmeth.3543

O'Brien, T. P., Feder, N., and Mccully, M. E. (1964). Polychromatic staining of plant cell walls by toluidine blue O. *Protoplasma* 59, 368–373. doi: 10.1007/bf01248568

Padmanabhan, M., Cournoyer, P., and Dinesh-Kumar, S. P. (2009). The leucine-rich repeat domain in plant innate immunity: a wealth of possibilities. *Cell. Microbiol.* 11, 191–198. doi: 10.1111/j.1462-5822.2008.01260.x

Pan, C., Ye, L., Qin, L., Liu, X., He, Y., Wang, J., et al. (2016). CRISPR/Cas9-mediated Efficient and Heritable Targeted Mutagenesis in Tomato Plants in the First and Later Generations. *Sci. Rep.* 6:24765.

Pehlivan, N. (2019). Stochasticity in transcriptional expression of a negative regulator of Arabidopsis ABA network. *3 Biotech* 9:15. doi: 10.1007/s13205-018-1542-2

Ranjan, A., Ichihashi, Y., Farhi, M., Zumstein, K., Townsley, B., David-Schwartz, R., et al. (2014). De Novo Assembly and Characterization of the Transcriptome of the Parasitic Weed Dodder Identifies Genes Associated with Plant Parasitism. *Plant Physiol.* 166, 1186–1199. doi: 10.1104/pp.113.234864

Robinson, M. D., Mccarthy, D. J., and Smyth, G. K. (2009). edgeR: a Bioconductor package for differential expression analysis of digital gene expression data. *Bioinformatics* 26, 139–140. doi: 10.1093/bioinformatics/btp616

Runyon, J. B., Mescher, M. C., Felton, G. W., and De Moraes, C. M. (2010). Parasitism by Cuscuta pentagona sequentially induces JA and SA defence pathways in tomato. *Plant Cell Environ.* 33, 290–303. doi: 10.1111/j.1365-3040.2009.02082.x

Saffer, A. M. (2018). Expanding roles for pectins in plant development. *J. Integr. Plant Biol.* 60, 910–923. doi: 10.1111/jipb.12662

Sato, S., Tabata, S., Hirakawa, H., Asamizu, E., Shirasawa, K., Isobe, S., et al. (2012). The tomato genome sequence provides insights into fleshy fruit evolution. *Nature* 485, 635–641. doi: 10.1038/nature11119

Shen, G., Liu, N., Zhang, J., Xu, Y., Baldwin, I. T., and Wu, J. (2020). Cuscuta australis (dodder) parasite eavesdrops on the host plants' FT signals to flower. *Proc. Natl. Acad. Sci.* 117, 23125–23130. doi: 10.1073/pnas.2009445117

Shimizu, K., and Aoki, K. (2019). Development of Parasitic Organs of a Stem Holoparasitic Plant in Genus Cuscuta. *Front. Plant Sci.* 10:1435. doi: 10.3389/fpls.2019.01435

Snowden, K., Simkin, A., Janssen, B., Templeton, K., Loucas, H., Simons, J., et al. (2005). The decreased apical dominance1/Petunia hybrida CAROTENOID CLEAVAGE DIOXYGENASE8 gene affects branch production and plays a role in leaf senescence, root growth, and flower development. *Plant Cell.* 17, 746–759. doi: 10.1105/tpc.104.027714.

Spallek, T., Melnyk, C. W., Wakatake, T., Zhang, J., Sakamoto, Y., Kiba, T., et al. (2017). Interspecies hormonal control of host root morphology by parasitic plants. *Proc. Natl. Acad. Sci.* 114, 5283–5288. doi: 10.1073/pnas.1619078114

Stefanović, S., Kuzmina, M., and Costea, M. (2007). Delimitation of major lineages within Cuscuta subgenus Grammica (Convolvulaceae) using plastid and nuclear DNA sequences. *Am. J. Bot.* 94, 568–589. doi: 10.3732/ajb.94.4.568

Stemmer, M., Thumberger, T., Del Sol Keyer, M., Wittbrodt, J., and Mateo, J. L. (2015). CCTop: an Intuitive, Flexible and Reliable CRISPR/Cas9 Target Prediction Tool. *Plos One* 10:e0124633. doi: 10.1371/journal.pone.0124633

Su, C., Liu, H., Wafula, E. K., Honaas, L., De Pamphilis, C. W., and Timko, M. P. (2020). SHR4z, a novel decoy effector from the haustorium of the parasitic weed Striga gesnerioides, suppresses host plant immunity. *New Phytol.* 226, 891–908. doi: 10.1111/nph.16351

Tada, Y., Sugai, M., and Furuhashi, K. (1996). Haustoria of Cuscuta japonica, a Holoparasitic Flowering Plant, Are Induced by the Cooperative Effects of Far-Red Light and Tactile Stimuli. *Plant Cell Physiol.* 37, 1049–1053. doi: 10.1093/pcp/pcd070

Taylor, A., Martin, J., and Seel, W. E. (1996). Physiology of the parasitic association between maize and witchweed (Striga hermonthica): is ABA involved? *J. Exp. Bot.* 47, 1057–1065. doi: 10.1093/jxb/47.8.1057

Tintor, N., Ross, A., Kanehara, K., Yamada, K., Fan, L., Kemmerling, B., et al. (2013). Layered pattern receptor signaling *via* ethylene and endogenous elicitor peptides during Arabidopsis immunity to bacterial infection. *Proc. Natl. Acad. Sci.* 110, 6211–6216. doi: 10.1073/pnas.1216780110

Tomilov, A. A., Tomilova, N. B., Abdallah, I., and Yoder, J. I. (2005). Localized hormone fluxes and early haustorium development in the hemiparasitic plant Triphysaria versicolor. *Plant Physiol.* 138, 1469–1480. doi: 10.1104/pp.104.057836

Valdés, A. E., övernäs, E., Johansson, H., Rada-Iglesias, A., and Engström, P. (2012). The homeodomain-leucine zipper (HD-Zip) class I transcription factors ATHB7 and ATHB12 modulate abscisic acid signalling by regulating protein

phosphatase 2C and abscisic acid receptor gene activities. *Plant Mol. Biol.* 80, 405–418. doi: 10.1007/s11103-012-9956-4

Van Ghelder, C., Parent, G. J., Rigault, P., Prunier, J., Giguère, I., Caron, S., et al. (2019). The large repertoire of conifer NLR resistance genes includes drought responsive and highly diversified RNLs. *Sci. Rep.* 9:11614. doi: 10.1038/s41598-019-47950-7

Vaughn, K. C. (2002). Attachment of the parasitic weed dodder to the host. *Protoplasma* 219, 227–237. doi: 10.1007/s007090200024

Veselov, D., Langhans, M., Hartung, W., Aloni, R., Feussner, I., Götz, C., et al. (2003). Development of *Agrobacterium tumefaciens* C58-induced plant tumors and impact on host shoots are controlled by a cascade of jasmonic acid, auxin, cytokinin, ethylene and abscisic acid. *Planta* 216, 512–522. doi: 10.1007/s00425-002-0883-5

Vieira Dos Santos, C., Delavault, P., Letousey, P., and Thalouarn, P. (2003). Identification by suppression subtractive hybridization and expression analysis of Arabidopsis thaliana putative defence genes during Orobanche ramosa infection. *Physiol. Mol. Plant Pathol.* 62, 297–303. doi: 10.1016/s0885-5765(03)00073-0

Vogel, A., Schwacke, R., Denton, A. K., Usadel, B., Hollmann, J., Fischer, K., et al. (2018). Footprints of parasitism in the genome of the parasitic flowering plant Cuscuta campestris. *Nat. Commun.* 9:2515. doi: 10.1038/s41467-018-04344-z

Wehrens, R., and Buydens, L. (2007). Self- and Super-organizing Maps in R: the kohonen Package. *J. Statist. Softw.* 21, 1–19.

Wormit, A., and Usadel, B. (2018). The Multifaceted Role of Pectin Methylesterase Inhibitors (PMEIs). *Int. J. Mol. Sci.* 19:2878. doi: 10.3390/ijms19102878

Yaakov, G., Lanini, W. T., and Wrobel, R. L. (2001). Tolerance of Tomato Varieties to Lespedeza Dodder. *Weed Sci.* 49, 520–523.

Yoder, J. I., and Scholes, J. D. (2010). Host plant resistance to parasitic weeds; recent progress and bottlenecks. *Curr. Opin. Plant Biol.* 13, 478–484. doi: 10.1016/j.pbi.2010.04.011

Yoshida, S., Cui, S., Ichihashi, Y., and Shirasu, K. (2016). The Haustorium, a Specialized Invasive Organ in Parasitic Plants. *Annu. Rev. Plant Biol.* 67, 643–667. doi: 10.1146/annurev-arplant-043015-111702

Conflict of Interest: MF was employed by company The Better Meat Co.

The remaining authors declare that the research was conducted in the absence of any commercial or financial relationships that could be construed as a potential conflict of interest.

Publisher's Note: All claims expressed in this article are solely those of the authors and do not necessarily represent those of their affiliated organizations, or those of the publisher, the editors and the reviewers. Any product that may be evaluated in this article, or claim that may be made by its manufacturer, is not guaranteed or endorsed by the publisher.

Frontiers in Plant Science

Cultivates the science of plant biology and its applications

The most cited plant science journal, which advances our understanding of plant biology for sustainable food security, functional ecosystems and human health.

Discover the latest Research Topics

See more →

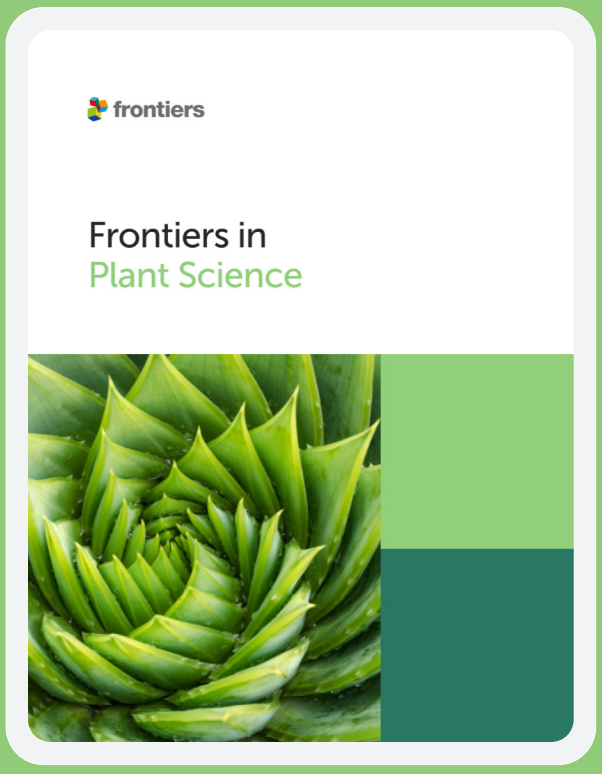

Frontiers

Avenue du Tribunal-Fédéral 34
1005 Lausanne, Switzerland
frontiersin.org

Contact us

+41 (0)21 510 17 00
frontiersin.org/about/contact